Evaluation of Composite Laminates Interleaved with Nanofibre and Microfibre Veils

A thesis submitted in fulfilment

of the requirements for the degree

of

Masters of Engineering

in Materials and Process Engineering

at

The University of Waikato

by

Rosalie Collins-Gargan

———————

The University of Waikato

2015

THE UNIVERSITY OF
WAIKATO
Te Whare Wānanga o Waikato

Abstract

The research covered in this thesis aimed to investigate the use of nanofibre and microfibre veils in carbon fibre reinforced composites and assessed the potential of the veils to improve damage resistance during impact and fatigue loading. It was hypothesised that the interleavings would increase the amount of energy required for crack propagation because of toughening due to fibre reinforcement mechanisms such as crack deflection, fibre pull out and fibre breakage. The work was undertaken as a combined project between the University of Waikato (Hamilton, New Zealand) and Revolution Fibres Ltd (Auckland, New Zealand).

During this investigation, six thermoplastic polymers were chosen (acrylonitrile butadiene styrene (ABS), acrylonitrile styrene acrylate (ASA), polystyrene (PS), chlorinated polyvinyl chloride (CPVC), polymethyl methacrylate (PMMA) and polycarbonate (PC)) that could potentially be used for the electrospinning of polymer nanofibre veils. Nanofibre veils were successfully produced from PMMA, and a polymer blend of polyamide 6,6 (PA6,6) and PMMA, (referred to as 'nanoNyplex'). These veils, along with three other nanofibre veils (nanoPA6,6, poly vinyl butyral (nanoPVB), and poly ether sulfone (nanoPES)), three microfibre veils (polyphenylene sulfide (microPPS), polyetherimide (microPEI), and woven polyamide 6 (microtricot)) procured from other manufacturers, and three veils combining one of the nanofibre veils with each of the microfibre veils (microPPSnanoPA6,6, microPEInanoPA6,6, and microtricotnanoPA6,6) were then used as interleaves in the manufacture of carbon fibre reinforced epoxy composite panels. Interleaves were placed between every ply of prepreg. After curing the panels, test specimens were created to assess fatigue, vibration damping and compression after impact performance.

From the vibration damping study, it was found that the nanoNyplex interleaving improved damping the most. It was thought that energy dissipation was due friction brought about by the movement of the interleaving fibres in the matrix, resulting in friction due to weak adhesion between the nanoNyplex fibres and the epoxy matrix.

From the compression after impact (CAI) section of this study, it was found that specimens interleaved with nanoPA6,6, microPPS and microPPSnanoPA6,6 had the highest CAI strengths. From optical inspection, it appeared (in general) that as the CAI strength of the specimen increased, the length of the damage region also increased. However, those identified with the highest CAI strengths had shorter damage regions.

From the fatigue section of this study, it was found that the use of most interleavings, (apart from microtricot) increased the number of cycles to failure. Post fatigue test scanning electron microscopy confirmed that crack deflection was present for most interleaved specimens. Some evidence of pull out and breakage of the interleaving fibres was seen on the fracture surfaces of the nanoPA6,6, microPPS, microPEI, microPEInanoPA6,6 and microPPSnanoPA6,6 interleaved specimens.

For both CAI and fatigue, it was found that improvement was generally greater with veils that had a large number of fibres per unit area and high adhesion strength with the matrix. However, for CAI it seems that high fracture toughness was also desirable.

Acknowledgements

I have found this whakataukī to be apt throughout this project:

He whakataukī:

"Ka tika a muri, ka tika a mua, ka rere pai ngā āhuatanga katoa".

Table of Contents

vii

List of Figures

xiii

xxiv

List of Tables

List of Abbreviations and Nomenclature

Polymers

Abbreviation	Full name
ASA	acrylonitrile styrene acrylate
ABS	acrylonitrile butadiene styrene
CPVC	chlorinated polyvinyl chloride
Nyplex	blend of PMMA and PA6,6
PA6,6	polyamide 6,6, also Nylon 6,6
PC	polycarbonate
PES	poly ethersulfone
PMMA	poly methyl methacrylate
PS (ExPS)	expanded polystyrene
PS (GPPS)	general purpose polystyrene
PS (HIPS)	high impact polystyrene
PVB	polyvinyl butyral
PPS	polyphenylene sulfide
PEI	polyetherimide
tricot	woven polyamide 6 (PA 6)

Solvents

Abbreviation	Full name
AA	acetic acid
BA	benzyl alcohol
EA	ethyl acetate
FA	formic acid
NPA or nPA	n-propyl acetate
MEK	methyl ether ketone
DMSO	dimethyl sulfoxide
DMF	dimethyl formamide

DMA	dimethyl acetamide
THF	tetrahydrofuran
IPA	2-propanol
NMP	n-methyl-2-pyrrolidone

Additives

Abbreviation	Full name
AgNO$_3$	silver nitrate
SDS	sodium dodecyl sulfate
LiCl	lithium chloride
AmmA	ammonium acetate
PSS	poly(sodium styrene sulfonate)
Citric	citric acid

Veil names

Veil Abbreviation	Details
nanoNyplex	Nyplex nanofibres (spun from a solution of PMMA and PA6,6)
nanoPMMA	PMMA nanofibres
nanoPA6,6	PA6,6 nanofibres
nanoPVB	PVB nanofibres
nanoPES	PES nanofibres
microPPS	PPS microfibres
microPEI	PEI microfibres
microtricot	Woven polyamide 6 (tricot) microfibres
microPPSnanoPA6,6	PPS microfibres and PA6,6 nanofibres
microPEInanoPA6,6	PEI microfibres and PA6,6 nanofibres
microtricotnanoPA6,6	tricot microfibres and PA6,6 nanofibres

Composite specimen names

Sample no	Abbreviation or interleaving type	Details
1	control	carbon fibre reinforced epoxy composite (CFRP) control, no interleaving
2	nanoNyplex	CFRP interleaved with Nyplex nanofibres
3	nanoPMMA	CFRP interleaved with PMMA nanofibres
4	nanoPA6,6	CFRP interleaved with PA6,6 nanofibres
5	nanoPVB	CFRP interleaved with PVB nanofibres
12	nanoPES	CFRP interleaved with PES nanofibres
6	microPPS	CFRP interleaved with PPS microfibres
7	microPEI	CFRP interleaved with PEI microfibres
8	microtricot	CFRP interleaved with tricot microfibres
9	microPPSnanoPA6,6	CFRP interleaved with PPS microfibres and PA6,6 nanofibres
10	microPEInanoPA6,6	CFRP interleaved with PEI microfibres and PA6,6 nanofibres
11	microtricotnanoPA6,6	CFRP interleaved with tricot microfibres and PA6,6 nanofibres

Miscellaneous:

Abbreviation	meaning
CAI	compression after impact
rpm	revolutions per minute
SEM	scanning electron microscope

Chapter 1

Introduction

The research covered in this thesis aimed to assess the use of nanofibre and microfibre veils in carbon fibre reinforced composite laminates to improve damage resistance during fatigue loading and impact, as well as improve damping performance. The work for this thesis was carried out at Revolution Fibres Ltd in Auckland, New Zealand and at the University of Waikato in Hamilton, New Zealand, from March 2014 to June 2015.

During this investigation, a range of thermoplastic polymer solutions that could potentially be used for the electrospinning of polymer nanofibre veils were developed and trialled. Two nanofibre veils previously not spun at Revolution Fibres were successfully produced during this solution development phase. These veils, along with three other nanofibre veils (manufactured at Revolution Fibres Ltd), three microfibre veils (bought from other manufacturers) and three nanofibre/microfibre combination veils were then incorporated between lamina (interleavings) in carbon fibre reinforced epoxy composite panels. These panels were converted into test specimens for evaluation of the performance of the veils as a method of energy dissipation and increasing toughening to resist damage in carbon fibre reinforced composites. Fatigue testing, vibration damping testing and compression after impact testing was undertaken to understand how the veils influenced the behaviour of the composites.

1.1 Veil production

The best method for production of fibre veils depends on the scale of fibre desired, specifically, whether nanofibres or microfibres are desired. Nanofibres are loosely classified as fibres that have a diameter of up to 1000 nm, whereas microfibres are classified as fibres that have a diameter larger than 1000 nm. Due to their small diameter, nanofibres have a high surface area to volume ratio, which makes them attractive for many applications, such as fibre reinforcement in nanocomposites, interleaves in fibre reinforced composite materials, membranes for filtration and scaffolds for tissue engineering [1]. Methods such as self assembly and phase

separation can be used to produce nanofibres, however, electrospinning has been identified as the easiest and most efficient method [2]. Electrospinning can also be used to produce polymer microfibres, but other conventional mechanical methods (such as melt spinning) are more efficient [3].

1.1.1   Electrospun fibre production

Electrospun nanofibres generally form nonwoven randomly aligned (or aligned) veils that have high porosity [3]. Alignment of the fibres can be bought about during production by using various methods, such as electrospinning on a rotating drum or spinning on an edge of a rotating wheel [4].
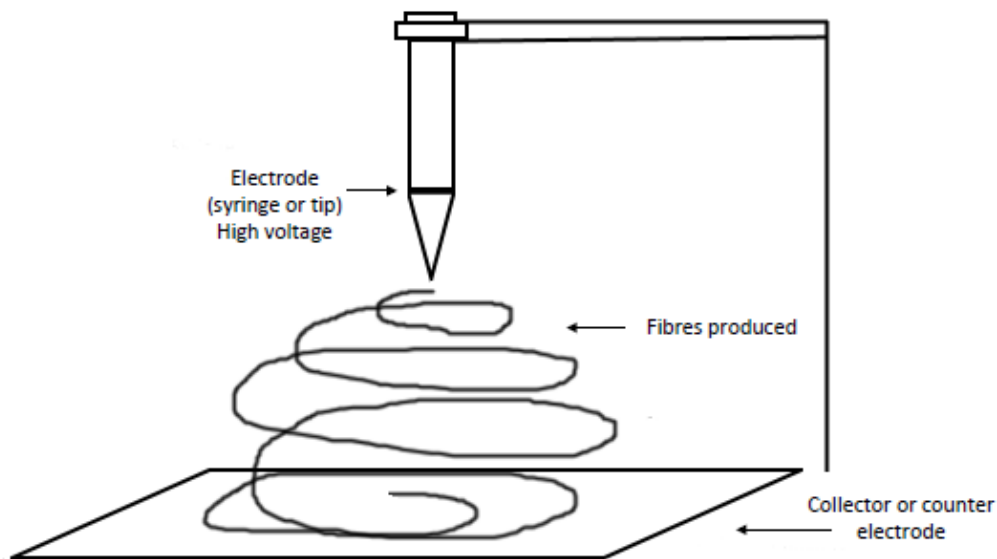
Figure 1.1: Simple electrospinning system schematic.

The basic requirements for electrospinning are shown schematically in Figure 1.1. The electrode contains an electrospinning solution, commonly delivered by a syringe. The solution to be spun is often a polymer which is dissolved in a solvent or solvent mixture, or could be a polymer melt. The electrode is usually charged to a large voltage, for example +30 kV, and the collector (also referred to as the 'counter electrode') is charged to a large oppositely charged voltage, for example - 10 kV.

The electrospinning process starts at the electrode, where the solution deforms due to the electrostatic force produced by the potential difference between the electrode and the collector (which overcomes the surface tension of the solution)

2

and forms a Taylor cone at the tip of the electrode. This results in a jet (thin stream of solution) which accelerates due to the oppositely charged collector plate after a threshold (potential) voltage has been met. The jet can 'spiral' toward the collector due to bending instabilities before depositing on the collector plate, as seen in Figure 1.2. This is often referred to by some researchers as 'whipping motion'. The jet is prevented from breaking up by the entanglement by its polymer chains [5].
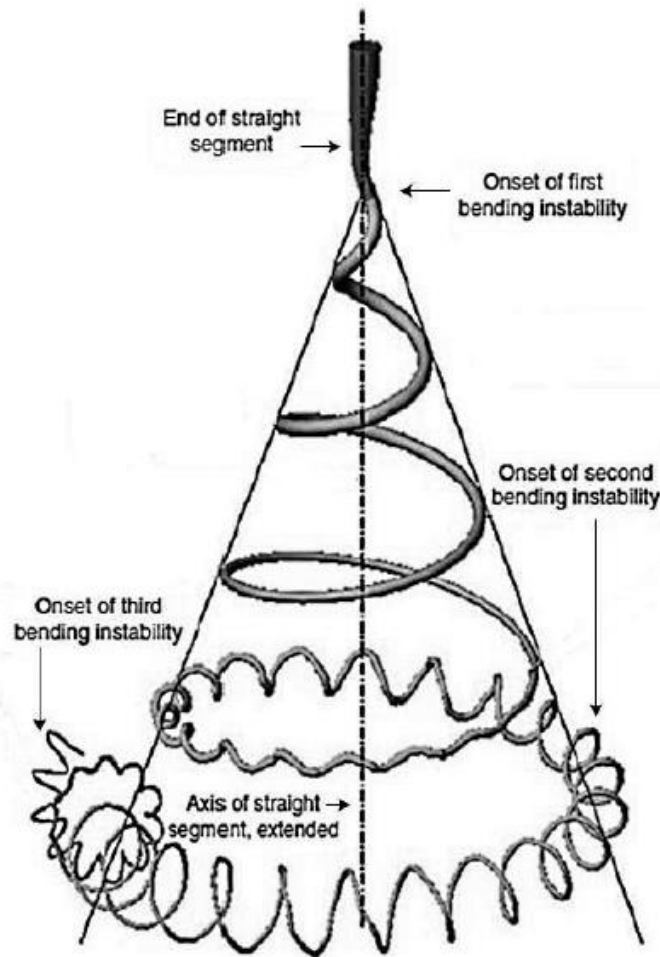
Figure 1.2: Bending instabilities in a jet (reprinted from [6] with permission).

The solvent usually evaporates during the drawing and bending of the jet from the tip to the collector plate, leaving only the polymer in a fibre form deposited on the collector. However, in some cases not all the solvent will evaporate from some electrospinning solutions, leaving the deposited fibres 'wet'; the evaporation of the solvent depends on the vapour pressure of the solvent used. The volatility of the solvent used can also affect the porosity of the fibres and the surface roughness of the fibres [7].

3

For a simple laboratory system consisting of an electrode fed by a syringe with a charged collector plate (see Figure 1.1), the ranges for constant electrospinning have been found to be:

- distance between electrodes: 8-25 cm (see Figure 1.1),
- electrode +10-30 kV, collector -10-30 kV,
- current: up to 10 mA [3].

High voltage generators in which the current and voltage can be varied are generally used in laboratory scale equipment. A substrate such as wax paper or aluminium foil can be used to cover the collector and make removal of the fibres easier.

1.1.2 History of electrospinning

Electrospinning started with the investigation of liquid deformation under the influence of electric fields. Bose (1745) investigated the spraying of aerosols using electrical potential and Lord Raleigh (1885) investigated the amount of charge needed to deform a droplet. In 1902 and 1903, Cooley and Moore filed patents detailing the apparatus used for spraying liquids by use of electrical charge [3]. The first patent for the electrospinning of plastics was made in 1937 by Formhals [3]. This patent outlined the process of electrospinning some polymers and several electrospinning setups.

During the period between 1937 and 1971, there was very little interest in electrospinning and its potential applications. In the 1970s, research was undertaken investigating the electrospinning of polymer melts [3]. Interest in electrospinning and the applications of nanomaterials grew dramatically throughout the 1990s. In 2010 alone, nearly 2000 publications were issued on electrospinning [3].

1.1.3 Electrospinning equipment parameters

Altering the electrospinning equipment parameters and solution parameters (if using a solution involving a polymer and solvent) has been found to influence the production rate, fibre diameter, fibre morphology and the ability of the polymer to electrospin.

Increasing the potential difference between the collector and the electrode has been shown to decrease the fibre diameter [1], as well as increase the number of Taylor cones and thus produce more fibres. The distance between the electrode and the collector has been shown to influence the quality of the fibre. Beads are where a uniform fibre is interrupted by a small spherical or elliptical 'beads' on the fibre (see Figure 1.3) and can be considered as a flaw in the fibre. An optimum distance can result in fibres without beads [1].

Vac-High   PC-Std.   10 kV   x 400 ———— 50 µm   002786
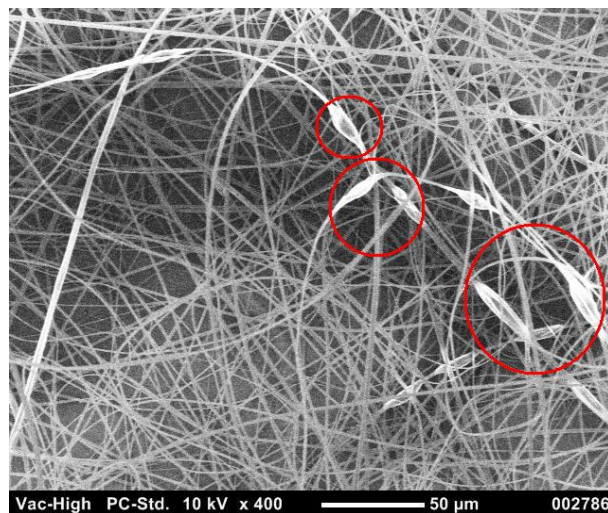
Figure 1.3: Beading on fibres shown in an SEM image (from the results of this research).

The distance between the electrode and the collector is also known to influence whether there is sparking between them. Sparking occurs when the breakdown voltage of the solvent and air mixture between the collector and electrode is exceeded. Smaller distances between the electrode and counter electrode increase the risk of sparking, as the breakdown voltage needed to cause dielectric breakdown of the air and solvent mixture can be met or exceeded by the potential voltage of the electrodes, causing a discharge. Sparking can be dangerous, particularly if flammable solvents are present.

The temperature and humidity have been found to influence how well a polymer will electrospin. These factors influence the rate at which the solvent evaporates, hence whether the fibres land wet or dry on the collector (or substrate). It has been found to be detrimental to the quality of the fibre mat if the solvent evaporates too quickly or too slowly. In a study by Kim *et al.* [8], the humidity was also found to influence the fibre diameter of polystyrene nanofibres. The diameter of the

nanofibres was found to increase as the humidity was increased. For some polymers, however, the opposite effect has been documented. In thesis research by Golin [9], a higher relative humidity was found to result in a decrease in fibre diameter of nanofibres.

The feeding rate of the solution also influences electrospinning. The solution feed rate must be equal to or greater than the amount of solution drawn off by the formation of fibres. When the feed rate is insufficient, interruption of the spinning occurs [10]. However, small variations in the feeding rate of the solution has been found to have no effect on the diameter of the fibres produced [11].

1.1.4 Electrospinning solutions

The solution parameters relating to the polymer, solvent and their interaction have been found to influence the electrospinning of solutions and affect the fibres produced.

In research to date, a large range of polymer nanofibres have been spun, such as PMMA, polyvinylidene fluoride (PVDF), PA6,6, PES, PVB, and polycaprolactone. Most polymers can be electrospun, however, in order to do so, the polymer must have a sufficiently high molecular weight, i.e. chain length [5].

In general, the higher the concentration of the polymer in the solution, the higher the viscosity of the solution, and the larger diameter of the fibres produced [1]. For fibre formation to occur in electrospinning, a minimum solution concentration is required, below which a mixture of beads and fibres are obtained. As the solution concentration increases, the shape of the beads change from spherical to flat, and finally uniform fibres are formed [1].

In a study by Pattamaprom *et al.* [12] to assess the influence of solvent properties, it was found that polystyrene solutions that used solvents such as dimethyl formamide (DMF) with higher dipole moments (due to carbonyl and nitrogen groups with free electrons) had a higher chance of being able to electrospin. It was also found that polystyrene solutions using solvents with high viscosity were more difficult to electrospin.

Solubility has also been found to affect the ability of a solution to electrospin. Solutions formed from solvents in which polymers fully dissolve have been found to not electrospin as well as solutions formed from solvents that only partially dissolve the polymer [13].

Solvents with a with high volatility can result in clogged electrode tips, and decrease productivity [7]. This is because the solvent evaporates and leaves the polymer on the tips (see Figure 1.1), causing blocking of the syringes. To alleviate this, solvents with a lower vapour pressure are used or the electrode tips are cleaned regularly during production. Solvents with a vapour pressure that is too low are also undesirable, as nanofibres can land too 'wet' (i.e. retain too much solvent) and combine together to produce a film instead. The ideal vapour pressure range for solvents has been found to be approximately 2.0-59.0 Torr for machines at Revolution Fibres Ltd.

The conductivity of the electrospinning solution has been found to affect stretching of the fluid jet and whipping motion during spinning [3]. The higher the conductivity, the more stretched the jet becomes, which results in fibres with a smaller diameter [1]. The stability of the jet or amount of whipping motion has also been found to depend on the solvent used and the voltage used. Increased voltage with a strongly conductive solvent results in an unstable jet, whereas increased voltage with solvents with low conductivity result in stable liquid jets [14].

Successful electrospinning can also be dependent on the dielectric constant of the solution. According to Wendorff, *et al.* [3], a spinning solution should have a dielectric constant of between 15 and 90, which largely depends on the choice of solvent to dissolve the polymer. Non-polar solvents have low dielectric constants, whereas polar solvents have medium to high dielectric constants [15]. The dielectric constant of the solution has also been found to have an effect on the diameter of the fibres produced. In a study by Luo, *et al.* [13], a direct correlation was found between the dielectric constant of the solvent used and the nanofibre diameters produced. In further research by Luo *et al.* [16] it was found that by increasing the dielectric constant of the solvent mixture, the required applied voltage to achieve stable jetting increased, the frequency of bead-on-string

morphology decreased, and the amount of space between the fibres increased without affecting the rate fibres were spun.

1.1.4.1 Electrospinning additives

Many additives can be used in electrospinning to alter solution properties or to functionalise the nanofibre product.

Sodium dodecyl sulfate (SDS) and lithium chloride (LiCl) are two solution additives which are commonly used in electrospinning. LiCl is a soluble salt used to increase the conductivity of an electrospinning solution, whereas SDS, an anionic surfactant, is commonly used to alter the surface tension of electrospinning solutions [7]. SDS has also been found to affect the fibres produced. In a study by Wu *et al.* [17], it was found that adding SDS to a cellulose acetate electrospinning solution prevented bead production. However, adding either cetyltrimethyl ammonium bromide (cationic surfactant) or Triton X-100 (non ionic surfactant) had no effect on bead production.

Functional nanofibres can be made by using fibre additives. Fibre additives are added to the spinning solution before spinning, and become part of the fibre after spinning. $AgNO_3$ is used as a fibre additive as it can photo-degrade to produce silver nanoparticles which become part of the electrospun nanofibre. Nanofibres with silver nanoparticles have been successfully used for antibacterial applications [18]. $AgNO_3$ can also used to alter the dielectric constant [19].

1.1.5 Large scale electrospinning

Production rates are a major bottleneck in the application of nanofibres [1]. To increase production rates, solution development and electrospinning variables (such as voltage, conductivity and surface tension) can be optimised. For example, higher voltages can mean that more Taylor cones and jets form, and thus more fibre can be produced. Alternatively, multiple tip electrodes or large rotating drum electrodes that produce multiple Taylor cones can be used to produce many jets to give higher yields [1].

1.1.6 Production issues

Production issues such as the lack of cohesion, 'fluffiness' of the fibre mat and 'cobwebbing' have been found to occur in past studies. Cobwebbing is where cobweb like filaments can form in an electrospinning machine due to fibres that have not landed on the collector. The filaments can form between tips which eventually cause the tips to clog. At present, it is unknown what causes cobwebbing. Lack of cohesion of fibres can mean the mat produced is too easy to pull apart.

Nanofibre mats can have different degrees of 'fluffiness' or 'loftiness' (some researchers also use the terms packing density or solidity [20]). In laboratory studies it has been found that the surface resistivity of the nanofibres influences the apparent fluffiness of the nanofibre mats. In a study by Cai [21], a 'fluffy nanofibrous scaffold' and a 'flat nanofibrous membrane' of zein and poly(ethylene glycol) were manufactured by altering the surface resistivity of the fibre using additives. The addition of sodium dodecyl sulfate lowered the surface resistivity of the fibres and resulted in a 'fluffy fibrous scaffold' while those with higher resistivity (no additive) formed a 'flat' membrane. It was thought that the addition of SDS converted the polymer from an insulator to a semi conductor, which increased the ability of the polymer to transfer static electricity, resulting in a 'fluffy' mat.

1.1.7 Nanofibre types

As well as polymer solutions, ceramics and melted polymer can also be spun, however the processes for doing so differ from those described previously. Instead of using a solvent to dissolve a ceramic sample, a sol-gel suspension can be used [22]. For a melted polymer, the polymer is cooled back to the solid state between the collector and the electrode and is fully cooled on the collector [7]. This method (often called 'meltspinning') is useful in applications where no trace of solvent is desired. Polymer melt spinning was not investigated during this research as the machines at Revolution Fibres Ltd did not have the capacity.

Polymer blends can also be electrospun. Polymer blend nanofibre mats can be produced by two methods. The first method is where the two polymers can

dissolve in the same solvent to produce a solution that is able to be electrospun. The second method is where two different polymer solutions are electrospun one after the other, in order to create a layered electrospun nanofibre mat.

1.2   Solution development

Previous research in laboratories has focussed on the use of solutions that frequently contain solvents that are potentially harmful, carcinogenic or mutagenic, such as chloroform, dimethyl formamide and dichloromethane. In laboratory scale electrospinning, very small quantities of solvent are required, which minimises the risk of inhalation and absorption when using these potentially harmful solvents. However, medium to large scale operations require larger quantities of solvents, which can present a health and safety risk. For example, Revolution Fibres Ltd has the ability to produce nanofibres on a large scale, but has to rely on respirators and extraction fans to ventilate the production area. Regardless of what safety measures are in place, there is a need to investigate electrospinning solutions which avoid harmful solvents.

Often it has been found that polymer solvent solutions that are used in laboratory scale experiments do not work on the machines at Revolution Fibres Ltd. This further enforces the need to develop new electrospinning solutions. Solution development is also important in order to optimise equipment and solution parameters (detailed in Sections 1.1.3 and 1.1.4).

1.2.1   Predicting solubility

In order for a solute to be dissolved by a solvent, the intermolecular forces holding the solute together must be overcome by solvent molecules (which move between and around the solute molecules) [23]. If the intermolecular forces of the solute molecules and solvent molecules are sufficiently different, the intermolecular forces of one molecule will not be able to overcome the intermolecular forces of the other.

Partial to high solubility of a polymer in a solvent is desirable for electrospinning solutions. Polymers that dissolve easily in a solvent decrease the overall production time of the electrospinning process, however, partially soluble

polymers are also noted in the literature to electrospin more successfully [13]. A more accurate prediction of solute solubility (in this case, polymer solubility) can be made using complex solubility scales.

1.2.2 Solubility parameters

There are many different solubility scales. These include the Kauri-Butanol number, aromatic character, wax number, and Hildebrand parameter, of which the latter is the most suitable and widely applicable solubility system.

The Hildebrand solubility parameter quantitatively reflects the intermolecular interactions and is given by:

$$\delta = \sqrt{c} = (\frac{\delta H - RT}{V_m})^{1/2}$$

(1-1)

Where:
c is the cohesive energy density, which is a direct reflection on the strength of the intermolecular forces holding the molecules together,
δH is the heat of vaporisation,
R is the universal gas constant,
T is the temperature and
V_m is the molar volume.

The Hildebrand solubility parameter of a blend of solvents is determined by taking the average of the Hildebrand values of the individual solvents by volume.

Inconsistencies can arise when just using Hildebrand parameters alone, as the Hildebrand parameters do not reflect the different forces that influence the total intermolecular force. The three main types of intermolecular forces considered in solubility theories are dispersion forces, polar forces, and hydrogen bonding [23] [24].

Dispersion forces are interactions caused by temporary dipoles which provide temporary attraction to the nucleus of another molecule. Dipoles are small local charge imbalances, which give rise to a molecule with a small magnetic effect, (i.e. a molecule with equal opposite poles - a 'dipole') [23]. In general, the larger the

molecule, the greater the surface area, and the greater the number of temporary dipoles, which in turn means the greater the intermolecular attractions between molecules [23].

Polar forces refer to the interactions between molecules caused by permanent dipoles [24].

Hydrogen bonding is a type of polar interaction force which is very strong. In molecules which exhibit hydrogen bonding, the electron of hydrogen is drawn toward a more electronegative atom (such as oxygen, nitrogen or fluorine), which creates a protonic bridge, which provides strong attraction to electrons in other molecules [23]. Polar protic solvents participate in hydrogen bonding due to the O-H or N-H bond. Acids are polar protic solvents, and are a source of protons in a solution [15]. Conversely, polar aprotic solvents do not participate in hydrogen bonding and do not provide protons in a solution.

The inconsistencies seen when using the Hildebrand solubility parameter alone are due to difference in hydrogen bonding [23]. Thus multi component prediction systems (such as the Hansen parameters) can be more useful for predicting solubility.

1.2.3 Hansen parameters

Hansen parameters divide the Hildebrand parameter into three separate parameters; dispersion, polar and hydrogen bonding (see previous section). The squares of each of the Hansen parameters are added to give the square of the Hildebrand parameter (1-2). Hansen parameters are useful in that the Hildebrand parameter can be further broken down into its individual components in order to see what type of intermolecular forces are most present in the solvent or polymer that is being investigated and that the Hildebrand parameter can be calculated from the individual Hansen parameters.

$$\delta^2 = \delta_D{}^2 + \delta_P{}^2 + \delta_H{}^2 \qquad \text{(1-2)}$$

Where:

δ is the Hildebrand parameter,

δ_D is the dispersion component,

δ_P is the polar component, and

δ_H is the hydrogen bonding component.

Many different texts give values for the dispersion, polar and hydrogen bonding Hansen parameters of many different solvents and polymers. HSPiP, 'Hansen solubility parameters in practice', is a software database that provides Hansen parameters for many different materials and can predict the solubility of a solute in a large range of solvents using a 'solubility sphere' [25].

A 'solubility sphere' is a three dimensional plot in which the Hansen parameters of a solute and a range of solvents are plotted. The solubility sphere indicates solvents that would be able to dissolve the polymer. This can also be worked out without plotting the three dimensional graph, as the distance of the solvent from the middle of the polymer solubility sphere can be calculated, and must be less than the radius of interaction for the polymer [23]. The equation for this is given in (1-3):

$$D_{(S-P)} = [4(\delta_a s - \delta_a p)^2 + (\delta_p s - \delta_p p)^2 + (\delta_h s + \delta_h p)2]^{1/2} \quad \text{(1-3)}$$

Where:

$D_{(S-P)}$ is the distance between the solvent and the centre of the polymer solubility sphere,

$\delta_D s/p$ is the dispersion component for the solvent (s) or polymer (p),

$\delta_p s/p$ is the polar component for the solvent (s) or polymer (p), and

$\delta_H s/p$ is the hydrogen bonding component for the solvent (s), or polymer (p).

Hansen parameters can also be used to create a Teas diagram which can be useful in predicting and assessing solubility for polymer-solvent solutions [23]. In a study by Luo, *et al.* [13], solubility windows for polymethylsilsesquioxane were made by plotting solvent solubilities on a Teas graph, which was able to be used to select binary solvent systems for the polymer.

1.2.4 Teas diagram construction

Hansen parameters are used in the creation of the Teas graph which uses fractional parameters on each of its three axes. They are derived from the type of force over the total force, shown in equations (1-4), (1-5), (1-6) and (1-7).

$$f_d = \frac{\delta_d}{\delta_d + \delta_P + \delta_h} \tag{1-4}$$

$$f_p = \frac{\delta_p}{\delta_d + \delta_P + \delta_h} \tag{1-5}$$

$$f_h = \frac{\delta_h}{\delta_d + \delta_p + \delta_h} \tag{1-6}$$

$$f_d + f_p + f_h = 100 \tag{1-7}$$

Where: f_d, f_p and f_h are fractional Hansen parameters.

However, the Teas diagram is based on the assumption that all materials have the same Hildebrand values, which is not true. However in practice, it is a useful tool as it can be used to plot solvent locations relative to each other.
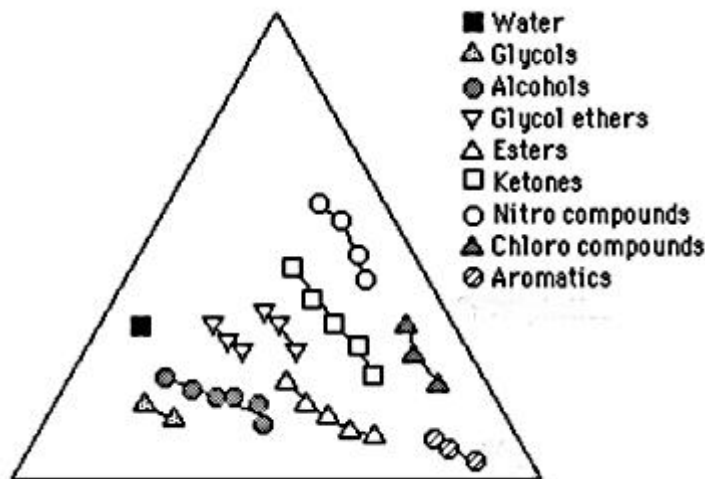
Figure 1.4: Example Teas diagram for basic solvent groups. Reprinted from [23] with permission.

14

A polymer solubility window can be created by plotting the results of experiments on the Teas graph. Small samples can be made, observed under a microscope and then plotted on the Teas graph to give an indication of what solvents the polymer could be soluble in. It can show the ideal amount of dispersion, hydrogen bonding and polar forces relative to other solvents.

1.2.5 Solubility reference data

In some cases, Hildebrand and Hansen solubility values are not available for all grades of polymers and solvents. Thus other resources are often needed. One such resource is the Chemical Resistance of Thermoplastics and Chemical Resistance of Specialty Thermoplastics series, by Woishnis and Ebnesajjad [26]. These books detail experimental trials undertaken to assess the resistance of a range of thermoplastics, including different grades of thermoplastics, in the presence of different solvents at different temperatures and concentrations. This reference text could also be used to verify solubility expectations after using Hildebrand and Hansen parameters to initially predict suitable solvents.

1.3 Similar processes to electrospinning used in industry

Similar processes to electrospinning that have been studied intensively may help the understanding and optimisation of electrospinning. Electrospraying is a functionally similar process to electrospinning and involves the spraying a liquid into a fine aerosol, via electrical repulsive forces. Electrostatic precipitators and pesticide sprayers are common examples of electrospraying processes [1].

Electrospray ionisation mass spectrometry (ESI-MS), is a laboratory application of electrospraying, which is an analytical chemistry technique used to find the composition of a particular sample. It works by transferring particles into the gas phase as ions, by spraying a solution. Many different types of solutes can be analysed, such as nucleic acids, polymers and proteins of high molecular mass [27].
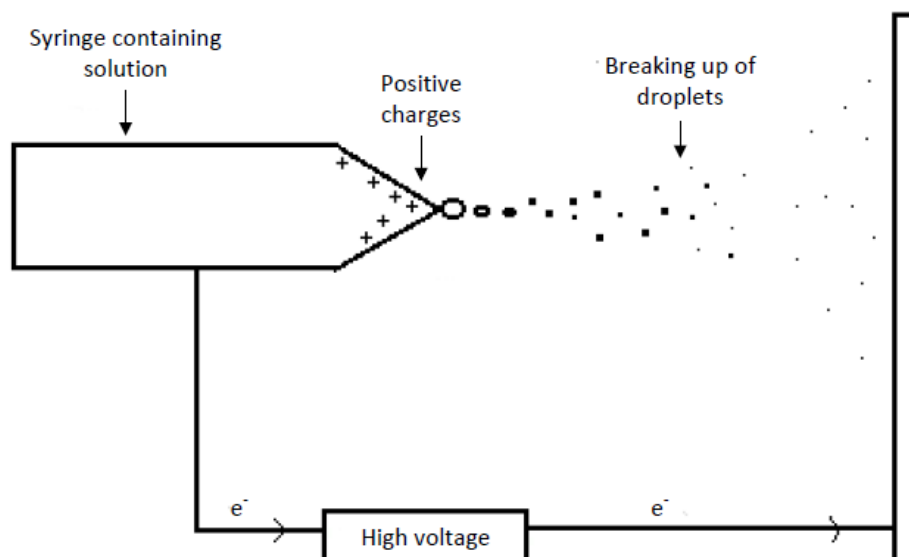
Figure 1.5: Basic schematic of electrospray ionisation mass spectrometry.

Electrospraying utilizes a charged electrode (such as a syringe containing the solution) and a collector. The charged electrode charges the droplets at the tip of the electrode and polarises the solvent, and positive and negative ions move under the influence of the high electric field at the tip. The polarisation forces create a Taylor cone which overcomes the surface tension of the solution. If the applied voltage is high enough, a jet erupts from the Taylor cone [27]. It is noted that if a positive voltage is applied the jet has positive ions at its surface. The jet then breaks up into droplets, which further break up due to solvent evaporation and increased repulsion of charges as the droplets move closer to the collector, (referred to as coulomb explosion or droplet fission) [27]. The broken up droplets result in gas phase ions [27].

Methanol, methanol/water (polar protic), acetonitrile (polar aprotic) and acetonitrile/water mixtures are often used for dissolving solutes in ESI-MS [27]. Non-polar aprotic or polar aprotic solvents can be used, however ionic additives such ammonium acetate may be required for stable spraying [27]. Ammonium acetate delivers NH_4^+ ions at the surface of the droplets formed [27]. This additive could also be used for electrospinning.

1.4 General information on composite materials

1.4.1 Overview

Composites reinforced with carbon fibre are becoming more popular in the aircraft and automotive industries and high end sports applications due to their high strengths, high stiffness to weight ratios and low density. These attributes enable these materials to be competitive in structural applications against more traditional materials such as aluminium alloys and steels, and can present advantages in fuel economy. Structures can also be built in one piece from composite materials, resulting in a substantial reduction in the number of parts needed. Boeing has stated that using composite materials for manufacturing the 787 fuselage as one-piece sections "eliminated 1,500 aluminium sheets and 40,000 - 50,000 fasteners per section" [28], which is a significant reduction in the number of parts required to assemble the structure.

For high performance applications, carbon fibre reinforced composites are commonly produced from prepreg. Carbon fibre prepreg consists of carbon fibre (either woven or unidirectional) and uncured epoxy resin in a rolled form that can be cut to size and laid up to a desired composite thickness. This is normally cured in an autoclave to form a carbon fibre reinforced laminate composite.

1.4.2 Limitations of carbon fibre reinforced composites

Although carbon fibre reinforced epoxy composites have become a viable replacement for some traditional materials, the brittleness of the epoxy resin matrix and poor delamination resistance of the composite has restricted implementation in structural components that require a high level of toughness and resistance to damage [29] [30]. In order to address these problems, methods of toughening and mechanisms of toughening need to be considered.

1.4.3 Current toughening techniques

At present, the two main methods of toughening are prepreg toughening and interlayer based toughening. Prepreg based toughening is where a thermoplastic, elastomer, nanoparticles or nanotubes are blended into the epoxy resin [31]. A thermoplastic material or elastomeric material which has a lower modulus than

the epoxy matrix is used for this approach. The thermoplastic or elastomer particles have been shown to act as 'crack stoppers'. More energy has to be used as a crack has to move around the particle to propagate [30]. However, the distribution of particles in the matrix can be uneven, resulting in agglomerations of particles which can cause stress concentrations and a reduction in strength [30]. Particles can also increase the laminate thickness (sometimes by around 20 %) and decrease in plane stiffness and strength [32].

Interlayer toughening is where a layer is placed between all or some plies in a laminate composite. Polymeric films, nanofibre veils and microfibre veils have all been investigated for use as interlayers (or interleavings) in previous research. Polymeric film interlayers have been found to prevent a crack from propagating from one ply to the next in a laminate composite. However, films can block resin flow and are impossible to use in liquid moulding [30]. Poor adhesion can also occur between the resin and the film [30].

Microfibres veils have been investigated for use as interlayers and have the advantage of being highly porous, resulting in little decrease in resin flow during curing. However, some microfibre veils can cause an undesirable increase in the weight and thickness of a composite [33]. Nanofibre veils however have been particularly attractive for researchers as they are also highly porous, and have a higher surface area to volume ratio than either films or microfibres. They also do not add a significant increase in the weight of the composite, even though the nanofibres have a high surface area, and are small enough to reinforce regions of the matrix located in between adjacent laminate plies [34]. In a study by Tsotsis [30], it was found that the compression after impact strengths of composite laminates were improved with the addition of microfibre interleaving veils, particularly if the diameter of the veil fibres was decreased.

It has been found previous research that nanofibres provide better toughening than films. In a study by Magniez, *et al.* [29], it was found that composites interleaved with polyvinylidene fluoride (PVDF) nanofibres were more resistant to crack propagation than composites interleaved with PVDF films. However, both composites were found to be less resistant to crack propagation to the control composite. It was established that the adhesion between the PVDF and the epoxy

was favourable, however the shear strength of the films was thought to be too poor. On the other hand, it was discovered that the nanofibre interleaved samples showed complex changes in the micromechanisms of failure, and the crack path moved from the mid section of the nanofibre interlayer to the resin/interlayer interface.

Nanofibres have been found to either phase separate or remain intact during the curing of the composite panel. A nanofibre with a lower melting temperature than the processing temperature of the composite would be likely to phase separate during curing. Some studies have found that nanofibres which phase separate to form particles provide enhanced mode I interlaminar fracture toughness than nanofibres that stayed intact during curing [35].

However, it would be expected that an interlayer based toughening method (such as nanofibre interlayers) would provide better toughening than matrix based particulate reinforcement methods (such as adding particles to the epoxy resin or the formation of particles in the resin by phase separation). Particulate reinforcement methods can only arrest the formation and propagation of cracks in the matrix by crack bowing and crack deflection. Crack bowing is where a crack can become blunt as it bows between two particles. Crack deflection is where a crack has to move around an obstacle such as a particle in order to propagate, which increases the amount of energy required to propagate the crack.

Fibre reinforcement methods can also use these two energy absorption methods, as well as fibre bridging, debonding and fibre pull out; hence the increased amount of energy absorption methods available make it more likely that better toughening would be achieved with fibre reinforcement rather than particulate reinforcement. Fibre bridging is where a crack tip is 'bridged' i.e. the sides of a crack are connected by a fibre, which usually happens before either fibre pull out or debonding. Debonding is where a crack has to break the bond between a fibre and the matrix before propagation can progress, which ensures that more energy is required in order for a crack to propagate. Fibre pull out is where fibres debond and pull out of the matrix during crack growth.

1.4.4 Fibre-matrix interface

The strength of the fibre-matrix interface depends on the degree of adhesion between the fibre and the matrix and can influence the amount of energy absorption for mechanisms such as fibre debonding. However, the adhesion first relies on the ability of the matrix material to 'wet' the fibre (related to the compatibility of both materials) or come into close contact with the fibre [36]. For carbon fibre reinforced epoxy composites (as tested in this study) wetting occurs during the curing of the composites when the epoxy matrix is capable of flowing around the carbon fibres and interleaving fibres.

The degree of adhesion between the fibres also depends on the following mechanisms:

- Mechanical: where the two surfaces can bond through interlocking of one surface on another, i.e. a rougher surface can have a better mechanical bond than a smooth surface.
- Chemical: chemical bonding can occur when the chemical groups of one material interact and are compatible with the chemical groups of the other material [36]. Often materials with polar groups such as -COOH, -OH and -NH$_2$ on the surface provide better adhesion with glues, because of the chemical reaction of the polar groups on the adhesive and the polar groups on the surface of the material [37].
- Electrostatic: bonding that occurs when one material surface is positively charged and one surface is negatively charged, which results in electrostatic attraction between them [36].
- Interdiffusion: where the molecules of two materials can entangle or react at the surface [36]. The intertwining of polymer chains at an interface of two polymeric surfaces is an example of interdiffusion.

In general, the main fibre reinforcements in composite materials that are strongly bonded to the matrix allow the load applied to the matrix to be transferred to the fibres [36]. A weak interfacial bond between fibre and matrix can result in a low stiffness and strength and high resistance to fracture, however an interfacial bond that is too strong can result in a low resistance to fracture and brittle behaviour, but high stiffness and strength [36].

The adhesion strength between the interleaving materials or other methods of toughening would also be important. In a study by Kaynak *et al.* [38], the affect of the strength of the interface between rubber particles and epoxy matrices on the mechanical properties was investigated. In this study it was discussed that the degree of adhesion between toughening phases (such as particles, interleaving fibres and other methods) and epoxy matrices is critical in governing the extent of toughening achieved, and suggested that an optimum intermediate level of adhesion between the phases would be required for optimum toughening. It was found that the use of silane coupling agents could be used to govern the amount of adhesion between the rubber particles and the epoxy, however although an increase in the tensile strength and modulus was obtained using rubber particles that were treated with coupling agents, the fracture toughness was not affected appreciably. It was envisaged however that with the use of a better coupling agent or surface treatment of the rubber particles, the fracture toughness would be improved.

1.5 Vibration damping

1.5.1 Overview

Micro-cracks in materials can propagate through the material because of fatigue caused by vibrations [39], therefore improvements in the vibration damping performance of composites can be of advantage, especially in military and aerospace applications, where the material is likely to be subjected to severe vibrations during service.

1.5.2 Testing

The ability of material to damp vibration can be investigated and analysed using a dynamic mechanical analysis (DMA) tester or a vibration test rig such as the one outlined in ASTM method E756, 2010.

During DMA testing, a sinusoidal load is applied to the sample and the strain response is measured [40]. The strain response is then translated by analysis software in order to obtain the storage modulus, loss modulus, and tan delta of the sample (detailed in Section 1.5.3). The strain response can be measured over a range of temperatures or frequencies. Specimens can be cooled with liquid nitrogen or heated in a furnace to obtain the desired range of temperatures. The frequency range is usually limited to 0-100 Hz (depending on machine).

During vibration rig testing, (outlined in ASTM E756), the test specimen is placed inside an environmental chamber and an excitation force to vibrate the beam is applied by a transducer. The vibration response of the beam is measured by another transducer. As for DMA, damping data can be obtained over a range of frequencies and temperatures. Although the ASTM method is more accurate [41] [40], the DMA tester was used in this study, as it is able to generate useful data more quickly, without requiring a large amount of user input [40], [42], requires smaller samples and was available in-house.

Since the DMA uses very small sample sizes, factors such as friction between sample and fixture clamps, and the fixture type can have a large influence on damping data [42]. There were six main types of clamping options (for the tester available):

- single cantilever (is recommended for polymeric specimens with a Young's modulus between 10^6 to 10^{10} Pa),

- double cantilever (is recommended for low stiffness specimens),

- tension (usually used for analysis of films and fibres),

- compression (usually used for foams, gels and food samples),

- shear (usually used for low stiffness samples) and

- three point bending (recommended for high stiffness specimens (with a Young's modulus between 10^8 to 10^{12} Pa), such as composites and cured thermosets) [43].

Specimens tested using three point bending are not held in place and are free to move, whereas specimens tested using cantilever fixtures are clamped at the ends of the specimen, which can increase shearing. It has been found that data measured using dual cantilever can be 10-30% different compared to data measured with three point bending, using the same material [44].

1.5.3 DMA damping theory

As outlined previously, analysis is carried out by applying a sinusoidal stress to a sample, and then measuring the sample's response to the stress. Vibration damping analysis is really measuring the materials ability to lose energy. A bouncing ball is a simple example or analogy for this concept [44]. The ball has energy when it is released and loses energy when it bounces. Some energy is stored as it bounces back but not enough to achieve the same height. The loss of energy is its damping ability (given by a ratio of the storage and loss modulus).

When a sample is subjected to a sinisoidal stress (σ), the resulting strain the sample is also sinuisoidal and lags behind the applied stress by phase angle δ [45] (see Figure 1.6).
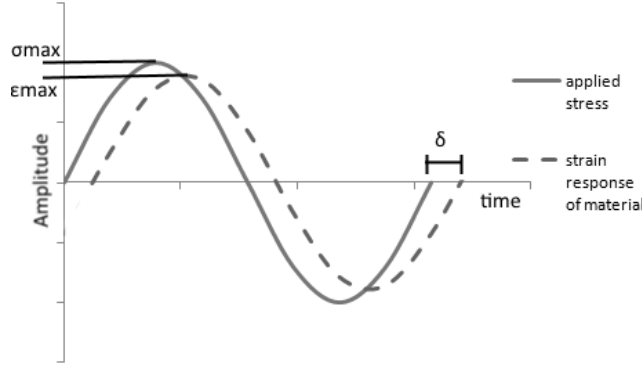
Figure 1.6: Applied stress and strain response of material.

The applied stress and the strain response can be written as:

$$\sigma(t) = \sigma_{max}e^{i(\omega t + \delta)} \tag{1-8}$$

$$\varepsilon(t) = \varepsilon_{max}\,e^{i\omega t} \tag{1-9}$$

where σ_{max} is the maximum stress, ε_{max} is the maximum strain, ω is the frequency of the applied stress, and t is the time.

The complex modulus (E^*) can be calculated by:

$$E^* = \frac{\sigma_{max}}{\varepsilon_{max}}e^{i\delta} \tag{1-10}$$

where δ is the phase lag shown in Figure 1.6.

The equation can also be written as:

$$E^* = \frac{\sigma_{max}}{\varepsilon_{max}}(\cos\delta + i\sin\delta) \tag{1-11}$$

and:

$$E^* = E'\cos\delta + iE''\sin\delta \tag{1-12}$$

E' and E'' are the real and imaginary parts of the complex modulus. E' is also referred to as the storage modulus and E'' is referred to as the loss modulus. Tan(δ) is the ratio of the loss modulus to the storage modulus of the sample [45].

Tan(δ) (also called the damping ratio) of the sample is given by:

$$tan(\delta) = E''/E' \tag{1-13}$$

24

1.5.4 Effect of toughening techniques on the vibration damping properties of composite materials

It has been found that many factors affect the vibration damping characteristics of carbon fibre reinforced composites. The direction of the reinforcing fibre in particular can significantly affect the damping properties of carbon fibre composites [41], but matrix modifications, such as polymer or rubber additives have also provided improvements in damping performance.

The addition of nanotubes into a matrix has been shown to have a positive effect on the vibration damping performance. A study by Tehrani *et al.* [46] showed that composite samples containing multi-walled carbon nanotubes had higher damping properties than composites without multi-walled nanotubes, which indicated a greater capability to dissipate energy and lose energy during impact. This was thought to be because energy could be dissipated by friction due to sliding at the interface of the nanotubes and matrix [46].

A study by Khan*, et al.* [39] showed that adding carbon nanotubes to the composite resulted in a higher dynamic loss modulus and loss factor, indicating higher damping performance when carbon nanotubes were added. This was also thought to be due to sliding of the carbon nanotubes within the matrix, resulting in friction and energy dissipation.

In another study by Palazzetti *et al.* [47], the impact resistance of carbon fibre reinforced composites with Nylon 6,6 nanofibres as interleavings in two different configurations was investigated. In this study, the samples were subjected to a range of tests, including static and dynamic tests before and after impact. Results from these tests showed that interaction between the resin and the nanofibre was an important factor in the reinforcement effect, and when the specimens were undamaged, the friction between the nylon nanofibres and the resin increased the amount of friction in the interleaved samples compared to the non-interleaved samples. This meant that the damping ability of the nanomodified specimens was higher compared to the specimens without interleaving. After the specimens were damaged, it was found that the nanofibres increased the damage tolerance of the

laminates compared to the non-interleaved samples, through the presence of the fibre bridging reinforcement mechanism.

In a study by Tehrani *et al.* [48], carbon nanotubes were grown on carbon fibres by a low temperature synthesis technique. These were used to create a carbon fibre carbon nanotube hybrid epoxy composite, which was then evaluated for damping performance using dynamic mechanical analysis. The results from this study showed that the addition of the carbon nanotubes decreased the storage modulus slightly, but increased the damping (tan delta) by approximately 56% compared to the reference samples with no carbon nanotubes or surface treatment.

In a study by Miller [42], the damping performance of an epoxy matrix with dispersed nanoparticles and an epoxy matrix with nanoparticles applied as a coating were evaluated by DMA. Since variation up to 50 percent was found in the results gathered, an increase of 50 percent or higher to be considered as significant. It was found that the nanoparticle dispersion composites did not lead to a greater than 50 percent increase in the damping compared to the control samples with no nanoparticles. However, it was found that the coated composites showed an improvement higher than 50 percent.

In another study, by Rajoria and Jalili [49], the damping performance of carbon fibre reinforced composites toughened with carbon nanotubes was investigated. The study suggested that the increase in damping could be due to energy dissipation via debonding and slippage of the nanotubes. It was thought that this movement occured when a critical tensile load was applied. It was identified in this study that the adhesion (or 'stick') between the epoxy matrix and the nanotubes dictated the extent of the damping performance. If the nanotubes were bonded well to the matrix then an increase in stiffness and natural frequency was found. If the adhesion was poor, there was more movement of the nanotubes in the epoxy matrix, resulting in higher damping, but a slight decrease in stiffness composite, as the load was not transferred to the nanotubes.

1.6 Compression after impact

1.6.1 Overview

Compression after impact testing is a two part test. The first part of the test involves impacting the sample with a single impact, bringing about damage in the sample. For the second part of the test, the sample is placed in a specially designed jig to avoid buckling and compressed until failure in order to measure the residual strength of the composite. The residual strength of the composite relates to the impact resistance of the specimen and the damage tolerance of the specimen during compression [50].

This test is an important test for composite materials that are to be used in applications where an impact event is likely, and where the composite must still retain a level of strength after the impact event. After an impact event, composites can show very little damage that can be detected visually, however, in actual fact, inside the composite structure, significant damage can occur which can cause severe reductions in strength and stability [51]. Laminated composites have been found to be more susceptible than metallic structures to the severe reduction in strength after an impact event. Small stones flicked up by aircraft tyres during takeoff and landing are an example of real life impact events. Stones are considered a ballistic type of impact due to the speeds the stones can travel at. Heavy tools dropped on composite panels of aircraft also provide another type of impact, even though the velocity is much lower.

Low velocity impacts initiate damage by producing small cracks inside the matrix material, which during service can create delaminations at the interfaces between plies with different fibre orientations [51]. Impact damage on stiff structures can cause cracks on the impacted face, which propagate downward through the sample, producing a 'pine tree' shape of damage created by intra ply cracks and interface delaminations. Thin specimens can experience bending the lowest ply, creating a 'reverse pine tree' shape of damage in the specimen.

The amount of damage brought about by the initial impact is crucial to the CAI strength of the composite. This is because the impact produces cracks and delaminations in the matrix, which during compressive loading, brings about

localised buckling of the plies and delamination growth. This is eventually followed by final failure which occurs by buckling of the composite in the impact region because the load bearing capacity of the composite is reduced by the damage accumulated [51]. In general, the lower energy impact, then the smaller the delamination areas and the higher the residual strength of the composite [51].

Thermoplastic matrices have been found to be more damage tolerant compared to thermoset matrices, as when subjected to the same impact, the damage region is far smaller for a thermoplastic matrix composite than thermoset matrix composite [51]. Toughened thermoset matrix composites have been shown to have less induced damage than untoughened thermoset matrix composites for a given impact energy. Laminates without resin toughening have the tendency to have low resistance to transverse stresses particularly at the interfaces of plies with different orientations, which leads to delamination and localised buckling of plies [51]. Toughening helps to arrest crack propagation particularly in the transverse direction [51].

The matrix material, the fibres, the strength of the bond between the main reinforcing fibres and the matrix and the layup sequence also affect the CAI strength [51]. Manufacturing defects, such as voids and fibre misalignment also can affect the CAI strength. Voids produce stress concentrations when under compressive loads and bring about premature buckling of the plies, resulting in a low CAI strength. Since the $0°$ plies are the primary load bearers during a compression test, any misalignment of the plies in this fibre direction would also bring about premature buckling and result in a low CAI strength. Thus, it is important that all care is taken during manufacture to avoid such flaws, and it is recommended to use an ultrasonic inspection method (such as C scanning) before testing to check for defects.

1.6.2 Testing

There are many different ways in which to simulate an impact phenomenon. In aerospace industry, small high velocity projectiles, such as stones impacting an aircraft panel, are often simulated by using a gas gun firing a small projectile of known mass, velocity, and energy. Lower velocity impacts such as heavy tools dropping onto a composite panel are often simulated by using a weight dropped

from a height, using an impact rig. A large mass with low velocity is known not have the same energy as a small mass with high velocity [51]. With so many different methods of simulating an impact event, it is hard to compare results between researchers. As a result, many different standards have been established by authorities such as ASTM and aircraft manufacturers such as Boeing and Airbus. The ASTM method D7137/D7137M for compression after impact testing used in this project is similar to the test method used by Boeing, and uses a similar impact rig and compression after impact jig.

This method of testing involves holding the sample in a specially designed impact rig, where the specimen is subjected to an impact event of enough energy to bring about damage in the specimen. The specimens are then measured for dent depth and then are compression tested in a specially designed jig, using a universal testing machine. The jig is designed to prevent failure through buckling by supporting the sample with anti buckling guides, which encourage failure by pure compression, in order to give an accurate idea of residual compressive strength after the impact event.

The drawback of this test, however, is it requires large test pieces and thus is expensive for researchers to perform. As a result, there have been many studies using smaller and thinner samples. One such study done in Japan, using a specimen size of 50 mm by 80 mm, rather than the sample size of 100 mm by 150 mm recommended by Boeing, has shown a high degree of correlation between the small scale specimens and the larger Boeing test specimens [50]. However, when using smaller samples it needs to be taken into account that the damage can saturate the sample at relatively low impact energies, meaning the damage zone can take up the entire sample, therefore making it hard to compare the extent of the damage zones between samples.

1.6.3 Effect of toughening techniques on the compression after impact properties of composite materials.

Previous research has shown that many different types of interleaving methods are capable of improving the compression after impact properties of carbon fibre composites. An in depth study by Tsotsis [30] details the effect of different

polymer microfibre interleaving in carbon fibre reinforced composites. It was shown from the initial round of test data that the CAI strengths of two microfibre interleavings, based on a polyamide based product and a ternary polymer blend, both increased the CAI strength with increasing veil interlayer weight. However, in specimens containing a polyester veil, the CAI strength decreased with increasing veil weight. C scan images of the specimens showed that the damage zone decreased when using increasing weights of both the polyamide and ternary polymer based microfibre interleaving compared to the control sample with no interleaving. However, this was not the case with the polyester based microfibre interleaving, for which the damage zone increased alongside the increasing veil weight. This was thought to be because the polyamide had a high polarity could have increased the amount of interaction with the epoxy matrix, resulting in a good bond between the polyamide fibres and the epoxy. Conversely, it was thought that since the polyester is a relatively non polar polymer, it would have interacted less with the epoxy, which would have resulted in a weaker bond between the two. It was hypothesised that when a crack encountered the interleaving, it would have taken a greater amount of energy to propagate the crack around the fibres that were well bonded to the matrix, resulting in less damage for a given impact energy for the polyamide based specimens. For the polyester interleaved specimens however, the weak bond between the interleaving fibres and the matrix material may have meant that less energy was required to propagate cracks through the matrix, resulting in an increase in the size of the damage region.

Another study by Akangah and Shivakumar [52] showed that using PA6,6 nanofibre interleavings in aerospace grade carbon fibre reinforced composites resulted in an increase in threshold impact force (the force required to initiate impact damage) of 12% and an increase in compressive strength of the samples by approximately 10%. It is noted that the interleavings had a light deposition of 0.7 g/m^2 for each interleaving, which took a production time of approximately eight hours.

In another study by Palazzetti, *et al.* [47], the impact resistance of carbon fibre reinforced composites interleaved with PA6,6 nanofibres in two different configurations was investigated. In this study, the samples were subjected to a

range of tests, including static and dynamic tests before and after impacting. It was suggested that the friction between the nylon nanofibres and the resin increased damping for the interleaved samples compared to the non-interleaved samples. The nanofibre interleaved specimens also showed less damage.

In another investigation by Shivakumar [53], the affect of polymer nanofibres on the dynamic properties and impact damage resistance was studied. It was found that the nanofibre interleavings increased the laminate thickness marginally by 3% and the damping ability of the composites with interleaving improved by 13%, which is a similar result to that found in the study by Palazzetti, *et al.* [47]. The study by Shivakumar [53] also found that the nanofibre interleaved samples had increased resistance to damage, as the damage size of interleaved samples was one-sixth the damage size of non-interleaved samples.

1.7 Fatigue

1.7.1 Overview

Fatigue failure refers to the failure of a structure under a cyclic load. Fatigue first starts in metals when a crack is initiated by a cyclic load. Under the cyclic load the crack slowly grows, until it reaches a critical size. At this critical crack size the material can fail, often at stresses lower than the stress required to bring about failure at static loads (flexural, tensile). In metals, often a ductile metal can fail in a brittle manner under excess cyclic fatigue loading. The number of cycles required in order for failure to occur depends on the stress levels, the mode of cycling, the material composition and the environmental conditions.

The overall trend between stress (or strain) and log (N) (where N is the number of cycles to failure) for metals that show a fatigue limit is the same for carbon fibre reinforced composite materials (CFRPs). CFRP materials will not fail at a stress or strain that is under the fatigue limit for any number of cycles. At high stress or strain, the material will only last for a small number of cycles before failure. At lower stresses failure will happen after a larger amount of cycles, up to the fatigue limit [54]. It is preferred to use strain rather than stress for composite materials, as the strain in a composite sample is the same throughout the sample, unlike stress, which is different for the fibre and the matrix.

The mechanisms by which a fibre reinforced composite fail under fatigue loading are more complex than for metals, and are related to damage accumulation in the sample rather than a single critical size crack propagating through the material [54]. Fibre buckling, matrix cracking, debonding, intraply cracking and delamination all contribute to the damage accumulation of a composite in fatigue loading [54]. Failure eventually occurs later in the life of the composite because the damage accumulation in a region causes the load bearing capacity to reduce to a critical level. This means the level of maximum stress the composite can bear decreases over time and the composite can fail if the fatigue stress reaches this. Fatigue tests have shown that composites fail by more than one mechanism and show a sequence of damage occurring throughout the fatigue life [54].

For unidirectional composites in particular, the fibres carry most of the load. At high stresses/strains they fail by fibre breakage, at a small number of cycles. For a medium strain level, matrix cracking can occur. Over time, more cracks can grow and couple together, leading to the initiation of other damage modes such as delamination, which leaves the reinforcing fibres unsupported. This (eventually) brings about fibre failure and failure of the overall composite. For low strains, matrix cracking between the fibres can also occur, but cracks do not grow very fast, and therefore the composite does not fail (for a chosen fatigue life) [55]. In general, for unidirectional carbon fibre reinforced epoxy composite materials, a conservative estimate of the composite fatigue limit is the epoxy fatigue limit [55].

In multidirectional laminates, the ultimate tensile fatigue failure is still determined by the unidirectional (0°) layers. However, the off-axis fibres (90° and ± 45°) are more easily damaged in fatigue, due to their mechanical properties being dependent on the matrix material [54]. Transverse cracks start to form in the 90° plies during the first cycle. Interply damage can develop between the 90° and 45° plies, which decreases the strength and stiffness of the composite. The stress concentrations at the ends of the interply cracks can initiate delamination which can leave the unidirectional load bearing fibres unsupported, leading to fibre failure and overall composite failure [54].

Thus, for both unidirectional and multidirectional laminates, fatigue performance is very dependent on the matrix material, and how easy it is for cracks to occur and propagate in the matrix. Some toughening methods aid debonding and encourage plastic deformation, which results in poorer fatigue properties [56]. However, toughening methods or processes that can increase resistance of the matrix to crack propagation are likely to improve amount of damage accumulation before failure and the number of cycles to failure of the composite [54].

1.7.2 Fatigue testing

Understanding the fatigue behaviour of a composite is important, particularly if the composite is to be used in applications where the part must withstand both vibration and cycling loads (such as helicopter rotor blades.). Vibration has the potential to cause fatigue because it has the potential to contribute to opening up cracks [39]. Although it is well known that carbon fibre composites have good

fatigue properties compared to metals, it is important that fatigue testing is undertaken, particularly if composites are to be utilised in high load situations [54].

Fatigue testing involves a simple test, usually undertaken on a servo hydraulic tester which can apply a controlled cycling load to give a constant load control, position control, or strain control. Fatigue tests are normally conducted at the highest cycling frequency possible in order to reduce the time taken to complete a fatigue test. However, if the frequency is too high, the specimen may generate too much heat which could result in reduced material properties and fatigue performance [54].

1.7.3 Effect of toughening techniques on the fatigue properties of composite materials

Some studies have been undertaken to evaluate the performance of interleaved composites compared to non interleaved composites. In a study by Phong *et al.* [57], tension-tension fatigue tests were used to evaluate the fatigue performance of interleaved and non-interleaved composites. The testing revealed that the interleaved composites had a fatigue life 10-30 times longer than non-interleaved composites. The composites consisted of an epoxy matrix with carbon fibre fabric as the reinforcing fibre. The interleaved composites contained polyvinyl alcohol nanofibres, which were directly mixed into the epoxy resin before curing rather than a layer of interleaving included during the composite layup process. This study also found that the nanofibre increased the fatigue life by delaying initiation of cracks.

In another study by Zhou *et al.* [58], the effect of modifying a satin weaved carbon fibre reinforced epoxy composite with various amounts of carbon nanofibres was investigated. It was found from this study that the tension-tension fatigue life increased with increasing amounts of carbon nanofibres, up until the amount of carbon fibre nanofibres reached 2 wt%. The resin for the composites tested was modified with the carbon nanofibres before being infused into a carbon fibre preform. It was thought that with a higher nanofibre content (above 2 wt%) the nanofibres did not disperse well, so stress concentration occurred, which

34

would have lowered the strength and the fatigue life. The increase in cycles to failure for the specimens containing less than 2 wt% was thought to be due to nanofibres providing obstacles that the crack had to move around to propagate. SEM imaging revealed that the carbon nanofibres bridged cracks and caused small cracks to change direction.

Mode I delamination fatigue is another type of fatigue test. This test was used by Hojo *et al.* [59] to investigate the delamination fatigue crack growth resistance in two different types of interleaved samples. One type of interleaving used was the T800H/3900-2 made with fine polyamide particles, which is currently used in the Boeing 777 [59]. The other type of interleaving tested was a type of thermoplastic resin (UT500/111/ionomer) film which was placed at the prepreg interface. It was chosen because of its high ductility and good adhesion strength with epoxy. The results found that the delamination fatigue crack resistance for the T800H/3900-2 interleaved samples was around three times the crack resistance of the control, which had no interleaving. The increase in the delamination fatigue crack resistance was thought to be due to the crack being deflected around the polyamide particles. UT500/111 ionomer film specimens also showed an increase in the delamination fatigue crack resistance in comparison to the control.

Chapter 2

Experimental

This section details the materials and methods used for each section of this thesis.

2.1   Solution development

2.1.1   Introduction

This section is focused on the development of solutions for various polymers not previously spun at Revolution Fibres Ltd. Solution development is extremely important as the electrospinning capability of a polymer not only depends on the polymer properties, but also the solution the polymer is dissolved in.

2.1.2   Polymer selection

Previously, Revolution Fibres Ltd has successfully produced nanofibre mats from three different polymers (PA6,6, PVB and PES). In previous studies by Revolution Fibres, it was found that interleavings of 4.5 gsm PA6,6 nanofibres gave good all round performance in mode I and mode II fracture toughness tests [33]. However, PA6,6, has the disadvantage of having high water absorption, which is not desirable for use in composite interleavings, although it is noted that minimal PA6,6 would be included in the composite when used as an interleaving nanofibre veil.

Thus a broader range of polymers was chosen for this research. Polymers with a low melting point were avoided, as it would be more likely that toughening would be obtained with polymer nanofibres that would retain their fibrous structure within the composite, due to the increased number of energy absorption mechanisms associated with fibre reinforcement compared to particle reinforcement (such as debonding, fibre pull-out, and fibre bridging, as discussed in Section 1.4.3). Therefore polymers with low moisture absorption and a melting temperature greater than the processing temperature of the composite panels to be produced were chosen; there is no general consensus on what other properties of polymers are desirable for producing veils that would provide toughening. The

polymers chosen for this part of the study were ABS, ASA, CPVC, PC, PMMA, and three grades of PS (expanded, general purpose and high impact).

Comparison of water absorption, melting point and some mechanical properties for these polymers, along with PA6,6, PVB and PES are shown in Table 2.1.

2.1.3   Solution development – polymer and solvent solubility

The first step of solution development was to choose an appropriate solvent for each polymer, as discussed in Section 1.2. The Hansen and Hildebrand solubility parameters and the polarity for the polymers to be investigated are shown in Table 2.2. It is noted that not all data was able to be found for each polymer from the available resources. Explanation of these solubility parameters can be found in Section 1.2.2 and 1.2.3).

Table 2.1: Polymer properties.

Polymer	Melting point (°C)	Tensile Strength (MPa) ASTM D638	Young's modulus (GPa) ASTM D638	Elongation at Break (%)	Izod Impact, Notched [J/cm] ASTM D256	Charpy Impact [J/cm] ISO 179	Water Absorption - 24hrs ASTM D570, [%]
ABS	230 - 250	42	2.1	20	4.1		0.3
ASA	238 - 260	47 - 66	1.5 - 2.3	25 - 40, 6	4.9		
CPVC	395	50 - 80	2.9 - 3.4	35	4.8		0.048 - 0.08
PC	155	55–75	2 - 2.4	80–150	6 - 8.5		0.1
PMMA	160	77	2.2 - 3.2	5.5*		20	0.1 - 0.4
PS (ExPS)							
PS (GP)	210 - 220	44	3.1	<3*	0.2	2.8	0.03 - 0.05
PS (HIPS)	230 - 240	24	1.6 - 2.2	52	1.1		0.1 - 0.6
PA6,6	260	83	2.4	30	0.6		1.2
PES	345 - 390	85 - 94	2.6	6.7*, 15 - 40	0.8		0.6
PVB	160-210	56	2.4	33	0.4 - 0.6		0.3 - 0.5
* Breaking stress							
		polymers not previously spun by Revolution Fibres		polymers already spun by Revolution Fibres			

**Data for this table was sourced from Polymer: A Properties Database [60] and manufacturers technical data sheets by Revolution Fibres Ltd.

Table 2.2: Hansen and Hildebrand parameters and polarity of various polymers.

| Polymer | Hansen Parameters (MPa$^{1/2}$) | | | Hildebrand Parameter | Partial Polarity (e) |
	δD (Dispersion)	δP (Polarity)	δH (Hydrogen Bonding)	δp (MPa$^{1/2}$)	
ABS	16.3	2.7	7.1	18.0	
ABS	17.6	8.6	6.4	20.6	
Average ABS	17.0	5.7	6.8	19.3	
ASA					
CPVC	17.5	6.5	5.5	19.5	
PC	18.2	5.9	6.9	20.3	0.246
PMMA	18.1	10.5	5.1	21.5	0.281
PMMA	18.6	10.5	5.1	22.0	0.281
PMMA	18.6	10.5	7.5	22.7	0.281
PMMA	19.3	16.7	4.7	26.0	0.281
Average PMMA	18.7	12.1	5.6	23.0	0.281
PS	18.5	4.5	2.9	19.3	0.168
PS	18.0	5.0	5.0	19.3	0.168
PS	22.3	5.8	4.3	23.4	0.168
Average PS	19.6	5.1	4.1	20.7	0.168

*Data for this table is sourced from HSPiP software [25] by Revolution Fibres Ltd

Solvents were chosen based on the understanding that an appropriate solvent would be expected to have a similar Hildebrand solubility parameter and a similar partial polarity to the polymer (see Section 1.2.2 and 1.2.3). The properties of the solvents available at Revolution Fibres are shown in Table 2.3. Solvents not available or not in stock at Revolution Fibres were not considered due to the amount of time taken for most solvents and additives to be ordered and delivered.

Table 2.3: Properties of available solvents.

	Solvent	Hansen Parameters (MPa$^{1/2}$)			Hildebrand Parameter	M_w	Partial Polarity (e)	Dielectric Constant	Vapour pressure (at 25°C) Torr
		δD (Dispersion)	δP (Polarity)	δH (Hydrogen Bonding)	δs (MPa$^{1/2}$)				
Non- polar solvents	cyclohexane	16.8	0	0.2	16.8	84	0.00	2.02	97.5
	toluene	18	1.4	2	18.2	92	0.00	2.38	28.4
	xylene	17.8	1	3.1	18.1	106	0.00	2.57	6.6
	methyl ethyl ketone (MEK)	16	9	5.1	19.1	72		18.50	94.5
	chloroform	17.8	3.1	5.7	18.9	119		4.81	196.5
Polar-aprotic Solvents	n-propyl acetate (NPA)	15.8	4.8	6.7	17.8	102		6.002 - 8.0	33.7
	acetone	15.5	10.4	7	19.9	58	0.69	20.70	231.0
	dichloromethane (DCM)	17	7.3	7.1	19.8	85		2.02	436.5
	ethyl acetate	15.8	5.3	7.2	18.2	88	0.17	6.02	94.5
	n-methyl-2-pyrrolidone (NMP)	18	12.3	7.2	23.0	99		33.00	0.3
	tetrahydrofuran	16.8	5.7	8	19.5	72		7.58	162.0
	n,n-dimethyl acetamide (DMA)	16.8	11.5	9.4	22.4	87		37.80	2.0
	dimethyl sulfoxide	18.4	16.4	10.2	26.7	78		46.70	0.6
	dimethyl formamide (DMF)	17.4	13.7	11.3	24.9	73	0.77	36.70	3.3
Polar protic Solvents	acetic acid	14.5	8	13.5	21.4	60	0.30	6.20	15.5
	benzyl alcohol	18.4	6.3	13.7	23.8	108		13.5	0.1
	formic acid	14.6	10	14	22.6	46		57.90	42.6
	2-propanol (IPA)	15.8	6.1	16.4	23.6	60		18.00	45.2
	ethanol	15.8	8.8	19.4	26.5	46	0.27	24.50	59.0
	water	15.5	16	42.3	47.8	18	0.82	80.10	23.7

*Data for this table was sourced from HSPiP software [25] and other sources by Revolution Fibres Ltd.

Partial polarity values could not be found for ASA, ABS, CPVC and some solvents, and the Hansen and Hildebrand values could not be found for ASA. Instead of using these parameters, potential solvents were chosen for these polymers by using a reference text (The Chemical Resistance of Thermoplastics by Woishnis and Ebnesajjad [26]). As discussed in Section 1.2.5, this reference text details experiments undertaken on solvents and solutes, and the PDL# ratings in the book specify to what extent the solute (in this case a polymer) was able to be dissolved in the solvent. For example, a PDL# rating of 0 denoted that the polymer was able to completely dissolve in the solvent. Thus, a summary table of potential solvents for the specific polymers was able to be created and is shown in Table 2.4.

Table 2.4: Potential solvents for specific polymers.

Polymer	Potential Solvent	Solubility Rating PDL# **	Solvent Hildebrand Parameter δ_s (MPa$^{1/2}$)	Solvent Partial Polarity (e)	Polymer Hildebrand Parameter δ_p (MPa$^{1/2}$)	Polymer partial Polarity (e)
ABS	ethyl acetate	0	18.2	0.17	18	-
	n-propyl acetate	-	17.8			
	MEK	0	19.1			
	DMF	0	24.9	0.77		
	o-xylene	0	18.1	0		
	toluene	0	18.2	0		
ASA	benzyl alcohol	0: dissolves	23.8			
	ethyl acetate	0: dissolves	18.2	0.17		
	n-propyl acetate	0: dissolves	17.8			
CPVC	acetic acid	-	21.4	0.3	19.5	-
	benzyl alcohol	0	23.8			
	n-propyl acetate	-	17.8			
	ethyl acetate	0	18.2	0.17		
	MEK	0	19.1			
	DMF	0	24.9	0.77		
	o-xylene	0	18.1	0		
Polycarbonate	benzyl alcohol	0: dissolves	23.8		20.3, 22.6	0.246
	chloroform	0: dissolves	18.9			
	DMF	0: dissolves	24.9	0.77		
	MEK	0	19.1			
	DCM	0: dissolves	19.8			
	xylene	0	18.1	0		
PMMA	ethyl acetate	0: dissolves	18.2	0.17	22.0, 22.7	0.281
	ethanol		26.5	0.27		

Polymer	Potential Solvent	Solubility Rating PDL# **	Solvent Hildebrand Parameter δs (MPa$^{1/2}$)	Solvent Partial Polarity (e)	Polymer Hildebrand Parameter δp (MPa$^{1/2}$)	Polymer partial Polarity (e)
	formic acid		22.6			
	MEK	0	19.1			
	toluene	0: dissolves	18.2	0		
	o-xylene	0	18.1	0		
PS (all grades)	benzyl alcohol	0	23.8		19.3	0.168
	ethyl acetate	0	18.2	0.17		
	n-propyl acetate		17.8			
	DMF	0	24.9	0.77		
	MEK	0	19.1			
	n-propyl acetate	0	17.8			
	o-xylene	0	18.1	0		
	toluene	0	18.2	0		

*Potential solvent table is sourced from information gathered from Chemical Resistance of Thermoplastics [26], HSPiP software [25] and other sources by Revolution Fibres Ltd.

** PDL# ratings (solubility ratings) from Chemical Resistance of Thermoplastics by Woishnis and Ebnesajjad [26].

Some potential solvents have associated health and safety concerns. A summary table of safety information made from available materials safety data sheets is shown in Section 6.1.1. For example, DMA, DMF, MEK, toluene, o-xylene are either carcinogenic and or mutagenic, so were avoided if possible.

2.1.4 Naming of solubility trials

In this thesis, solubility trial names were written in the form shown by the following example:

Example solubility trial name: 12% PA6,6 and 3% PMMA in 80% formic acid and 20% acetic acid + 1.5% AgNO3 + 0.05%LiCl

The first part of the name refers to the type of polymer and the concentration (in wt %). If the solution contained two polymers (called a polymer blend) the concentration of the major polymer and the major polymer name is stated, followed by the concentration of the minor polymer and minor polymer name.

The polymer concentration refers to the total amount of polymer in solution. For example, 12% PA6,6 and 3% PMMA means that 12% of the solution mass is PA6,6 and 3% is PMMA. If the total solution mass was 100 g, the amount of

PA6,6 would be 12 g and PMMA would be 3 g. Therefore a solvent mix of 85 g would have been added to make up a 100 g solution.

The second part of the name shows the ratio of the solvents mixed with the polymer. This needed to be read separately to the polymer, as often a solvent mix was made, and then the polymer added. For example, a solvent mix of 80% formic acid and 20% acetic would mean that if a total of 85 g of solvent was needed, 80% formic acid (68 g) and 20% acetic acid (16 g) would be used.

Fibre additives such as PSS, TiO_2, and $AgNO_3$ were added relative to the concentration of polymer in the solution. Thus if 1.5% $AgNO_3$ means that if there was 15 g of a polymer in the solution, then the amount of the additive added would be 0.255 g, which corresponds to 1.5% of 15 g.

Solution additives were added to enhance solution properties (such as conductivity, surface tension). SDS, LiCl, ammonium acetate, ammonium chloride and citric acid are examples of solution additives used. These additives are added in addition to the total solvent mass. For example, if 0.05% LiCl additive was to be added, then the amount of additive to be added was 0.05% of the total mass of solvent in the solution. If there was 85 g of solvent in the solution, then the amount of the additive to be added was 0.0425 g of LiCl. More information on solution additives and fibre additives is given in Section 1.1.4.1.

2.1.5 Solubility assessment of trials

Polymers, additives and their respective potential solvents were mixed together in a small beaker with a mechanical stirrer in order to visually assess the solubility of the polymer in the solvent. If the polymer appeared to fully dissolve within two hours or less, then the polymer was deemed soluble. If the polymer appeared to mostly dissolve within two hours, the polymer was deemed partially soluble. If the polymer only swelled, showed no degradation or only a small amount of polymer dissolved, the polymer was deemed insoluble. For some partially soluble and insoluble polymers, heat was applied using a hot plate at 60 °C. After 10-30 minutes, solubility was reassessed. If heated solutions precipitated after cooling to room temperature, the polymer was deemed insoluble within that solvent. If the

polymer was insoluble in the solvent it was not electrospun and another possible solvent was investigated, and the process repeated.

2.1.5.1 Compositions of solubility trials

This section shows the composition of the solubility trials undertaken for each polymer. Information on the grades and suppliers of the polymers and solvents used are located in Section 6.1.2.

Initial solubility trial compositions using PMMA are shown in Table 2.5. Once a suitable solution was found (PMMA-FA-AA), further trials involving the use of various additives to increase the dielectric constant (to improve upon the fluffiness/low packing density) of the PMMA nanofibre veil were undertaken. The compositions used in these trials are shown in Table 2.6.

Solubility trial compositions involving PC and ABS are shown in Table 2.7 and Table 2.8 respectively. Solubility trial compositions using ASA are shown in Table 2.9. Further solubility trials for ASA involving the use of additives and solvent blends are shown in Table 2.10. Compositions for the solubility trial involving CPVC are shown in Table 2.11. Solubility trial compositions for the three chosen grades of polystyrene (general purpose (GPPS), high impact (HIPS) and expanded (ExPS)) are shown in Table 2.12.

Table 2.5: Solubility trial compositions for PMMA.

Composition abbreviation	Composition Name	Polymer content PMMA/100g soln	Total solvent in solution (g /100 g soln)	Major solvent (g /100 g soln)	Minor solvent (g /100 g soln)	Additive type	additive g/100g soln	Heated
PMMA-FA	■■■■	■	■	■				
PMMA-E	■■■	■	■	■				Yes
PMMA-EA	■■■■	■	■	■	-	-	-	Yes
PMMA-FA-LiCl	■■■ ■	■	■	■	-	LiCl	▮	
PMMA-FA-SDS	■■■ ■	■	■	■	-	SDS	▮	
PMMA-FA-AA	■■■ ■	■	■	■	■	-	-	
PMMA-FA-AA-LiCl	■■■ ■■■	■	■	■	■	LiCl	▮	
PMMA-FA-AA-SDS	■■■ ■■■	■	■	■	■	SDS	▮	

Table 2.6:Further PMMA trial compositions.

Abbreviation	Composition name	Polymer content PMMA/100g soln	Total solvent in solution (g /100 g soln)	Major solvent (g /100 g soln)	Minor solvent (g /100 g soln)	Additive type	additive g/100g soln
PMMA-FA-AA-1.5AgNO$_3$	■■■ ■■■	■	■	■	■	AgNO$_3$	0.225
PMMA-FA-AA-0.5AgNO$_3$	■■■ ■■■	■	■	■	■	AgNO$_3$	0.075
PMMA-FA-AA-TiO$_2$	■■■ ■■■	■	■	■	■	TiO$_2$	0.15

Table 2.7: Polycarbonate solubility trial compositions.

Composition Abbreviation	Composition Name	Polymer content PC g/100g solution	Total solvent in solution (g /100 g solution)	Major solvent (g /100 g solution)	Minor solvent (g /100 g solution)	Additive type	amount of additive g/100g solution
20PC-BA	approx 20% PC in 100% benzyl alcohol	20	80	80	-	-	-
13PC-THF-NMP-LiCl	13% PC in 80% tetrahydrofuran & 20% n-methylpyrollidone + 0.075% LiCl	13	87	69.6	17.4	LiCl	0.06525
PC-X	15% PC in 100% xylene	15	85	85	-	-	-

Table 2.8: ABS solubility trial compositions.

Abbreviation	Composition name	Polymer content ABS/100g solution	Total solvent in solution (g /100 g solution)	Major solvent (g /100 g solution)
ABS-EA	15% ABS in 100% ethyl acetate	15	85	85
ABS-NPA	15% ABS in 100% n-propyl acetate	15	85	85
ABS-DMF	15% ABS in 100% dimethylformamide	15	85	85
ABS-X	15% ABS in 100% xylene	15	85	85

Table 2.9: ASA solubility trial compositions.

Abbreviation	Composition Name	Polymer content ASA/100g solution	Total solvent in solution (g /100 g solution)	Solvent (g /100 g solution)
ASA10-BA	10% ASA in 100% benzyl alcohol	10	90	90
ASA-EA	15% ASA in 100% ethyl acetate	15	85	85
ASA-BA	15% ASA in 100% benzyl alcohol	15	85	85
ASA-NPA	15% ASA in 100% n-propyl acetate	15	85	85

Table 2.10: Further ASA solubility trial compositions.

Abbreviation	Composition Name	Polymer content ASA/100g solution	Total solvent in solution (g /100 g solution)	Major solvent (g /100 g solution)	Minor solvent (g /100 g solution)	Additive type	amount of additive g/100g solution
ASA-EA-LiCl	15% ASA in 100% ethyl acetate + 0.05% LiCl	15	85	85	-	LiCl	0.0425
ASA-EA-SDS	15% ASA in 100% ethyl acetate + 2% SDS	15	85	85	-	SDS	1.7
ASA-50BA-50EA	15% ASA in 50% benzyl alcohol and 50% ethyl acetate	15	85	42.5	42.5	-	-
ASA-80BA-20EA	15% ASA in 80% benzyl alcohol and 20% ethyl acetate	15	85	68	17	-	-
ASA-50BA-50A	15% ASA in 50% benzyl alcohol and 50% acetone	15	85	42.5	42.5	-	-

Table 2.11: CPVC solubility trial compositions.

Abbreviation	Composition Name	Polymer content PC/100g solution	Total solvent in solution (g /100 g solution)	Major solvent (g /100 g solution)	Heated
CPVC- NPA	15% CPVC in 100% n-propyl acetate	15	85	85	Yes
CPVC-AA	CPVC in 100% acetic acid	unknown	excess	excess	Yes
CPVC-EA	15% CPVC in 100% ethyl acetate	15	85	85	Yes
CPVC-DMF	15% CPVC in 100% DMF	15	85	85	Yes
CPVC-MEK	15% CPVC in 100% MEK	15	85	85	Yes
CPVC-X	15% CPVC in 100% xylene	15	85	85	Yes

Table 2.12: Solubility trial compositions for PS.

Block	Trial Abbreviation	Trial Name	Polymer content PS/100g solution	Total solvent in solution (g /100 g solution)	Major solvent (g /100 g solution)	Minor solvent (g /100 g solution)	Additive type	amount of additive g/100g solution	Heated
1	ExPS20-EA	20% expanded polystyrene in 100% ethyl acetate	20	80	80	-	-	-	
	ExPS20-BA	20% expanded polystyrene in 100% benzyl alcohol	20	80	80	-	-	-	
	ExPS-nPA	15% expanded polystyrene in 100% n-propyl acetate	15	85	85	-	-	-	
	ExPS-NPA-AA	15% expanded polystyrene in 95% n-propyl acetate and 5% acetic acid	15	85	80.75	4.25	-	-	
	ExPS-95NPA-5E	15% expanded polystyrene in 95% n-propyl acetate and 5% ethanol	15	85	80.75	4.25	-	-	
	ExPS-90NPA-10E	15% expanded polystyrene in 90% n-propyl acetate and 10% ethanol	15	85	76.5	8.5	-	-	
2	HIPS-EA	15% HIPS in 100% ethyl acetate	15	85	85	-	-	-	
	HIPS-NPA	15%HIPS in 100% n-propyl acetate	15	85	85				
	HIPS-NPA-SDS	15% HIPS in 100% n-propyl acetate + 2.5% SDS	15	85	85	-	SDS	2.125	
3	GPPS-EA	15% GPPS in 100% ethyl acetate	15	85	85	-	-	-	
	GPPS-NPA	15% GPPS in 100% n-propyl acetate	15	85	85	-	-	-	
	GPPS20-NPA	20% GPPS in 100% n-propyl acetate	20	80	80	-	-	-	
	GPPS-NPA-0.1LiCl	15% GPPS in 100% n-propyl acetate + 0.1% LiCl	15	85	85	-	LiCl	0.085	Yes
	GPPS-NPA-0.6LiCl	15% GPPS in 100% n-propyl acetate + ~ 0.6% LiCl	15	85	85	-	LiCl	0.51	
	GPPS-NPA-	15% GPPS in	15	85	85	-	TiO2	0.15	

Block	Trial Abbreviation	Trial Name	Polymer content PS/100g solution	Total solvent in solution (g /100 g solution)	Major solvent (g /100 g solution)	Minor solvent (g /100 g solution)	Additive type	amount of additive g/100g solution	Heated
	TiO2	100% n-propyl acetate +1% TiO2							
4	GPPS-MEK	15% GPPS in 100% MEK	15	85	85	-	-	-	
	GPPS-NPA-MEK-TiO2	15% GPPS in 70% n-propyl acetate and 30% MEK + 1% TiO2	15	85	59.5	25.5	TiO$_2$	0.15	
	GPPS-DMF	15% GPPS in 100% DMF	15	85	85	-	-	-	
	GPPS10-DMF	10% GPPS in 100% DMF	10	90	90	-	-		
	GPPS10-DMF-0.05LiCl	10% GPPS in 100% DMF + 0.05% LiCL	10	90	90	-	LiCl	0.045	
	GPPS-NPA-2PSS	15% GPPS in 100% n-propyl acetate + 2% PSS	15	85	85	-	PSS	0.85	
5	GPPS-NPA-1Citric	15% GPPS in 100% nPA +1% citric acid.	15	85	85	-	citric acid	0.85	
	GPPS-NPA-2AmmA	15% GPPS in 100% nPA +2% ammonium acetate	15	85	85	-	ammonium acetate	1.7	Yes @ 40 °C
	GPPS-NPA-2AA	15% GPPS in 100% nPA + 2% acetic acid	15	85	85	-	acetic acid	1.7	
	GPPS-NPA-2FA	15% GPPS in 100% nPA +2% formic acid	15	85	85	-	formic acid	1.7	
	GPPS-NPA-3AA	15% GPPS in 100% nPA +3% acetic acid	15	85	85	-	acetic acid	2.55	
	GPPS-NPA-4AA	15% GPPS in 100% nPA +4% acetic Acid	15	85	85	-	acetic acid	3.4	

Polymer blend solution trials (PA6,6 and PMMA)

███

███

████████████████████████████████████ Therefore a polymer blend was investigated in order to see if the electrospinning of the polymer blend (particularly production rate or packing density) improved compared to the electrospinning of the individual PMMA or PA6,6 solutions.

The composition of the solubility trials for this investigation is shown in Table 2.13.

Table 2.13: Polymer blend solubility trial compositions.

███	███	███ ███ ███	███ ███	███ ███	███ ███ ███ ██
█	███ ███ █	█	█	█	█
█	███ ███	█	█	█	█
███ █	███ ███ █	█	█	█	█
███ █	███ ███ █	█	█	█	█
███ █	███ ███ ███	█	█	█	█
███ █	███ ███	█	█	█	█
███ █	███ ███	█	█	█	█

2.1.6 Electrospinning trials

Electrospinning trials were undertaken on the 'Skink', a laboratory scale electrospinning machine at Revolution Fibres Ltd. If required due to machine availability, the medium scale machine ('Chameleon') at Revolution Fibres Ltd was configured to a laboratory scale set up and used for some trials. Only solubility trial compositions in which polymer was found to be partially soluble or soluble in the solvent chosen (see Section 2.1.5) were electrospun. Revolution

Fibres Ltd standard operating procedures were used while operating the electrospinning machines. Observations such as the formation of fibres or electrospraying (spraying of solution without formation of fibres) and visual assessment of production rate, cobwebbing, clogging of tips and other production issues that contributed to the overall spinning rating were recorded.

2.1.6.1 Laboratory scale trial conditions

This section describes the conditions used for the laboratory scale electrospinning of the chosen solubility trial compositions. The temperature and relative humidity were not able to be controlled for these experiments. The current for each experiment was fixed at 0.5 mA.

The electrospinning conditions for PMMA solubility trial compositions are shown in Table 2.14. The PMMA packing density trial electrospinning conditions are shown in Table 2.15. The electrospinning conditions for solubility trial compositions involving PC and ABS are shown in Tables 2.16 and 2.17 respectively. Electrospinning conditions for solubility trial compositions containing ASA are shown in Table 2.18 and the electrospinning conditions for further ASA trial compositions are shown in Table 2.19. Electrospinning conditions for solubility trial compositions involving CPVC and PS are shown in Table 2.20 and Table 2.21 respectively.

Table 2.14: Conditions for electrospinning trial compositions containing PMMA.

Abbreviation	Electrode Voltage (+kV)	Collector voltage (-kV)	Temperature (°C)	Relative Humidity (%)
PMMA-FA	42	0	-	-
PMMA-EA	42	0	23	51
PMMA-FA-LiCl	48	0	22	50
PMMA-FA-SDS	48	0	22.5	47
PMMA-FA-AA	48	0	25	42
PMMA-FA-AA-LiCl	48	0	22	48
PMMA-FA-AA-SDS	48	0	23	46

Table 2.15: Conditions for electrospinning the PMMA packing density trials.

Abbreviation	Electrode Voltage (+kV)	Collector voltage (-kV)	Temperature (°C)	Relative Humidity (%)
PMMA-FA-AA-1.5AgNO$_3$	48	0	24.8	41
PMMA-FA-AA-0.5AgNO$_3$	48	0	24.8	41
PMMA-FA-AA-TiO$_2$	50	0	26.9	38

Table 2.16: Conditions for electrospinning trial compositions containing PC.

Abbreviation	Electrode Voltage (+kV)	Collector voltage (-kV)	Temperature (°C)	Relative Humidity (%)
20PC-BA	48	0		
13PC-THF-NMP-LiCl	50	0		

Table 2.17: Conditions for electrospinning trial compositions containing ABS.

Abbreviation	Electrode Voltage (kV)	Collector voltage (kV)	Temperature (°C)	Relative Humidity (%)
ABS-EA	48	0	24.4	43
ABS-NPA	48	0	24.9	41
ABS-DMF	50	0		

Table 2.18: Conditions for electrospinning trial compositions containing ASA.

Abbreviation	Electrode Voltage (+kV)	Collector voltage (-kV)	Temperature (°C)	Relative Humidity (%)
ASA10-BA	Unsuccessful, was not recorded			
ASA-EA	35	0, 15	28.8	46
ASA-BA	Unsuccessful, was not recorded			
ASA-NPA	48-50	0	24.9	41

Table 2.19: Conditions for electrospinning further trial compositions containing ASA.

Abbreviation	Electrode Voltage (+kV)	Collector voltage (-kV)	Temperature (°C)	Relative Humidity (%)
ASA-EA-LiCl	35	10	28.8	46
ASA-EA-SDS	35	10	28.5	43
ASA-50BA-50EA	Not recorded			
ASA-80BA-20EA	Not recorded			
ASA-50BA-50A	Not recorded			

Table 2.20: Conditions for electrospinning trial compositions containing CPVC.

Abbreviation	Electrode Voltage (+kV)	Collector voltage (kV)	Temperature (°C)	Relative Humidity (%)
CPVC- NPA	50	0	24.5	44

*Please note that only one solution was suitable to be electrospun for CPVC

The electrospinning conditions used for trial compositions containing polystyrene (general purpose (GPPS) high impact (HIPS) and expanded (ExPS) grades) are shown in Table 2.21.

Table 2.21: Conditions for electrospinning trial compositions containing PS.

	Abbreviation	Electrode Voltage (+kV)	Collector voltage (-kV)	Temperature (°C)	Relative Humidity (%)
Block 1	ExPS20-EA	48	0	-	-
	ExPS20-BA	48	0	-	-
	ExPS-nPA	50	0	25.7	41
	ExPS-NPA-AA	-	-	-	-
	ExPS-95NPA-5E	-	-	-	-
	ExPS-90NPA-10E	-	-	-	-
Block 2	HIPS-EA	48	0	24.1	44
	HIPS-NPA	50	0	25.7	41
	HIPS-NPA-SDS	50	0	25.4	44
Block 3	GPPS-EA	48	0	24.1	44
	GPPS-NPA	50	0	25.7	41
	GPPS20-NPA	50	0	26.2	42
	GPPS-NPA-0.1LiCl	50	0	24.3	42
	GPPS-NPA-0.6LiCl	50	0	24.3	42
	GPPS-NPA-TiO$_2$	50	0	26.5	36

	Abbreviation	Electrode Voltage (+kV)	Collector voltage (-kV)	Temperature (°C)	Relative Humidity (%)
Block 4	GPPS-MEK	50	0	23.9	46
	GPPS-NPA-MEK-TiO2	50	0	21.2	63
	GPPS-DMF	50	0	23.9	46
	GPPS10-DMF	50	0	25.5	43
	GPPS10-DMF-0.05LiCl	50	0	25.9	41
	GPPS-NPA-2PSS	50	0	26	41
Block 5	GPPS-NPA-1Citric	50	0	21.3	63
	GPPS-NPA-2AmmA	50	0	20.6	62
	GPPS-NPA-2AA	50	0	20.6	62
	GPPS-NPA-2FA				
	GPPS-NPA-3AA	50	0	20.6	62
	GPPS-NPA-4AA	50	0	20.6	62

The conditions for the PA6,6 PMMA polymer blend electrospinning trials are shown in Table 2.22.

Table 2.22: Polymer blend electrospinning trial conditions.

Abbreviation	Electrode Voltage (+kV)	Collector voltage (-kV)	Temperature (°C)	Relative Humidity (%)
███	50	0	23.5	51
██	50	0	22.3	59
█████	50	0	22.9	57
█████	50	0	23.6	50
█████	50	0	23.4	52
█████	50	0	23.4	52
█████	50	0	23.5	51

* Polymer blends trials were all spun for one minute on foil for comparison.

2.1.7 SEM imaging

SEM images were taken in order to estimate the fibre diameters, or confirm the presence of fibres after electrospinning. Specimens were attached to stubs by carbon tape and images of the samples were taken on a Jeol NeoScope benchtop SEM at 10 - 15 kV, using a range of magnifications. Samples were not coated before imaging.

2.1.8 Assessment and rating of trials

After solubility trials, electrospinning trials and SEM imaging (if applicable or necessary), trials were given a rating from zero to five, which depended on if the

polymer dissolved and whether the solution created was successful in electrospinning; for details see Table 2.23.

Table 2.23: Assessment and rating of trials.

Rating	Meaning
0	Polymer did not appear to dissolve or polymer appeared to dissolve and solution electrosprayed (no fibres produced)
1	Polymer appeared to dissolve but electrospun very poorly with near to no fibres produced
2	Polymer appeared to dissolve but electrospun poorly with low production rate of microfibres or nanofibres
3	Polymer appeared to dissolve, and electrospun fairly well with a good production rate and produced nanofibres, or electrospun well, but the nanofibre mat produced had low cohesion.
4	Polymer appeared to dissolve and electrospun with a medium production rate and produced nanofibres
5	Polymer appeared to dissolve and electrospun well with a high production rate and produced nanofibres

2.1.9 Viscosity, surface tension and conductivity

If the trial composition successfully electrospun on the laboratory scale machine with a rating of either four or five and was electrospun on the medium scale electrospinning machine, then the viscosity, surface tension and conductivity of the solution was measured and recorded. These tests were not carried out for the PMMA/PA6,6 blends due to time constraints.

Surface tension

Surface tension tests were carried out with a surface tension tester (SKZ21013 Surface Tension Meter, made by SKZ Industrial Co. LTD). Solution was poured into a clean glass surface tension bath until it was approximately half full. The glass bath was then placed into the tester. To assess whether the platinum probe was clean, the probe was hung gently on the probe connection at the top of the surface tension tester and a reading was taken. If the reading was 191.6 ± 0.1 mN/m^2, then the testing was able to proceed. However, if not, then the platinum probe was to be cleaned thoroughly, using distilled water and/or an ultrasonic jewellery cleaner, then dried thoroughly with a hairdryer. The measurement was taken again and cleaning repeated if necessary.
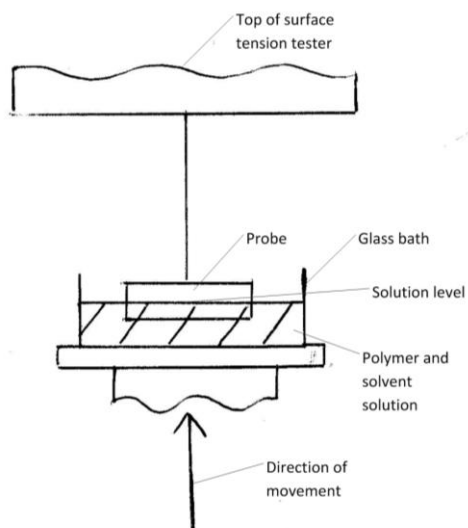
Figure 2.1: Raising the solution bath of the surface tension tester to meet the probe.
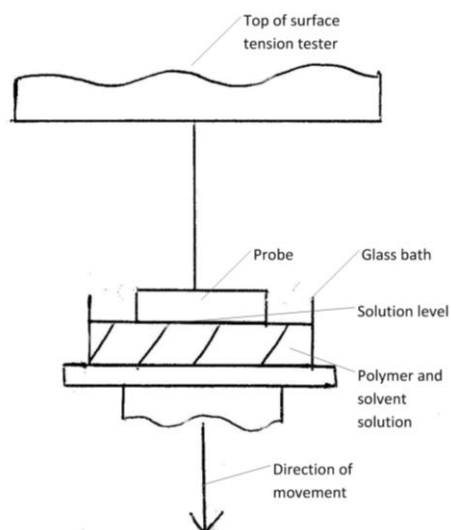
Figure 2.2: Lowering the solution bath of the surface tension tester so the solution just touched the bottom of the probe.

After repeating the process to confirm the platinum probe was clean, the solution bath was raised to meet the probe (Figure 2.1). The bath was then gently lowered until the solution was just touching along the width of the probe (Figure 2.2). The surface tension measurement was recorded and measurements taken. The average of six measurements was recorded.

Conductivity

Conductivity tests were undertaken using a conductivity probe (a Yokogawa ISC450g-a-u/um EXAxt450 inductive conductivity converter (s7) with a Yokogawa ISC40g-gg-t3-05 sensor). Approximately 400 g of the polymer and solvent solution to be tested was placed in a 500 ml beaker. The conductivity probe was then lowered into the middle of the beaker, so that the probe was fully covered by solution. It was also made sure that the bottom of probe was approximately 30 mm from the base of the beaker to prevent the conductivity readings being affected by the sides of the beaker. The probe was left in solution for approximately five minutes, then the conductivity reading and the testing temperature reading was taken. The conductivity probe was then washed

thoroughly with solvent used in the solution tested, followed by distilled water. The probe was then dried with a paper towel. The probe was cleaned between measuring each different solution.

Viscosity

The viscosity of the solutions was measured using the Zahn cup method. A Zahn viscosity cup was chosen and dipped into the solution to be tested until the cup was full. The Zahn cup was then raised quickly, letting the solution run through the hole in the bottom of the cup. A stopwatch was started as soon as the cup was raised from the beaker. The stopwatch was stopped when a break in the solution stream was observed. This was repeated five times in order to get an average time. The time was then converted using a Zahn cup conversion chart to a measurement of viscosity, in centistokes (cSt). If the time taken was in the extremes of the conversion chart, an alternative Zahn cup was chosen and the process repeated.

2.1.10 Medium scale trial conditions

Two polymer solutions (PMMA-FA-AA and GPPS-NPA-3AA) and a range of polymer blend solutions were chosen to be electrospun using the medium scale configuration on the 'Chameleon' electrospinning machine because these trial compositions were successful (had a high rating) during earlier electrospinning trials (refer to Sections 3.1.1 and 3.1.6 for more information). After electrospinning, SEM images were taken of the nanofibre created in order to verify if fibres were present and obtain fibre diameter measurements (using the same procedure outlined in Section 2.1.7).

Solutions were assessed and rated as per the previous trials (see Section 2.1.8). If the trial had a rating of five, then the veils were produced by Revolution Fibres for interleaving in composite panels.

The medium scale electrospinning trial conditions for the PMMA-FA-AA, GPPS-NPA-3AA and PMMA/PA6,6 blends are shown in Tables 2.24 - 2.26 respectively.

Table 2.24: PMMA-FA-AA medium scale solution electrospinning trial conditions.

Table 2.25: Polystyrene medium scale trial conditions (GPPS-NPA-3AA).

Table 2.26: Medium scale PA6,6 PMMA polymer blend trial conditions.

2.2 Laminate production

2.2.1 Panels

This section details the process undertaken in order to create the composite panels that were tested in order to evaluate the toughening effect of the interleaving veils. Twelve panels were created in total:

- Carbon fibre reinforced composite (CFRC) with no interleaving (control),

- CFRC with Nyplex nanofibre (nanoNyplex) (PMMA/PA6,6 blend created during solution development) interleaving,

- CFRC with PMMA nanofibre (nanoPMMA) interleaving (created during solution development),

- CFRC with PA6,6 nanofibre (nanoPA6,6) interleaving,

- CFRC with PVB nanofibre (nanoPVB) interleaving,

- CFRC with PES nanofibre (nanoPES) interleaving,

- CFRC with PPS microfibre (microPPS) interleaving,

- CFRC with PEI microfibre (microPEI) interleaving,

- CFRC with tricot (polyamide 6) microfibre (microtricot) interleaving,

- CFRC with PPS microfibre and PA6,6 nanofibre (microPPSnanoPA6,6) interleaving,

- CFRC with PEI microfibre and PA6,6 nanofibre (microPEInanoPA6,6) interleaving,

- CFRC with tricot microfibre and PA6,6 nanofibre interleaving (microtricotnanoPA6,6).

The areal weights of each veil used for interleaving are shown in Table 2.27.

Panels were created using unidirectional 200 gsm Gurit brand prepreg. The prepreg contained Volvo ocean race carbon fibre (VRC) and the Gurit SE70 epoxy resin system. Each interleaved panel had veils between each ply of unidirectional carbon fibre epoxy prepreg. All nanofibre interleavings were made by Revolution Fibres Ltd. Microfibre PPS and PEI interleavings were supplied by Technical Fibre Products Ltd, UK. Microfibre PPS was chosen because the bulk polymer has a high melting point, high tensile strength (approximately 100 MPa)

and has a strain at break of approximately 1-4 %, depending on the grade of polymer. Microfibre PEI was chosen because the bulk polymer also has a high melting point and tensile strength (approximately 115 MPa), and has an elongation at break of approximately 1-5.3 % depending on manufacturer and grade of polymer. Microtricot (made from polyamide 6) has similar properties to PA6,6, an approximate tensile strength of 85 MPa and elongation to break around 7 %. Approximate properties were sourced from various manufacturers data sheets [61].

Table 2.27: Areal weights of veils used.

#	Veil	Average nanofibre areal weight g/m^2	Average microfibre areal weight g/m^2	Average total areal weight g/m^2
2	nanoNyplex	4.3	-	4.3
3	nanoPMMA	4.5	-	4.5
4	nanoPA6,6	4.8	-	4.8
5	nanoPVB	4.7	-	4.7
12	nanoPES	3.75	-	3.75
6	microPPS	-	5.5	5.5
7	microPEI	-	4.9	4.9
8	microtricot (woven)	-	12.4	12.4
9	microPPSnanoPA6,6	3.85	5.5	9.35
10	microPEInanoPA6,6	3.7	4.9	8.6
11	microtricotnanoPA6,6	4.75	12.4	17.15

2.2.2 Panel construction

2.2.2.1 Prepreg and nanofibre veil cutting

The carbon fibre unidirectional prepreg was taken from a freezer and allowed to reach room temperature overnight in a plastic bag before cutting into plies required for the composite panels. The plies were cut into rectangles measuring 400mm by 500 mm with fibres aligned in the appropriate direction (0°, 90° or 45°). Cutting of prepreg was done with a sharp Stanley knife. The nanofibre and microfibre veils were cut into the same size with a sharp scalpel.

2.2.2.2 Layup

A quasi-isotropic symmetrical layup schedule was used, in which the ply fibres were stacked in a 0 °, -45°, +45° and 90° mirrored sequence, until 16 plies in total

were stacked. An interlayer was placed between all plies of prepreg. The control sample, however, had no interleaving veils. A layup sheet for each panel was created and filled out to ensure all layers of the composite were included.

After every four plies of carbon fibre was laid up, the block was put in a vacuum bag and held under vacuum to reduce air bubbles for at least 8-10 minutes using a small vacuum pump attached to the bag (referred to as 'debulking'). After debulking each block, the blocks were laid up in order to complete the panel and debulked again for at least 8-10 minutes. The panels were then stored in a plastic bag and put in a freezer until bringing to room temperature prior to autoclave curing.

2.2.2.3   Curing

Composite panels were vacuum bagged, with breather material, peel ply and glass breather material included in the bag (see Figure 2.3.
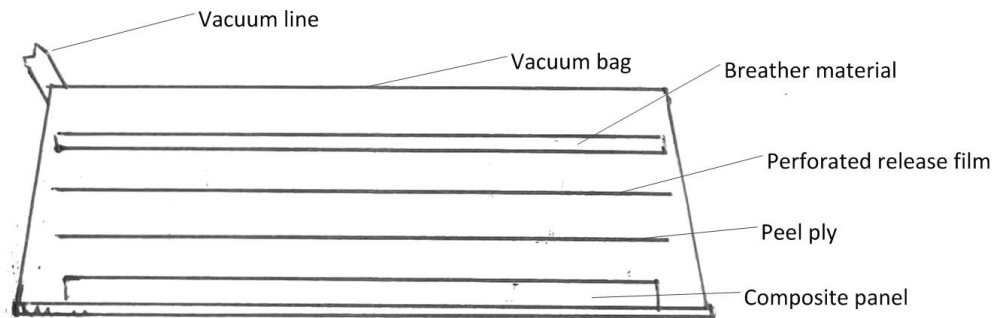
Figure 2.3: Schematic of a vacuum bagged composite panel.

The composites panels were then cured in an autoclave at Rivers Carbon Ltd, using a stepped cure with a dwell step of 80°C for 60 minutes followed by a cure temperature of 120°C for 90 minutes (see Figure 2.4). The composite panels were held under vacuum and an autoclave pressure of 3.5 bar was maintained during the curing of the panels.
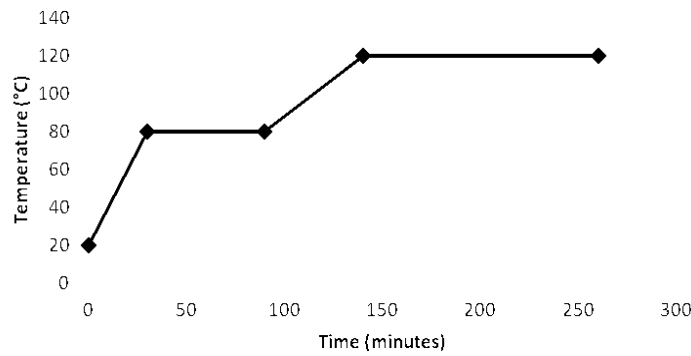
Figure 2.4: Autoclave cure schedule for the panels created.

2.2.2.4 Specimen creation

Panels were cut with a waterjet cutter in order to produce compression after impact (CAI), fatigue and vibration testing specimens. CAI specimens measured 100 x 150 mm, fatigue specimens measured 25 x 250 mm and vibration damping samples measured 10 x 50 mm. All panels were approximately 3.6 mm thick.

2.3   SEM inspection of veils used for interleaving

Clean SEM stubs were numbered and two pieces of carbon tape (sized differently to enable identification of samples) were attached to the top face of the stub. Two different veil samples were cut out using a scalpel and attached to the stub on one piece of the carbon tape. The samples were then sputter coated with platinum using a Hitachi E1030 ion sputter for 80 seconds. Samples were then observed and pictures taken at various magnifications in order to see surface morphology and fibre diameters on a Hitachi S4700 SEM at 3 kV. Images were then used by Revolution Fibres Ltd to find the diameters of the fibres using ImageJ software.

2.4   SEM imaging of composite panel cross sections

Small slivers of cross sections of each composite panel were mounted in epoxy resin. After curing for approximately 24 hours, the samples were then taken out of the moulds and polished to produce a smooth surface for imaging. The samples were polished firstly with a Struers Rotopol-21 rotary polisher at 300 rpm using 320 grit paper and water. This was done until the sample had flat surfaces. The samples were then rinsed with water and inserted in an automatic Struers Tegramin-25 rotary polisher and polished using 320 grit paper and water for two minutes, at a sample mover head speed of 150 rpm and polishing paper speed of

300 rpm. Both paper and sample mover head rotated the same direction. This was followed by with a Struers Largo polish with a Struers 9μm DiaPro diamond suspension for 20 minutes. This was polished at a speed of 150 rpm for both the polisher and the sample mover head. The direction of rotation was also the same for both the polisher and the sample mover head. The machine and samples were then thoroughly washed with soap to remove all traces of the DiaPro diamond suspension particles. The samples were then polished using the same machine with a fine Struers 'Chem' paper, followed with a Struers OP-S colloidal silica suspension. This was done at a sample mover head and polisher speed of 150 rpm. This time however, the direction of rotation was opposite. After a polishing time of 10 minutes, the samples were then removed and washed with soap to remove all traces of polishing solution. Samples were then dried with a hairdryer.

Samples were coated in platinum using a Hitachi E1030 ion sputter for 80 seconds, and carbon paint was applied to minimise charging. Specimens were observed using a Hitachi S4700 SEM under various magnifications, in order to evaluate the panel cross sections, including the thickness of the interlayer region of the panels.

2.5 Vibration damping tests using DMA

For the vibration damping tests, a Perkin Elmer DMA8000 was used in a three point bending clamping mode. For this clamping mode, the machine was orientated in the vertical position, rather than horizontal position (see Figure 2.5).
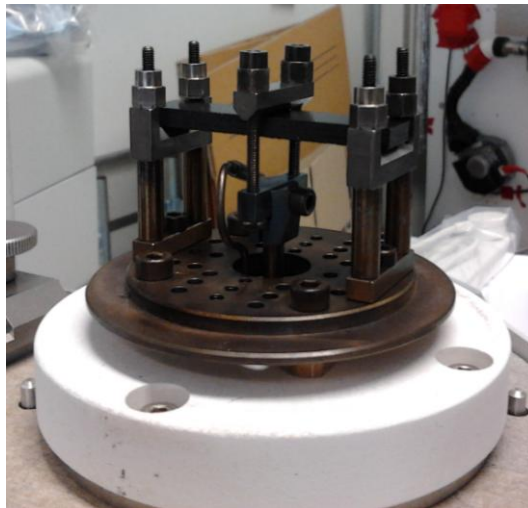
Figure 2.5: Three point bending DMA setup.

The frequency scan was carried out over a frequency range of 0.1 to 100 Hz (at logarithmic intervals). The strain amplitude was fixed at 0.05 mm. Three samples were initially tested at room temperature. However, due to too much variation between samples of the same set in the initial tests, four repeatability trials using the same frequency range and strain amplitude were undertaken using one control sample (sample 1 b):

a. Sample was clamped in position and tested at 23 °C (Trial A),

b. Sample was re-tested at 23 °C, without being taken out of the clamps (Trial B),

c. Sample was taken out, re clamped and re-tested at 23 °C (Trial C),

d. Sample was taken out, re clamped tighter and re-tested at 23 °C (Trial D).

It was found that there was too much variation in the laboratory temperature (more information in Section 3.3). All samples previously tested, along with a fourth sample from each set were then tested using the same frequency range and strain amplitude at approximately 23 °C (see Table 2.28 for exact temperatures) and were covered using the furnace attachment (disconnected) of the DMA to prevent variation in temperature during the test.

Table 2.28: Retest testing temperatures.

Sample type	Sample #	Test Temperature (°C)	Sample type	Sample #	Test Temperature (°C)
Control	1a	23.2	microPEI	7a	23.2-23.3
	1b	23.6		7b	23
	1c	22.8		7c	23.2-23.3
	1d	23.5-23.6		7d	23.2
nanoNyplex	2a	23.3	microtricot	8a	23.9
	2b	23.6		8b	23.2
	2c	23.3		8c	23.4
	2d	23.6		8d	23.0-23.1
nanoPMMA	3a	23.2	microPPSnanoPA6,6	9a	22.7
	3b	22.8		9b	23.2
	3c	23.7		9c	23.2
	3d	23.6		9d	23
nanoPA6,6	4a	23.6	microPEInanoPA6,6	10a	23.3
	4b	23.3		10b	23.4
	4c	23.2		10c	23.5
	4d	23.6-23.7		10d	23.1
nanoPVB	5a	23.4	microtricotnanoPA6,6	11a	23.6
	5b	23.2		11b	23.6
	5c	22.9		11c	23.4-23.5
	5d	23.5-23.7		11d	23.1
microPPS	6a	23.7-23.6	nanoPES	12a	23.6-23.7
	6b	23.8-23.9		12b	23.8
	6c	22.9-23.0		12c	23.5-23.6
	6d	23.8-23.9		12d	23.5-23.6

2.6 Compression after impact testing (CAI)

Compression after impact testing was a two step test, initially involving a single impact to the specimen, followed by a compression test.

2.6.1 Drop weight impacting

Six specimens from each sample type were impacted once at six different drop heights using an in-house made drop tower designed to satisfy ASTM International standard D7136/D7136M. The tower was equipped with a 5.40 kg drop weight which had a 16 mm spherical tip. The drop heights, impact energies

and impact velocities used for this test are shown in Table 2.29. Drop heights were measured from the top surface of the specimens.

The impact velocity was calculated using equation (2-1), and the impact energy was calculated using equation (2-2).

$$V_0 = \sqrt{2gH} \qquad\qquad (2\text{-}1)$$

$$E_0 = \frac{1}{2}MV_0^2 \qquad\qquad (2\text{-}2)$$

where V_o is the impact velocity (m/s),

g is equal to 9.81 m/s^2 (gravitational constant),

H is the drop height (m)

E_0 is the impact energy (J) and

M is the mass of the impactor (kg).

Table 2.29: Drop heights, impact velocities and impact energies.

Drop Height (mm)	Calculated Impact Velocity (m/s)	Actual (calculated) Impact Energy (J)
197	1.97	10.4
269	2.30	14.3
384	2.74	20.3
479	3.07	25.4
573	3.35	30.4
666	3.61	35.3

2.6.2 Compression after impact

After impact, specimens were inserted individually into an in-house made compression after impact jig designed to satisfy ASTM International standard D7137/D7137M. The jig containing a specimen was then placed between two parallel compression platens in a servo-hydraulic Instron 8801 Universal tester. The specimens were preloaded to 450 N and then compressed until failure using a

cross head speed of 1.25 mm/min. The failure load (kN) was recorded and from this, the compressive strength was calculated using equation (2-3).

$$C = \frac{F}{w.t}$$ (2-3)

where C equals compression after impact strength (Pa),

F = failure load (N),

w = specimen width (m),

and t = specimen thickness (m).

During testing, it was found that some specimens did not fail in an acceptable failure mode (i.e. they failed across the top of the specimen rather than near the impact area - see Figure 2.3 and 2.4). This was found to be because the specimens were not square and parallel, particularly across the thickness, due to being cut with a waterjet cutter. Specimens that had not yet been compression tested were trimmed by approximately 2 mm across the top with a diamond cutter to improve this. The exact specimen measurements are shown in Section 6.4. Since the compressive strength depends on the thickness and width rather than the length of the samples it should not have affected the results or comparison between samples significantly.

Figure 2.6: Acceptable failure mode.

Figure 2.7: Unacceptable failure mode.

2.6.2.1 Visual inspection and optical microscopy of specimens (post CAI)

The front and reverse of the CAI specimens (post CAI) were visually inspected and a range of photographs were taken using a Canon 1000D DSLR camera.

The sides of the specimens were also observed under a WILD optical microscope under magnifications of 6x, 16x and 40x. Optical micrographs were taken of the sides using a Nikon digital sight camera attached to the WILD optical microscope in order to create photomontages of the specimen sides. Measurements of the damage region length on the sides of the specimens subjected to impact energies of 25 and 30 J were also taken with the aid of the optical microscope (see Figure 2.8).
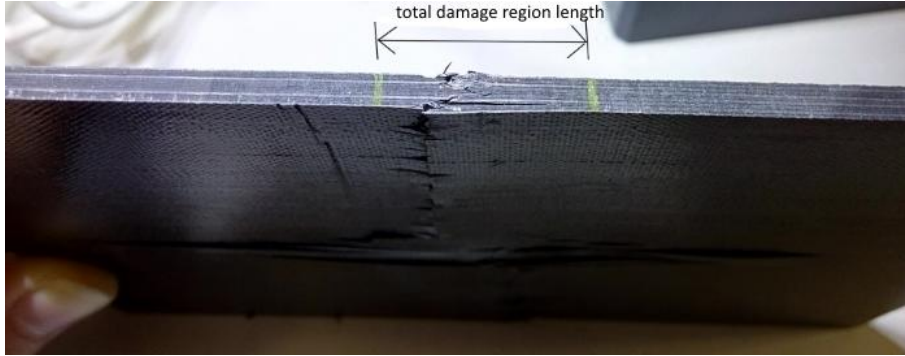
Figure 2.8: Damage region length measurement on the side of a CAI specimen (post impact and compression test).

2.7 Fatigue testing

Three specimens from each sample set were tested under tension-tension fatigue according to ASTM International standard D3479 with a servo hydraulic Instron 8801 Universal tester. One specimen from each set was tested at σ_{max} 400, 450 and 500 MPa. Each test had a stress ratio of 0.1. Emery cloth was used to ensure that the specimen did not slip while being held in the grips during testing for some samples, however, it was found this did not work for all specimens, so tabs were made for the remainder of specimens (this is noted for each specimen in Section 6.5). Initially some trial tabs were made which measured 60 mm x 26 mm and were made from 2 mm thick aluminium sheet. The tabs were bonded using Adhesive Technologies (Ltd) HPR25 two part adhesive and cured under pressure at room temperature for 12 hours and post cured in an oven at 60 °C for more than 12 hours. After these initial experiments, the tabs for the remaining specimens were modified slightly, measuring 55 mm x 26 mm x 2mm thick, with a 45° bevel, as per ASTM International standard D3039. Specimens measured approximately 25 x 3.6 x 250 mm (see Section 6.5).

2.7.1 Post fatigue visual inspection, optical microscopy and SEM analysis

Fatigue specimens were visually inspected and a range of photographs were taken using a Canon 1000D camera.

The fractured surfaces of the specimens were also observed under a WILD optical microscope under magnifications of 6x, 16x and 40x. Optical micrographs were taken using a Nikon digital sight camera attached to the WILD optical microscope.

Areas of interest near the break points of these specimens were further inspected using a scanning electron microscope (SEM). The areas were cut from the specimens using a small Shanghai Jiaodo wheel saw with a sintered diamond blade at 400 rpm. The pieces were mounted on stubs and coated in platinum using a Hitachi E1030 ion sputter for 80 seconds. Specimens were then observed using a Hitachi S4700 SEM under various magnifications.

Chapter 3

Results and Discussion

3.1 Solution development

3.1.1 Poly methyl methacrylate

From the potential solvents shown in Table 2.4, there were six possible solvents that could be trialled for use with poly methyl methacrylate (PMMA). Initially, trials were undertaken using formic acid (FA), ethyl acetate (EA) and ethanol (E) as the solvents for PMMA; these solvents were chosen because they were readily available.

After mixing vigorously at room temperature for two hours with each of the solvents (compositions shown in Table 2.5), PMMA appeared to dissolve in FA and in EA, but not E, supporting that FA and EA were suitable solvents for PMMA, as could be expected due to the similar Hildebrand parameters for FA, EA and PMMA. The two solutions produced were suitable for trialling on the laboratory scale electrospinning machine. When PMMA and E was transferred to a hotplate and stirred vigorously for approximately two hours at 60 °C, the PMMA still did not dissolve. It was concluded that E was not a suitable solvent for PMMA, which could be explained by the solubility parameters.

Electrospinning of the PMMA-EA solution produced fibres, however some electrospraying occurred during spinning, and the observed deposition rate of fibres was low. SEM imaging revealed that the fibres produced were heavily beaded and had a large fibre diameter range. The electrospinning was given a rating of one (refer to Table 2.23); therefore EA was not investigated further in conjunction with PMMA in this research.

The PMMA-FA solution produced fibres when spun on the laboratory scale electrospinning machine; however, the poor cohesion between the nanofibres meant that resulting nanofibre mat was too easy to pull apart. It also appeared fluffy, with low cohesion between nanofibres. The production rate of fibres seemed good. The electrospinning was given a rating of three (see Table 2.23). It

was thought that the solution could potentially be improved by blending with different solvents or additives (such as salts or surfactants, see Section 1.1.4.1). Examination of the nanofibres produced under the scanning electron microscope (SEM) (shown in Figure 3.1) showed the fibres to be around 500-600 nm in diameter, with no beading.
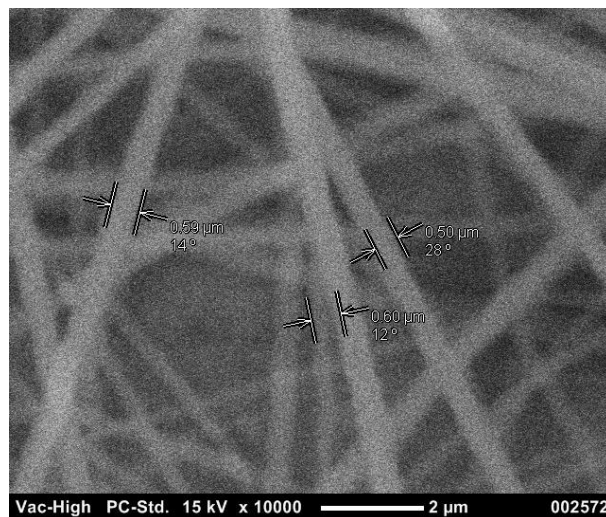
Figure 3.1: Fibres spun from PMMA-FA.

Acetic acid (AA) was identified as a possible solvent to blend with FA to dissolve PMMA. ██ ████████████████████████████████████ The results for the trials are given in Table 3.1.

Table 3.1: Electrospinning results for further PMMA trials.

Abbreviation	Observations	Fibres	Fibre Diameter	Beading	Other Observations	Rating
PMMA-EA	Some spraying occurred. Low deposition rate. Solution had a low viscosity.	Yes	600-1500 nm	Heavily beaded	Wide fibre diameter variation	1
PMMA-FA-LiCl	Solution was possibly too conductive. Cobwebs formed. Poor spinning overall	Yes	-	-		1
PMMA-FA-SDS	Some cobwebbing, however spun better than PMMA-FA-LiCl	Yes	-	-	Unknown if SDS had any effect	3
PMMA-FA-AA	Spun very well, with very little build up on tips. Spun better than PMMA-FA, and was less 'lofty' than PMMA-FA, but still had low packing density	Yes	400-500 nm	No		5
PMMA-FA-AA-LiCl	Did not spin as well as PMMA-FA-AA, some cobwebs, solution thought to be too conductive.	Yes	-	-		2
PMMA-FA-AA-SDS	Cobwebbing, but spun very well, unknown whether SDS had any effect on the spinning.	Yes	100-300 nm	-		3

74

From the results shown in Table 3.1 it can be seen that the PMMA-FA-AA solution spun the best of all the solutions containing both FA and AA. The addition of LiCl was found to be detrimental. This was thought to be because the conductivity of the solution was too high. It was also found that the addition of SDS to PMMA-FA-AA did not improve the spinning. Low quality SEM analysis of some of the more successfully spun fibres confirmed that fibres were produced from PMMA-EA, PMMA-FA-AA, PMMA-FA-AA-SDS and PMMA-FA-AA-LiCl solutions. PMMA nanofibres spun from PMMA-EA, PMMA-FA-AA and PMMA-FA-AA-SDS are shown in Figures 3.2, 3.3 and 3.4 respectively. The nanofibres spun from PMMA-EA had large diameter variability compared to fibres spun from PMMA-FA-AA and PMMA-FA-AA-SDS.
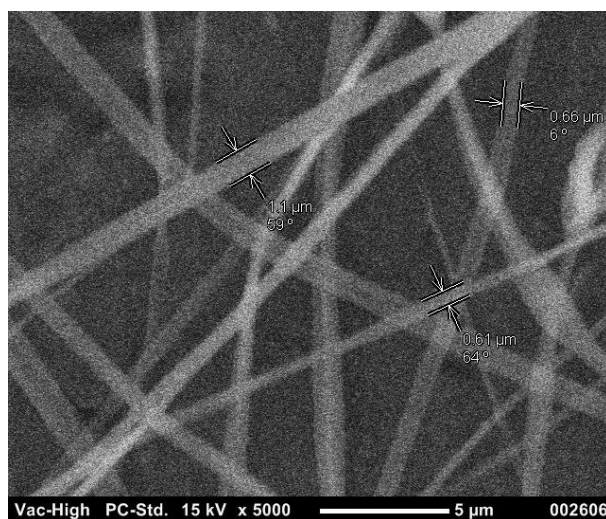
Figure 3.2: Fibres spun from PMMA-EA.
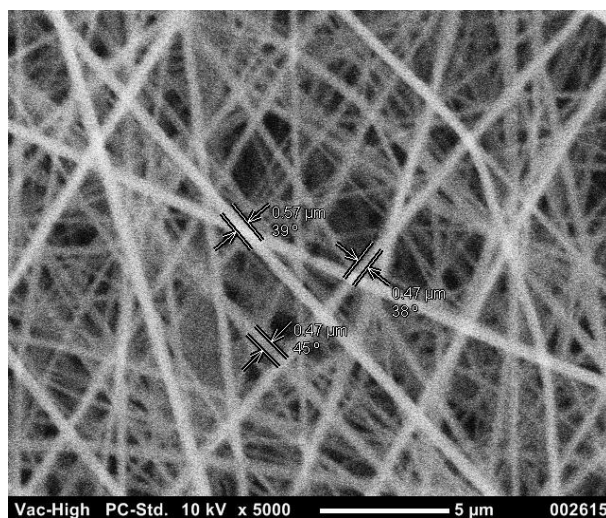
Figure 3.3: SEM image of PMMA nanofibres produced from PMMA-FA-AA.
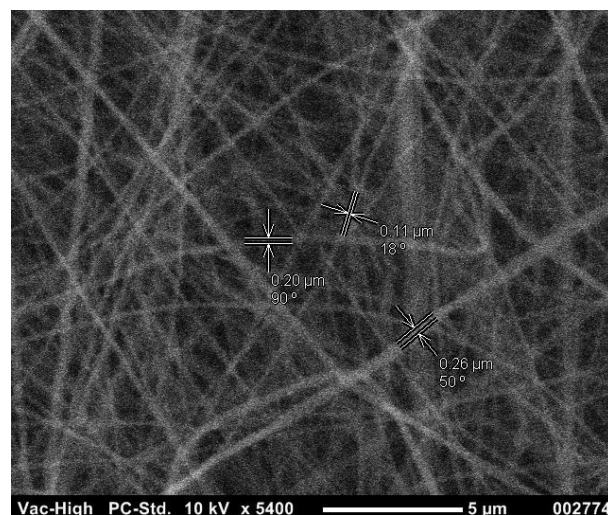
Figure 3.4: SEM image of PMMA nanofibres produced from PMMA-FA-AA-SDS.

3.1.1.1 Influence of dielectric constant

Adding $AgNO_3$ or TiO_2 to a polymer can influence the dielectric constant (see Section 1.1.4.1). Three trials were undertaken in order to determine whether increasing the dielectric constant of the fibres affected the observed 'loftiness' of the nanofibre mat and cohesion of the fibres, using $AgNO_3$ and TiO_2 as fibre additives in the PMMA-FA-AA solution. The composition of the solutions trialled is shown in Table 2.6. The results from these trials are shown in Table 3.2.

Table 3.2: Electrospinning of further PMMA trials.

Abbreviation	Observations	Fibres	Fibre Diameter	Beading
PMMA-FA-AA-1.5AgNO₃		Yes	200-500 nm	No
PMMA-FA-AA-0.5AgNO₃	All solutions spun very well. No improvement in the spinning or loftiness was observed compared to PMMA-FA-AA	Yes	200-500 nm	No
PMMA-FA-AA-TiO₂		Yes	200-500 nm	No

From the results, it was found that adding $AgNO_3$ or TiO_2 to the PMMA-FA-AA solution did not change the observed loftiness or cohesion of the PMMA fibres produced (see Section 1.1.6). It also did not affect the ability of the solution to electrospin. The cause of the loftiness and low cohesion of the PMMA nanofibre mat was unknown. Due to time constraints this not investigated further during this research.

SEM images of the nanofibres produced from the solutions trialled (Table 3.2) were taken in order to confirm the presence of nanofibres. Figures 3.5, 3.6, and

3.7 show fibres spun from PMMA-FA-AA-0.5AgNO$_3$, PMMA-FA-AA-1.5AgNO$_3$ and PMMA-FA-AA-TiO$_2$ respectively. No significant differences were observed, however, the diameters of the fibres produced were found to be between 200 - 400 nm, which was slightly smaller than the fibres produced from the PMMA-FA-AA solution (see Figure 3.3). No beading was found.
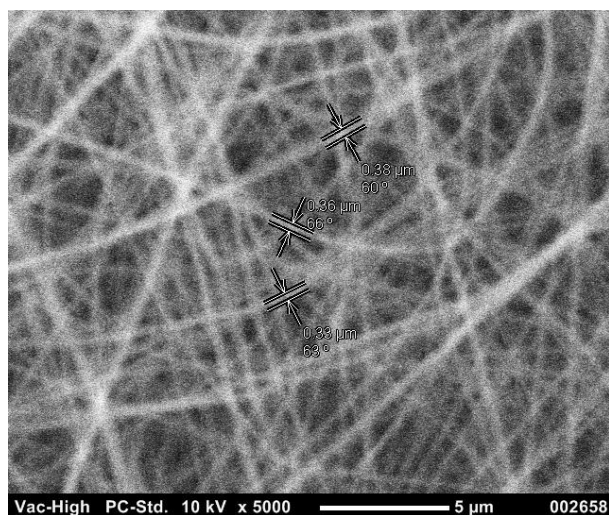
Figure 3.5: SEM image of PMMA nanofibres produced from PMMA-FA-AA-0.5AgNO$_3$ taken at Revolution Fibres, with diameter measurements.
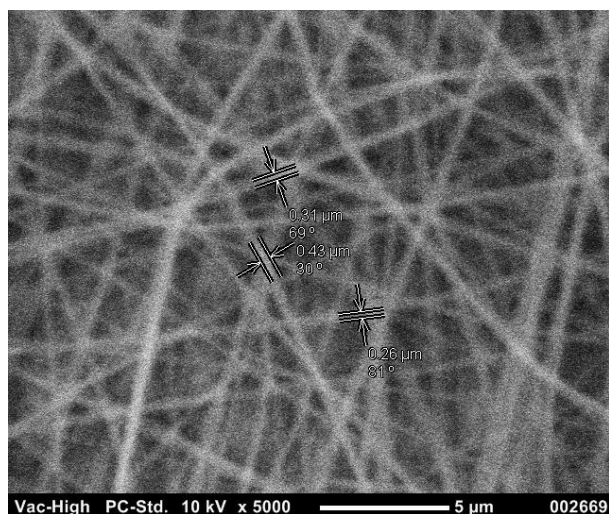
Figure 3.6: SEM image of PMMA nanofibres produced from PMMA-FA-AA-1.5AgNO$_3$ taken at Revolution Fibres, with diameter measurements.
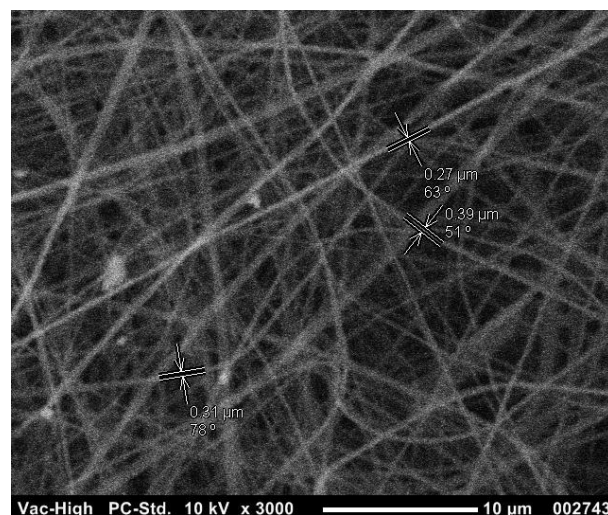
Figure 3.7: SEM image of PMMA nanofibres produced from PMMA-FA-AA-TiO$_2$ taken at Revolution Fibres, with diameter measurements.
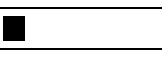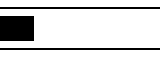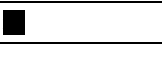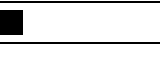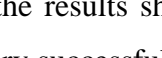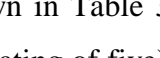
3.1.1.2 Medium scale trials

Since the PMMA-FA-AA solution was successful at electrospinning (rating of five), the solution was trialled on the medium scale machine. The surface tension, viscosity and conductivity of the solution were measured before spinning and are shown in Table 3.3. The key parameters and results for this trial are shown in Table 3.4.

Table 3.3: General properties of PMMA-FA-AA.

General Properties of PMMA-FA-AA				
	Surface Tension (mN/m)	Viscosity (cST)	Conductivity (μS/cm)	Test Temperature (°C)
PMMA-FA-AA	228.9	28	88	20

Table 3.4: PMMA-FA-AA trial results.

			Fibres	Rating	Deposition
▮	▮	▮	Yes	5	-
▮	▮	▮	Yes	5	-
▮	▮	▮	Yes	5	4.1 gsm
▮	▮	▮	Yes	5	3.6 gsm

From the results shown in Table 3.4 it can be seen that the spinning of PMMA was very successful (rating of five). The electrode speeds were adjusted to ensure a complete layer was produced. The substrate speed was also increased in order to achieve a low deposition of nanofibres. Although the loftiness of the nanofibre mat made the nanofibre hard to peel from the substrate, the solution was

78

successfully spun and the veils produced (referred to as 'nanoPMMA') were used as interleaving in the composite panels tested in the subsequent parts of this thesis.

3.1.2 Polycarbonate

The potential solvents table (Table 2.4) showed that chloroform, dichloromethane (DCM), dimethyl sulfoxide (DMSO), methyl ether ketone (MEK), dimethyl formamide (DMF), benzyl alcohol (BA) and xylene (X) could be suitable solvents for PC. However, chloroform, DMSO and MEK were avoided as the vapour pressures of these solvents were outside the optimal range for Revolution Fibre's machines (refer to Section 1.1.4 for more information). DMF and DCM were also avoided because of the associated health and safety risks.

Three trials were investigated for polycarbonate (shown in Table 2.7) using BA, X, and a combination of n-methylpyrrolidone (NMP) and tetrahydrofuran (THF). NMP and THF were used as solvents in a 13PC-THF-NMP-LiCl solution and were chosen based on industrial experience at Revolution Fibres Ltd.

The observations in the table below show the results from the three trial solutions.

Table 3.5: Results from PC trials.

Abbreviation	Observations	Fibres
20PC-BA	Did not fully dissolve, even when heated, therefore unknown concentration was trialled. Electrosprayed rather than electrospun.	No
13PC-THF-NMP-LiCl	Low packing density, cobwebbed, appearance was almost like 'candy floss'. Large fibres, but not useable	Yes
PC-X	Did not dissolve.	No

From Table 3.5 it can be seen that PC appeared to dissolve in the mix of THF and NMP, but did not dissolve fully in benzyl alcohol (BA) or xylene (X). THF has a Hildebrand parameter of 19.5 MPa$^{1/2}$ and 23.0 MPa$^{1/2}$ for NMP, shown in Table 2.3. PC was thought to be soluble in THF and NMP rather than BA or X, as THF, the predominant solvent, had a Hildebrand parameter closer to the value of polycarbonate (20.3 MPa$^{1/2}$) than either BA (23.8 MPa$^{1/2}$) or X (18.1 MPa$^{1/2}$).

However, no usable material was produced from 13PC-THF-NMP-LiCl trial, as the fibres produced were very large, and did not form a mat. Usually, large fibres indicate that the conductivity of the solution is low; suggesting that the amount of LiCl added was insufficient. The unsuccessful spinning of the 13PC-THF-NMP-

LiCl could have also been due to the low dielectric constant of the major solvent, THF (see Table 2.3) (also see Section 1.1.4). While the dielectric constant of the solution would have increased with the addition of NMP (as it had a higher dielectric constant), the dielectric constant of the overall solution may still have been too low for successful electrospinning.

As THF and NMP are polar aprotic solvents, it is possible that additives such as ammonium acetate that provide NH_4^+ ions could improve electrospinning as they have been shown to assist electrospraying as discussed earlier (Section 1.3).

It would be recommended for future research that a more pure form of polycarbonate be used, rather than the extruder granules used for these trials, as the granules may have contained additives to enhance extrusion, which could have affected solubility and electrospinning performance. It was also assumed during the potential solvent analysis that the Hildebrand and Hansen parameters for a pure form of polycarbonate would have been applicable to the polycarbonate granules used during the experiments. However, this may not have been the case and this assumption could have resulted in unsuitable solvents being chosen for the experiments. Due to time constraints, solutions containing polycarbonate were not investigated further during this project.

3.1.3 Acrylonitrile butadiene styrene

The possible solvents for ABS are shown in Table 2.4. Some of the solvents, such as dimethyl formamide (DMF), methyl ether ketone (MEK), toluene, and xylene (X), pose health and safety concerns. However, due to the small range of solvents suitable, DMF and X were trialled as well as ethyl acetate (EA) and n-propyl acetate (NPA). Four trials were investigated (see Table 2.8) and the results are shown in Table 3.6.

Table 3.6: ABS solution spinning conditions and observations.

Abbreviation	Initial Observations	Fibres	Fibre Diameter	Beading	Other Observations	Rating
ABS-EA	Tips clogged fast, possibly due to the evaporation of the solvent. Was spun on PE fabric, and was hard to remove where the polymer spun wet.	Yes	600 + nm	Yes		3
ABS-NPA	ABS appeared to be soluble in NPA, but the trial did not spin well (was worse than ABS-EA).	Yes				2
ABS-DMF	Solution splashed. Fine electrospraying with low deposition rate.	No			SEM images - no fibre, just particles	0
ABS-X	Did not fully dissolve.	-				0

DMF, NPA and EA appeared to be suitable solvents for ABS (see Table 3.6). However, X was not suitable, although Hildebrand parameters for X and ABS were similar. It seems likely that if heated, the ABS may have dissolved.

Only the ABS-EA, ABS-DMF and ABS-NPA trials were electrospun. The ABS-DMF trial electrosprayed rather than electrospun (Figure 3.8), and was given a rating of zero. However, both the ABS-EA and ABS-NPA trials produced fibres.
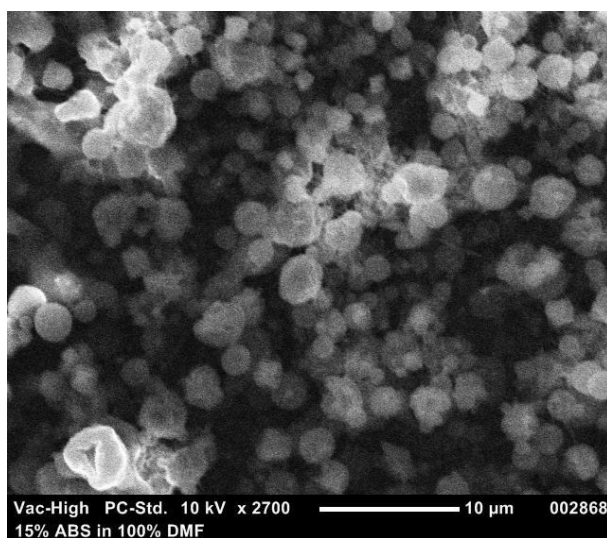
Figure 3.8: ABS-DMF trial electrosprayed rather than electrospun and resulted in particles.
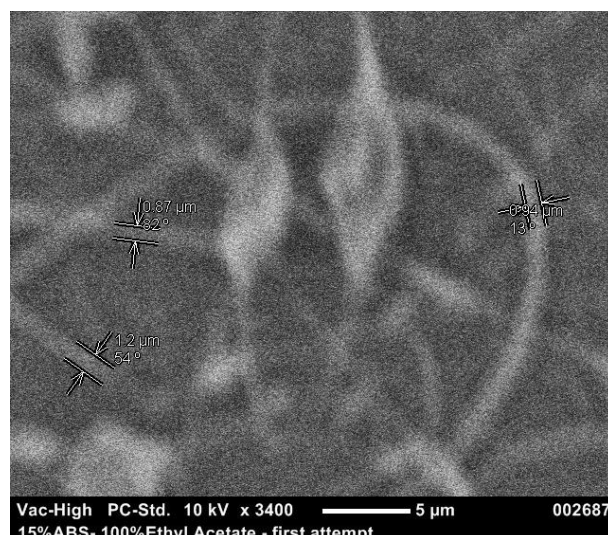
Figure 3.9: ABS nanofibres from ABS-EA trial.

Of these two solutions, ABS-EA was the most successful, but the electrodes clogged within a short time, likely due the high vapour pressure of EA. SEM images of the fibres produced from the ABS-EA solution showed that the fibres were large and had beads (see Figure 3.9). The ABS-NPA trial did not spin well, even though NPA had a lower vapour pressure than EA.

The poor electrospinning results for the ABS trials could have been due to the low conductivity of the solvents chosen; a solution must be sufficiently conductive in order to electrospin successfully (see Section 1.1.4). A table of in-house conductivity measurements of the solvents used is shown in Table 3.7. It can be seen that the conductivities of the solvents are very low, particularly when compared to successful electrospinning solutions such as PMMA-FA-AA (shown in Table 3.3).

Table 3.7: Table of conductivities of solvents used for ABS.

	Test temperature (°C)	Conductivity (µS/cm)
n-propyl acetate	21.1	0
ethyl acetate	20.5	0.1
dimethyl formamide	21.6	0.6
xylene	17.4	0.2

It is noted, that although there were small variations in electrode voltages, temperature and humidity between the trials, it is unlikely that they would have had a large influence on results.

82

As mentioned in Section 3.1.2, it was assumed that Hildebrand and Hansen parameters of pure ABS would be applicable to the grade of polymer used in this study. Therefore, if it was not applicable then the potential solvent analysis may not have been accurate. Any additives in the polymer used may have affected the solubility, so in future research a known grade of ABS with no additives should be used and the trials repeated.

Also, in future research, a different solvent with higher conductivity could be trialled, or an additive such as LiCl could be added to the solution to increase the conductivity. A different solvent system could also be investigated to decrease the clogging of the tips and increase the production rate. For this research, however, ABS was not investigated further due to time constraints.

3.1.4 Acrylonitrile styrene acrylate

From potential solvent analysis it was found that benzyl alcohol (BA), ethyl acetate (EA) and n-propyl acetate (NPA) could be used with acrylonitrile styrene acrylate (ASA) (see Table 2.4). Four trials were initially conducted (compositions shown in Table 2.9). The results for these trials are shown below in Table 3.8.

Table 3.8: ASA electrospinning trials.

Abbreviation	Observations	Fibres	Other Observations/ Notes	Rating
ASA10-BA	Electrosprayed	No	Stayed wet	0
ASA-EA	Very low production rate, solvent evaporated too fast. Possible nanofibres.			1
ASA-BA	Electrosprayed, probably because BA had low vapour pressure	No	The substrate (tin foil) stayed wet after being left overnight	0
ASA-NPA	Electrosprayed.	No		0

Although ASA appeared to dissolve in all of the solvents chosen, the solutions did not electrospin well (see Table 3.8). ASA-EA was the most successful and fibres were produced, but the electrodes clogged within a short time, likely due the high vapour pressure of EA. The clogged tips resulted in a very low production rate.

Fibres were not produced from any of the other solutions. The solutions that contained BA and NPA electrosprayed and landed wet on the collector, as the solvent had not evaporated to the extent required during electrospinning. The resulting material from solutions containing BA were extreme in that they did not

dry out overnight, which is likely to be because the low vapour pressure of BA. The resulting material for the solution with NPA was less wet, probably due to the higher vapour pressure of NPA relative to BA, albeit apparently too low still.

The second round of trials investigated using blends in order to adjust the vapour pressures, and additives to adjust surface tension and conductivity (see Table 2.10 and Table 3.9).

Table 3.9: Electrospinning results for extra ASA trials.

Abbreviation	Observations	Fibres	Fibre Diameter	Beading	Other Observations/ Notes	Rating
ASA-EA-LiCl	Solvent evaporated very fast, and tips clogged.	Yes	400+ nm	Yes	███████	1
ASA-EA-SDS	Very little spinning, solvent evaporated too fast.	Yes	500+ nm		███████	2
ASA-50BA-50EA	Electrosprayed, suspect because BA has low vapour pressure	No				0
ASA-80BA-20EA	Electrosprayed, suspect because BA has low vapour pressure	No				0
ASA-50BA-50A	Electrosprayed, suspect because BA has low vapour pressure	No				0

It can be seen from Table 3.9 that all of the trials had low ratings. From the results for ASA-50BA-50EA and ASA-80BA-20EA, it seems that blending BA with EA did not improve the spinning. From the results of the ASA-50BA-50A trial, it seems that adding acetone (A) did not provide any improvement either. It seems likely that the vapour pressure for these trials was still not suitable for electrospinning.

The ASA-EA-LiCl and ASA-EA-SDS trials did produce fibres when electrospun (see Figure 3.10 and Figure 3.11). However, the spinning was poor, most likely due to the high vapour pressure of EA.

It is noted that some trials were electrospun on the medium scale electrospinning machine rather than the laboratory machine, due to machine availability. For these trials, the conditions and set up of this machine was kept as similar as possible to the laboratory spinning machine. However, it would have contributed to some variation in electrospinning between solutions, but the quality of the electrospinning should have been similar.
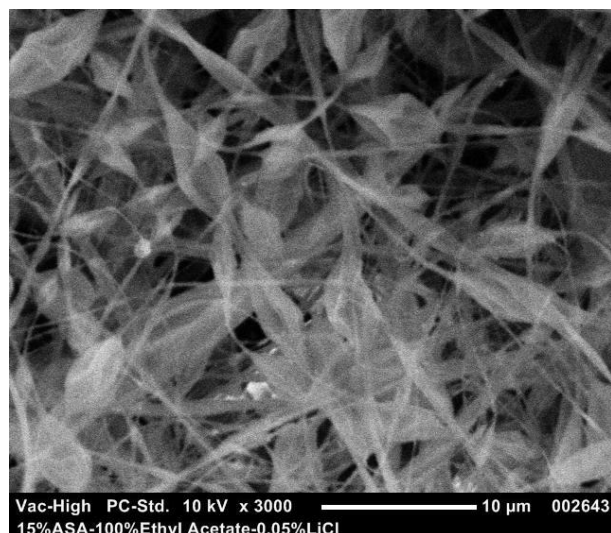
Figure 3.10: Fibres produced from ASA-EA-LiCl.
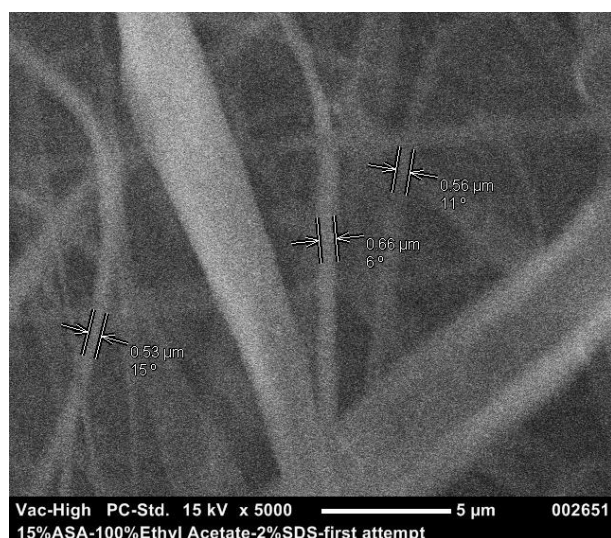
Figure 3.11: Fibres produced from ASA-EA-SDS.

Although all of the solvents used did appear to dissolve ASA, more trials involving different solvents would be recommended in order to achieve an acceptable vapour pressure for spinning. This was not undertaken during this investigation due to the limited solubility data available for ASA and time constraints.

3.1.5 Chlorinated poly vinyl chloride

The possible solvents for chlorinated poly vinyl chloride (CPVC) are shown in Table 2.4. Although dimethyl formamide (DMF), methyl ether ketone (MEK) and xylene (X) presented health and safety risks, these solvents were trialled along with ethyl acetate (EA), acetic acid (AA) and n-propyl acetate (NPA). Benzyl

alcohol was not trialled because it had been found to have a vapour pressure too low for spinning (see research covered in the previous sections). Therefore six trials containing CPVC were investigated (see Table 2.11).

Table 3.10: CPVC solution electrospinning trials.

Abbreviation	Observations	Fibres
CPVC- NPA	Polymer did not fully dissolve, spun mostly solvent. Was mixed again and appeared to not fully dissolve even when heated	No
CPVC-AA	Polymer did not dissolve.	-
CPVC-EA	Polymer swelled	-
CPVC-DMF	Polymer swelled and appeared to dissolve.	-
CPVC-MEK	CPVC swelled, did not dissolve.	-
CPVC-X	CPVC swelled, did not dissolve.	-

From the results shown in Table 3.10 it can be seen that for most trials the CPVC particles swelled rather than dissolved. DMF was the only solvent that appeared to dissolve CPVC, however much of the solvent evaporated before electrospinning could be carried out. This solution was not investigated further due to time constraints.

To encourage the CPVC to dissolve in the solvents used (other than DMF), heat could have been applied. However, this could have resulted in too much solvent evaporating, resulting in an increased polymer concentration, which could be too high for electrospinning. Alternatively, on cooling, the polymer may have also precipitated out of the solution. This would not be desired as precipitation could happen during electrospinning, as trials could not be kept warm in the machines at Revolution Fibres.

As mentioned in the previous sections, it was assumed that Hildebrand and Hansen solubility parameters of pure CPVC could be used during the potential solvent analysis. However, the CPVC used in the experiments was of unknown grade and molecular weight, as it was sourced from a ground up high temperature application CPVC pipe (extrusion granules were not available), which could have contained additives that may have affected the solubility. Thus, unsuitable solvents may have been chosen as a result of the assumption. Therefore future trials using a pure form of CPVC would be recommended. However, due to time

constraints, solutions containing CPVC was not investigated further during this project.

3.1.6 Polystyrene

The potential solvents list for polystyrene (Table 2.4) showed a large range of solvents available that could be used to dissolve polystyrene. The trials comprised of the solvents and additives shown in Table 2.12. The results from each trial are shown in Table 3.11. The first three blocks of Table 3.11 detail initial trials with ExPS, HIPS and GPPS using ethyl acetate (EA), benzyl alcohol (BA), n-propyl acetate (NPA), acetic acid (AA) and ethanol (E).

The fourth block covers trials with GPPS using n-propyl acetate (NPA), methyl ether ketone (MEK), and dimethyl formamide (DMF), as well as additives (PSS and TiO$_2$). The fifth block shows results from trials with GPPS using NPA and additives such as citric acid, ammonium acetate, AA and formic acid (FA).

Table 3.11: Observations and ratings for the polystyrene trials.

	Abbreviation	Observations	Fibres	Rating
Block 1	ExPS20-EA	Spun, but the electrodes clogged up after a short amount of time. Thought to be because the solvent evaporated too quickly.	Yes	3
	ExPS20-BA	Electrosprayed, thought to be because benzyl alcohol had a low vapour pressure.	No	0
	ExPS-nPA	Appeared to dissolve easily, but did not spin well.	Yes	1
	ExPS-NPA-AA	Polymer precipitated.		0
	ExPS-95NPA-5E	Polymer precipitated and seemed to dissolve when mixed. Was not spun		0
	ExPS-90NPA-10E	Polymer precipitated		0
Block 2	HIPS-EA	Appeared to have finer nanofibres to the eye than with GPPS. Had a lower deposition than GPPS. Did not spin well.	Yes	2
	HIPS-NPA	Did not dissolve as easily as GPPS,the carbon black additive present in HIPS made it hard to observe how much had dissolved. Splashed after a few minutes of spinning. Spun well after an electrode clean.	Yes	3
	HIPS-NPA-SDS	Spun better than without the SDS additive. Splashed at the bottom of the sample rather than electrospun.	Yes	3
Block 3	GPPS-EA	Spun readily, but filaments stuck to the electrode tips, thought to be because of the high evaporation rate of the solvent used.	Yes	2
	GPPS-NPA	Seemed to dissolve easily, but was observed to cobweb when electrospun.	Yes	3
	GPPS20-NPA	Solution was too concentrated. It was possible that there was electrospraying or large fibres formed (microfibres).		2
	GPPS-NPA-0.1LiCl	No difference when spun with LiCl additive compared to no additive.	Yes	3
	GPPS-NPA-0.6LiCl	Some of the LiCl did not dissolve. Spun ok. .	Yes	3
	GPPS-NPA-TiO2	Did not electrospin well.	Yes	2
Block 4	GPPS-MEK	Electrospun well, but only on the bottom of the foil, even when belt speed was increased. Solvent evaporated too fast.	Yes	2
	GPPS-NPA-MEK-TiO2	Approximately 1% TiO_2. Some solution splashed off the tips and some cobwebbing occured, but overall it seemed to spin better than 100% nPA solution	Yes	2
	GPPS-DMF	Too concentrated. Splashing and formation of large fibrous webs meant the tips fouled up too quickly.		0
	GPPS10-DMF	Very short spinning distance. Not as fibrous as GPPS-DMF, however some cobwebbing was observed. Possibly this solution had low conductivity.	Yes	1
	GPPS10-DMF-0.05LiCl	Low packing density of fibres and fast build up on tips. No improvement was observed when LiCl was added. Possibly large fibres were formed.	Yes	2
	GPPS-NPA-2PSS	Spun similar to previous GPPS solutions. PSS stayed as particles rather than dissolved (a suspension was created).	Yes	2
Block 5	GPPS-NPA-1Citric	Very little cobwebbing was observed compared to 15% GPPS in 100%nPA + 2% Ammonium acetate solution. Was an improvement upon 15% GPPS in 100% nPA solution. There was also a higher deposition rate observed.	Yes	4
	GPPS-NPA-2AmmA	This solution was mixed at 40 °C until as much as possible could be dissolved. Cobwebs between electrode tips when the solution was electrospun. Low deposition.		2
	GPPS-NPA-2AA	Polymer precipitated when acetic acid was added, but seemed to dissolve after the solution was mixed. Good deposition rate was observed and the electrode tips did not clog. However some filaments did adhere to the tips.	Yes	4
	GPPS-NPA-2FA	Polymer precipitated.	No	0
	GPPS-NPA-3AA	Polymer precipitated and but seemed to dissolve after it was mixed. Spun well, was not sure if the solution spun better than GPPS-NPA-2AA.	Yes	4
	GPPS-NPA-4AA	Very little whipping motion was observed when this solution was spun. The electrode tips clogged and the solution did not spin as well as GPPS-NPA-3AA.	Yes	2

It can be seen from the first three blocks that the solutions trialled with the three grades of polystyrene did not have high ratings, which was mostly due to problems such as filaments (long strands of nanofibre) which stuck to the electrodes and did not land on the collector, and low production rates.

It was also found that additives such as LiCl, SDS and TiO_2 did not provide significant improvement. SEM analysis confirmed that the electrospinning trials did however produce fibres (see Figure 3.12 - Figure 3.16). It is interesting to note that the GPPS nanofibres produced from GPPS-NPA seemed to have a rough surface (Figure 3.13).
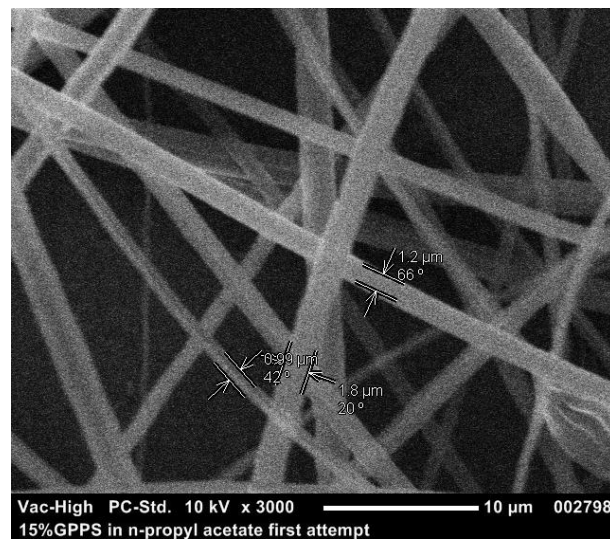
Figure 3.12: GPPS nanofibres from GPPS-NPA trial. It can be seen that the fibres had a large diameter.
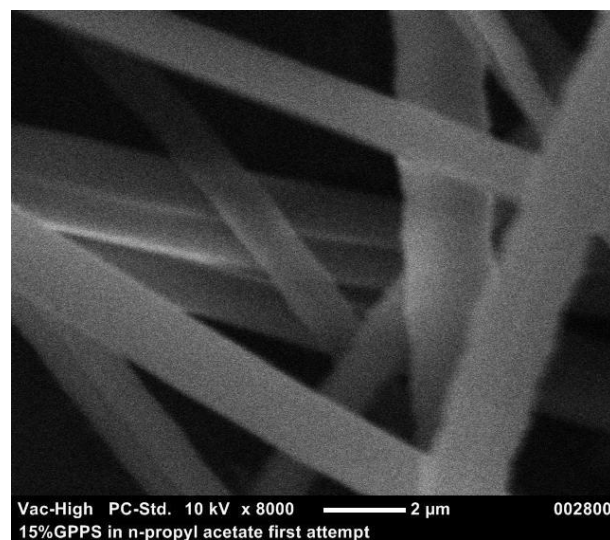
Figure 3.13: GPPS nanofibres from GPPS-NPA trial. A rough fibre surface can be seen.
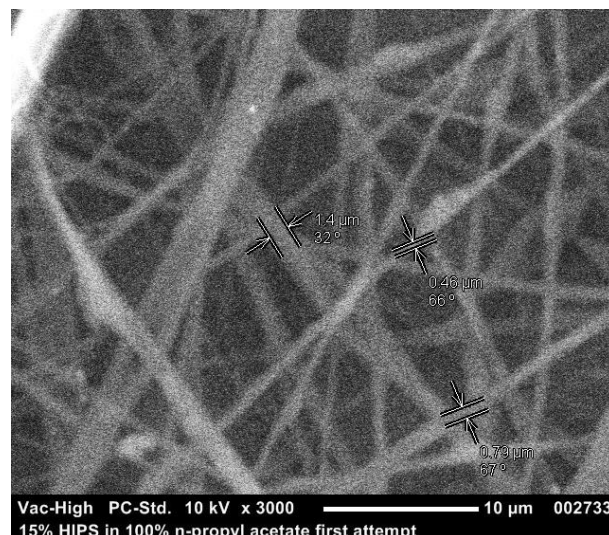
Figure 3.14: HIPS nanofibres from HIPS-NPA trial. Some beads were present.

The HIPS mat (see Figure 3.16) had low deposition, a high range of nanofibre sizes and more beading than the GPPS mat (shown in Figure 3.15), even though the two trials used the same solvent. Thus GPPS was chosen to be further investigated out of all of the grades of PS as GPPS solutions produced a higher quality mat. GPPS also had the least amount of additives in it compared to the other two grades used (the carbon black additive in HIPS made it hard to observe whether the polymer was completely dissolved).
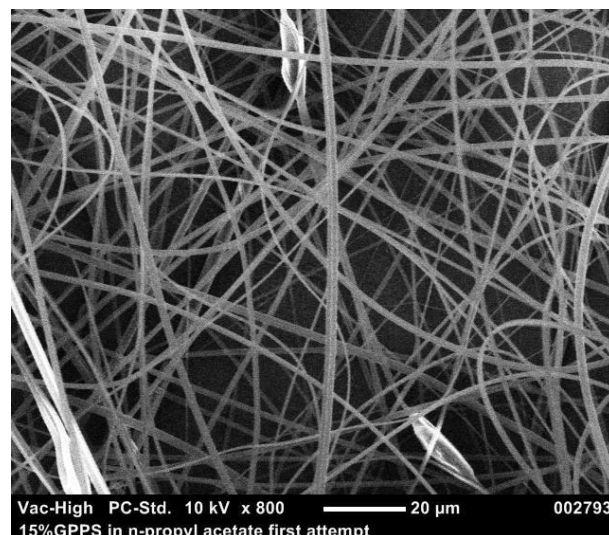
Figure 3.15: GPPS nanofibres from GPPS-NPA solution at 800 x magnification.

Vac-High   PC-Std.   10 kV   x 800   ————— 20 μm   002729
15% HIPS in 100% n-propyl acetate first attempt

Figure 3.16: Low quality mat of HIPS nanofibres produced from HIPS-NPA at 800 x magnification. It can be seen that there is a low deposition and high range of nanofibre sizes, along with some beading.

Block four of Table 3.11 shows results from trials using GPPS and solvents that posed health and safety concerns, which were undertaken to investigate whether the choice of solvents was affecting the ability of the polymer to spin. However, it seems that the use of these solvents did not improve the electrospinning ability of GPPS compared to the other solvents used previously.

It is noted that the solvents trialled with PS in blocks 1 - 4 (see Table 3.11) were either non-polar aprotic, or polar aprotic solvents (refer to Table 2.3). Therefore additives thought to increase the number of protons in solution were investigated in order to see if the electrospinning ability of GPPS was improved (see Table 2.12 and block five of Table 3.11). The additives trialled were ammonium acetate, an electrospray ionisation mass spectrometry (EIS) additive (see Section 1.3), citric acid powder, formic acid (FA), and acetic acid (AA). It was found that minimal citric acid and ammonium acetate were able to be dissolved in the solution, even when the solution was mixed and heated. From the electrospinning results shown in block five of Table 3.11, it seems that addition of citric acid as well as a small amount of AA improved the electrospinning of GPPS. It was also found that there was a peak amount of AA that could be added to the solution before it became detrimental to the electrospinning. The addition of FA however was found to be unsuccessful as the polymer precipitated when the acid was added.

91

SEM images revealed that GPPS-NPA-2AmmA, GPPS-NPA-1citric and GPPS-NPA with acetic acid all produced fibres, as shown in Figure 3.17, Figure 3.18 and Figure 3.19.
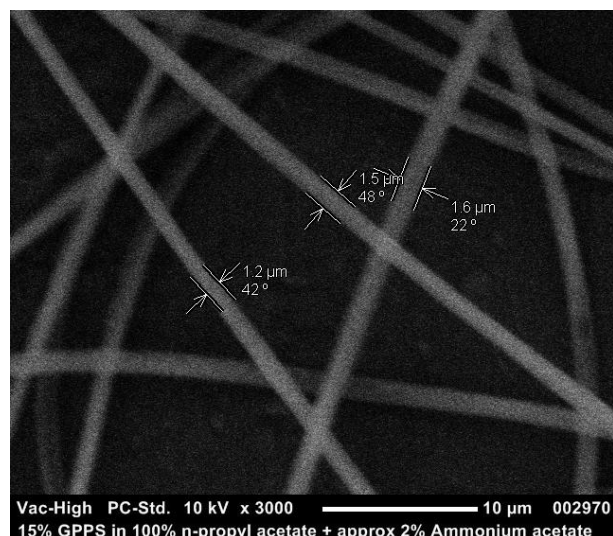
Figure 3.17: GPPS fibres produced from GPPS-NPA-2AmmA.
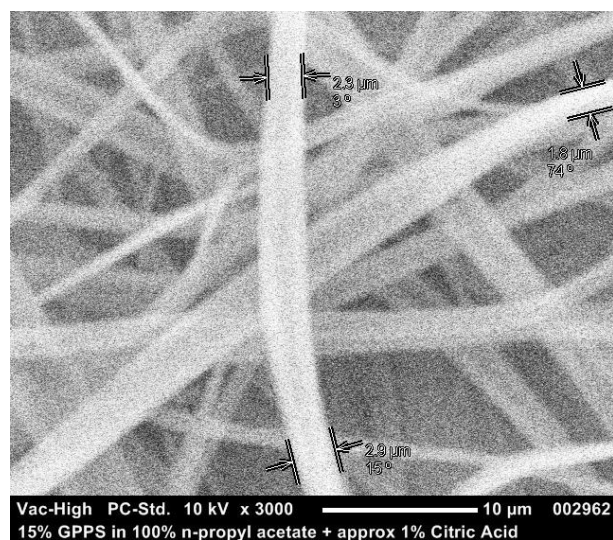
Figure 3.18: GPPS fibres from GPPS-NPA-1citric solution. It is hard to tell whether the fibres produced were ribbons or just very large fibres.
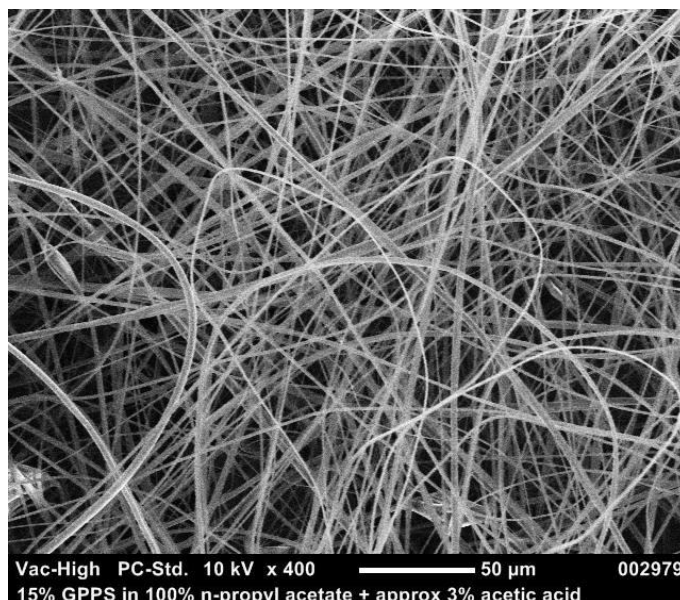
Figure 3.19: GPPS fibres produced from GPPS-NPA-3AA.

3.1.6.1 Medium scale trials

Of the trials with the highest ratings (4), GPPS-NPA-3AA was chosen to be trialled on the medium scale machine. GPPS-NPA-1Citric was not chosen to be trialled because of the difficulty in dissolving citric acid. GPPS-NPA-2AA was not selected to be trialled due to time constraints. Results for the GPPS-NPA-3AA medium scale trials are shown below in Table 3.13 and general properties of the solution spun on the medium scale machine are shown in Table 3.12. It can be seen that the addition of acetic acid increased the conductivity.

Table 3.12: General properties of the GPPS-NPA-3AA solution.

General Properties			
	Surface Tension	Conductivity (µS/cm)	Test Temp (°C)
GPPS-NPA-3AA (before acetic added)	24.18	0	20.8
GPPS-NPA-3AA (after acetic added)	-	0.1	20.8

Table 3.13: Results for Chameleon trials of GPPS-NPA-3AA.

Run #	Abbreviation					Observations	Fibres	Rating
1	GPPS-NPA-3AA	■	■	■	■	Filaments did not land properly. Noticed very little whipping motion and lots of sparking between collector and electrodes.	Yes	3
2	GPPS-NPA-3AA	■	■	■	■	Filaments did not land properly. Noticed very little whipping motion and some sparking, even with lower voltage and increased spinning distance.	Yes	3
3	GPPS-NPA-3AA	■	■	■	■	Filaments did not land properly. Noticed very little whipping motion and some cobwebbing occurred when the spinning distance increased. Very low deposition of nanofibre was observed.	Yes	3
4	GPPS-NPA-3AA	■	■	■	■	Filaments did not land properly. Noticed very little whipping motion, and some cobwebbing occurred at increased spinning distance. Very low deposition of nanofibre was observed.	Yes	3
5	GPPS-NPA-3AA	■	■	■	■	Changed spinning distance. Low deposition of nanofibre in middle of the substrate was observed.	Yes	3
6	GPPS-NPA-3AA	■	■	■	▌	Changed voltage. Low deposition of nanofibre in middle of the substrate was observed.	Yes	3
7	GPPS-NPA-3AA	■	■	■	■	Cobwebbing occurred. Low deposition of nanofibre was observed.	Yes	3

It can be seen from Table 3.13 that low ratings were given for the spinning of GPPS-NPA-3AA, despite the trial having a higher rating when spun on the laboratory scale electrospinning machine. The low ratings were given because of the low nanofibre deposition and because fibres were not landing on the collector. It was found that the collector and electrode voltage could not be increased as sparking occurred, even at increased spinning distance between the collector and the electrode (i.e. a low bed height). Due to time constraints and solvent availability, this polymer was not investigated further in this research.

Further recommendations for research include investigating the use of soluble additives as well as a solvent or solvent blend with a suitable vapour pressure which may help to prevent the fibres adhering to the electrodes and encourage the fibres to land on the collector. Another suggestion would be to trial the solutions with a pure form of polystyrene, rather than using extruder pellets, in case any additives present in the polymer granules caused production problems.

3.1.7 Polymer blend trials: PA6,6/PMMA blend (Nyplex)

It was noted that both the PMMA solution developed earlier in this research (see Section 3.1.1) and a PA6,6 solution previously developed by Revolution Fibres Ltd ██ ██████████. So for this investigation, five ratios of PA6,6:PMMA in FA and AA were investigated and compared to the PMMA and PA6,6 only solutions. It was found from the laboratory scale trials that all solutions were able to be electrospun successfully (see Table 3.14), and displayed different nanofibre deposition rates, cohesion and packing density characteristics.

Table 3.14: Results from Skink electrospinning trials - PMMA PA6,6 blends.

Abbreviation	Observations	Fibres	Rating
PMMA	Spun for comparison, did not spin well compared to past tests, cobwebbing, poor cohesion, low packing density.	Yes	5
PA6,6	Spun for comparison, low deposition and high packing density, high cohesion between fibres. Few splashes.	Yes	5
████████	Higher deposition no splashing. Spun better than PA6,6 on skink. Good cohesion, low production rate compared to PMMA	Yes	5
████████	Lower packing density, no splashing, clean break, cohesive fibres. Low deposition rate, tips clogged up quickly. Clean break when nanofibre mat was pulled apart.	Yes	5
████	Solution separated, but was re mixed. Higher packing density but started to show a fibrous break when the nanofibre mat was pulled apart. Stirred before spun. Higher deposition rate - better than PA6,6.	Yes	5
████████	Spun better than with less PMMA. Mat was not as strong but fibres had a good deposition rate. Not 'lofty', had good cohesion, and started to fibrous break when the nanofibre mat was pulled apart.	Yes	5
████████	Had higher deposition rate than lower amounts of PMMA. Fibre pullout when nanofibre mat was pulled apart. Very fibrous break, poor cohesion, but not too 'lofty'.	Yes	5

The blends produced nanofibres which had a diameter of 300 - 400 nm (see below in Figure 3.20, Figure 3.21 and Figure 3.22). All blends were given a rating of five, and were suitable for trialling on the medium scale electrospinning machine
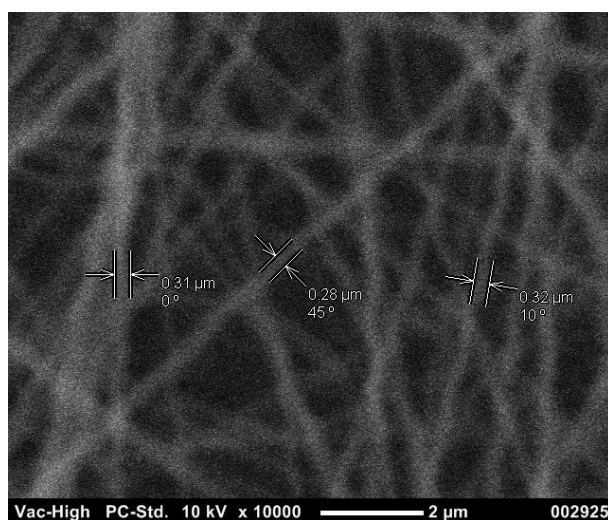
Figure 3.20: PA6,6/PMMA nanofibres produced from ████████████████.
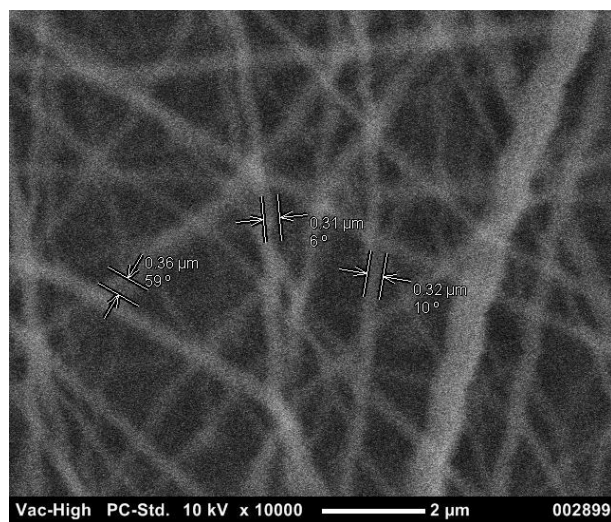
Figure 3.21: PA6,6/PMMA nanofibres produced from ██████████████.
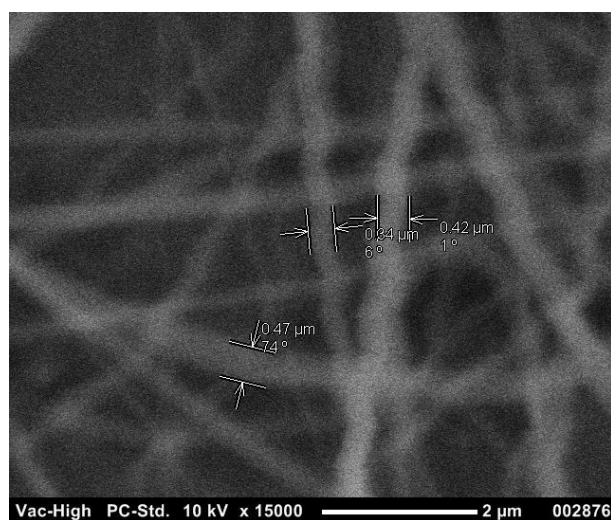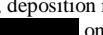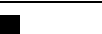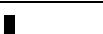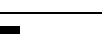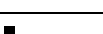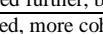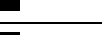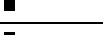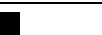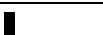
Figure 3.22: PA6,6/PMMA nanofibres produced from ██████████████.
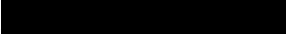
3.1.7.1 Medium scale trials

The key parameters and results for the medium scale trial runs are shown in Table 3.15.

Table 3.15: PA6,6 PMMA blend trials ██████████████████

	Abbreviation	██	██	Observations	Fibres	Rating
First Run	PA6,6	██	██	Cohesive mat, spun well.	Yes	5
	████████████	██	██	Cohesive, deposition rate not as good as ███████ only	Yes	5
	████████████	██	██	Not very good deposition - was not investigated further, bad quality.	Yes	4
	████████████	██	██	Cobwebbed, more cohesive than ██████ only solution.	Yes	5
	PMMA	██	██	Low packing density - 'Lofty'.	Yes	5
Second Run	████████████	██	██	Cobwebbed on tips and cobwebbed more than pure PMMA, but was less lofty and easy to peel off wax paper. Improved cohesion compared to PMMA	Yes	5
	PMMA	██	██	Very lofty poor cohesion	Yes	5
Third Run	PA6,6	██	██	Same as run 1	Yes	5
	████████████	██	██	Cobwebbed to one side, lower deposition rate.	Yes	5

From the first run of medium scale trials shown in Table 3.15, it can be seen that the most successful compositions were ████████████████████ ████. Therefore these solutions were trialled further (see second and third runs), along with the pure PMMA and PA6,6 solutions for comparison. It is noted that the PMMA solution was spun with ████████████████, to ensure a complete layer was produced. This would not have affected the overall success of the spinning of the trial.

It was found from the further trials that only ████████████████ trial showed improvement over the pure PMMA solution, as the higher packing density and higher cohesion between fibres improved the ability of the nanofibre to peel off the wax paper. This nanofibre veil was used in subsequent composite panels. The veil is referred to as 'nanoNyplex' for the remainder of the research.

3.2   Analysis of veils and composite cross sections

Analysis of the veils used for interleaving and the cross sections of the composite panels produced in this research are detailed in this section. The diameters of the fibres were calculated and the approximate width of the interlayer thickness of the composite panels produced was estimated from scanning electron microscope (SEM) imaging.

3.2.1   Veil analysis

A SEM image for each nanofibre or microfibre-only veil is shown below in Figures 3.23 - 3.30. Veils made from both nanofibres and microfibres are shown in Figures 3.31 - 3.33 (only the PA6,6 nanofibres are shown however). Generally, the fibres were evenly distributed and randomly oriented. However, nanoNyplex fibres appeared to be clumped together (or could be joined). The microtricot fibres were woven (see Figure 3.30). It is also noted that there was a 'cobweb' like structure amongst the fibres of nanoPA6,6 (Figure 3.25), and other veils containing nanoPA6,6 fibres (see Figures 3.31, 3.32 and 3.33).
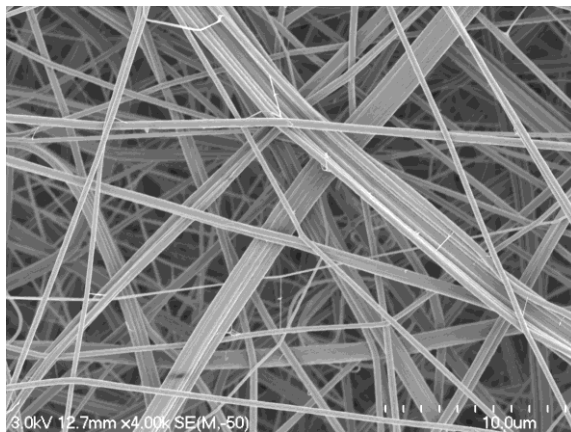
Figure 3.23: SEM image of nanoNyplex fibres at 4000x magnification.
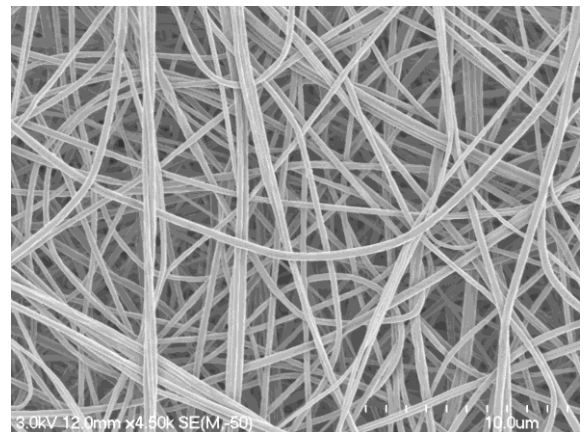
Figure 3.24: SEM image of nanoPMMA fibres at 4500x magnification.
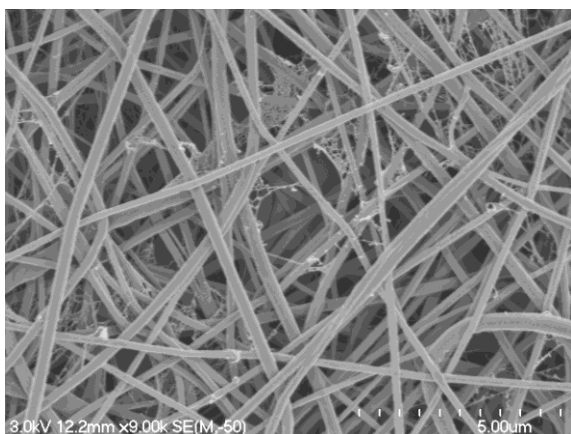
Figure 3.25: SEM image of nanoPA6,6 fibres at 9000x magnification.
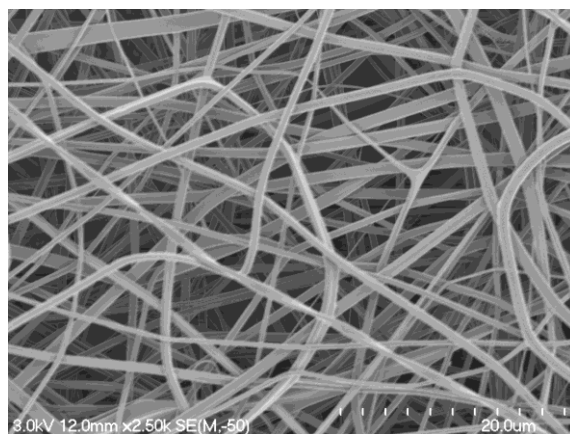
Figure 3.26: SEM image of nanoPVB fibres at 2500x magnification.
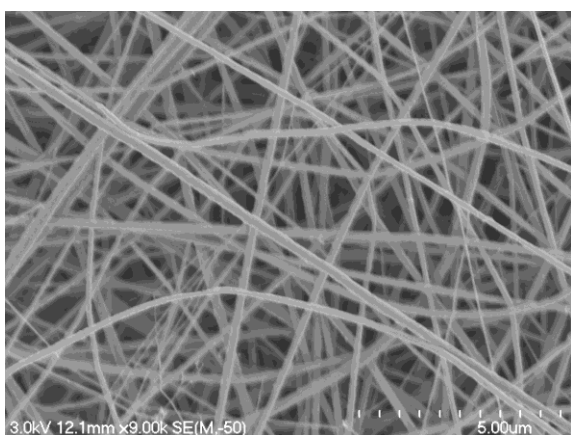
Figure 3.27: SEM image of nanoPES fibres at 9000x magnification.
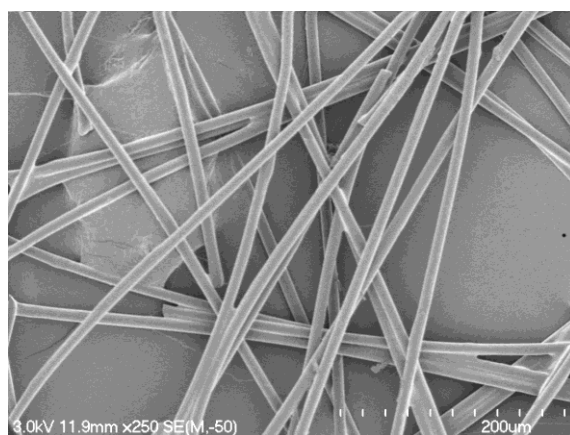
Figure 3.28: SEM image of microPPS at 250x magnification.
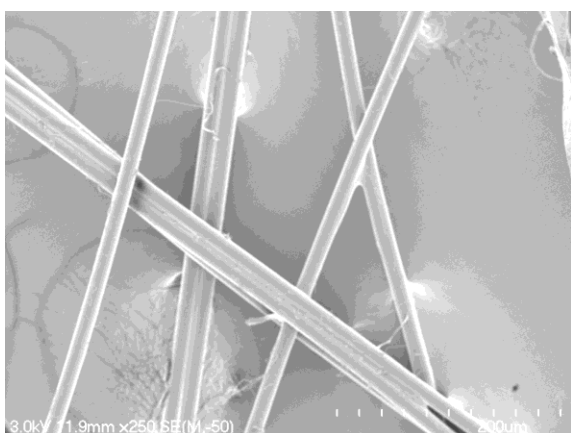
Figure 3.29: SEM image of microPEI at 250 x magnification.
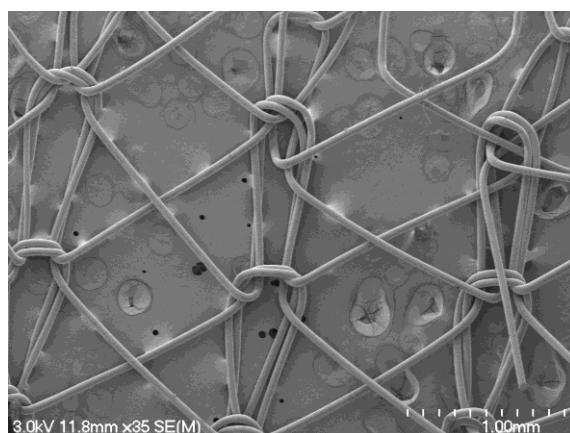
Figure 3.30: SEM image of microtricot at 35x magnification.
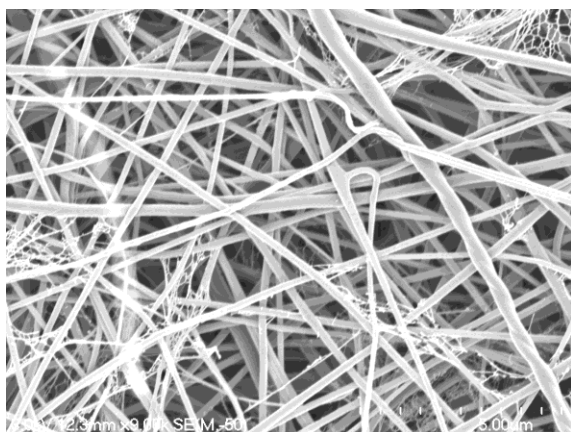
Figure 3.31: MicroPPSnanoPA6,6 veil at 9000x magnification.
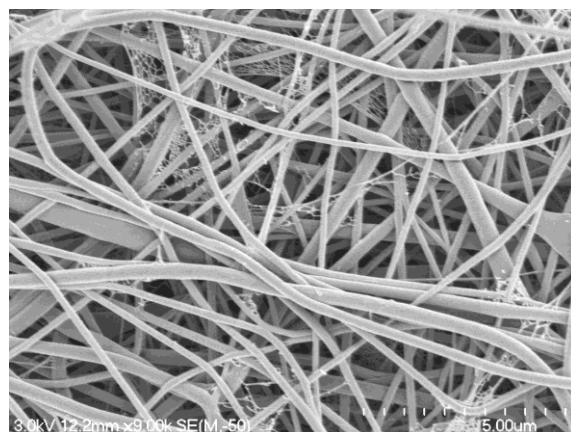
Figure 3.32: MicroPEInanoPA6,6 veil at 9000x magnification.
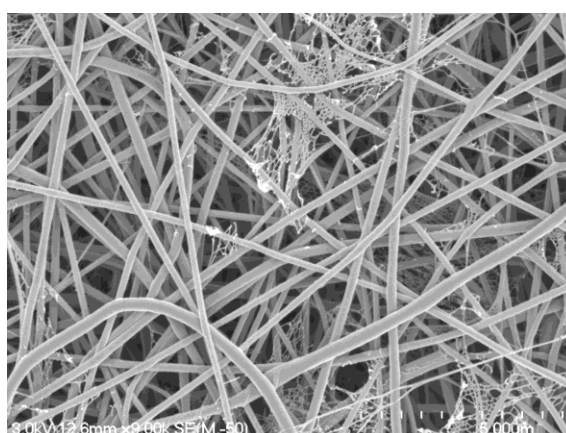
Figure 3.33: MicrotricotnanoPA6,6 veil at 9000x magnification.

3.2.1.1 Veil fibre diameter analysis

It was found that the fibres had a range of fibre diameters (see Table 3.16); the smallest average diameter nanofibre sample was nanoNyplex (0.141 μm) and the nanofibre sample with the largest diameter was nanoPVB with an average diameter of 0.651 μm. The microfibre sample with the largest diameter was microtricot, followed by microPEI and microPPS. It should be noted that for samples consisting of both nanofibre and microfibre, the average diameter was for the nanofibre content of the sample only (more information is shown in Section 6.2.1).

Table 3.16: Veil diameters.

Veil Type	Fiber Diameter (μm)			# of Measurements
	Average	Std Dev	Median	
nanoNyplex	0.141	0.070	0.138	1339
nanoPMMA	0.274	0.108	0.265	1455
nanoPA6,6	0.204	0.087	0.183	1057
nanoPVB	0.651	0.330	0.628	1097
nanoPES	0.150	0.066	0.148	1135
microPPS	9.465	1.640	9.641	429
microPEI	15.405	3.372	16.404	79
microtricot	37.627	6.802	36.807	503
microPPSnanoPA66	0.179	0.080	0.160	1197
microPEInanoPA66	0.200	0.082	0.177	1092
microtricotnanoPA66	0.173	0.062	0.163	1312

3.2.2 Panel cross section analysis

The cross sections of each of the panels were observed using a SEM (see Section 2.4) and are shown in Figures 3.34 - 3.45. It was found that no nanofibres could be seen, however, the area containing the interlayer (shown by arrows) could clearly be distinguished from the plies of carbon fibre. Of the microfibres, only microtricot fibres could be seen using the SEM. This is evident in both Figure 3.42 and Figure 3.45, in which the cross sections of the microtricot fibres can be seen in the area containing the interlayer.
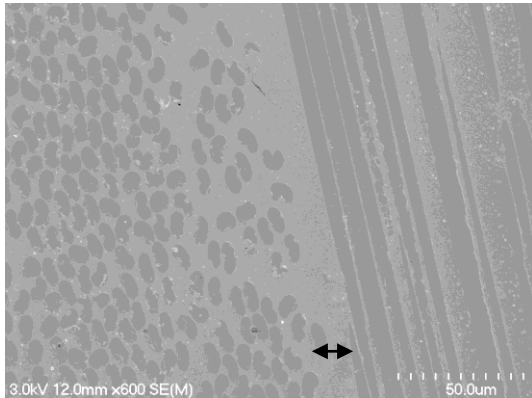
Figure 3.34: Control composite cross section (arrow indicates the interlayer region).
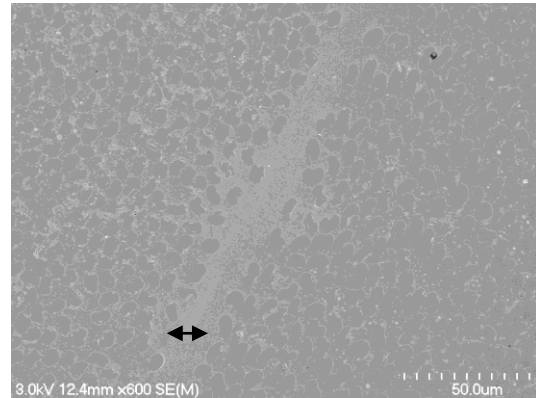
Figure 3.35: NanoNyplex interleaved composite cross section (arrow indicates the interlayer region).
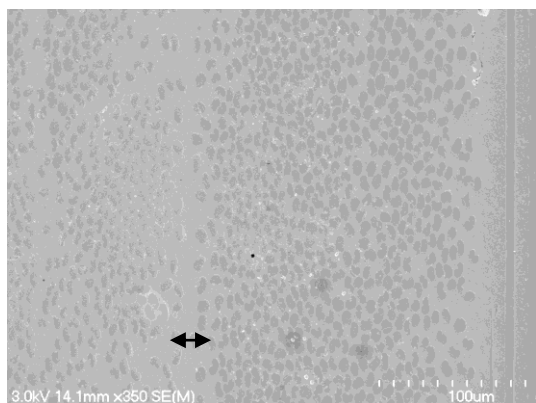
Figure 3.36: NanoPMMA interleaved composite cross section (arrow indicates the interlayer region).
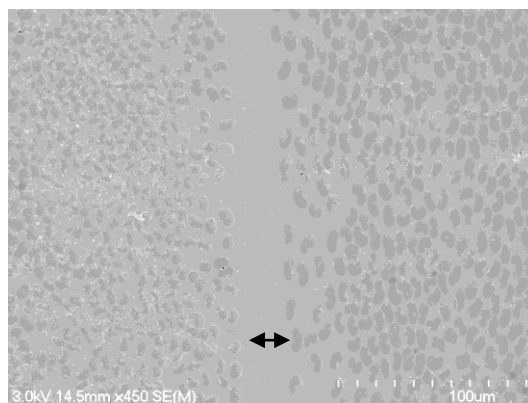
Figure 3.37: NanoPA6,6 interleaved composite cross section (arrow indicates the interlayer region).
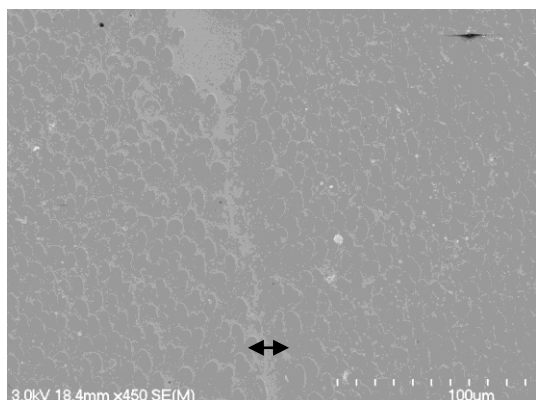
Figure 3.38: NanoPVB interleaved composite cross section (arrow indicates the interlayer region).
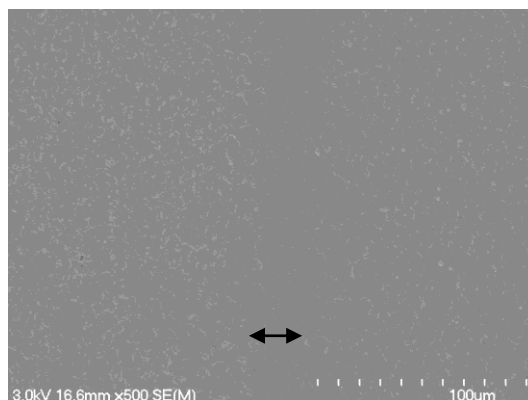
Figure 3.39: NanoPES interleaved composite cross section (arrow indicates the interlayer region).
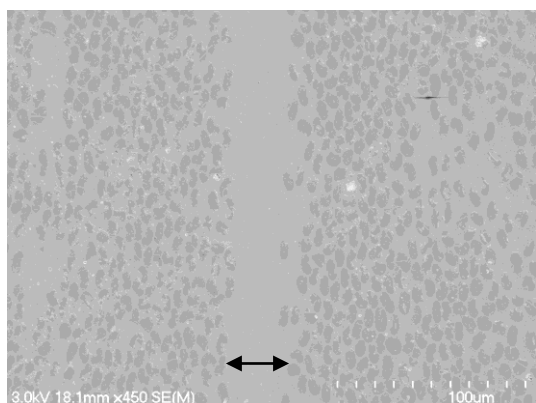
Figure 3.40: MicroPPS interleaved composite cross section (arrow indicates the interlayer region).
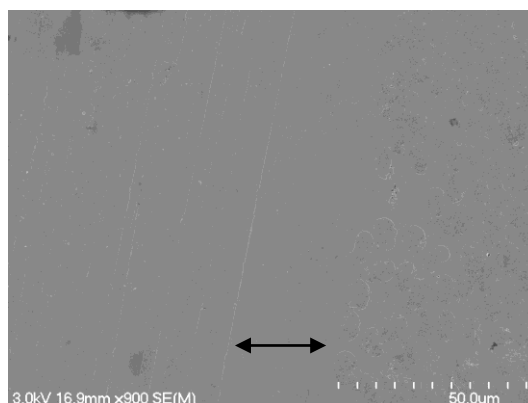
Figure 3.41: MicroPEI interleaved composite cross section (arrow indicates the interlayer region).

103
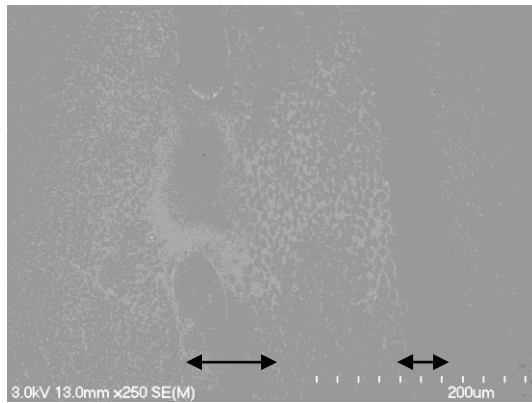
Figure 3.42: Microtricot interleaved composite cross section (arrows indicate the interlayer region).
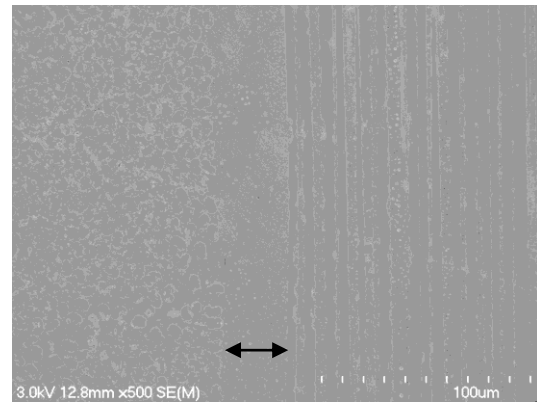
Figure 3.43: MicroPPSnanoPA6,6 interleaved composite cross section (arrow indicates the interlayer region).
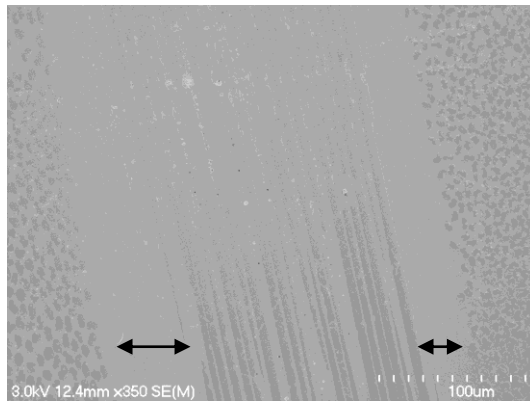
Figure 3.44: MicroPEInanoPA6,6 interleaved composite cross section (arrows indicate the interlayer region).
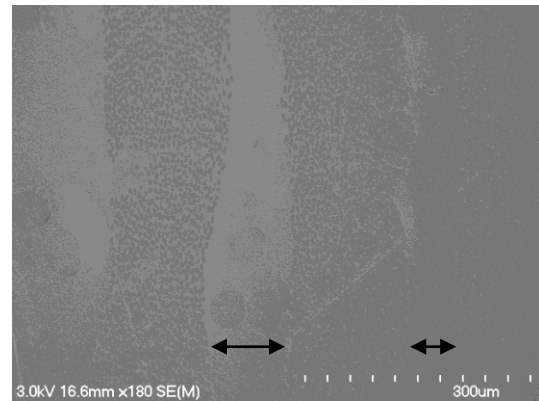
Figure 3.45: MicrotricotnanoPA6,6 interleaved composite cross section (arrows indicate the interlayer region).

3.2.2.1 Panel interlayer thicknesses

From imaging of the cross sections of each panel it was observed that there was a difference in the interlayer thickness between samples. The interlayer thickness for each specimen is shown in Table 3.17.

Table 3.17: Veil diameters and composite interlayer thicknesses.

Veil diameters and interlayer thicknesses for each resulting composite.			
Sample no	Specimen type	Composite Interlayer thickness (um)	Veil Diameter (um)
1	Control	8.2	-
2	nanoNyplex	20.3	0.141
3	nanoPMMA	11.1	0.274
4	nanoPA6,6	25.4	0.204
5	nanoPVB	20.0	0.651
12	nanoPES	24.7	0.150
6	microPPS	37.9	9.465
7	microPEI	25.5	15.405
8	microtricot	56.4	37.627
9	microPPSnanoPA66	40.8	0.179 (nanoPA6,6 diameter)
10	microPEInanoPA66	44.3	0.2 (nanoPA6,6 diameter)
11	microtricotnanoPA66	73.1	0.173 (nanoPA6,6 diameter)

The thicknesses of the interlayer region for interleaved samples were significantly larger than the control specimen with no interleaving (see Table 3.17) and all samples interleaved with microfibres (or a combination of microfibres and nanofibres) had a larger interlayer thickness than specimens with nanofibre only (see Table 3.17 and Figure 3.46).
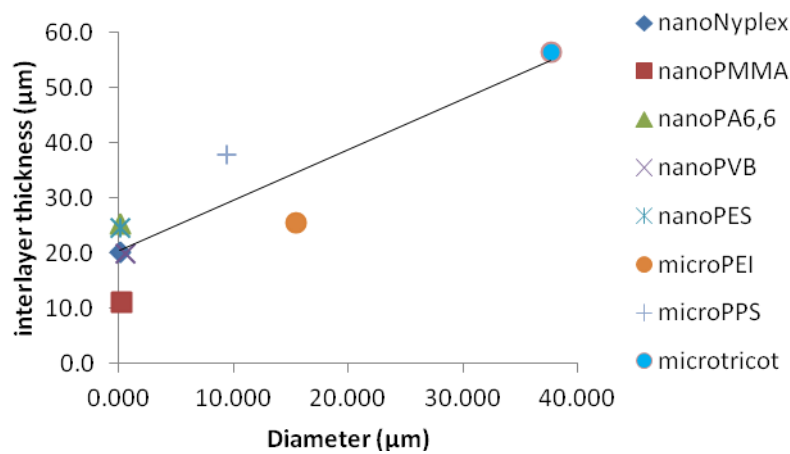
Figure 3.46: Interlayer thickness vs. diameter for microfibre and nanofibre only samples.

It can also be seen in Figure 3.47 that within the nanofibre only interleaved samples there was no relationship between diameter of the nanofibre and interlayer thickness. However, with microfibre interleaved samples it seemed that the larger the diameter the larger the interlayer thickness (shown in Figure 3.48).
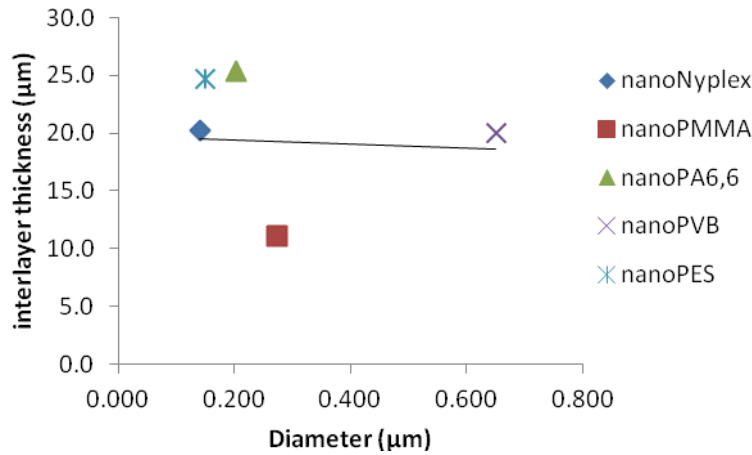
Figure 3.47: Interlayer thickness vs. diameter for nanofibre only samples.
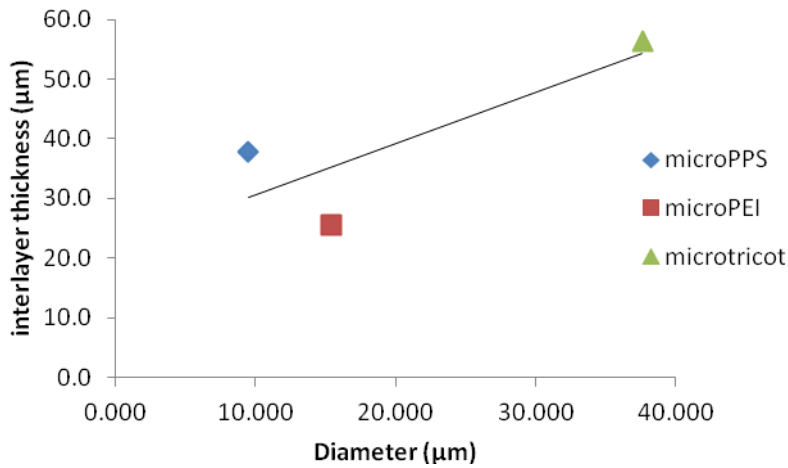
Figure 3.48: Interlayer thickness vs. diameter for microfibre only interleaved samples.

However, the interlayer thickness could depend on the areal weight of the veils. A table of areal weights of each veil is given in Table 2.27. Nanofibre areal weights were lower than the microfibre or microfibre and nanofibre veils. A graph of interlayer thickness vs. areal weight is given in Figure 3.49.

106
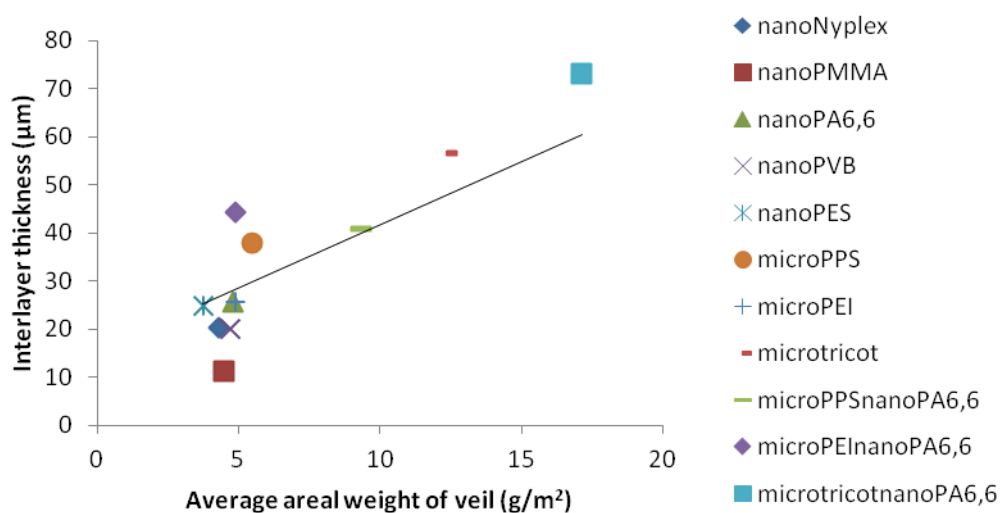
Figure 3.49: Interlayer thickness vs. areal weight of veil.
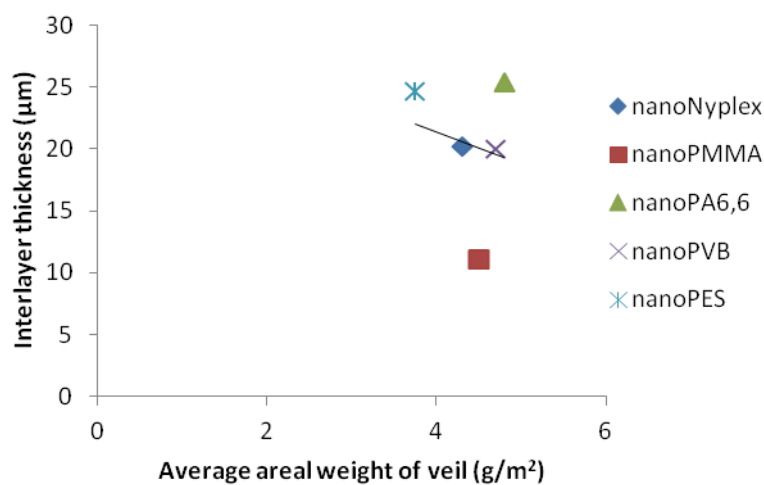
Figure 3.50: Interlayer thickness vs. areal weight of veil for nanofibre only veils.

From Figure 3.49, it can be seen that overall there was an increase in interlayer thickness as the areal weight of the interleaving veil increased. However, from Figure 3.50 there was no clear correlation between the areal weight and interlayer thickness for the nanofibre-only samples.

3.3 Vibration damping studies using dynamic mechanical analysis

This section of research aimed to evaluate the vibration damping performance of the interleaved composites. Values for storage modulus, loss modulus and tan delta (damping ratio) were obtained for a range of frequencies, at laboratory temperature.
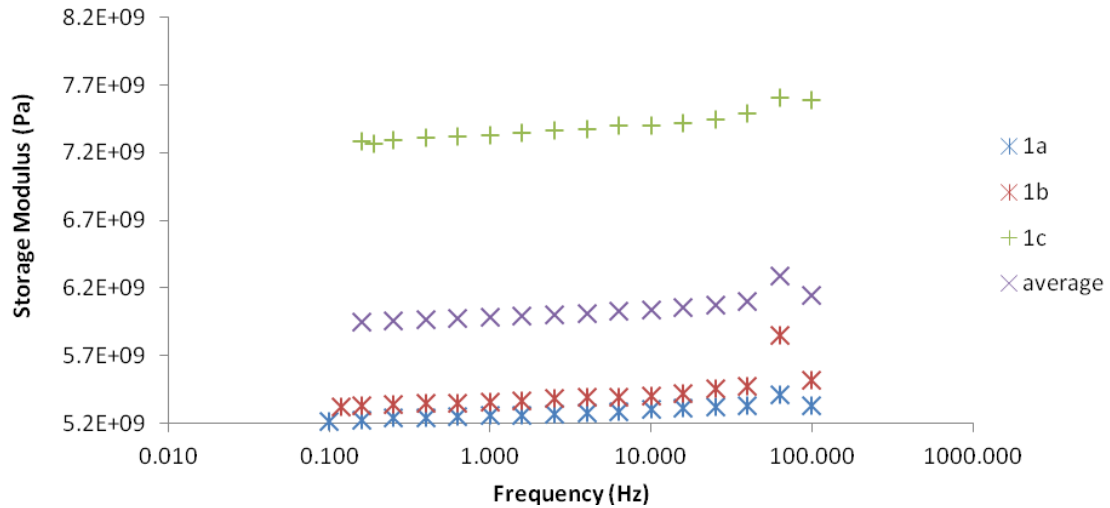
Figure 3.51: Storage modulus vs. frequency for three control specimens.

Figures 3.51, 3.52 and 3.53 show the initial results for the carbon fibre reinforced control samples. From Figure 3.51 it seems that the storage modulus generally increased slightly as the frequency increased, except for a peak at 63.1 Hz. This peak could be due to resonance as seen in the literature [62]. Resonance can result in anomalous data, including negative values, as can be seen for loss modulus (Figure 3.52) and for tan delta (Figure 3.53). There is also another variation occurring at 0.4 Hz for loss modulus and tan delta, which could also be due to the same effect.

Generally, however, the loss modulus (see Figure 3.52) appeared to decrease as the frequency increased. Overall, the tan δ (see Figure 3.53) had the same trend as loss modulus, suggesting this was more influential than storage modulus.
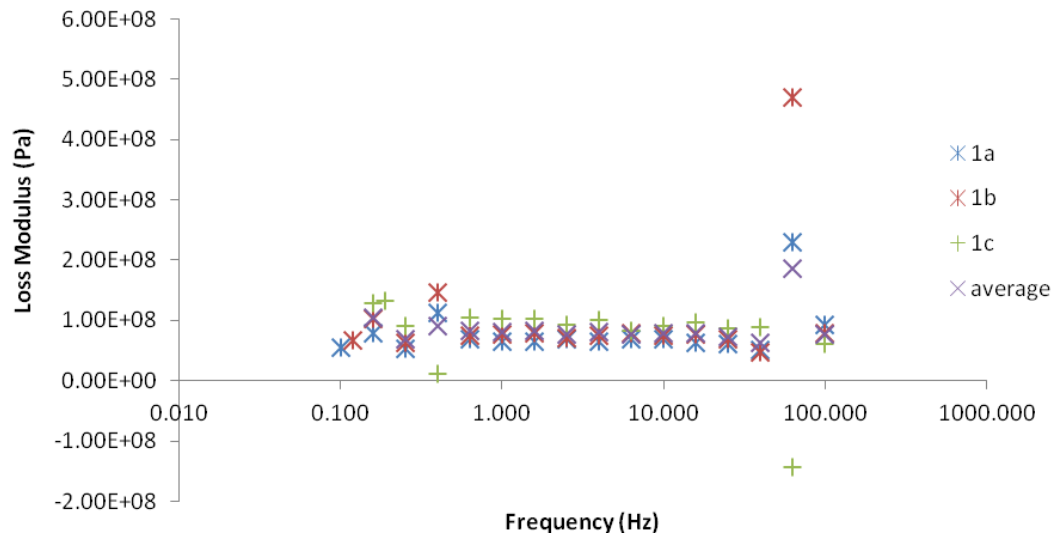
Figure 3.52: Loss modulus vs. frequency for control specimens.
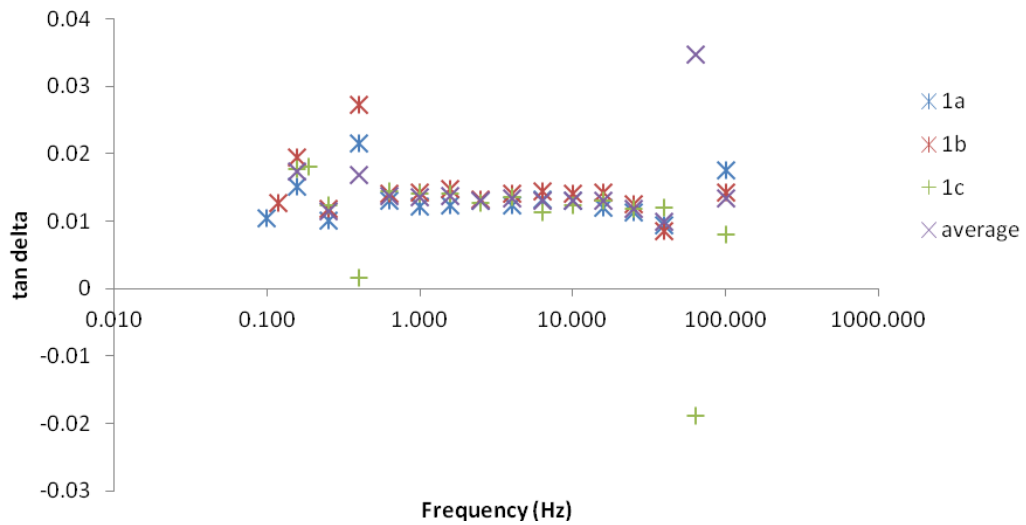
Figure 3.53: Tan delta vs. frequency for control specimens.

The variability seen between specimens for storage modulus and loss modulus was of concern with this initial data. Thus, using control specimen 1b, a study was undertaken check the reproducibility by repeating the test with the same sample (see Section 2.5 for details). It was assumed that the sample could be tested multiple times without significant change occurring within the sample. The results from this trial are shown in Figures 3.54 - 3.56.
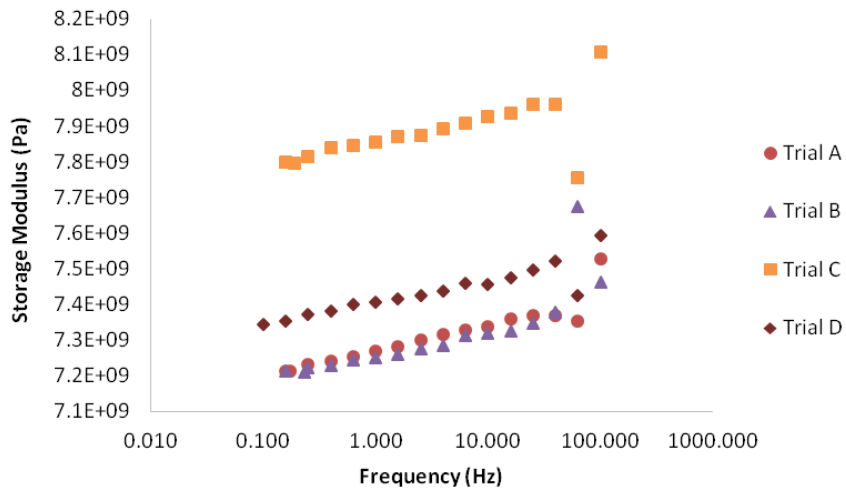
Figure 3.54: Storage modulus vs. frequency for repeatability trial.
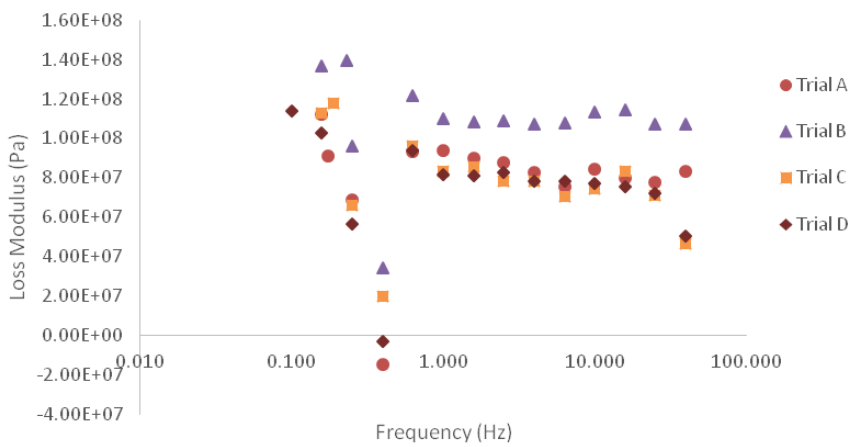
Figure 3.55: Loss modulus vs. frequency for repeatability trial.
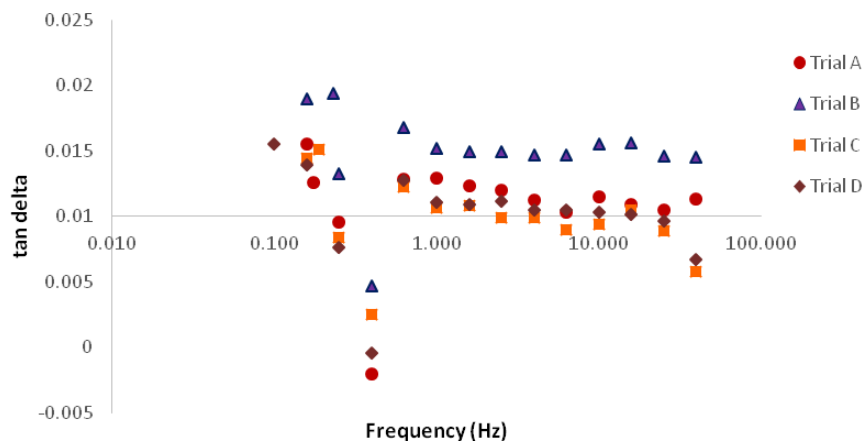
Figure 3.56: Tan delta vs. frequency for repeatability trial.

110

It can be seen that the storage modulus, loss modulus and tan delta were very similar for trials A and B, where the sample remained clamped between frequency scans. However, there was found to be a much larger difference in storage modulus between trials B, C and D, which suggested that variation could be attributed to clamping. The variation here though was not as large as the variation seen in the original tests. Temperature discrepancies during testing would be likely to be another main source of variation, as the samples were uncovered while being tested. The temperatures of the original tests are shown in Table 3.18:

Table 3.18: Original DMA tests - laboratory temperatures.

Sample #		Test Temperature (°C)	Sample #		Test Temperature (°C)
Control	1a	26.7	microPEI	7a	27.9-28
	1b	27		7b	28.65-28.75
	1c	23-23.1		7c	28.3-28.7
nanoNyplex	2a	24.1-24.3	microtricot	8a	24.9-25.5
	2b	22.7-22.9		8b	23.3-23.4
	2c	22.8-22.9		8c	25.1-25.2
nanoPMMA	3a	22.2-22.9	microPPSnanoPA6,6	9a	22.8
	3b	27.2-27.3		9b	22.8-23.3
	3c	22.8		9c	24.5-24.6
nanoPA6,6	4a	28.3	microPEInanoPA6,6	10a	29.-29.1
	4b	27.9-28.7		10b	24.1-24.3
	4c	22.8		10c	24.3
nanoPVB	5a	23.2-23.3	microtricotnanoPA6,6	11a	23.2
	5b	23.1		11b	23.5-24.4
	5c	22.9		11c	24.2-24.3
microPPS	6a	23.1-23.2	nanoPES	12a	27.5-27.6
	6b	23.7-24.3		12b	28.9
	6c	27.3-27.5		12c	24.2

There was a large amount of variation in the temperature of the laboratory, which was not expected, as the laboratory was meant to be temperature controlled. For control samples 1a and 1b the test temperature was approximately 27 °C, and the results for the similar storage modulus, loss modulus and tan delta were similar. However, sample 1c was tested at a temperature of approximately 23 °C and had different storage modulus, loss modulus and tan delta results compared to specimens 1a and 1b, which seems to suggest that the test temperature was a major source of variation in the original tests. Thus samples were re tested

111

covered at a controlled temperature, along with an untested sample for each sample type (see Section 2.5) at temperatures within 23.3 ± 0.6 °C (see Table 2.28).
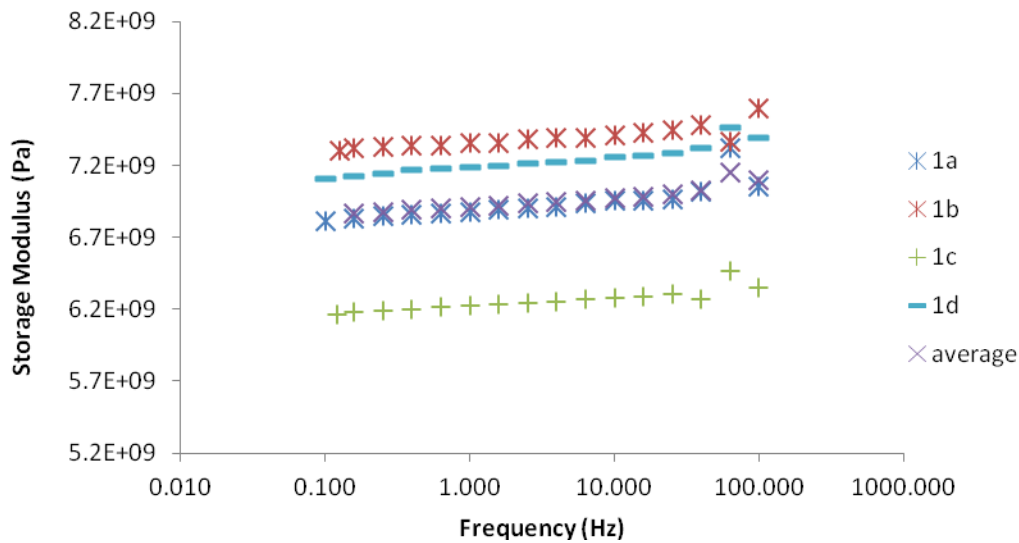
Figure 3.57: Storage modulus vs. frequency for control specimens.

From Figures 3.57, 3.58 and 3.59, it can be seen that the results for storage modulus, loss modulus and tan delta are less variable, but follow the same rends as the original tests.
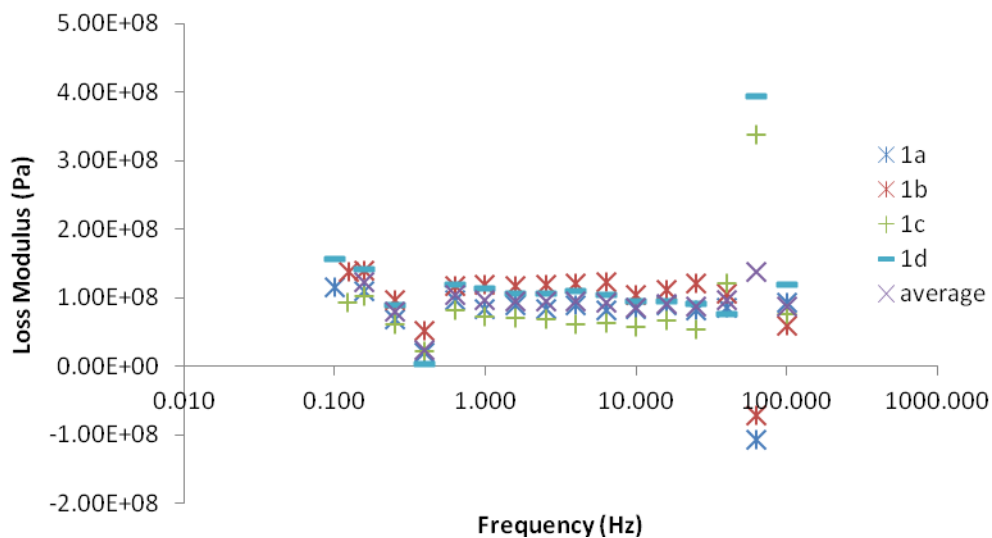
Figure 3.58: Loss modulus vs. frequency for control specimens.
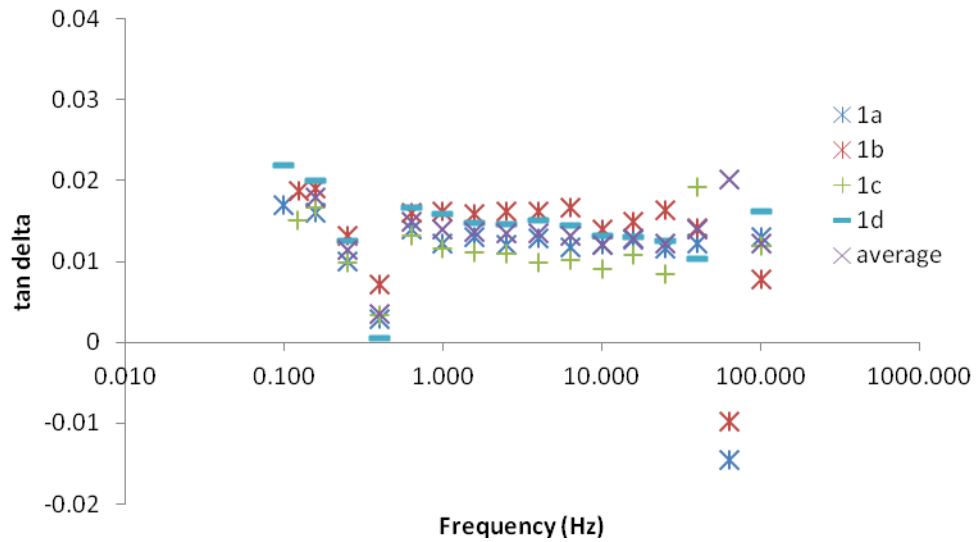
Figure 3.59: Tan delta vs. frequency for control specimens.

Results for the nanoNyplex interleaved samples are shown in Figures 3.60 - 3.62. The trends for all of the parameters studied were the same for nanoNyplex as well as the other sample types (see Section 6.3.2).
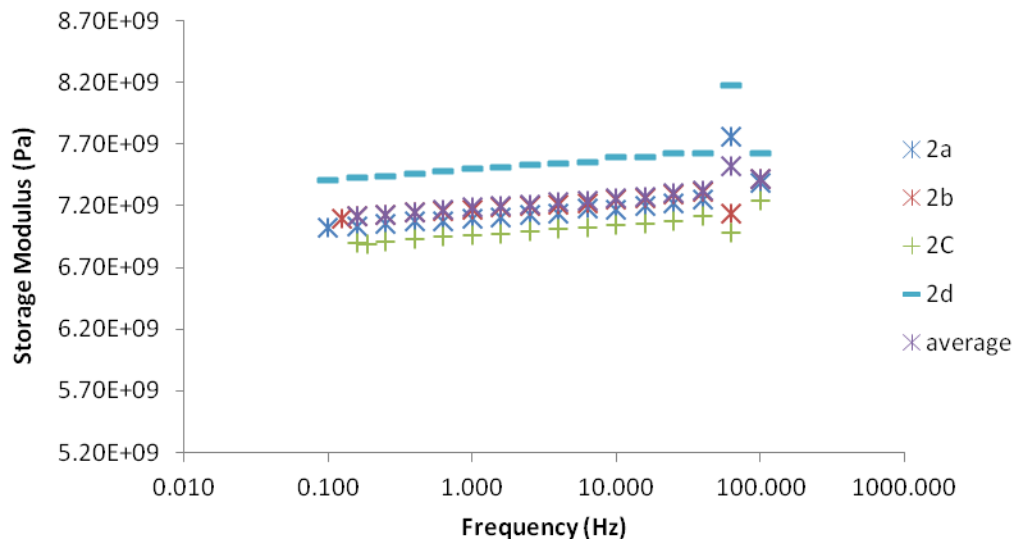
Figure 3.60: Storage modulus vs. frequency for nanoNyplex interleaved specimens.
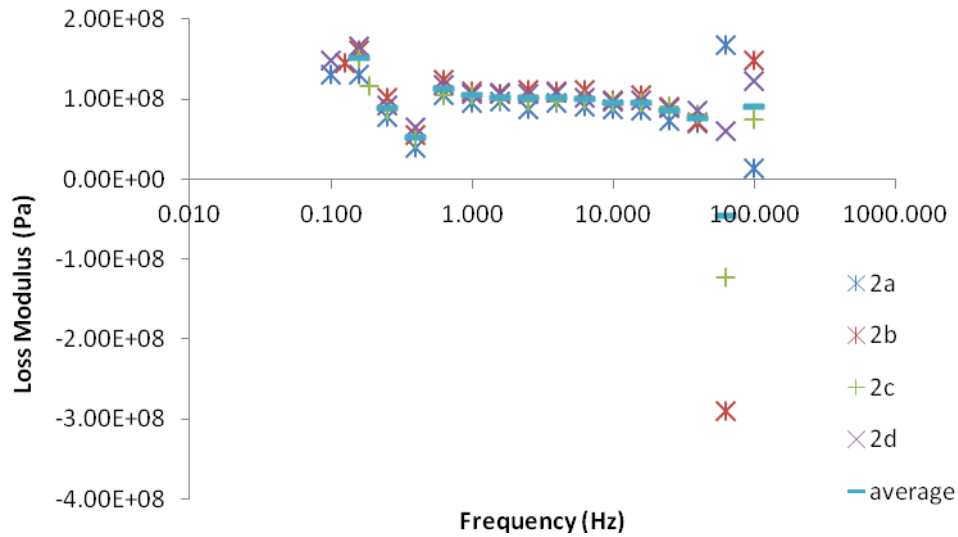
Figure 3.61: Loss modulus vs. frequency for nanoNyplex interleaved specimens.
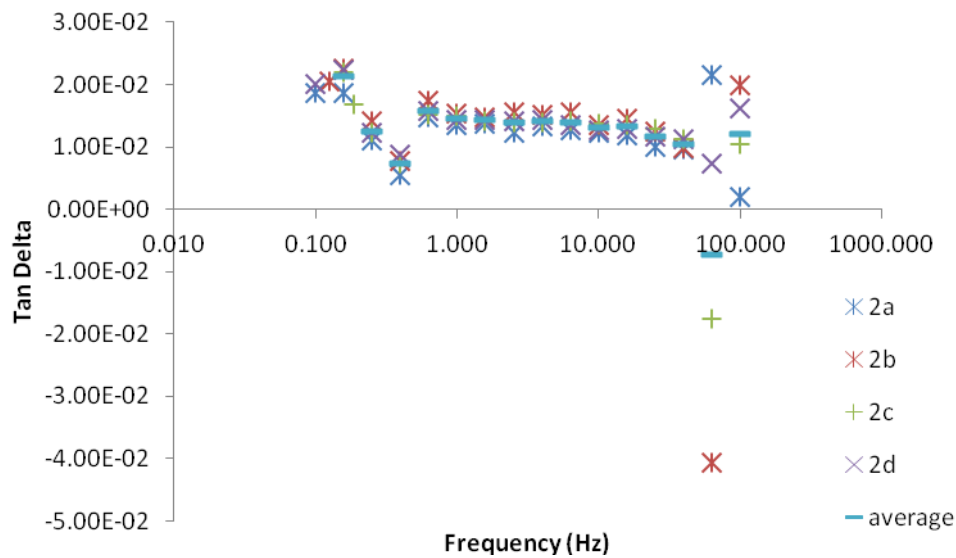
Figure 3.62: Tan delta vs. frequency for nanoNyplex interleaved specimens.

Comparison of storage modulus for all specimens (shown in Figure 3.63) shows that all interleavings, except nanoPMMA, increased the average storage modulus over the frequency range tested. NanoPA6,6 interleaved samples had the highest storage modulus out of all of the samples. Factors likely to be of influence include adhesion which is dependent on surface area and chemistry. High adhesion would limit movement of interleaving fibres [49]. It is possible that the high storage modulus for the nanoPA6,6 interleaved specimens is linked to a high degree

114

adhesion between these nanofibres and the matrix. Conversely, a lower degree of adhesion would encourage slippage between fibres and matrix and thus result in energy dissipation via friction, and result in a higher loss modulus and tan delta, rather than a high storage modulus [49]. A good degree of adhesion is likely between nanoPA6,6 interleaving fibres and the matrix, as PA6,6 has good compatibility with epoxy [33], can hydrogen bond to epoxy [63], and the veil itself has potential for good mechanical bonding (due to the cobweb type structures between the nanoPA6,6 fibres (see Section 3.2).
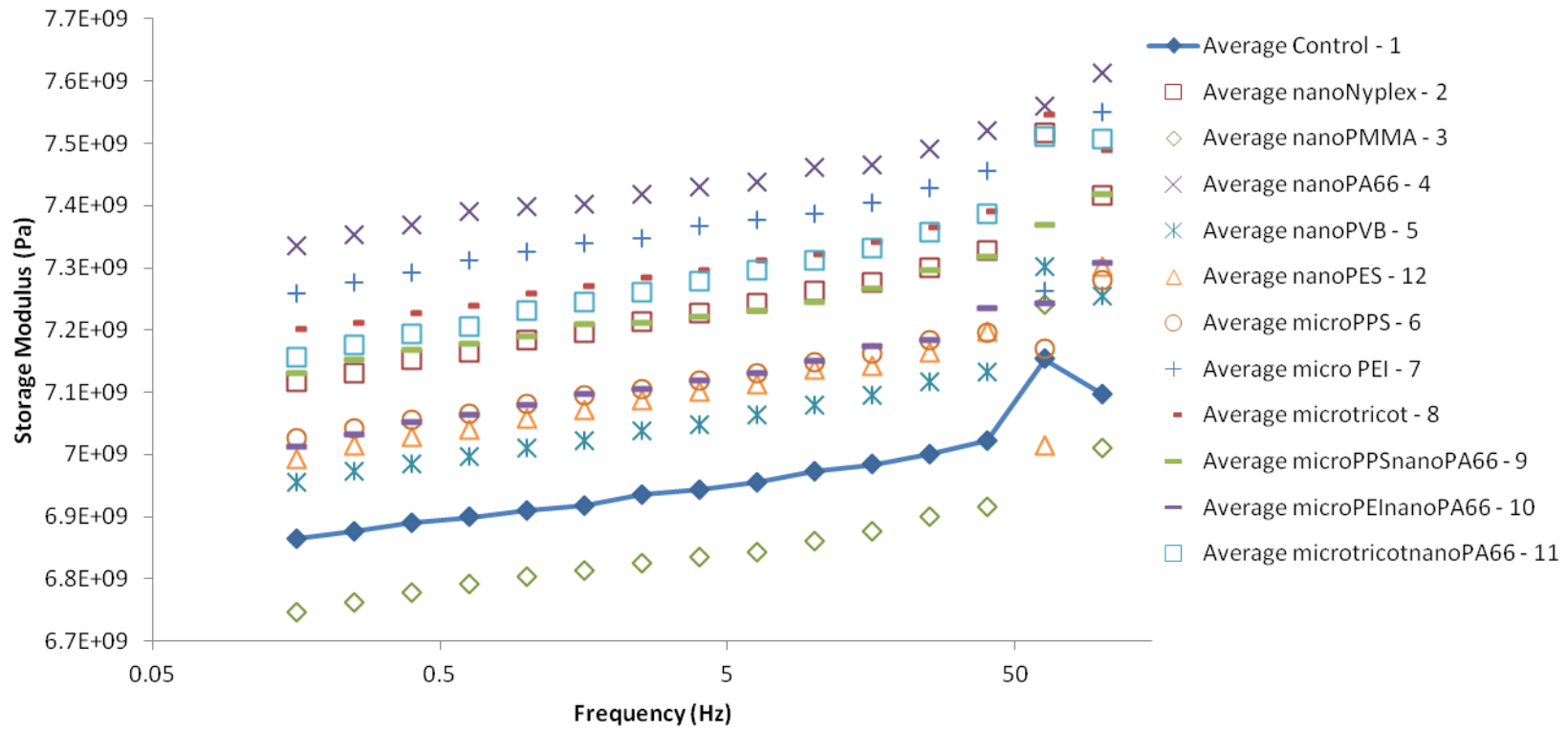
Figure 3.63: Comparison of average storage modulus vs. frequency for all specimen types.
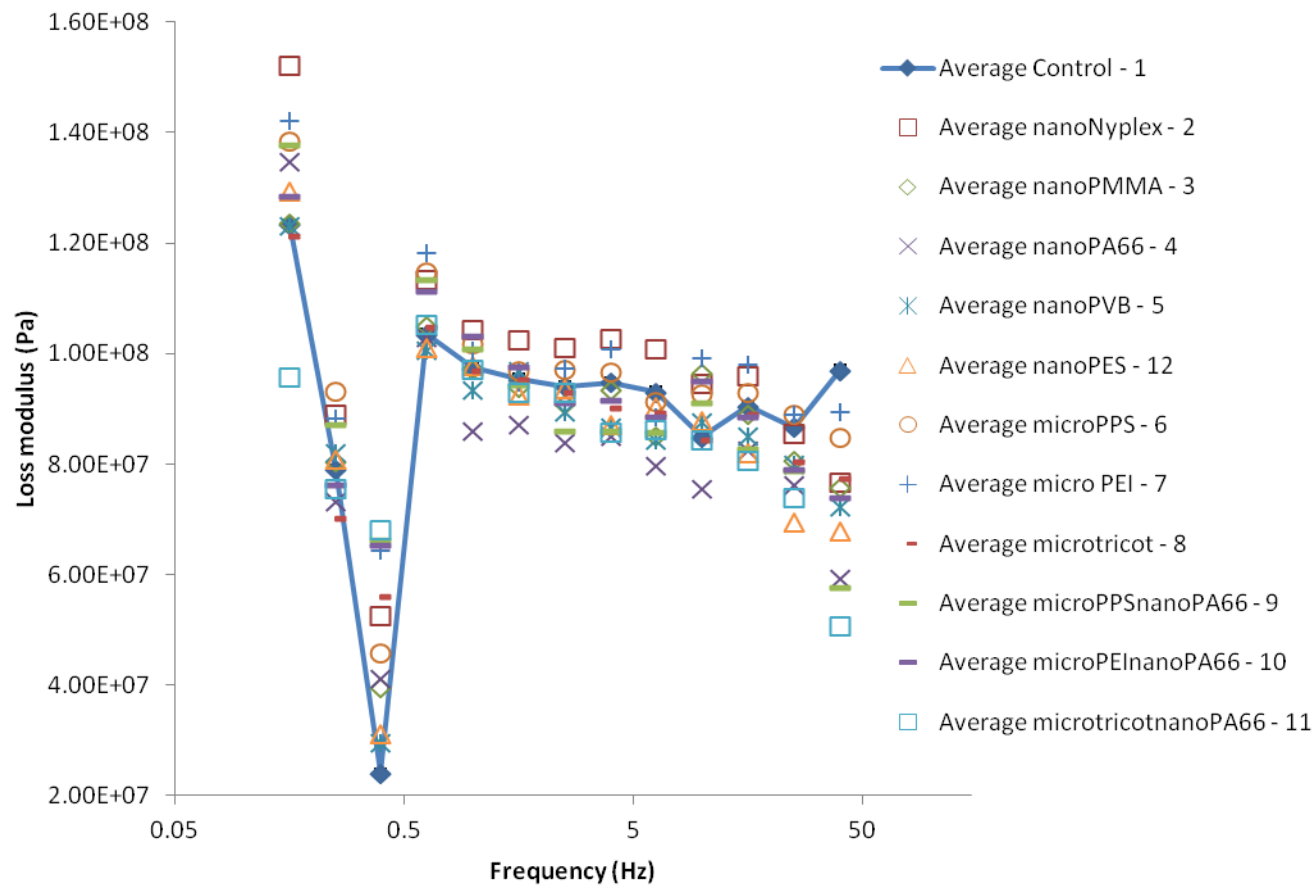
Figure 3.64: Comparison of average loss modulus vs. frequency for all specimen types, excluding 63 and 100 Hz..

Comparison of the loss modulus (see Figure 3.64) showed that nanoNyplex and microPEI interleaved samples generally appeared to have the highest loss modulus of all the specimen types tested, including the control, until a frequency of 25.1. At frequencies above 25.1 Hz, all specimens that contained interleaving veils had a loss modulus lower than (or approximately equal to) the control.

For clearer assessment, the data is split and displayed in Figure 3.65 (nanofibre only interleaved specimens) and Figure 3.66 (microfibre interleaved specimens).

Comparison of nanofibre interleavings

From Figure 3.65, it can be seen that the nanoNyplex interleaved specimens had a higher average loss modulus than any other interleaved sample for frequencies between 1.0 Hz and 6.3 Hz. In contrast, the nanoPA6,6 interleaved samples had the lowest loss modulus between 1.0 Hz and 39.8 Hz. The loss modulus of the specimens containing nanoPES, nanoPMMA or nanoPVB interleaving was similar to the control specimens. As discussed in Section 1.5.4, high loss modulus is likely to be due to energy dissipation due to a higher degree movement of interleaving fibres within the matrix. Fibres would be able to move if the adhesion between the fibres and the matrix was weak. NanoNyplex fibres (predominately PMMA) would be likely to have a lower degree of adhesion to the matrix than interleavings such as nanoPA6,6, as nanoNyplex was less likely to hydrogen bond with the epoxy than PA6,6 (PMMA had a lower hydrogen bonding Hansen parameter than PA6,6, of which the latter was also more similar to that of epoxy than PMMA - see Table 3.19). In addition, nanoNyplex was likely to have reduced mechanical adhesion as the veil fibres seemed clumped together (which would have lowered surface area available for bonding).

Table 3.19: Hansen and Hildebrand parameters for the bulk veil polymers.

| Polymer type | Hansen Parameters (MPa$^{1/2}$) | | | Hildebrand parameter δp MPa$^{1/2}$ |
	δD (Dispersion)	δP (Polarity)	δH (Hydrogen Bonding)	
PMMA	18.7	12.1	5.6	23
PA6,6	18.2	8.8	10.8	22.9
PVB	18.6	4.4	13	23.1
PES	19	11	8	23.4
PPS	18.8	4.8	6.8	20.6
PEI	17.3	5.3	4.7	18.7
Tricot (PA 6)	17	3.4	10.6	20.3
Epoxy (amine hardener)	17.4	10.5	9	22.2

* information gathered from HSPiP software [25]

118
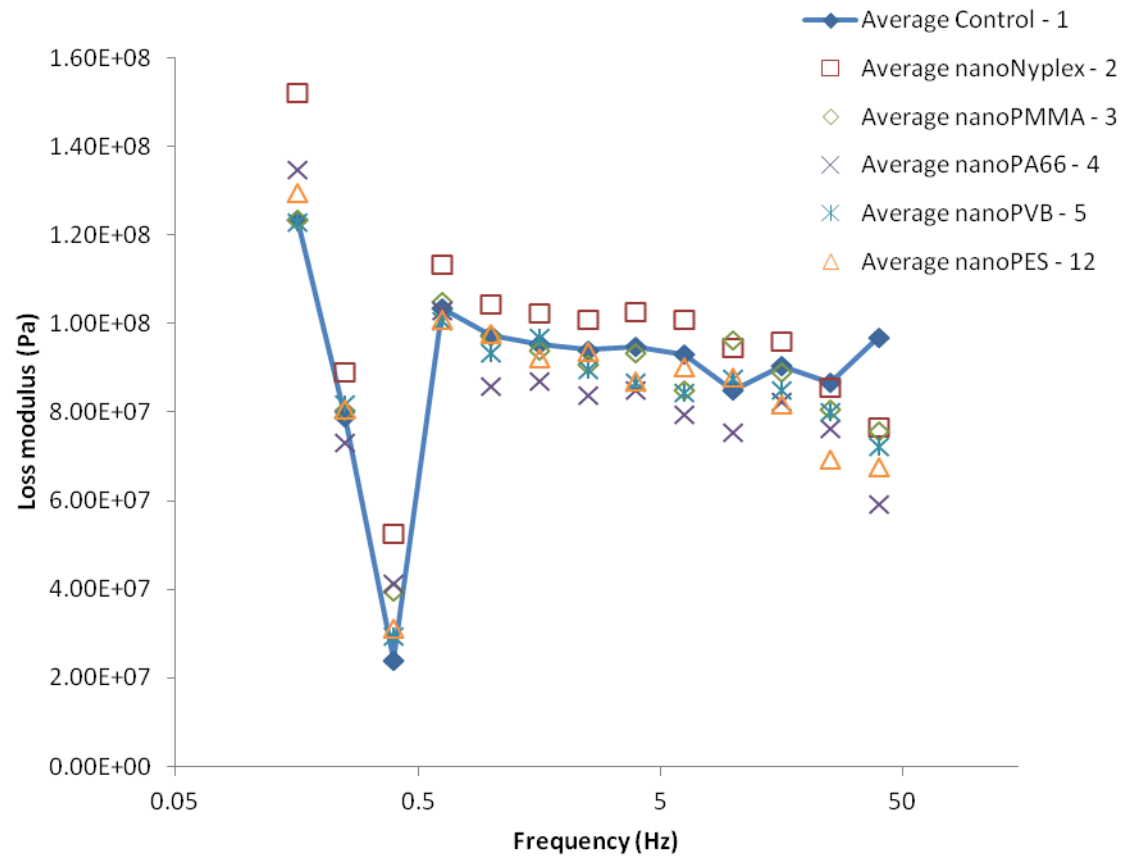
Figure 3.65: Comparison of average loss modulus vs. frequency for all nanofibre interleaved specimen types.
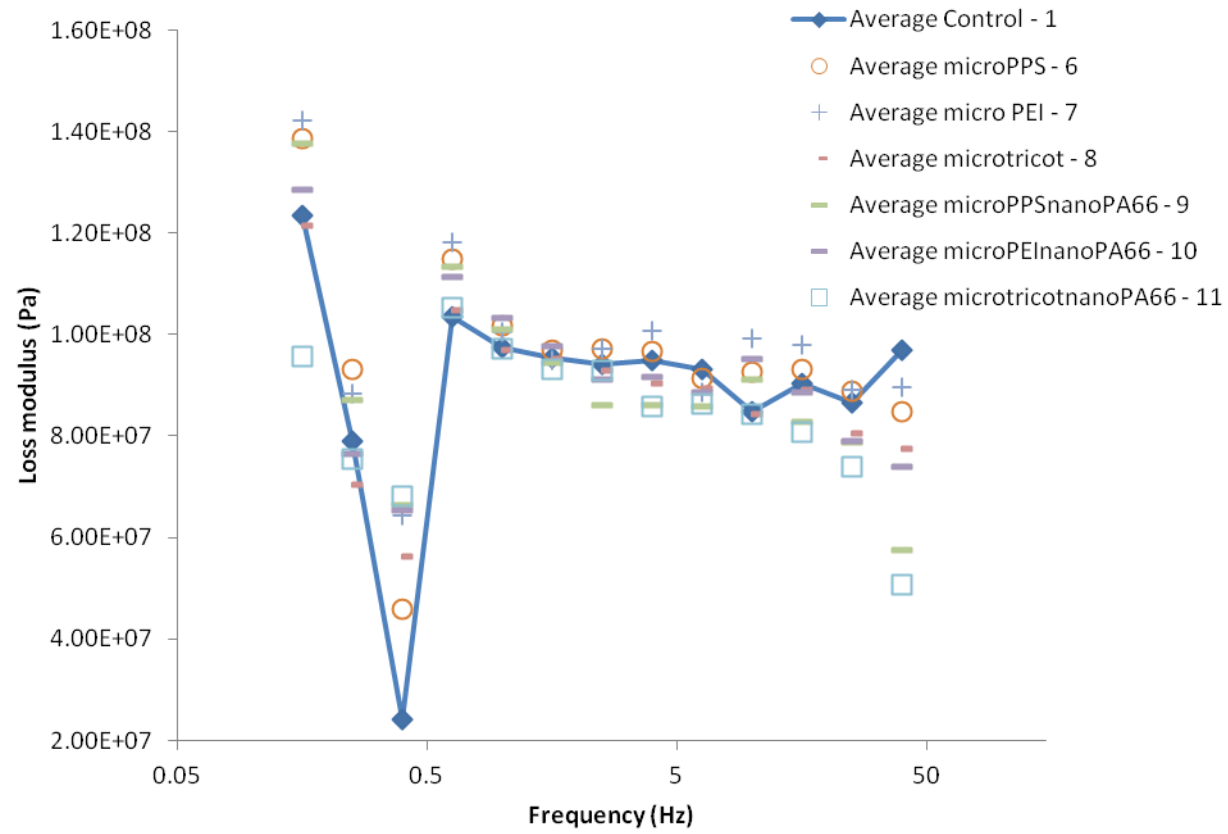
Figure 3.66: Comparison of average loss modulus vs. frequency for all microfibre interleaved specimen types.

Comparison of loss modulus for microfibre interleaved specimens

It can be seen in Figure 3.66 that generally microPPS and microPEI interleaved samples had a higher average loss modulus compared to the control. However, microtricot interleaved samples had a lower loss modulus than the control. It is likely that the microtricot (polyamide 6) fibres were bonded more strongly to epoxy than either microPPS and microPEI fibres, as although microPPS and microtricot were more likely to be compatible with the epoxy (see Hildebrand parameters shown in Table 3.19), microtricot was more likely to hydrogen bond with the epoxy, as it had a hydrogen bonding Hansen parameter similar to epoxy (see Table 3.19).

From Figure 3.66, microfibre and nanofibre combination interleavings generally had a lower loss modulus compared to the microfibre only interleavings. Thus it seems that adding PA6,6 nanofibres in conjunction with microfibre veils decreased the loss modulus, even though the potential for energy dissipation through friction should have increased due to the larger number of interfaces associated with using both veils. This has possibly been negated by strong interfacial bonding.

From comparison of tan delta (see Figures 3.67 - 3.69) it can be seen that the nanoNyplex interleaved samples and microPPS interleaved samples had a consistently higher average tan delta than the control and most other specimens from 0.2 - 15.8 Hz. However, the increase was under 10% for most frequencies, except for 0.2 and 0.4 Hz (shown in Table 3.20).

At frequencies above 25.1 Hz, the tan delta was not improved with the addition of any kind of interleaving, as found for loss modulus.
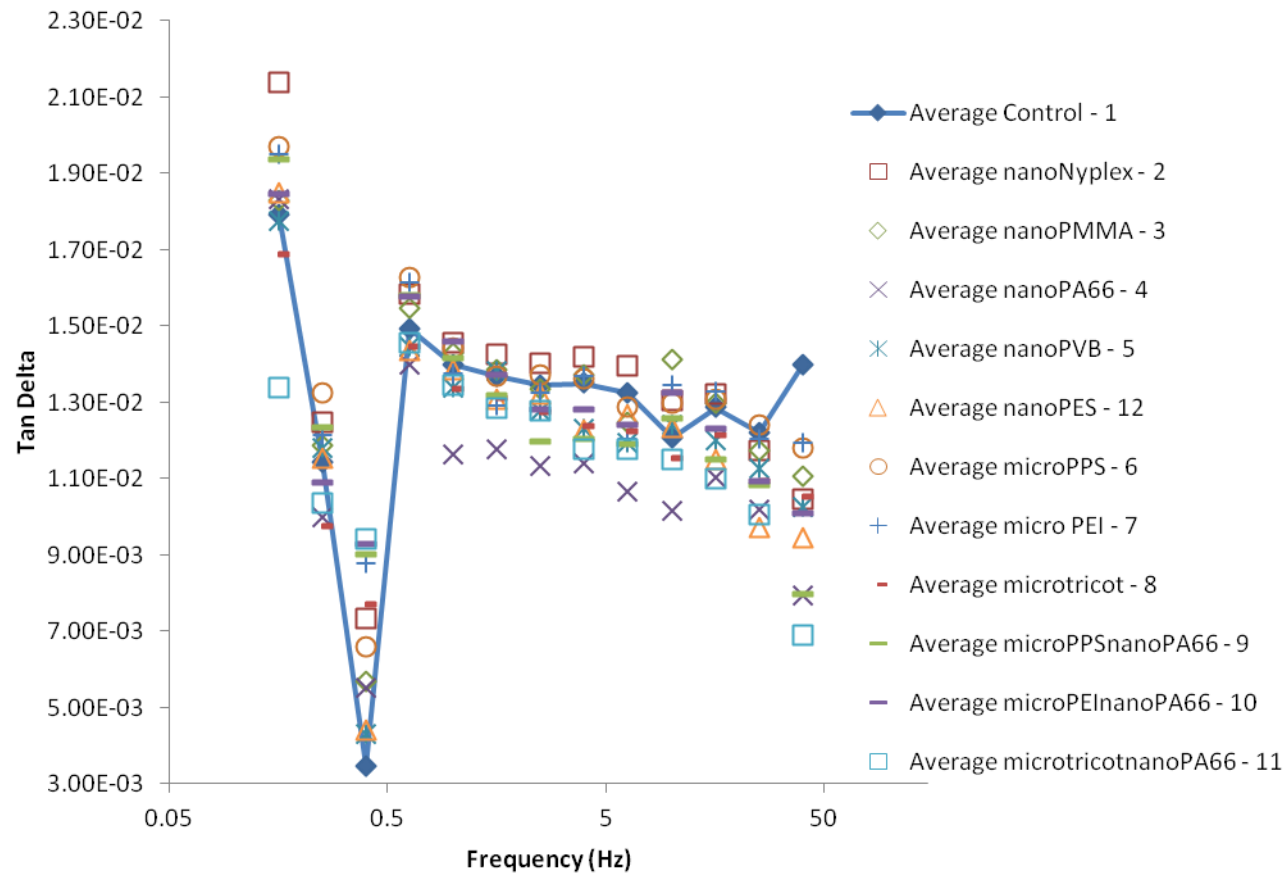
Figure 3.67: Comparison of average tan delta vs. frequency for all specimen types.
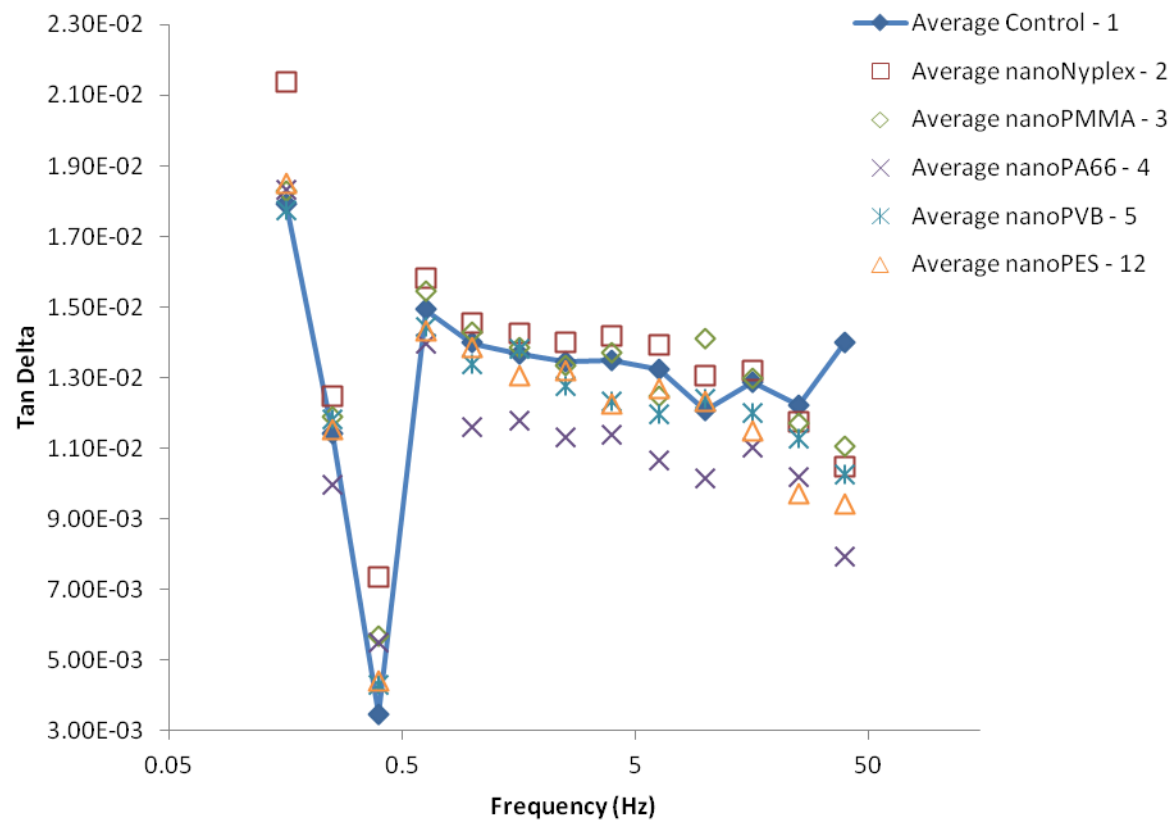
Figure 3.68: Comparison of average tan delta vs. frequency for all nanofibre specimen types.

Table 3.20: Percentage increase in the average tan delta for nanoNyplex samples compared to the control samples.

Frequency (Hz)	Percentage increase in tan delta for nanoNyplex compared to Control (%)
0.2	19
0.3	9
0.4	112
0.6	6
1.0	4
1.6	4
2.5	4
4.0	5
6.3	5
10.0	8
15.8	3
25.1	-4
39.8	-25
63.1	-136
100.0	-1

It is interesting to note that nanoPMMA interleaved specimens performed differently to nanoNyplex interleaved specimens, even though nanoNyplex fibres were predominately made from PMMA (see Section 3.1.7). This is possibly because the nanoPMMA fibres may not have been able to move to the same degree as nanoNyplex fibres due to a higher degree of adhesion. This seems likely, as nanoPMMA fibres seemed separated from each other (rather than clumped), so more area would have been available for bonding.
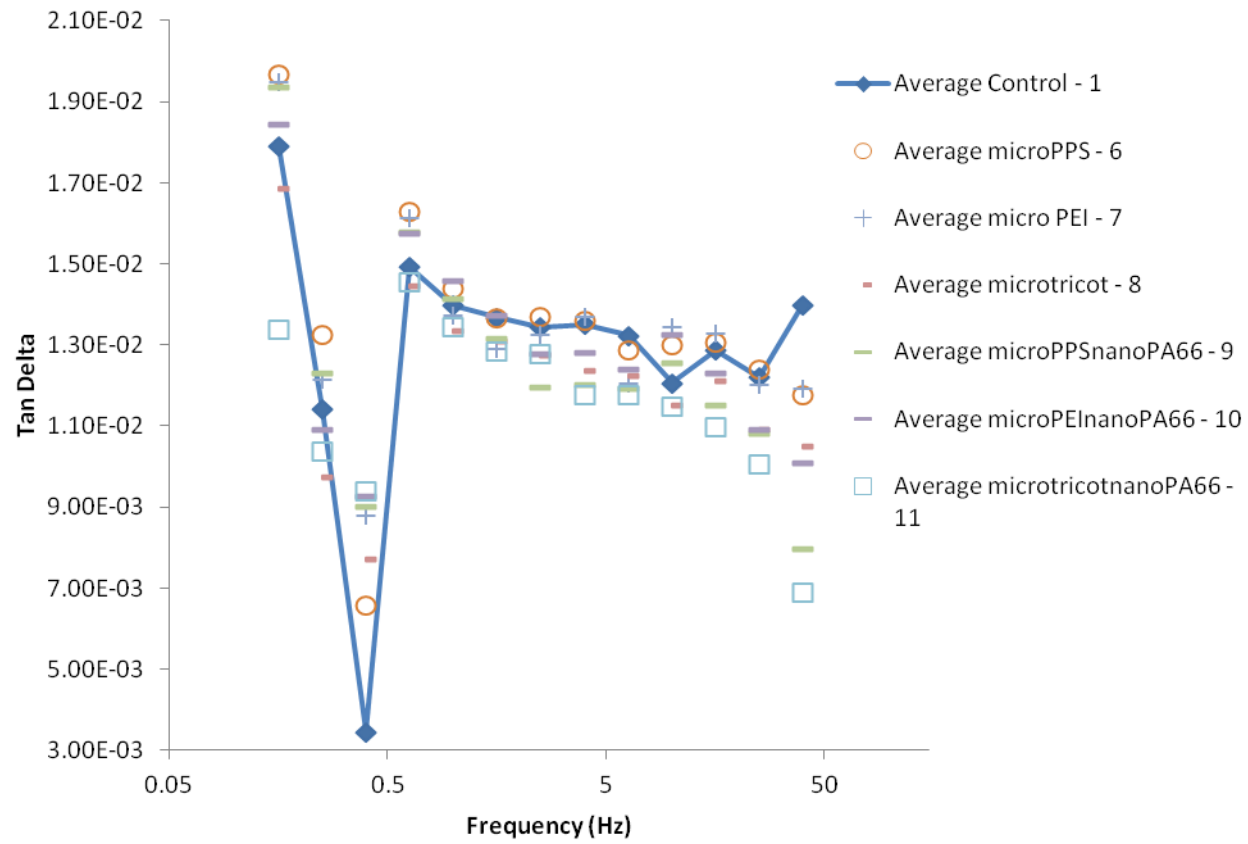
Figure 3.69: Comparison of average tan delta vs. frequency for all microfibre interleaved specimen types.

From the closer assessment of the microfibre interleaved specimens (see Figure 3.69) it seems that the microPPS interleaved specimens appeared to have a lower tan delta than microPPSnanoPA66 interleaved specimens, which suggested that adding PA6,6 nanofibre did not increase the amount of energy dissipated, even though the number of interfaces was increased through using both nanofibre and microfibre, as discussed previously. The same trend could be seen for microPEI, microtricot and the respective combination interleaved specimens (microPEInanoPA6,6 and microtricotnanoPA6,6,) further highlighting that the addition of PA6,6 nanofibres decreased the tan delta of the composites.

3.4 Compression after impact

As the impact energy increased, the amount of visual damage increased. For specimens with 10 and 15 J impacts, a small dent but very little other damage could be observed. Specimens with 20, 25, 30 and 35 J impacts showed increasing amounts of damage including delamination and fibre breakage on the reverse side. However, without ultrasonic C-scanning equipment, the extent of damage (or damage region) inside the samples could not be determined or compared.

3.4.1 General trends and variability

The compression after impact strengths are shown below in Figure 3.70 (raw data is contained in Section 6.4). Impacts energies were regarded as low (10 and 15 J), medium (20 and 25 J) or high (30 and 35 J).
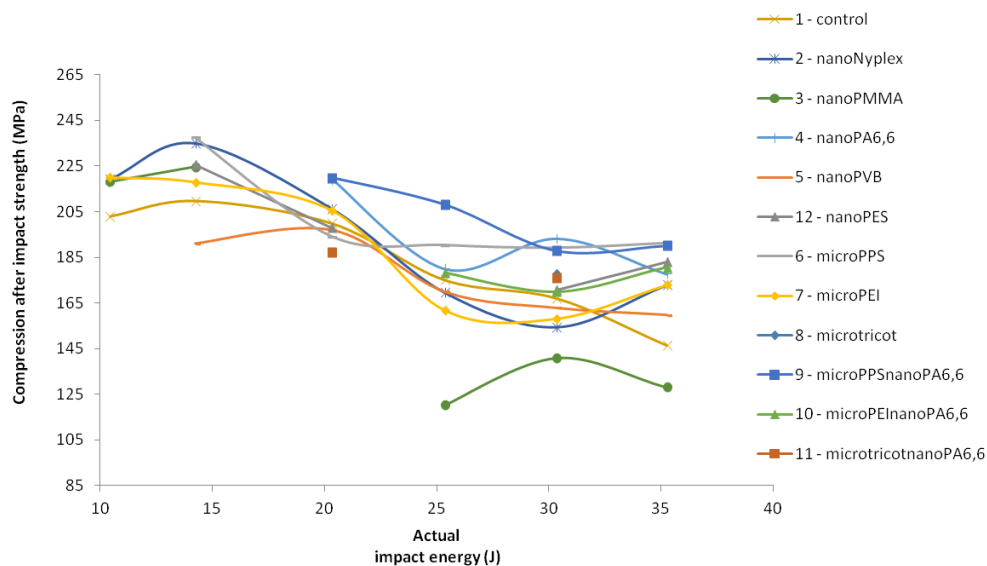
Figure 3.70: Compression after impact strength vs. actual impact energy for all sample types.

General trends

It can be seen from Figure 3.70 that for all specimen types, there was generally a reduction in the compression after impact (CAI) strength as the impact energy increased. The CAI strength decreased very little between specimens subjected to impact energies of 10 and 15 J, suggesting that little damage occurred during the initial impact. However, the CAI strength decreased substantially at medium impact energies, suggesting there was a threshold impact force needed to induce

127

significant damage in the sample before the CAI strength would be affected. The CAI strength of the specimens also appeared to level off at high impact energies, which could be due to the impact damage reaching the sides of the specimens (damage 'saturation') [50].

Variability

For some specimen types, the CAI strength was lower with lower impact loads which was contrary to expectation and highlights the issue of variability. It has been noted in literature that compression after impact test procedures (such as the ASTM D7137 method used for this study) produce data with a large amount of scatter [50]. Scatter in CAI strength results have been seen to be as much as ± 20 to ± 50 MPa [50].

It was not possible to quantify the amount of variability in this study, as only one specimen of each sample type was tested per impact energy due to materials availability and time constraints. Also, limited impact energies were assessed for some sample types. Data was further limited due to the tendency of samples to fail incorrectly at the edges (see Section 2.6.2), particularly at low impact energies, probably due to sample geometry as discussed previously (see Section 2.6.2), or because the specimens were not damaged enough to produce failure in the correct area [52].

Sources of variability include that due to sample variation such as defects including fibre misalignment and voids, which can bring premature buckling and result in low CAI strengths (see Section 1.6.1). Also variability could be introduced from the testing jig; this was an in-house built version of the one specified in ASTM D7137.

In addition the specimens used for this project were thinner than specified in the ASTM D7137 standard. Thinner specimens have been noted in other studies to be prone to some bending or out of plane deformation [64], which could also provide some variation in the CAI strengths.

3.4.2 Comparison of CAI strengths

Overall, from Figure 3.70, it can be seen that for specimens subjected to medium and high impact energies, the highest CAI strengths were found with specimens that were interleaved with nanoPA6,6, microPPS, and microPPSnanoPA6,6.

For clearer assessment, the CAI data was separated into Figure 3.71 (nanofibre interleaved specimens), Figure 3.72 (microfibre interleaved specimens) and Figure 3.73 (nanoPA6,6, microPPS and microPPSnanoPA6,6 interleaved specimens only).

Comparison of nanofibre interleavings
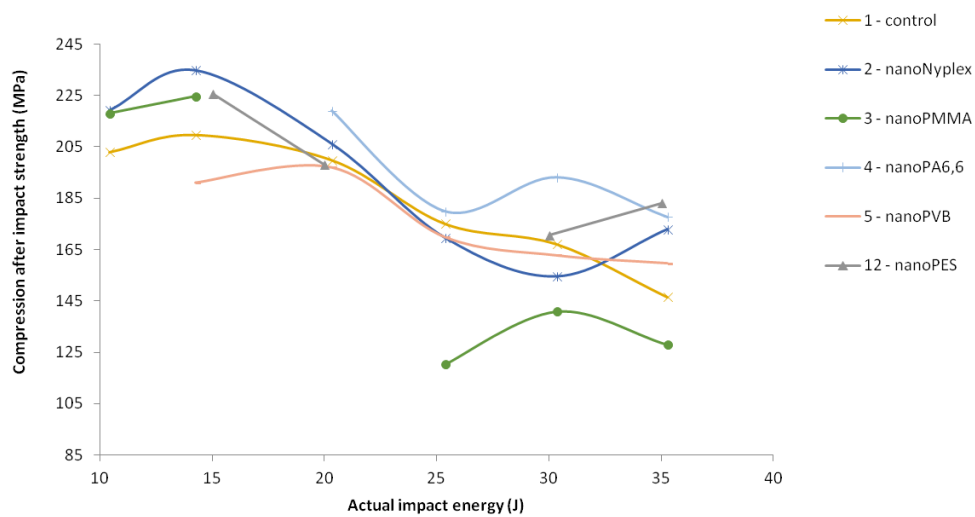
Figure 3.71: CAI strengths vs. actual impact energy for nanofibre interleaved sample types.

From Figure 3.71, it appears that the nanoPA6,6 and nanoPES interleaved specimens had higher CAI strengths for specimens subjected to high energy impacts, with nanoPA6,6 generally having the highest. NanoPVB and nanoNyplex interleaved specimens subjected to high energy impacts had CAI strengths that were clustered around the CAI strengths for the control specimens. NanoPMMA interleaved specimens however had CAI strengths much lower than any other specimen type for high impact energies.

The CAI strengths for the nanoPVB and nanoNyplex interleaved specimens were similar to the CAI strengths for the control specimens for medium impact energies.

For nanofibre specimens subjected to low impact energies not many data points were gained due to the specimens failing across the top of the specimen rather than through the impact zone (see Section 2.6.2). However, from the limited data it seems that nanoPES, nanoNyplex and nanoPMMA interleaved specimens subjected to low energy impacts had higher CAI strengths than the control. However, since these interleaved specimens had low CAI strengths when subjected to higher impact energies, it was difficult to confirm if the veils had an effect only at low impact energies, or the apparent increase in CAI strength for the low impact energy specimens was due to variability in the test.

Comparison of microfibre interleaved specimens
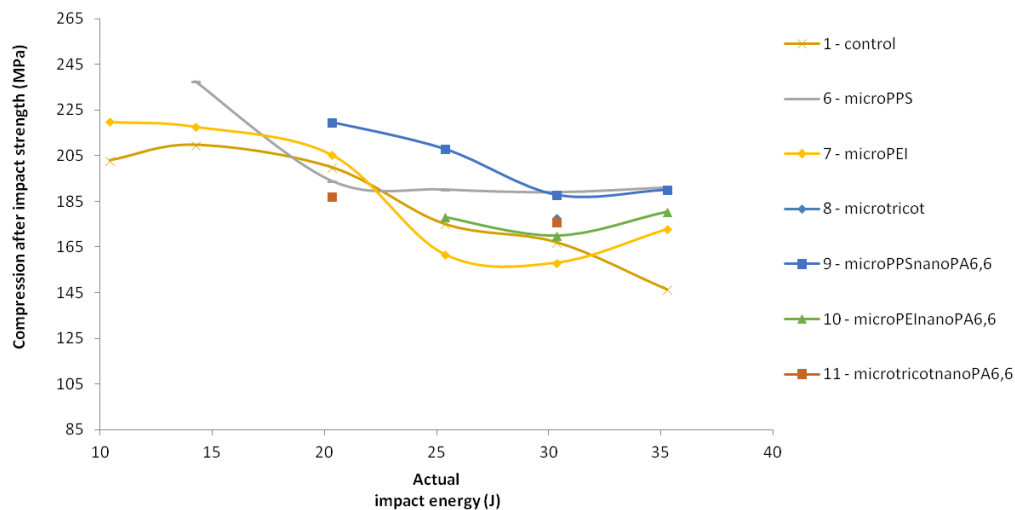
Figure 3.72: CAI strength vs. impact energy for microfibre interleaved specimens.

For the microfibre specimens, it can be seen that samples interleaved with microfibre PPS and nanofibre PA6,6 ('microPPSnanoPA6,6') had higher CAI strengths for specimens impacted with medium and high energy impacts compared to the control and the other microfibre interleaved specimens.

Comparison between specimens subjected to low energy impacts was not considered useful since limited data was collected.

130

Comparison of microfibre-nanofibre combination specimens
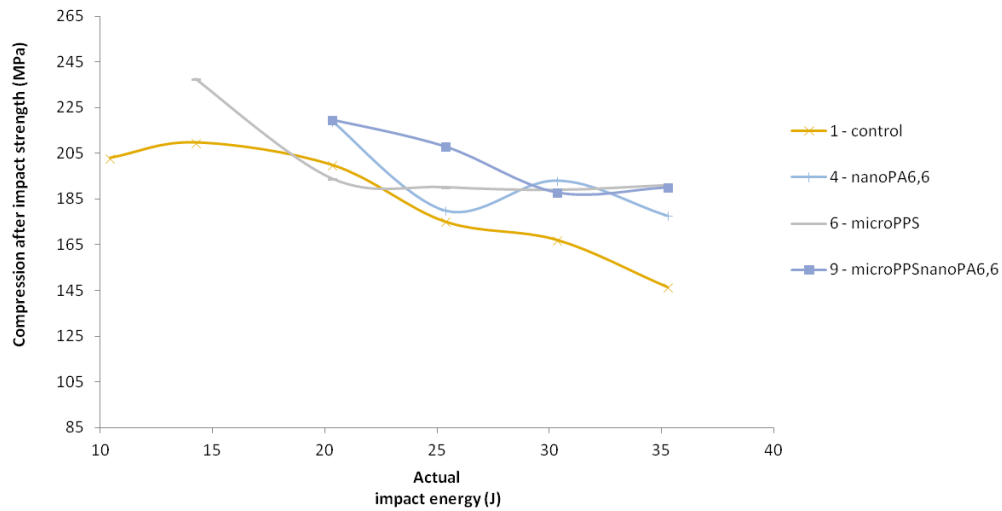
Figure 3.73: CAI strength vs. impact energy for nanoPA6,6, microPPS and microPPSnanoPA6,6 specimens.

The microPPSnanoPA6,6 specimens had similar CAI strengths to microPPS interleaved specimens with high energy impacts, but microPPSnanoPA6,6 specimens had higher CAI strengths for specimens subjected to medium impacts (see Figure 3.73), suggesting that adding PA6,6 nanofibre increased the CAI strength (possibly due to the nanofibre providing toughening in the spaces between the microfibres). The curve for the microPPSnanoPA6,6 interleaved specimens seems offset from the microPPS curve, suggesting adding PA6,6 nanofibre also increased the 'threshold' impact energy (by approximately 10 J).

From Figure 3.73, it can be seen that the CAI strengths and the threshold impact energies were similar for the nanoPA6,6 and microPPSnanoPA6,6 interleaved specimens subjected to medium and high energy impacts (except lower for the nanoPA6,6 specimen subjected to a 25 J impact, as discussed earlier). However, the threshold impact energy for the microPPS only interleaved specimens appeared to be significantly lower in comparison. Thus, it appears that the increase in CAI for the microPPSnanoPA6,6 interleaved specimens could be mostly due to the PA6,6 nanofibre component of this veil, rather than the microfibre component.

With regards to the microPEI interleaved samples and microfibre PEI with nanofibre PA6,6 (microPEInanoPA6,6) interleaved samples, it is difficult to tell if

the threshold impact energy was increased with the addition of PA6,6, due to the lack of data for microPEInanoPA6,6 samples (see Figure 3.72). However, it can be seen that microPEI interleaved samples had a CAI strength lower than the control and microPEInanoPA6,6 interleaved specimens for medium and high energy impacts, indicating that the addition of PA6,6 nanofibre was beneficial to the CAI performance, possibly because the nanofibre provided toughening between the microfibres.

Since very little data was obtained for microfibre only interleaved specimens subjected to low energy impacts, microtricot, and microtricotnanoPA6,6 interleaved specimens, the performance of these veils was not compared.

3.4.2.1 Assessment of toughening mechanisms

As discussed in Section 1.4.3 and 1.6.3, the interleaving fibres would have been likely to provide obstacles and potentially deflect any cracks that formed in the matrix during the initial impact and the compression test, which would increase the amount of energy required for crack growth. Other fibre reinforcement mechanisms such as fibre bridging, debonding and pull out could also have increased the energy required for crack propagation, as discussed in Section 1.4.3 and reduced the overall degree of damage for a particular impact energy, resulting in higher CAI strengths. The degree of toughening achieved by each interleaving would be likely to be affected by variables such as:

- the fracture toughness of the polymer the veil was manufactured from,
- the interfacial area available for bonding (related to veil fibre diameter, areal weight and density),
- the compatibility of the veil with the epoxy matrix (related to the Hildebrand parameters - see Section 1.2.2) and
- the adhesion strength between the veil and the epoxy (related to compatibility, mechanical factors and chemical adhesion mechanisms such as hydrogen bonding - see Section 1.4.4).

The properties of the veils that potentially influenced toughness are shown in Tables 3.21 and 3.22.

132

Table 3.21: Veil properties and corresponding bulk polymer properties.

Veil Type	Fibre diameter (um)*	Areal weight (g/m²)*	Bulk polymer density (g/m³)**	Interfacial area (m²) per square metre of veil***	Bulk polymer fracture toughness K1c (MPa. m^0.5)**	Average fracture toughness: K1c (MPa. m^0.5)**
nanoNyplex	0.141	4.3	1.20E+06****	102	-	1.62****
nanoPMMA	0.274	4.5	1.17E+06	56.1	0.7-1.6	1.15
nanoPA6,6	0.204	4.8	1.30E+06	72.4	3.32-3.66	3.49
nanoPVB	0.651	4.7	1.10E+06	26.3	High toughness [65] (exact value not found)	-
nanoPES	0.15	3.75	1.36E+06	73.5	1.14-2.26	1.7
microPPS	9.465	5.5	1.34E+06	1.7	1.23-1.75	1.49
microPEI	15.405	4.9	1.26E+06	1.0	1.99-4.03	3.01
microtricot (PA 6)	37.627	12.4	1.13E+06	1.2	3.1-3.42	3.26

* see Section 3.2
** General values from CES 2014 Edupack materials database
*** Calculation based on assumption of one continuous fibre.
**** weighted average of PMMA and PA6,6 using ratio 80:20 (see 3.1.7)

Table 3.22: Hansen parameters, Hildebrand parameters and partial polarity values for the veils used.

Polymer Type	Hansen Parameters (MPa^1/2)			Hildebrand parameter δp (MPa^1/2)	Partial polarity (e)
	δD (Dispersion)	δP (Polarity)	δH (Hydrogen Bonding)		
PMMA	18.7	12.1	5.6	23.0	0.281
PA6,6	18.2	8.8	10.8	22.9	0.344
PVB	18.6	4.4	13.0	23.1	-
PES	19.0	11.0	8.0	23.4	0.347
PPS	18.8	4.8	6.8	20.6	-
PEI	17.3	5.3	4.7	18.7	-
Tricot (PA 6)	17.0	3.4	10.6	20.3	0.188
Epoxy (amine hardener)	17.4	10.5	9.0	22.2	0.432

* General data gathered from HSPiP database software [25].

The degree of adhesion between the veils and the epoxy was assessed and ranked by taking into account the wettability (precursor to adhesion), the likelihood of hydrogen bonding between the polymer and the epoxy (indicated by the Hansen hydrogen bonding parameters) and any other chemical or mechanical bonding factors (presented in following information):

- **PA6,6** has good compatibility with epoxy [33]. PA6,6 has a high hydrogen bonding Hansen parameter, indicating that hydrogen bonding could possibly occur between the polymer and the hydroxyl groups present on

the epoxy [63], which could encourage strong bonding (see Section 1.4.4). From previous SEM work (see Section 3.2, Figure 3.25) it appears that there were 'cobwebs' present between the nanoPA6,6 fibres (which were not present in any other type of polymer veil), which would increase the surface area and encourage good mechanical adhesion.

- **PVB** is a polymer made from three monomers (vinyl butyral, vinyl alcohol and vinyl acetate) with hydroxyl groups which can cross link with epoxy resins to form a very strong bond [66].

- **PMMA** has a low hydrogen bonding Hansen parameter (see Table 3.22), and therefore it should be less likely to hydrogen bond (than polymers such as PA6,6) therefore the adhesion strength between nanoPMMA and epoxy would be likely to be weaker than with nanoPA6,6.

- **NanoNyplex** was made from a blend of PA6,6 and PMMA, (predominantly PMMA) so it is likely that (in general) the adhesion strength between the epoxy and nanoNyplex would be similar to nanoPMMA and epoxy. However, as noted from SEM micrographs (Section 3.2.1) some nanoNyplex fibres were joined together which could have reduced (mechanical) adhesion between the epoxy matrix and the nanoNyplex fibre.

- The adhesion strength between **microPPS, microPEI** and **microtricot** (made from polyamide 6) and the epoxy would be likely to be proportional to the likelihood of hydrogen bonding occurring between the fibres and the matrix (see hydrogen bonding parameters, Table 3.22).

The rankings for the adhesion strength between the epoxy and each of the veils are shown in Table 3.23. High adhesion strength was given a ranking of one, whereas low adhesion strength was given a seven.

Table 3.23: Adhesion rankings for the nanofibre and microfibre veils.

Type	Adhesion rank
nanoNyplex	4
nanoPMMA	4
nanoPA6,6	2
nanoPVB	1
nanoPES	3
microPPS	5
microPEI	7
microtricot	4

An assessment of factors potentially influential to toughness follows.

CAI strength of the corresponding nanofibre interleaved specimen vs. the fracture toughness of the bulk polymer is shown in Figure 3.74. Note that the nanoPVB specimen was excluded, as a fracture toughness value could not be obtained from available data. From Figure 3.74, it seems that for the nanofibre veils as the fracture toughness of the bulk polymer of the veil increased, the CAI strength also increased.
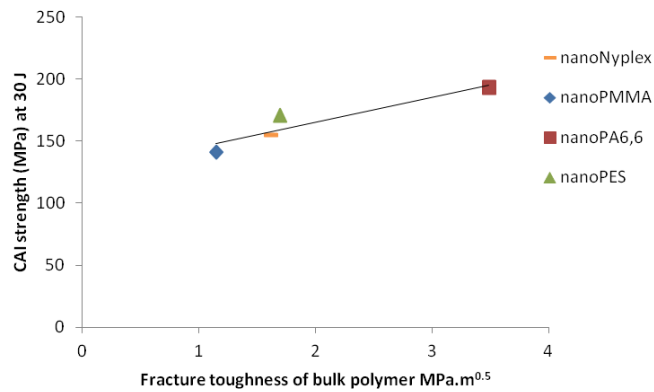
Figure 3.74: CAI strength for nanofibre interleaved specimens subjected to 30 J impacts vs. the corresponding fracture toughness of the bulk polymer.

However, from Figure 3.75, it seems that the CAI strengths decreased as the fracture toughness of the bulk polymer increased for microfibre interleaved specimens. Figure 3.76 shows the bulk polymer fracture toughness and CAI strengths for both the nanofibre and microfibre interleaved specimens. From this graph it seems that there was a slight increase in CAI strength of the specimens as the fracture toughness increased.
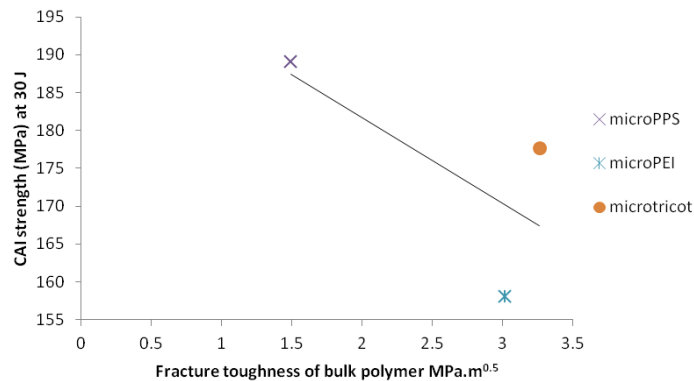
Figure 3.75: CAI strengths for microfibre interleaved specimens subjected to 30 J impacts vs. the fracture toughness of the corresponding microfibre veil bulk polymer.

135
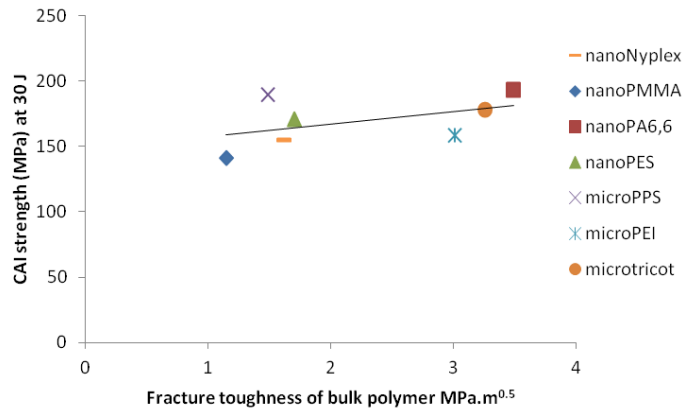
Figure 3.76: CAI strengths for the nanofibre and microfibre interleaved specimens subjected to 30 J impacts vs. fracture toughness of the nanofibre and microfibre veil bulk polymers.

Veil characteristics such as diameter and areal weight could have also affected the CAI strength (see Section 1.6.3). In this study, it seems that nanoPVB interleaved specimens had lower CAI strengths than nanoPA6,6 interleaved specimens which had smaller diameter fibres than nanoPVB fibres. Although the nanoPVB veil had a similar areal weight to the nanoPA6,6 veil, the larger diameter would have meant there was less fibres to act as barriers for crack deflection and other mechanisms for specimens interleaved with nanoPVB in comparison to nanoPA6,6. In addition, it was found that microPPS interleaved specimens had higher CAI strengths than microPEI interleaved specimens which had larger diameter interleaving fibres (see Table 3.21 and Section 3.2.1.1).

Veils with a large fibre diameter would also have less surface area available for bonding with the epoxy matrix than a veil with a smaller fibre diameter but similar areal weight. An estimate of the interfacial area per square metre of veil was calculated (see Table 3.21) and assessed in Figures 3.77 - 3.79.
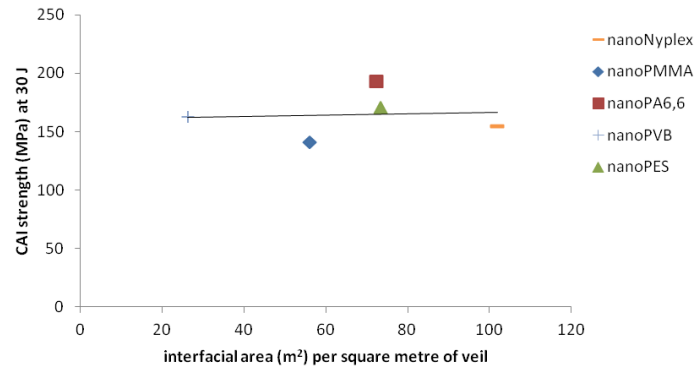
Figure 3.77: CAI strength for the corresponding nanofibre interleaved specimens impacted with 30 J vs. interfacial area per square metre of veil.
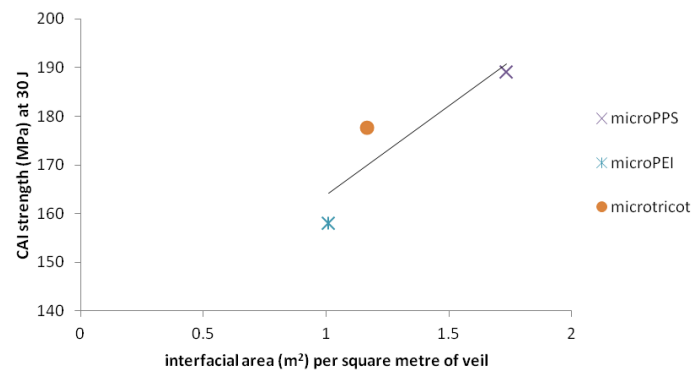
Figure 3.78: CAI strength of the microfibre interleaved specimens impacted with 30 J vs. interfacial area per square metre of veil for microfibre veils.
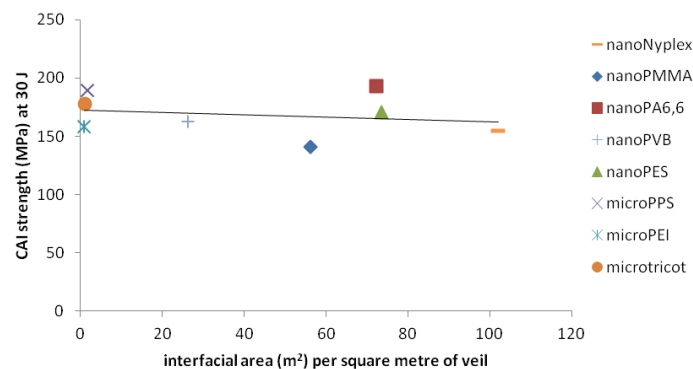
Figure 3.79: CAI strength of the microfibre and nanofibre interleaved specimens impacted with 30 J vs. the interfacial area per square metre of veil for microfibre veils and nanofibre veils.

From Figure 3.77, it seems that there was almost no correlation between interfacial area and the CAI strength. However, for microfibre interleaved specimens (shown in Figure 3.78), it appears that increasing the interleaving interfacial area increased the CAI strength. However, overall (see Figure 3.79), it

seems that there was almost no correlation between interfacial area and CAI strength.

In addition, factors such as the compatibility and the adhesion strength between the veil and the epoxy matrix would be important, as these affect the amount of energy required for debonding and pull out of the interleaving fibres. The compatibility was assessed by the difference in Hildebrand parameters between the epoxy and the bulk polymer (see Figure 3.80 and Figure 3.81). A smaller difference in Hildebrand parameters would suggest a higher compatibility between the two materials.
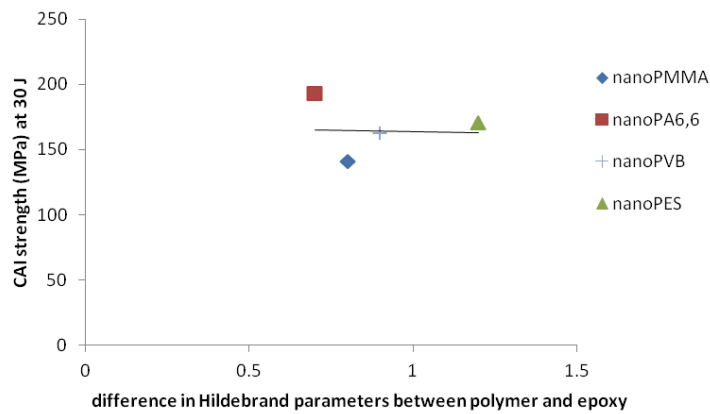
Figure 3.80: CAI strength for the corresponding nanofibre interleaved specimens subjected to impacts of 30 J vs. the difference in the Hildebrand parameters between the bulk polymers and the epoxy.
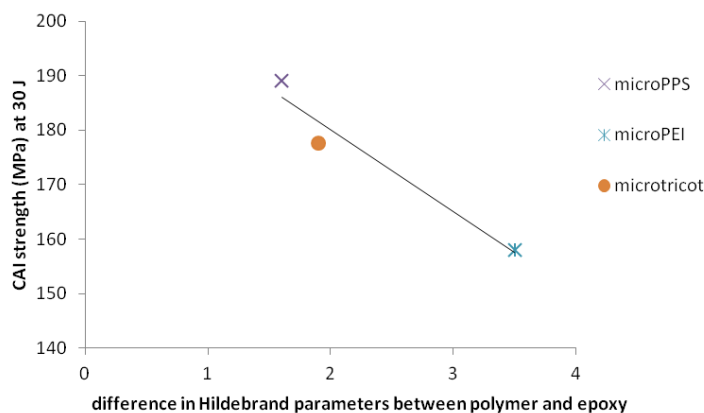
Figure 3.81: CAI strength for the corresponding microfibre specimens subjected to 30 J impacts vs. the difference in the Hildebrand parameters between the bulk polymer and the epoxy vs.

138
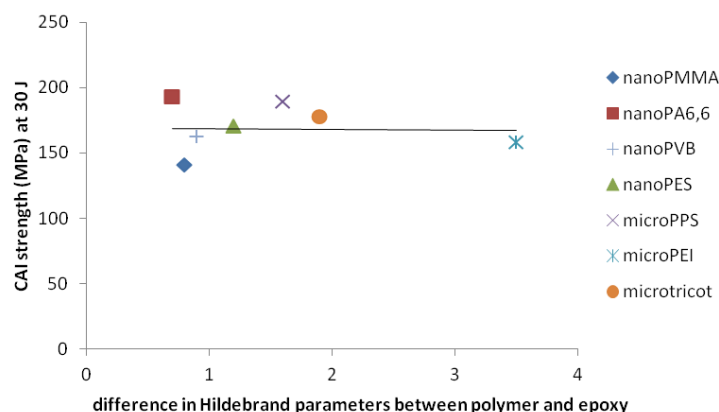
Figure 3.82: CAI strength for the corresponding microfibre and nanofibre specimens subected to 30 J impacts vs. the difference in the Hildebrand parameters between the bulk polymer and the epoxy.

From Figure 3.80 it appears that there was no correlation between the compatibility of the nanofibre interleavings and the CAI strength. However, it is noted that all of the nanofibre veils were made from polymers that had relatively similar Hildebrand parameters compared to the epoxy. In contrast, Figure 3.81 suggests that microfibre veils made with polymers with a similar Hildebrand parameter to the epoxy had higher CAI strengths. However, overall (see Figure 3.82) it appears that there was no correlation between the compatibility of the veils with the epoxy and the CAI strength.

The affect of the adhesion strength between the interleaving fibres and the epoxy was also assessed (see Figures 3.83 to 3.85).
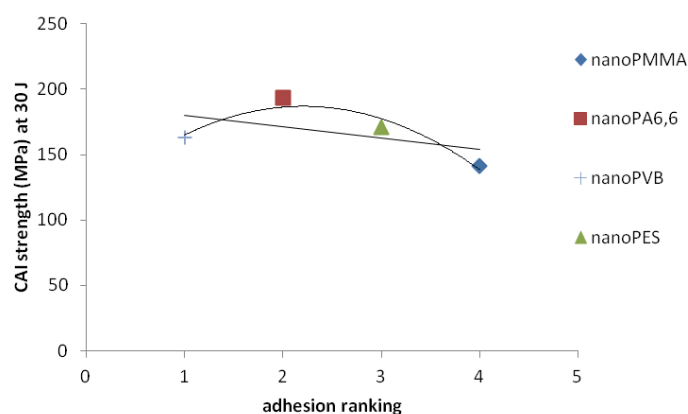
Figure 3.83: CAI strength for the nanofibre interleaved specimens subjected to a 30 J impact vs. the adhesion ranking for the nanofibre veils (one indicates high adhesion whereas five indicates weak adhesion strength).

139
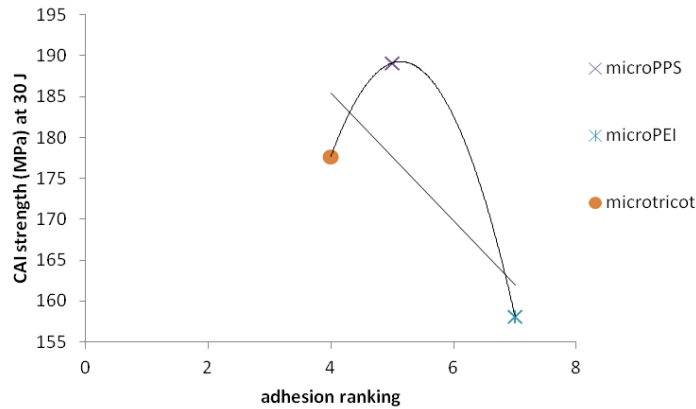
Figure 3.84: CAI strength for microfibre specimens subjected to 30 J impacts vs. adhesion strength ranking for the microfibre veils (one indicates high adhesion whereas seven indicates weak adhesion strength).
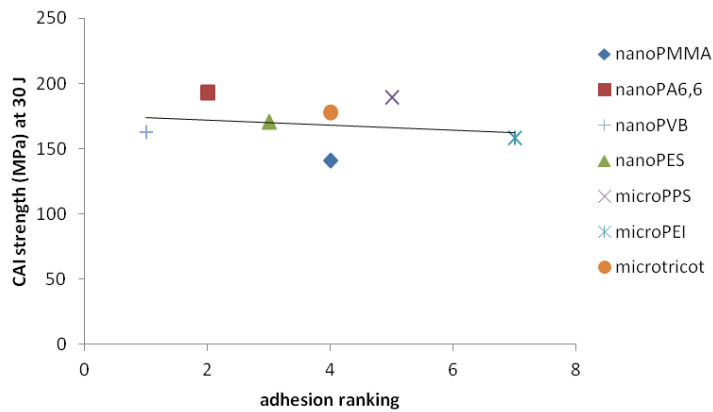
Figure 3.85: CAI strength for nanofibre and microfibre specimens subjected to 30 J impacts vs. adhesion strength ranking for the microfibre and nanofibre veils (one indicates high adhesion whereas seven indicates weak adhesion strength).

From Figure 3.83, the results suggest that a high degree of adhesion achieved the highest CAI strength. From Figure 3.84 it can be seen that the microPPS specimen had the highest CAI strength and had medium adhesion ranking for the microPPS and the epoxy. This compliments suggestions made in other studies that an medium interfacial strength was required for toughening, rather than low or high adhesion strength, (see Section 1.4.4 and [38]). Overall, (see Figure 3.85) it appears that there was a slight decrease in CAI strength as the adhesion strength between the fibre and the epoxy decreased.

Although it seems that one dominant factor could not be identified from this analysis, it seems that in general, a veil with a high bulk polymer fracture toughness, a large number of interleaving fibres per unit area, and a medium to

140

high degree of adhesion strength (between the interleaving fibres and the matrix) was more likely (when used as interleavings) to produce composites with higher CAI strengths.

3.4.3 Visual inspection and optical microscopy of CAI specimens

Visual inspection of nanofibre interleaved specimens:

Specimens were photographed on both sides after impact and compression in order to assess the extent of damage and the failure modes. The photographs of the front and back faces of the control and the nanofibre only interleaved specimens are shown in Figures 3.86 - 3.97.

Front
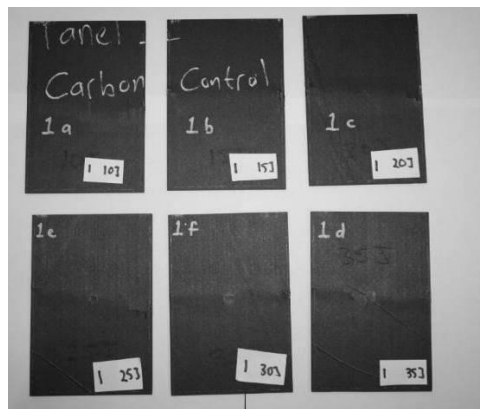
Figure 3.86: Front of control specimens (top from left: specimens impacted at 10, 15 and 20 J, bottom from left: specimens impacted at 25, 30 and 35 J).

Back

Figure 3.87: Back of the control specimens (top from left: specimens impacted at 10, 15 and 20 J, bottom from left: specimens impacted at 25, 30 and 35 J).
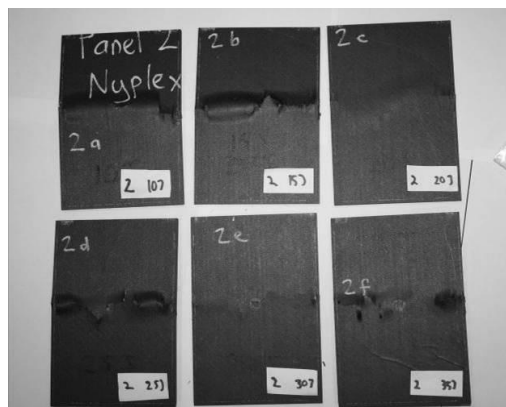
Figure 3.88: Front of nanoNyplex interleaved specimens (top from left: specimens impacted at 10, 15 and 20 J, bottom from left: specimens impacted at 25, 30 and 35 J).
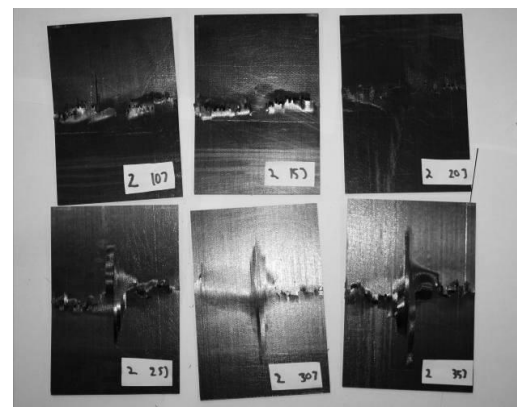
Figure 3.89: Back of nanoNyplex interleaved specimens (top from left: specimens impacted at 10, 15 and 20 J, bottom from left: specimens impacted at 25, 30 and 35 J).
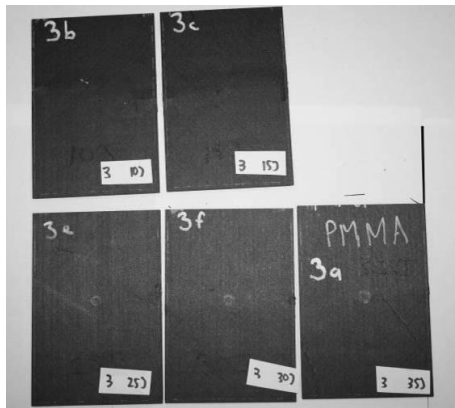
Figure 3.90: Front of nanoPMMA interleaved specimens (top from left: specimens impacted at 10 and 15 J, bottom from left: specimens impacted at 25, 30 and 35 J).
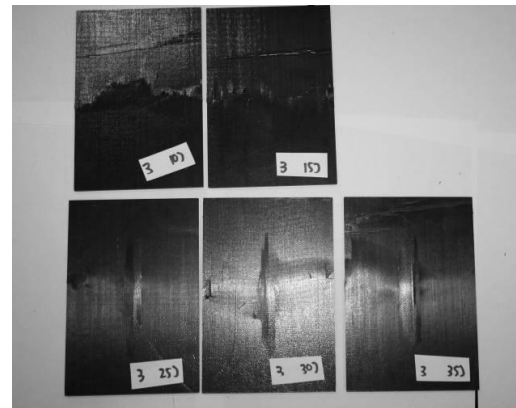
Figure 3.91: Back of nanoPMMA interleaved specimens (top from left: specimens impacted at 10 and 15 J, bottom from left: specimens impacted at 25, 30 and 35 J).
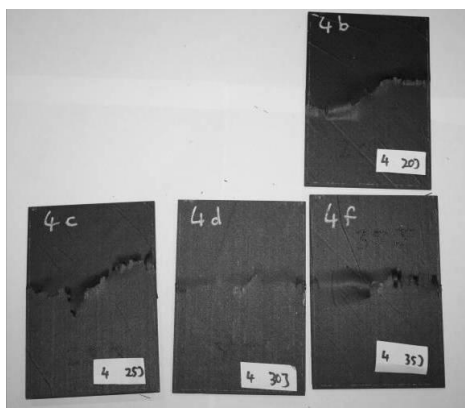
Figure 3.92: Front of nanoPA6,6 interleaved specimens (top: specimen impacted at 20J, bottom from left: specimens impacted at 25, 30 and 35 J).
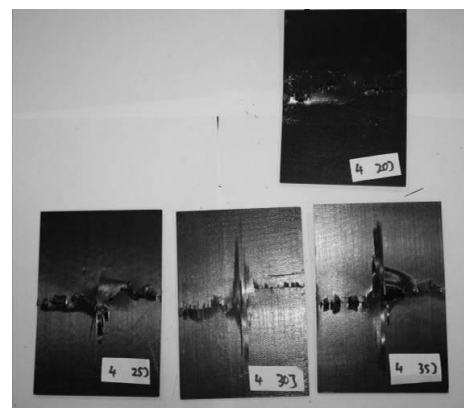
Figure 3.93: Back of nanoPA6,6 interleaved specimens (top: specimen impacted at 20J, bottom from left: specimens impacted at 25, 30 and 35 J).
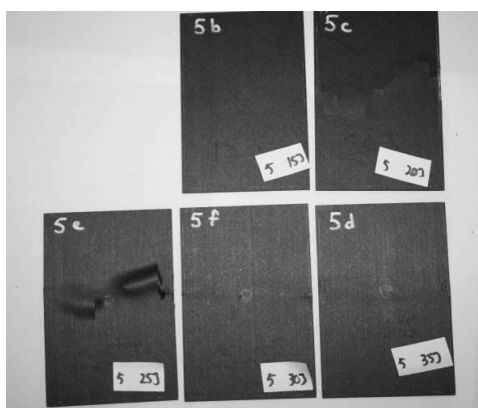
Figure 3.94: Front of nanoPVB interleaved specimens (top from left: specimens impacted at 15 and 20 J, bottom from left: specimens impacted at 25, 30 and 35 J).
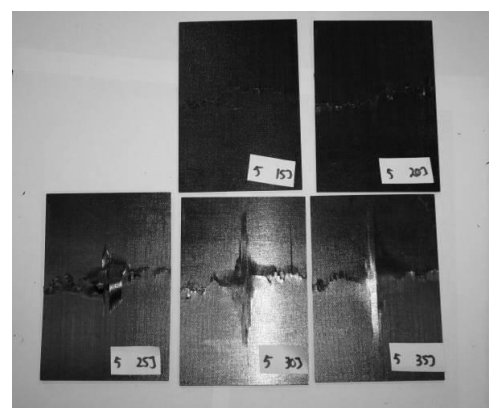
Figure 3.95: Back of nanoPVB interleaved specimens (top from left: specimens impacted at 15 and 20 J, bottom from left: specimens impacted at 25, 30 and 35 J).
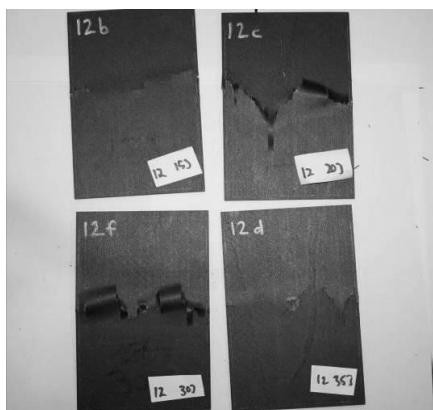
Figure 3.96: Front of nanoPES interleaved specimens (top from left: specimens impacted at 15 and 20 J, bottom from left: specimens impacted at 30 and 35 J).
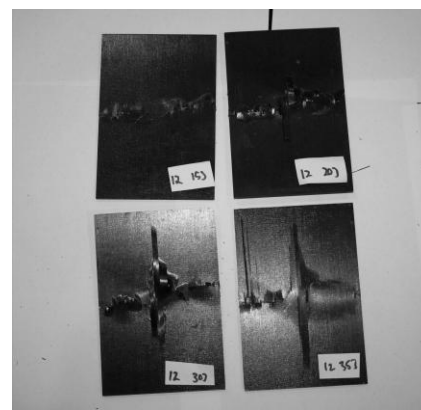
Figure 3.97: Back of nanoPES interleaved specimens (top from left: specimens impacted at 15 and 20 J, bottom from left: specimens impacted at 30 and 35 J).

There was very little visual damage on the front faces of the control specimens (shown in Figure 3.86), apart from a small dent on specimens subjected to impact energies of 25, 30 and 35 J. For specimens interleaved with nanoNyplex, nanoPA6,6, nanoPVB and nanoPES, (see Figures 3.90, 3.92, 3.94 and 3.96 respectively) the front of the specimens showed more damage (such as bulges and fibre breakage) than the control specimens. The front face of the nanoPMMA interleaved specimens however were almost pristine (Figure 3.90). Less damage was also observed for the back faces of the nanoPMMA interleaved specimens compared to the other nanofibre interleaved specimens and the control specimens. NanoPMMA interleaved specimens subjected to medium and high energy impacts failed at lower loads than the control specimens. It is likely that:

- during impact, there was less energy absorbed by fibre reinforcment mechanisms so more damage was sustained within the specimen, or
- less energy was absorbed during compression due to lower maximum loads, so less damage was sustained on the front face,

or quite likely a combination of both of the above.

Visual inspection of microfibre interleaved specimens

The photographs of the front and back faces of the microfibre interleaved specimens are shown in Figures 3.98 - 3.109. From these photographs, it appears that the front faces of all of the microfibre interleaved specimens appeared to be more damaged than the control specimens, although the extent of damage on the

back faces of the microPPS, microPEI, microtricot, microPEInanoPA6,6 and microtricotnanoPA6,6 interleaved specimens appeared to be similar to the control specimens. The microPPSnanoPA6,6 interleaved specimen, as an exception, appeared to have less damage on the back face (so given the greater damage on the front face may have had similar damage overall to the control) which correlated with the improved CAI performance of the specimen.

Front
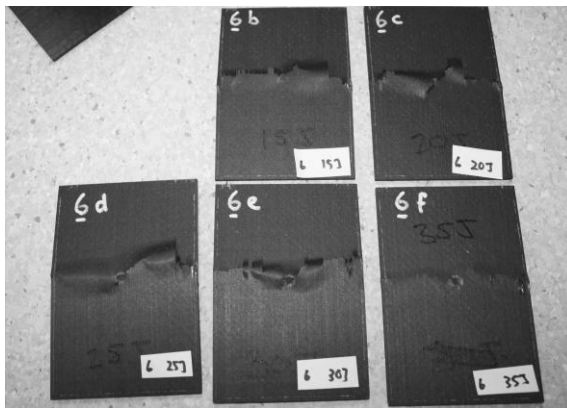
Figure 3.98: Front of microPPS interleaved specimens (top from left: specimens impacted at 15 and 20 J, bottom from left: specimens impacted at 25, 30 and 35 J).

Back

Figure 3.99: Back of microPPS interleaved specimens (top from left: specimens impacted at 15 and 20 J, bottom from left: specimens impacted at 25, 30 and 35 J).
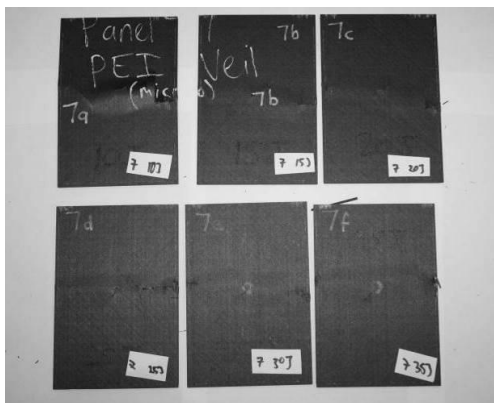
Figure 3.100: Front of microPEI interleaved specimens (top from left: specimens impacted at 10, 15 and 20 J, bottom from left: specimens impacted at 25, 30 and 35 J).
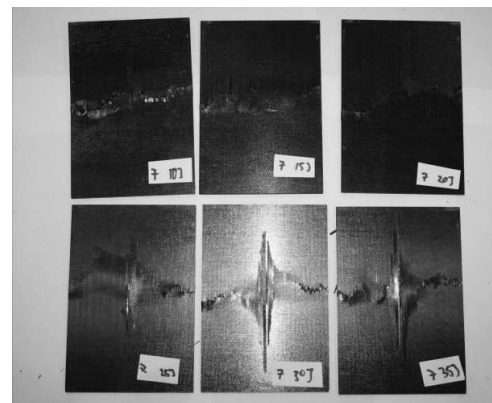
Figure 3.101: Back of microPEI interleaved specimens (top from left: specimens impacted at 10, 15 and 20 J, bottom from left: specimens impacted at 25, 30 and 35 J).
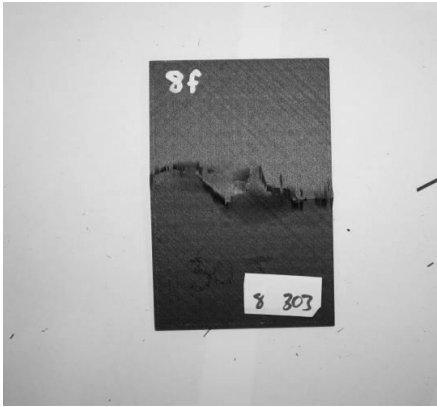
Figure 3.102: Front of microtricot interleaved specimen subjected to 30 J impact.
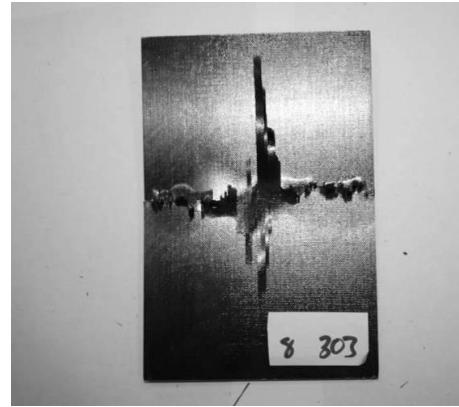
Figure 3.103: Back of microtricot interleaved specimen subjected to 30 J impact.
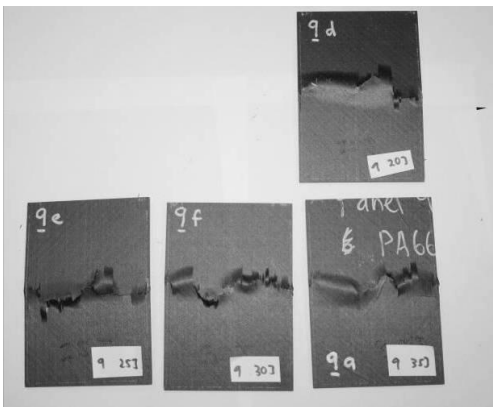
Figure 3.104: Front of microPPSnanoPA6,6 interleaved specimens (top from left: specimen impacted at 20 J, bottom from left: specimens impacted at 25, 30 and 35 J).
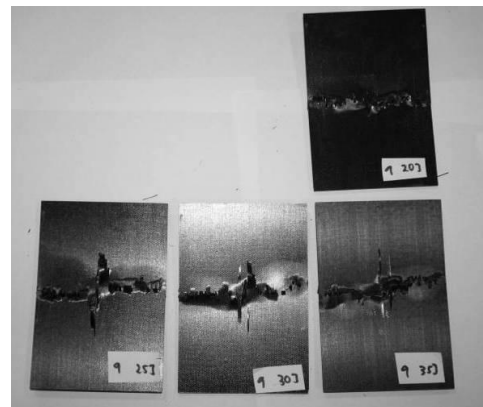
Figure 3.105: Back of microPPSnanoPA6,6 interleaved specimens (top from left: specimen impacted at 20 J, bottom from left: specimens impacted at 25, 30 and 35 J).
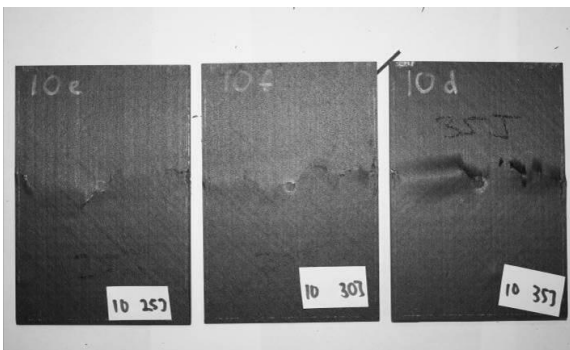
Figure 3.106: Front of microPEInanoPA6,6 interleaved specimens (from left: specimens impacted at 25, 30 and 35 J).
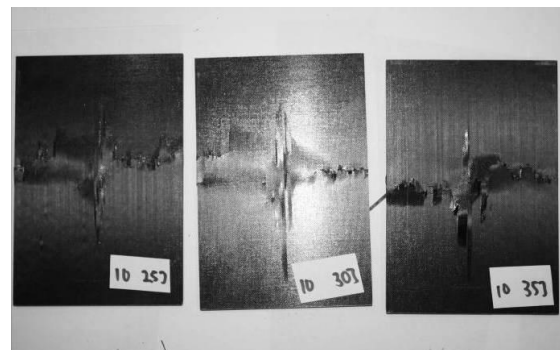
Figure 3.107: Back of microPEInanoPA6,6 interleaved specimens (from left: specimens impacted at 25, 30 and 35 J).

145
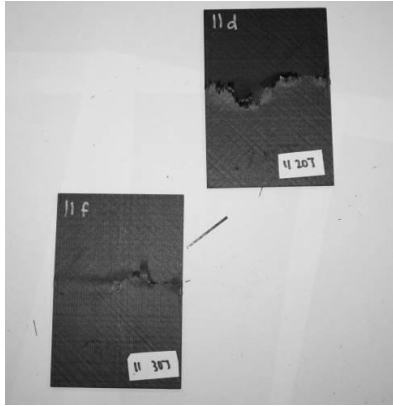
Figure 3.108: Front of microtricotnanoPA6,6 interleaved specimens (top: specimen impacted at 20 J, bottom: specimens impacted at 30 J).
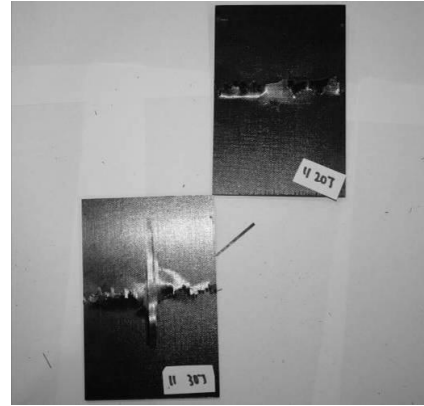
Figure 3.109: Back of microtricotnanoPA6,6 interleaved specimens (top: specimen impacted at 20 J, bottom: specimens impacted at 30 J).

Optical microscopy of nanofibre and microfibre interleaved specimens

The sides of the CAI specimens subjected to 25 and 30 J impacts were examined under the optical microscope after being compressed. Photo montages of the sides of the control specimens and the nanofibre interleaved specimens subjected to 30 J impacts are shown in Figures 3.110 - 3.115. The microfibre interleaved specimens are shown in Figures 3.116 - 3.121 (also subjected to 30 J impacts).
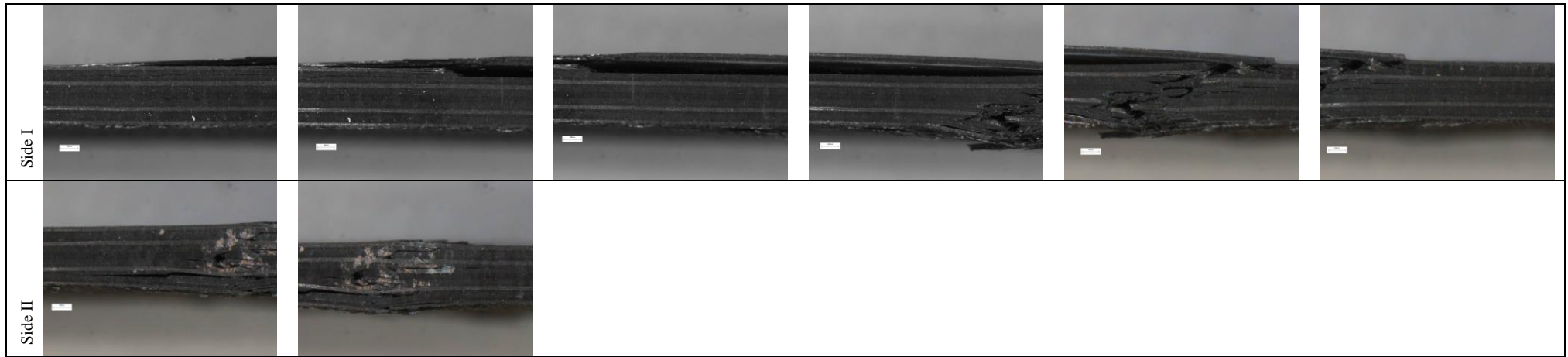
Figure 3.110: Photomontage of the control specimen sides (subjected to a 30 J impact).
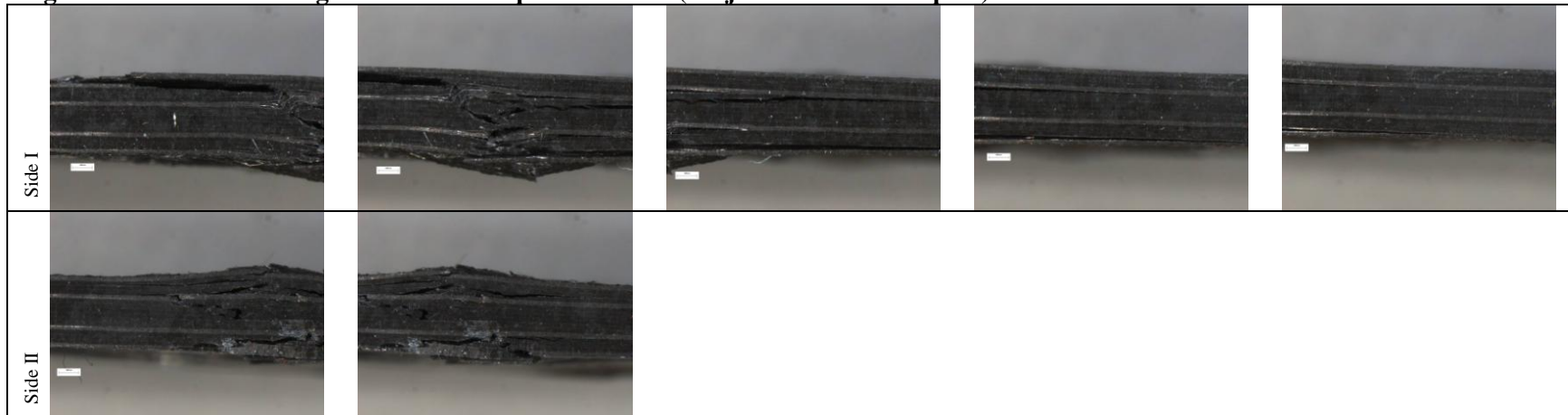
Figure 3.111: Photomontage of the nanoNyplex interleaved specimen sides (subjected to a 30 J impact).
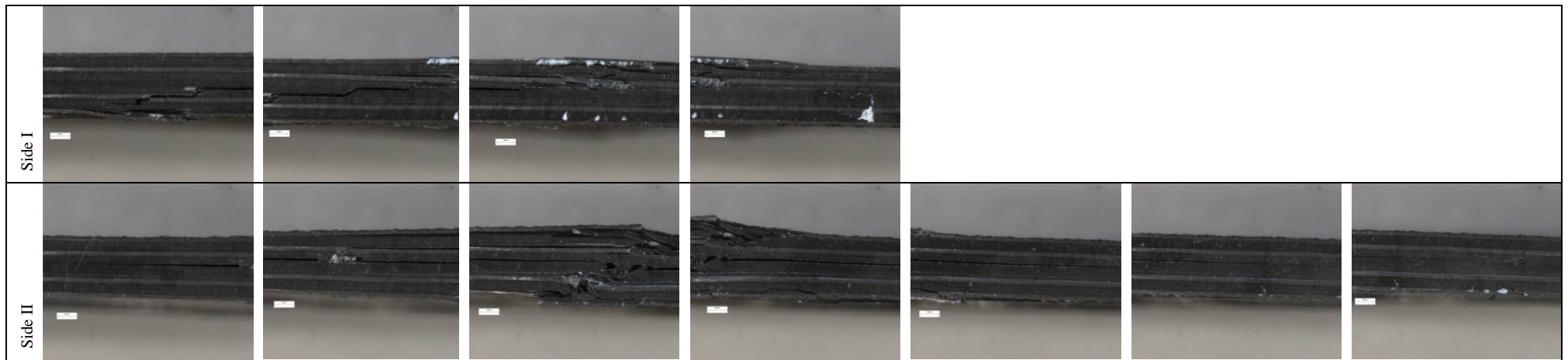
Figure 3.112: Photomontage of the nanoPMMA interleaved specimen sides (subjected to a 30 J impact).
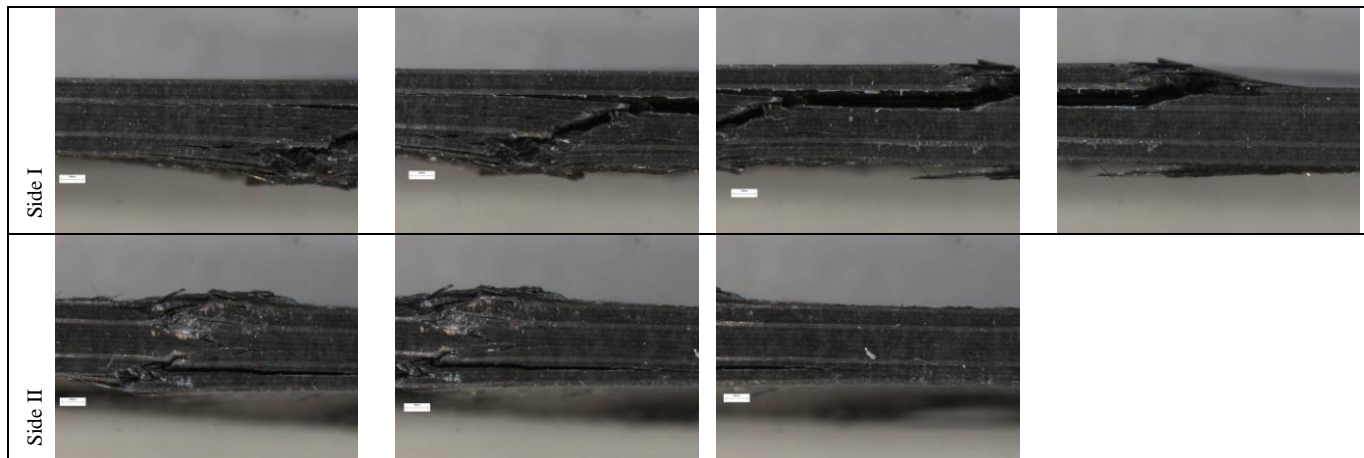
Figure 3.113: Photomontage of the nanoPA6,6 interleaved specimen sides (subjected to a 30 J impact).
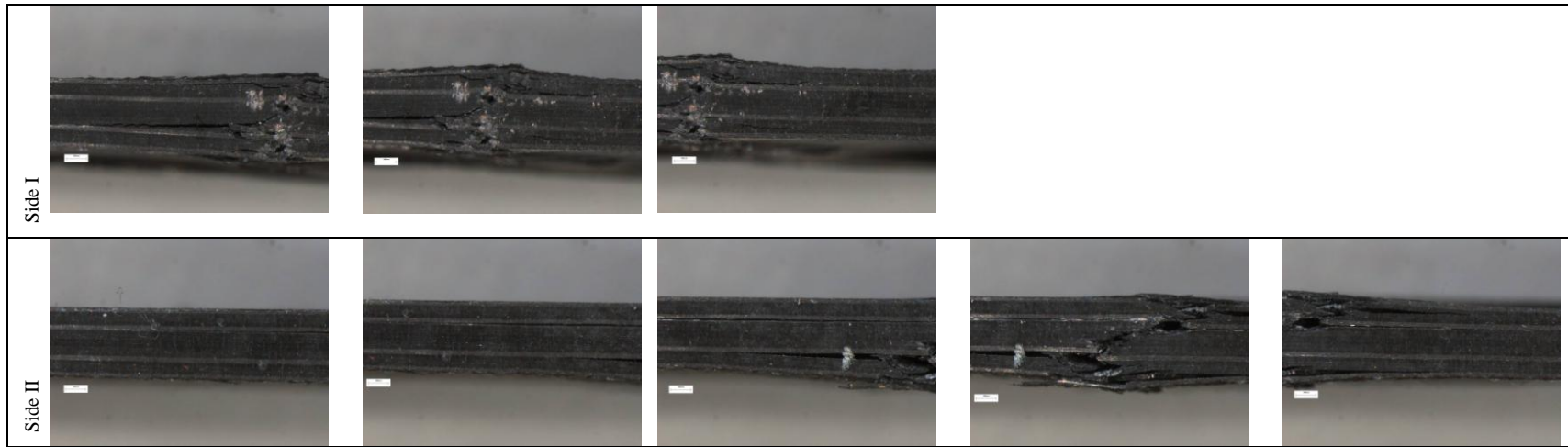
Figure 3.114: Photomontage of the nanoPVB interleaved specimen sides (subjected to a 30 J impact).

149
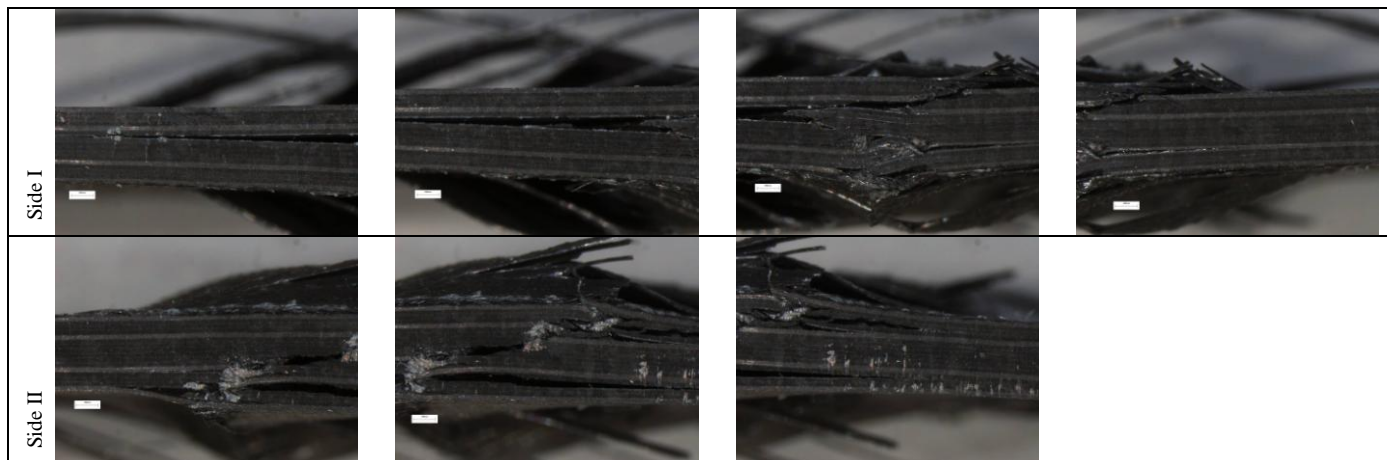
Figure 3.115: Photomontage of the nanoPES interleaved specimen sides (subjected to a 30 J impact).
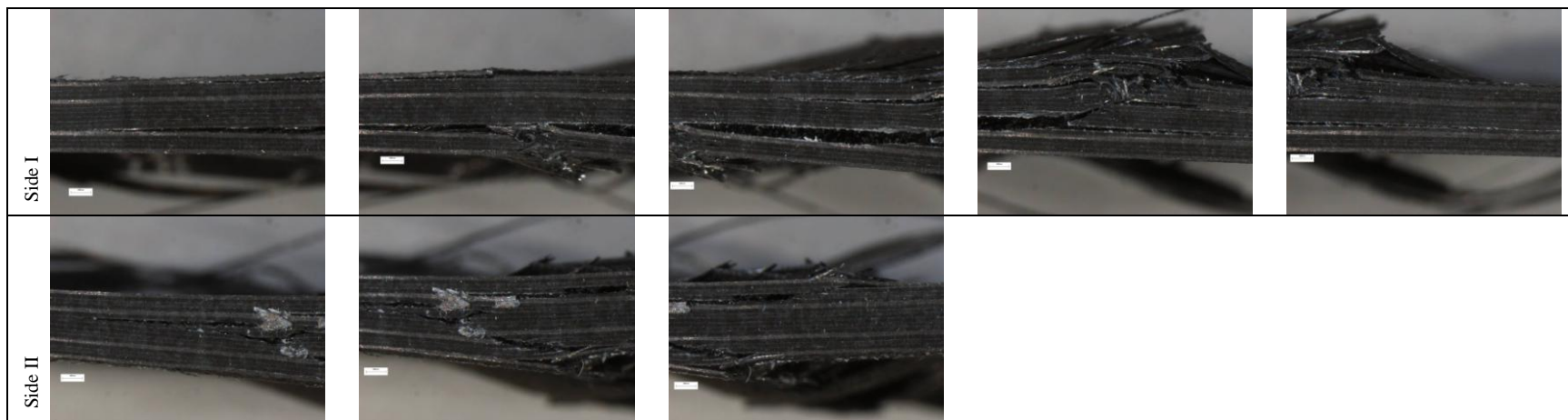
Figure 3.116: Photomontage of the microPPS interleaved specimen sides (subjected to a 30 J impact).
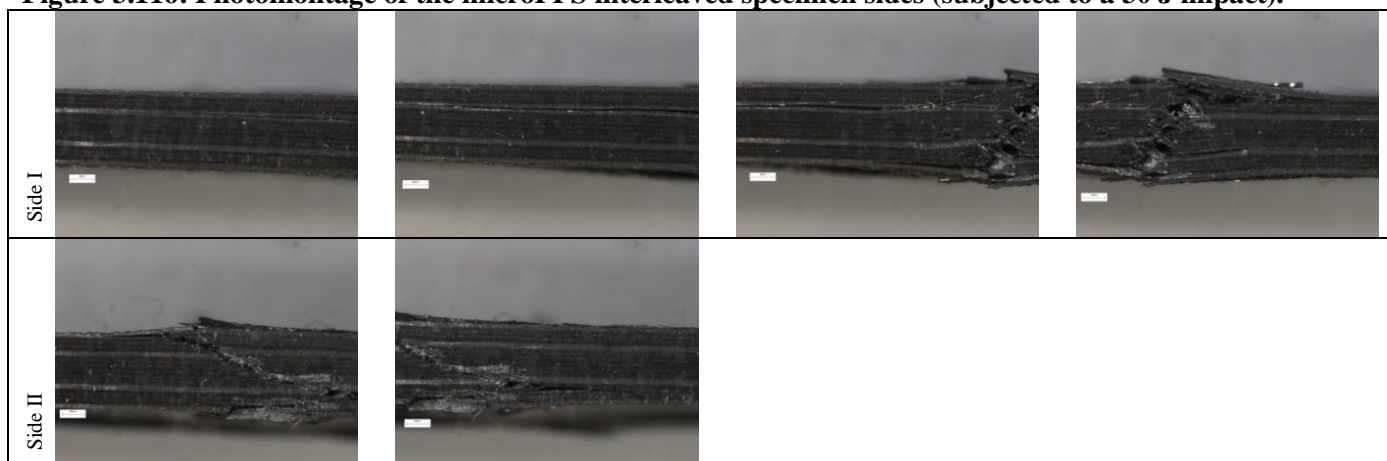
Figure 3.117: Photomontage of the microPEI interleaved specimen sides (subjected to a 30 J impact).
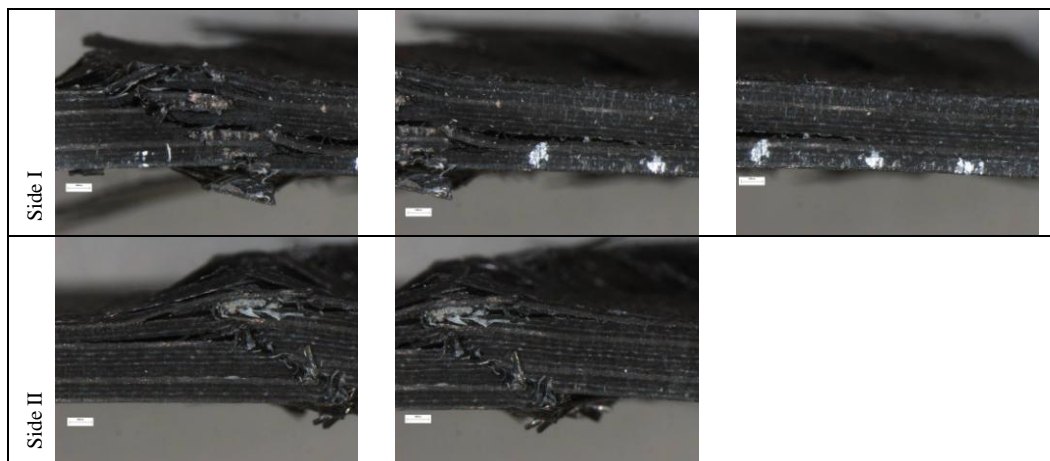
Figure 3.118: Photomontage of the microtricot interleaved specimen sides (subjected to a 30 J impact).

151
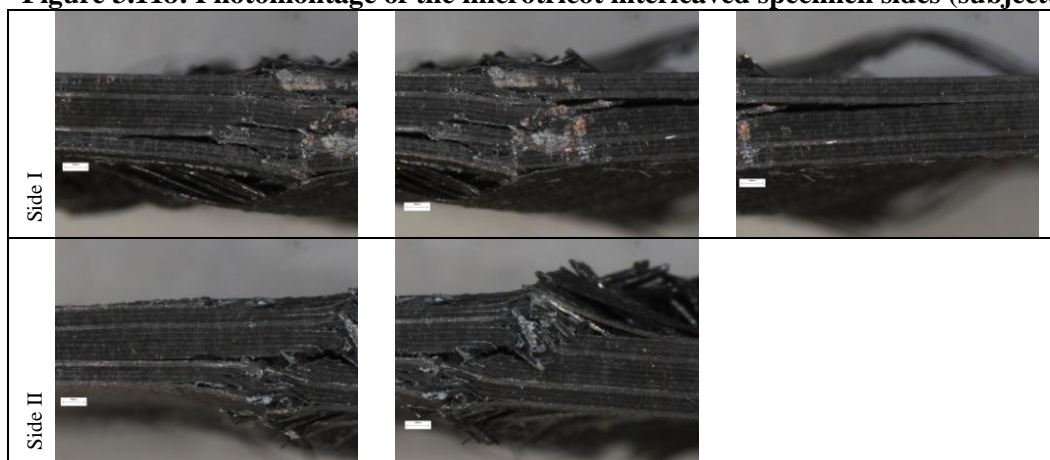
Figure 3.119: Photomontage of the microPPSnanoPA6,6 interleaved specimen sides (subjected to a 30 J impact).
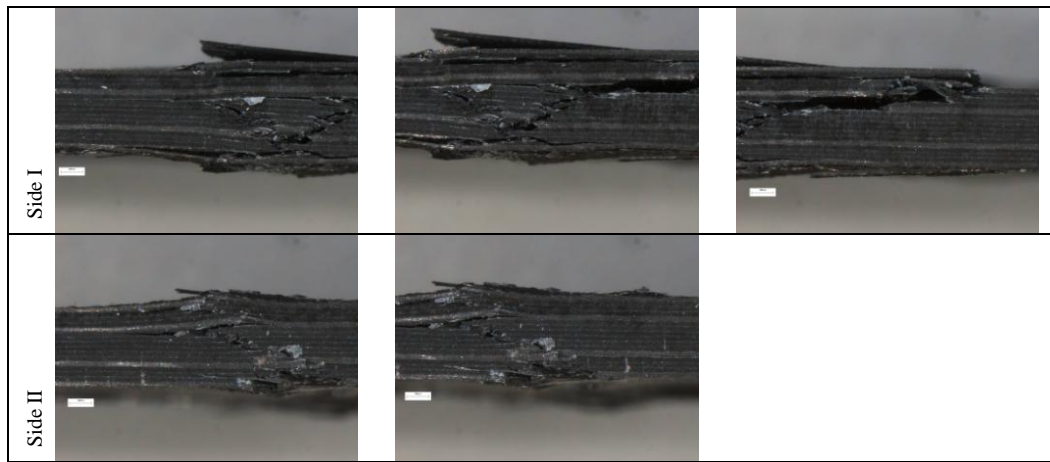
Figure 3.120: Photomontage of the microPEInanoPA6,6 interleaved specimen sides (subjected to a 30 J impact).
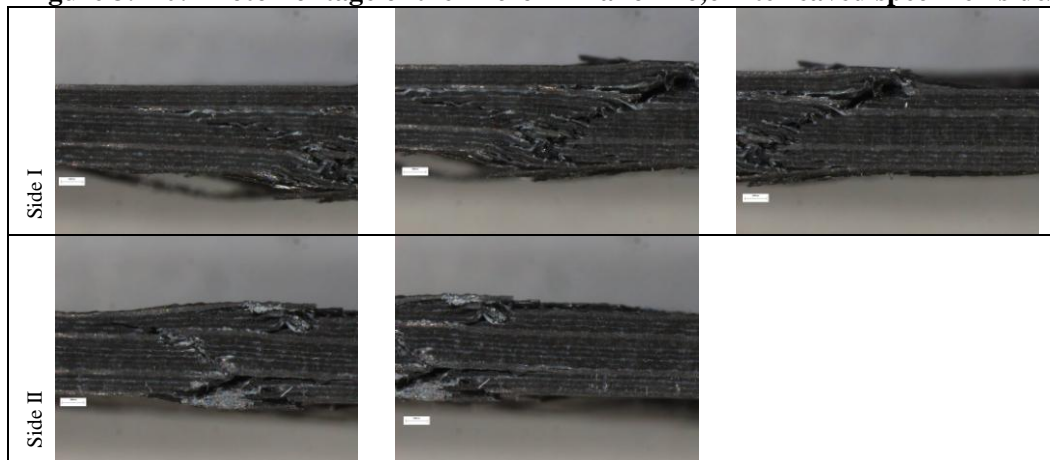
Figure 3.121: Photomontage of the microtricotnanoPA6,6 interleaved specimen sides (subjected to a 30 J impact).

From these images, it seems that more delamination or damage occurred on one side compared to the other, which could be due to uneven loading across the top of the specimen during the compression testing. It also appears that all specimens had multiple cracks or delaminations extending from the break zone.

For a more effective comparison and analysis of the damage, the length of the damage region, on the sides of the specimens (see Section 2.6.2.1) subjected to impact energies of 25 and 30 J were recorded and an average value was taken (see Tables 3.25 and 3.24).

Table 3.24: Damage region length for specimens subjected to a 25 J impact.

		length of damage region for 25 J impacted specimens		
	specimen	side a	side b	average
1	control	45	21	33
2	nanoNyplex	20	14	17
3	nanoPMMA	17	0	9
4	nanoPA6,6	37	15	26
5	nanoPVB	10	17	14
12	nanoPES	-	-	
6	microPPS	41	14	28
7	microPEI	12	54	33
8	microtricot	-	-	
9	microPPSnanoPA6,6	47	29	38
10	microPEInanoPA6,6	31	30	31
11	microtricotnanoPA6,6	-	-	

Table 3.25: Damage region length for specimens subjected to a 30 J impact.

		length of damage region for 30 J impacted specimens		
	specimen	side a	side b	average
1	control	43	18	31
2	nanoNyplex	35	12	24
3	nanoPMMA	30	51	41
4	nanoPA6,6	28	19	24
5	nanoPVB	17	37	27
12	nanoPES	34	22	28
6	microPPS	45	24	35
7	microPEI	35	17	26
8	microtricot	18	16	17
9	microPPSnanoPA6,6	24	21	23
10	microPEInanoPA6,6	22	16	19
11	microtricotnanoPA6,6	20	16	18
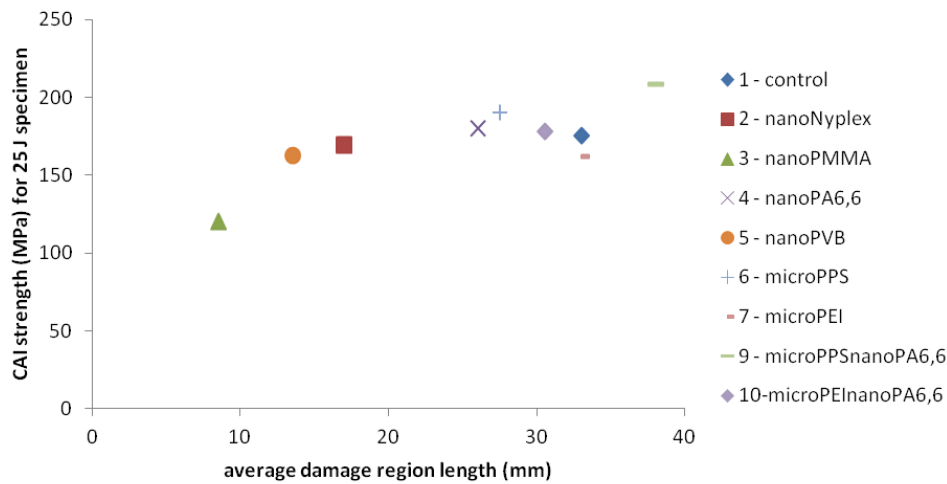
Figure 3.122: CAI strength for all specimens subjected to an impact of 25 J vs. average damage region length.
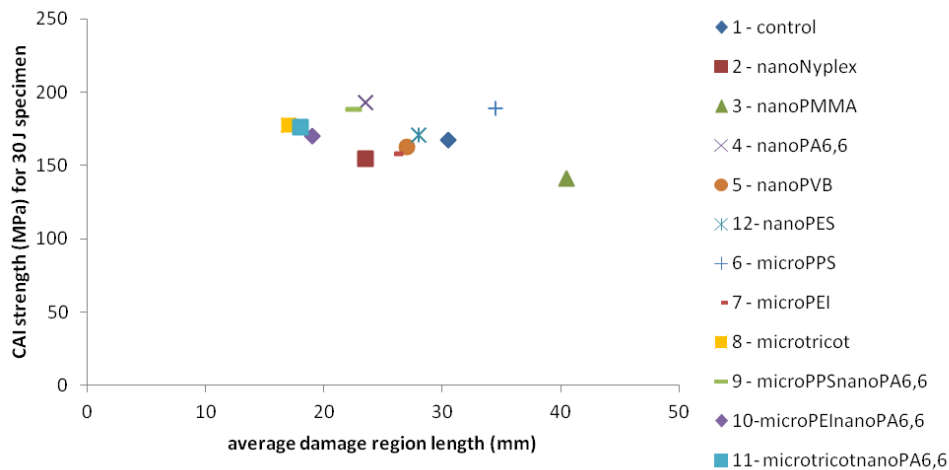
Figure 3.123: CAI strength for all specimens subjected to an impact of 30 J vs. average damage region length.

Figures 3.122 and 3.123 show the CAI strengths vs. the length of the damage region for the 25 and 30 J impacted specimens. From Figure 3.122, it appears in general that the damage zone generally increased as the CAI strength increased.

From Figure 3.122 it seems that the nanoPA6,6, microPPS and microPEInanoPA6,6 interleaved specimens had a smaller damage region and higher CAI strengths than the control specimens, suggesting these interleavings did help to restrict damage which lead to improved CAI strengths.

From Figure 3.123 it appears that there was no general correlation between the length of the damage zone and the CAI strength, which contrasts to the results

154

shown in Figure 3.122. From Figure 3.123 it can be seen that nanoPA6,6, nanoPES, microPPSnanoPA6,6, microPEInanoPA6,6 and microtricotnanoPA6,6 interleaved specimens had a smaller damage region lengths and higher CAI strengths than the control. It was also noted that microPEI interleaved specimen had a lower CAI strength and longer damage zone than the microPEInanoPA6,6 specimen, suggesting that the length of the damage zone was decreased by the addition of the PA6,6 nanofibre.

3.5 Tension - tension fatigue testing

The results are shown below in Figure 3.124 and the raw data is shown in the appendix (see Section 6.5). The percentage increase in the number of cycles to failure for each cyclic stress for specimen is shown in Table 3.26.
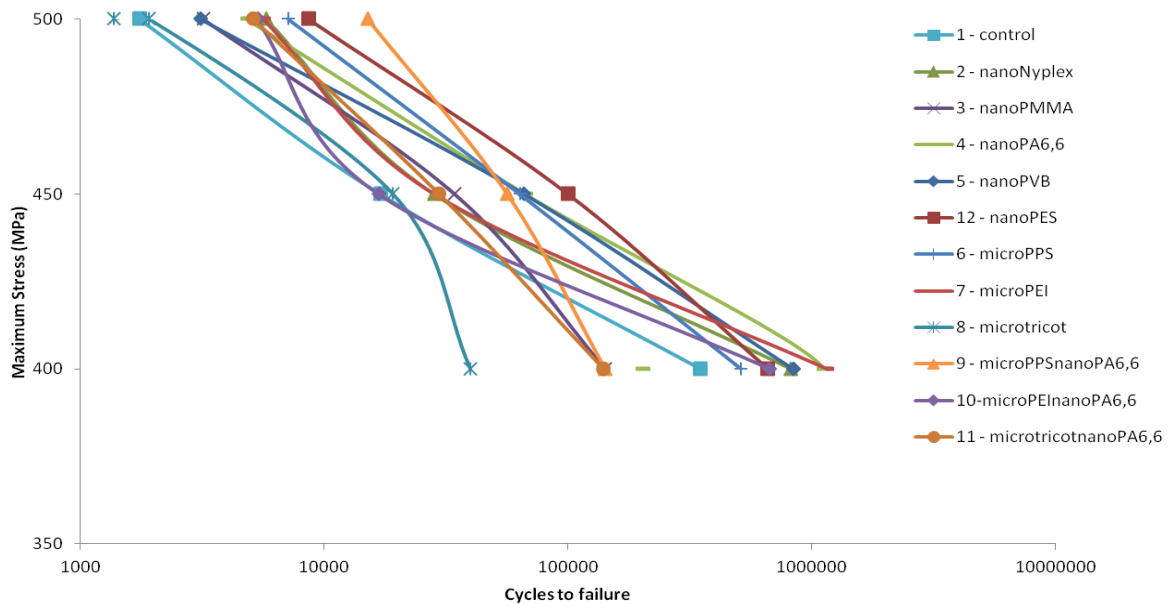
Figure 3.124: Maximum cyclic stress vs. cycles to failure for all specimen types.

Table 3.26: Percentage increases in the number of cycles to failure for all specimens.

Max cyclic stress (MPa)	500	450	400
Specimen	% increase compared to control specimen	% increase compared to control specimen	% increase compared to control specimen
Control	-	-	-
nanoNyplex	329	166	234
nanoPMMA	182	201	41
nanoPA6,6	275	394	321
nanoPVB	177	388	239
nanoPES	493	589	189
microPPS	407	373	147
microPEI	322	167	330
microtricot	109	113	11
microPPSnanoPA6,6	859	331	40
microPEInanoPA6,6	303	99	192
microtricotnanoPA6,6	292	174	40

3.5.1 General trends and variability

From Figure 3.124 it can be seen that generally as the cyclic stress decreased, the number of cycles to failure increased for all specimen types.

156

Fatigue data is well known to have a large amount of variation, particularly at longer fatigue lives [67]. In addition, further variability would have been introduced due to inexpert specimen preparation and conduct of tests; particularly in early tests (a new machine was installed). This was highlighted by the results for the two nanoPA6,6 interleaved specimens (see Figure 3.124) tested at a maximum stress of 400 MPa. One nanoPA6,6 interleaved specimen was not tabbed properly and failed at a very low number of cycles, however, a second specimen tested at the same conditions, but tabbed properly, failed at a considerably larger number of cycles to failure. The results for the initial nanoPA6,6 specimen were therefore excluded.

Some of the variability could have been caused by the test machine fittings becoming loose during testing, which could have occurred for nanoPMMA, microPPSnanoPA6,6, and microtricotnanoPA6,6 interleaved specimens at a maximum of 400 MPa cyclic stress. This could explain the steeper gradient between 450 MPa and 400 MPa for these specimens.

Furthermore, some variation may also have been introduced due to the interruption of the nanoNyplex (400MPa), nanoPMMA (500 MPa), nanoPES (450 MPa) microPEI (400 MPa), and microtricot (450 and 400MPa) specimen tests (see Section 6.5). However, the results did not seem greatly affected by this.

As noted in Section 2.7 and Section 6.5, most specimens had 55 mm tabs, although some had 60 mm tabs or no tabs (in this case emery paper was used). This may have also introduced some variation between specimens; however, it was thought that the amount of variation would be minimal since all specimens failed within the gauge length, where the stress would not have been affected.

Other sources of variability include that caused by sample variation due to defects including fibre misalignment and voids.

3.5.2 Comparison of fatigue lives

At a maximum cyclic stress of 500 MPa, all specimens, apart from the microtricot interleaved specimen, failed at a higher number of cycles than the control specimen.

At a maximum cyclic stress of 450 MPa, however, all interleaved specimens showed considerable improvement in the number of cycles to failure compared to the control specimen.

At a maximum cyclic stress of 400 MPa, only the nanoNyplex, nanoPVB, nanoPES, microPPS, microPEI and microPEInanoPA6,6 interleaved specimens showed an improvement in the number of cycles to failure compared to the control specimen, while the nanoPMMA, microtricot, microPPSnanoPA6,6 and microtricotnanoPA6,6, interleaved specimens failed at less cycles than the control specimen (likely due to variation in the test as discussed earlier).

Of nanofibre interleaved specimens, nanoPA6,6, nanoPVB and nanoPES interleaved specimens failed at the highest number of cycles. Of the microfibre interleaved specimens, microPPS and microPEI interleaved specimens failed at the highest number of cycles.

For clearer assessment, the data for microfibre interleaved specimens is displayed in Figure 3.125.
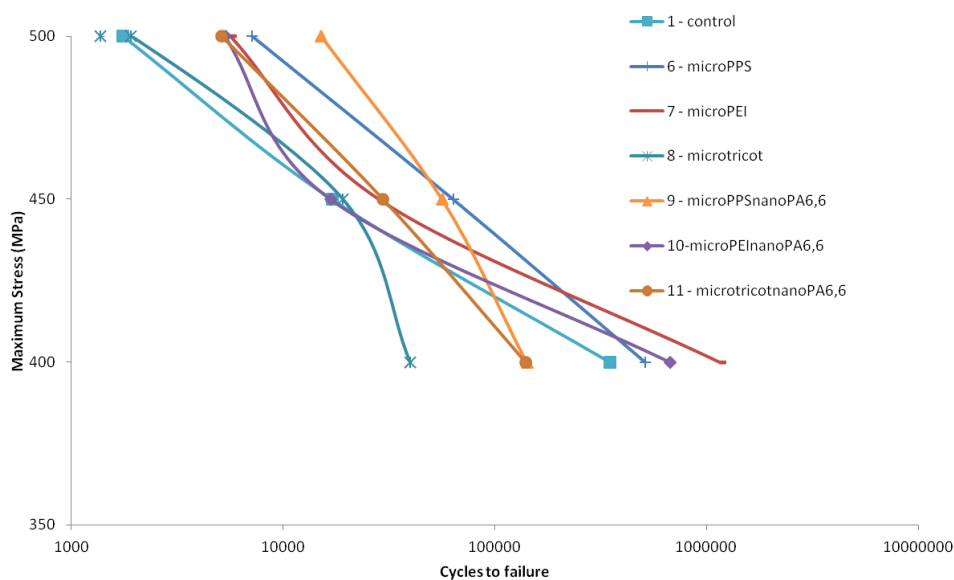
Figure 3.125: Maximum cyclic stress vs. cycles to failure for microfibre interleaved specimens.

Upon closer inspection, it seems that cycles to failure for the microPPS interleaved specimens was higher than for the other microfibre only interleaved

specimens. As discussed in Section 3.4.2.1, the PPS microfibre had a smaller diameter than the PEI microfibre, but similar areal weight, so there would be more PPS fibres per unit area to act as barriers to inhibit crack propagation. More barriers would have been likely to increase the energy required for crack growth and decrease the damage accumulation rate.

The microtricot interleaved specimens had the lowest cycles to failure of the specimens with interleavings in general. It is noted that the diameter of the microtricot fibres was very large compared to any of the other interleaving fibres, and were much larger than the carbon fibres (see Section 3.2.2). In previous SEM work it appears that the thickness of the interlayer region varied due to the large microtricot fibres (see Section 3.2.2, Figures 3.42 and 3.45). This may have disrupted the fibre alignment or 'wrinkled' the plies of carbon fibre, introducing stress concentrations which could have lowered the cycles to failure.

At a maximum cyclic stress of 500 MPa, it appears that the number of cycles to failure was higher for the microPPSnanoPA6,6 interleaved specimen compared to the microPPS interleaved specimen, suggesting that the number of cycles to failure was extended with the addition of the PA6,6 nanofibre. It also seemed that PA6,6 fibres increased the number of cycles to failure for microtricotnanoPA6,6 specimens compared to microtricot only specimens, but reduced the number of cycles for microPEInanoPA6,6, specimens compared to microPEI only specimens. The increase in the number of cycles to failure for specimens interleaved with microPPSnanoPA6,6 and microtricotnanoPA6,6 (compared to their microfibre only counterparts) would most likely be due to the reinforcement of the matrix by the PA6,6 nanofibre in between the microfibres.

3.5.3   Assessment of toughening mechanisms

It is clear from the results that most interleavings were effective in improving the fatigue life. This is most likely because the interleavings provided barriers for cracks (crack deflection) and provided reinforcement via other mechanisms such as fibre bridging, debonding and pull out. These mechanisms would increase the energy required in order for cracks to propagate, as discussed in Section 3.4.2.1 (also see Section 1.4.3). An increase in the amount of energy required for crack growth would have been likely to decrease the damage accumulation rate.

However, the effectiveness of the fibres in providing toughening would be likely to be affected by factors identified in Section 3.4.2 (such as the fracture toughness of the polymer that the veil was made from). An assessment of each factor was undertaken in the following sections using information from Tables 3.21 - 3.23 (see Section 3.4.2.1).
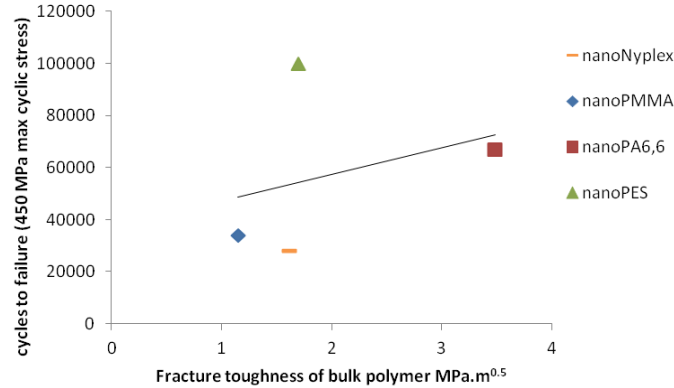
Figure 3.126: Number of cycles to failure for 450 MPa cyclic stress for nanofibre interleaved specimens vs. fracture toughness of the bulk polymers.
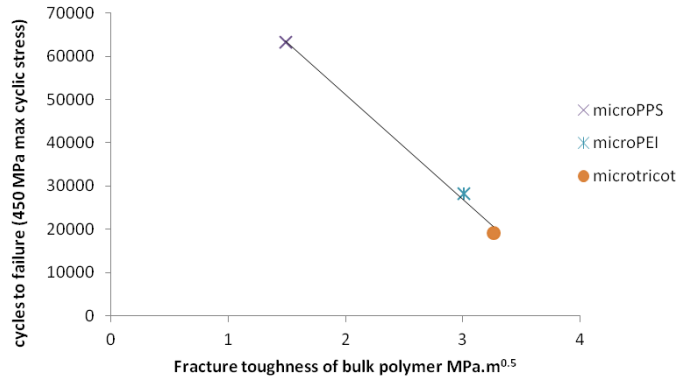
Figure 3.127: Number of cycles to failure for specimens interleaved with microfibre veils tested at 450 MPa maximum cyclic stress vs. fracture toughness of bulk polymer.
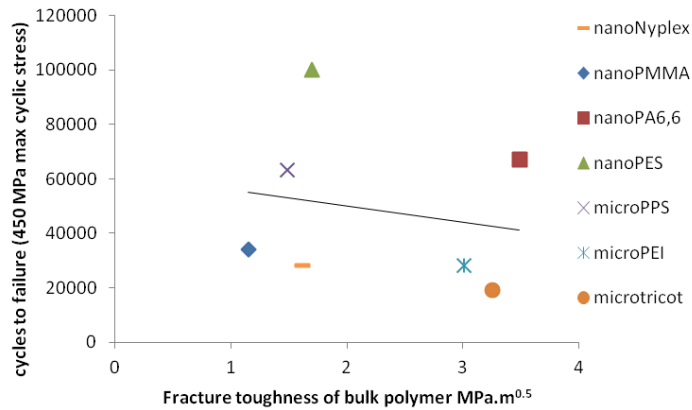
Figure 3.128: Number of cycles to failure for specimens interleaved with nanofibre and microfibre veils tested at 450 MPa maximum cyclic stress vs. fracture toughness of bulk polymer.

From Figure 3.126 (nanofibre specimens) it appears that as the fracture toughness of the bulk polymer increased, so did the number of cycles to failure, however, the opposite was found for microfibre interleaved specimens (see Figure 3.127). However, overall (see Figure 3.128) it seems that there was no correlation between fracture toughness of the bulk polymer and the number of cycles to failure. Note that nanoPVB was excluded as a fracture toughness value could not be obtained from available data.

From Figure 3.129, it appears that there was generally a decrease in the number of cycles to failure as the interfacial area increased for nanofibre specimens. In contrast, from Figure 3.130 it appears that as the interfacial area increased so did the number of cycles to failure for the microfibre interleaved specimens.
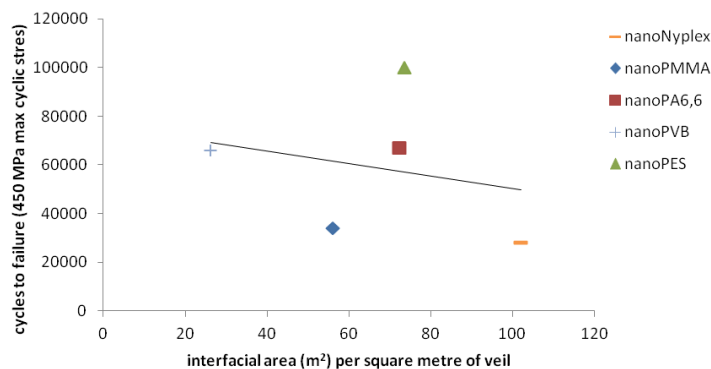
Figure 3.129: Number of cycles to failure at a maximum cyclic stress of 450 MPa vs. interfacial area per square metre of veil for nanofibre interleaved specimens.

161
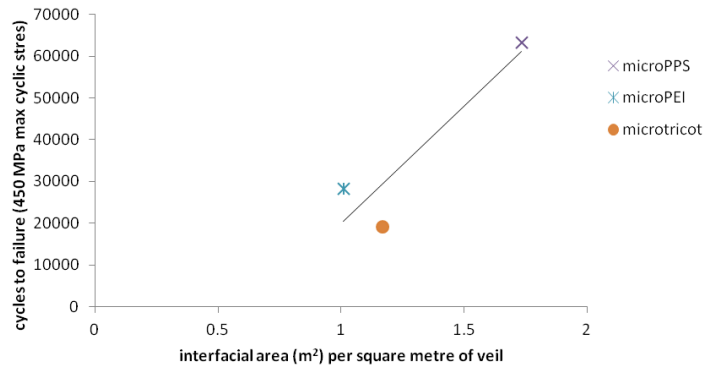
Figure 3.130: Number of cycles to failure for 450 MPa maximum cyclic stress for specimens interleaved with microfibre veils vs. interfacial area per square metre of veil.
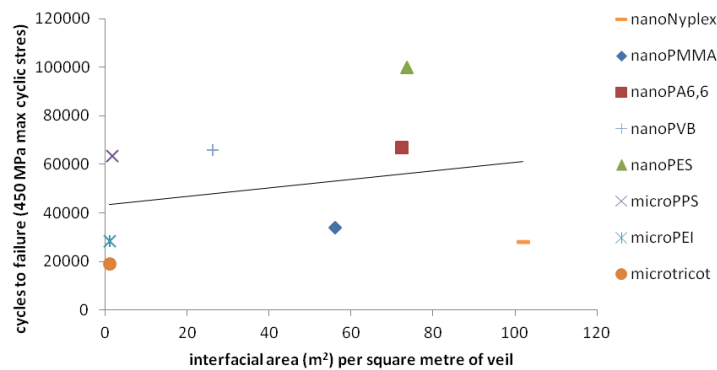
Figure 3.131: Number of cycles to failure for 450 MPa maximum cyclic stress for specimens interleaved with nanofibre and microfibre veils vs. interfacial area per square metre of veil.

Overall, from Figure 3.131 it seems the higher the interfacial area the higher number of cycles to failure.

From Figure 3.132, it appears that the more incompatible the polymer veil (i.e. the larger the difference in Hildebrand parameters between the bulk polymer and the epoxy), the greater the number of cycles to failure for the nanofibre interleaved specimens. However, it is noted that all of polymers used for nanofibre veils had relatively similar Hildebrand parameters to the epoxy.

162
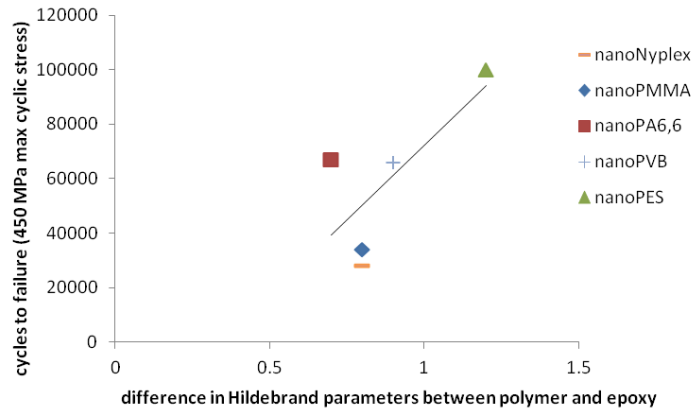
Figure 3.132: Number of cycles to failure at a maximum cyclic stress of 450 MPa for corresponding specimens interleaved with nanofibre veils vs. the difference between the Hildebrand parameters for the polymers and epoxy.
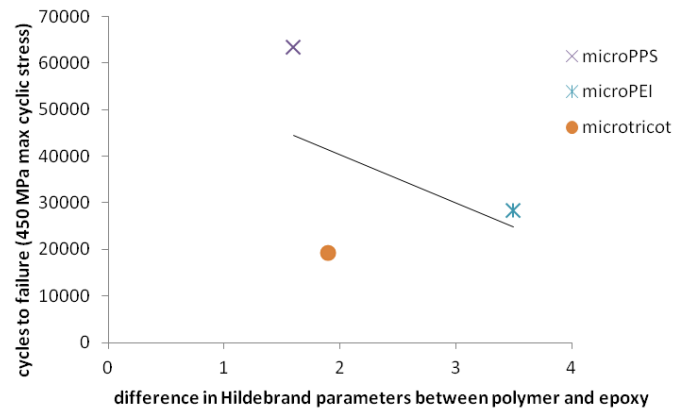
Figure 3.133: Number of cycles to failure for 450 MPa maximum cyclic stress for the corresponding specimens interleaved with microfibre veils vs. the difference in Hildebrand parameters between the bulk polymers and epoxy.
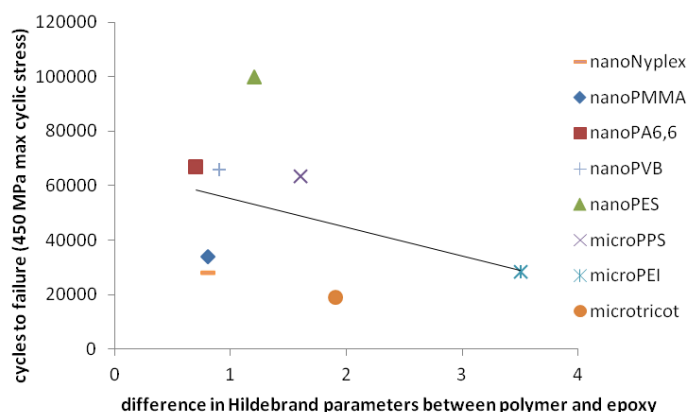
Figure 3.134: Number of cycles to failure for 450 MPa maximum cyclic stress for corresponding specimens interleaved with nanofibre and microfibre veils vs. the difference in Hildebrand parameters between the bulk polymers and epoxy.

For microfibre specimens (see Figure 3.133), it appears that the more compatible the fibre was with the epoxy (i.e. the smaller the difference in Hildebrand parameters) the greater the number of cycles to failure (apart from microtricot interleaved specimens, but this is likely due to the large diameter fibres, as discussed previously). Overall from Figure 3.134, it also seems that the specimens that were interleaved with fibres that were more compatible had longer fatigue lives.
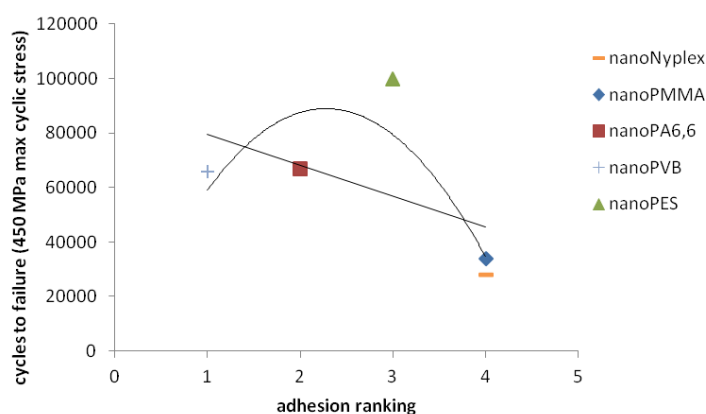
Figure 3.135: Number of cycles to failure for a maximum cyclic stress of 450 MPa for specimens interleaved with nanofibre veils vs. adhesion ranking (where 1 indicates strongest adhesion strength and 7 indicates weakest adhesion strength).

164
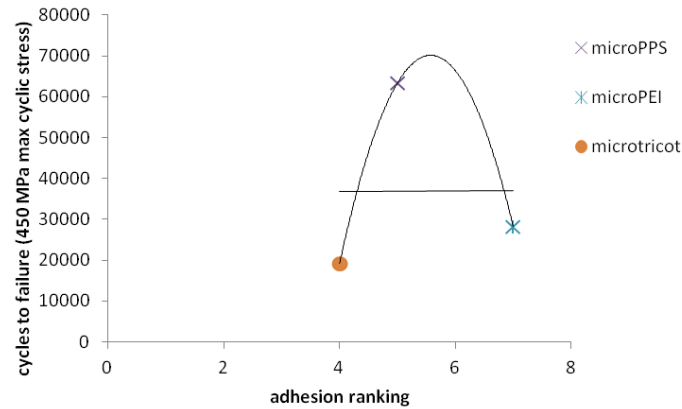
Figure 3.136: Number of cycles to failure for 450 MPa maximum cyclic stress for specimens interleaved with microfibre veils vs. adhesion ranking (where 1 indicates strongest adhesion strength and 7 indicates weakest adhesion strength).
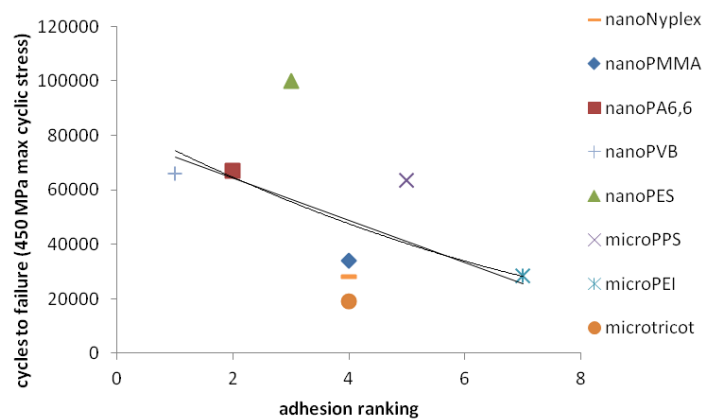
Figure 3.137: Number of cycles to failure for 450 MPa maximum cyclic stress for specimens interleaved with nanofibre and microfibre veils vs. adhesion ranking (where 1 indicates strongest adhesion strength and 7 indicates weakest adhesion strength).

It appears from Figure 3.135 (nanofibre interleaved specimens) that higher adhesion strength between the interleaving fibre and matrix resulted in the highest number of cycles to failure. This result is consistent with theory discussed in Section 1.4.4. However, from Figure 3.136 (microfibre specimens) it seems that there was no clear correlation. From Figure 3.137, however, it seems (in general) that specimens with the highest number of cycles to failure had higher adhesion strength between the interleaving fibres and the matrix.

Although one dominant factor could not be identified from this analysis, it seems that in general, a veil with a large number of interleaving fibres per unit area, and a medium to high degree of adhesion strength (between the interleaving fibres and

165

the matrix) was more likely (when used as an interleaving) to increase the fatigue performance (when used as an interleaving) to the greatest extent.

3.5.4 Post fatigue visual inspection, optical microscopy and SEM analysis

3.5.4.1 Visual inspection

Nanofibre interleaved specimens

Photographs of the nanofibre interleaved specimens and the control specimen tested at a maximum cyclic stress of 400 MPa are shown in Figure 3.138. In general, specimens presented more damage with higher number of cycles to failure.
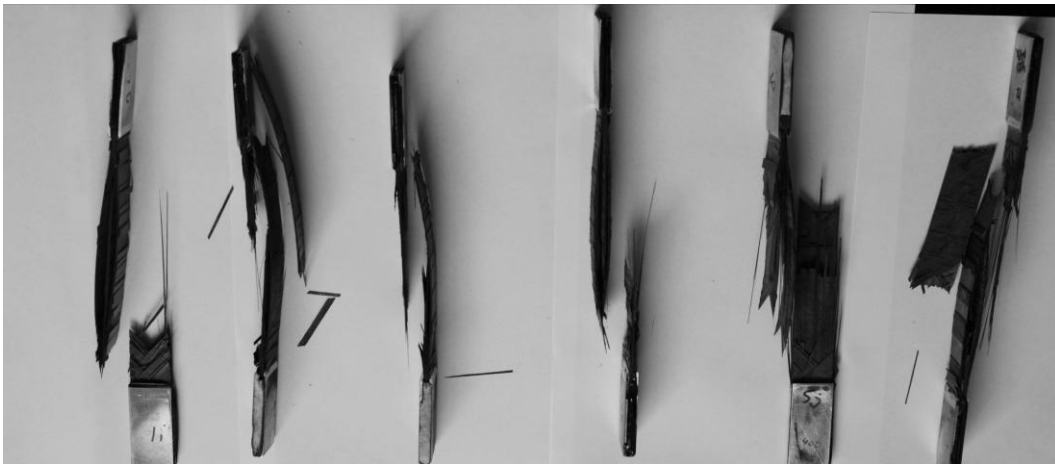
Figure 3.138: From left: fatigued control specimen, nanoNyplex interleaved specimen, nanoPMMA interleaved specimen, nanoPA6,6 interleaved specimen, nanoPVB interleaved specimen and nanoPES interleaved specimen (all tested at a maximum cyclic stress of 400 MPa).
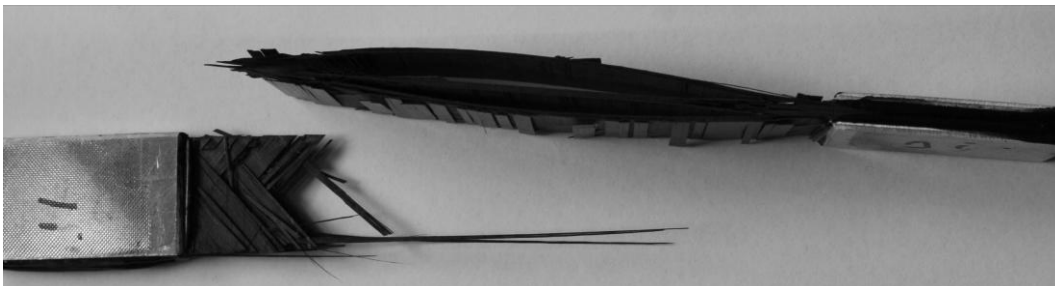
Figure 3.139: Fatigued control specimen.

The control specimen (shown in Figure 3.139) had delaminated between the 90° and 45° plies (separating the composite into three parts). It seems that most of the

90° plies on the outside of the specimen had separated from the composite. Some of the 45° plies near the break point had also separated and some of the 0° fibres had splayed (giving a brush like appearance).
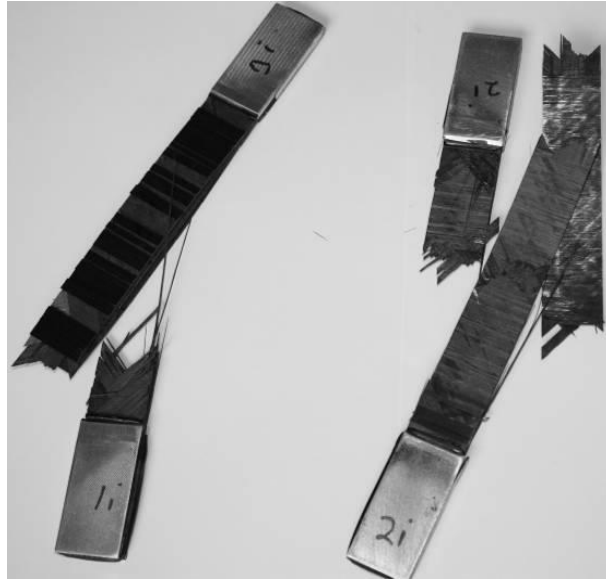
Figure 3.140: Fatigued control specimen (left) and nanoNyplex interleaved specimen (right).

The nanoNyplex specimen (see Figure 3.140) showed similar damage to the control specimen, but was broken into three main parts. The nanoPMMA specimen (see Figure 3.141) appeared to have more damage than the control specimen, as a lot of the specimen was missing (possibly pieces broke off during the final break). Some of the nanoPMMA specimen fracture surfaces appeared to be an opaque white (see Figure 3.142). The control specimen did not appear to have white areas on the fracture surfaces.
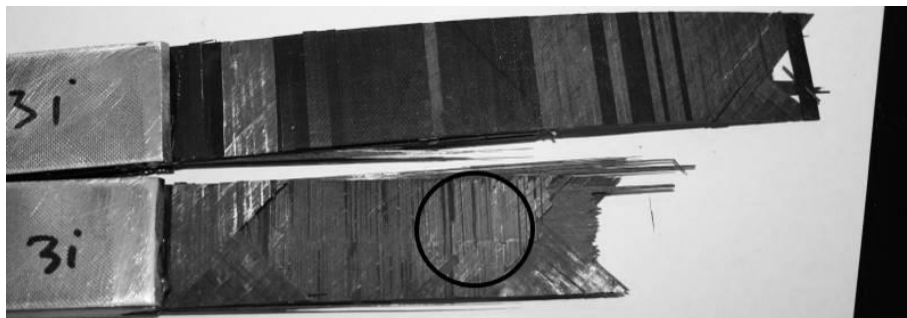
Figure 3.141: Fatigued nanoPMMA interleaved specimen (white area circled).
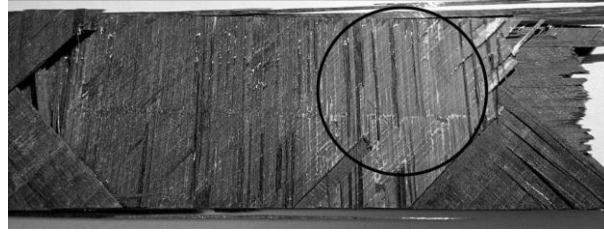
Figure 3.142: Fatigued nanoPMMA specimen showing white area (circled) at higher magnification.

Figure 3.143: Fatigued control specimen (left) and nanoPA6,6 interleaved specimen (right).

The delamination and damage of the nanoPA6,6 specimen (Figure 3.143) was similar to control specimen, except less of the outside 90° plies had separated from the composite. Some white rough surfaces were observed on some of the ply surfaces of the nanoPA6,6 specimen (see Figure 3.144), which were similar to those seem on the nanoPMMA specimen.
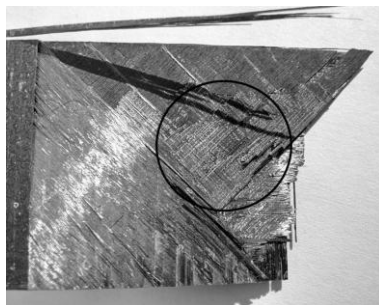
Figure 3.144: Fatigued nanoPA6,6 specimen showing rough surface (circled).

Figure 3.145: Fatigued control specimen (left) and nanoPVB interleaved specimen (right).

From Figure 3.145, it seems that the nanoPVB interleaved specimen had delaminated more than the control specimen, as a large amount of the ±45° plies and most of the 90° plies had separated from the specimen. It also appeared that more 0° fibres had splayed compared to the control specimen. No white areas were seen on the surfaces of this specimen.
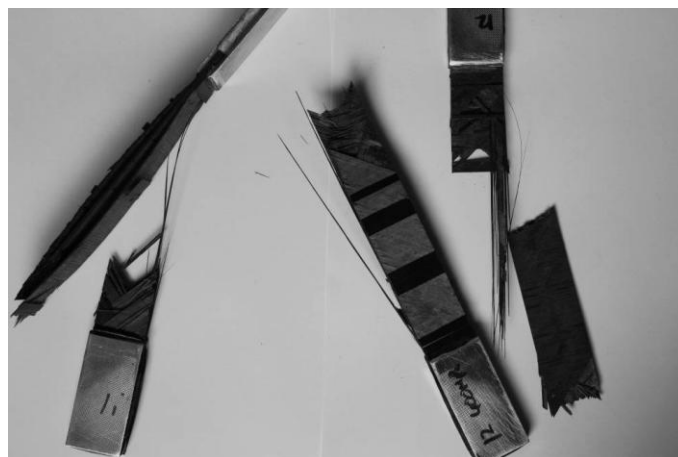
Figure 3.146: Fatigued control specimen (left) and nanoPES interleaved specimen (right).

The broken nanoPES interleaved specimen appeared to be similar to the broken control specimen, however, it did appear that more of the 90° ply on the outside of the laminate had separated from the specimen (Figure 3.146). There did not appear to be any white areas as seen for other specimen types.

A photograph of the microfibre and microfibre/nanofibre interleaved specimens and the control specimen tested at a maximum cyclic stress of 400 MPa are shown in Figure 3.147.

Figure 3.147: From left: fatigued control specimen, microPPS interleaved specimen, microPEI interleaved specimen, microtricot interleaved specimen, microPPSnanoPA6,6 interleaved specimen, microPEInanoPA6,6 interleaved specimen, microtricotnanoPA6,6 interleaved specimen, all tested at maximum cyclic stress of 400 MPa.

Figure 3.148: Fatigued control specimen (left) and microPPS interleaved specimen (right).

The microPPS interleaved specimen is shown in Figure 3.148. From visual inspection it appears that less 45° plies had separated and more outside 90° plies had stayed intact compared to the control specimen, even though the microPPS specimen had a higher number of cycles to failure. Some of the fracture surfaces

appeared to be white, similar to those seen on some nanofibre interleaved specimens.

Figure 3.149: Fatigued control specimen (left) and microPEI interleaved specimen (right).

The microPEI interleaved specimen is shown in Figure 3.149. From inspection, it appeared that less 45° plies had separated, but more 90° plies (on the outside of the specimen) had separated compared to the control specimen. Like the microPPS specimen, some rough white areas were seen on the specimen fracture surfaces.

Figure 3.150: Fatigued control specimen (left) and microtricot interleaved specimen (right).

The microtricot interleaved specimen (see Figure 3.150), was very different from the control specimen, as there was very little delamination, separation or splaying of the 0° fibres. The microtricot fibres were clearly visible on the fractured surfaces.

Figure 3.151: Fatigued control specimen (left) and microPPSnanoPA6,6 interleaved specimen (right).

Figure 3.152: Fatigued control specimen (left) and microPEInanoPA6,6 interleaved specimen (right).

The 90° plies were more intact on the outside of the microPPSnanoPA6,6 specimen (Figure 3.151) and microPEInanoPA6,6 interleaved specimen (Figure

3.152) than the control specimen. It also appeared that less 0° fibres were splayed. There were also some white rough areas on the fracture surfaces of these specimens. It was hard to distinguish if there was more or less damage overall for the microPPSnanoPA6,6 and microPEInanoPA6,6 specimens compared to the microPPS and microPEI interleaved specimens.

Figure 3.153: Control specimen (left) and microtricotnanoPA6,6 specimen (right).
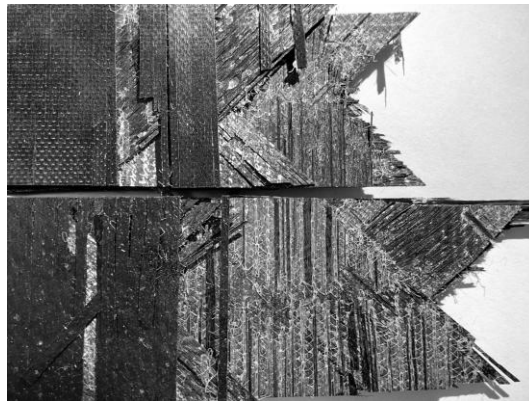
Figure 3.154: Fractured microtricotnanoPA6,6 specimen. The microtricot fibres were clearly visible.

The microtricotnanoPA6,6 specimen (Figure 3.153) had more delamination than the microtricot only specimen (but less than the control specimen). It appeared that significantly more 90° plies on the outside of the specimen were intact than the control specimen, but less were intact than the microtricot only specimen. There were less splayed 0° fibres than on the control specimen. The microtricot

fibres were clearly visible on some of the fracture surfaces (see Figure 3.154). It is noted that the microtricotnanoPA6,6 specimen failed at a larger number of cycles than the microtricot specimen, so it would be more likely that the specimen would be more damaged overall due to the increased amount of energy absorbed before failure.

3.5.4.2 Optical microscopy

Optical microscopy was used to inspect the fractured plies of the specimens more closely (see Section 2.7.1). A range of images of the fractured ply surface for the control specimen and the nanofibre interleaved specimens tested at a maximum cyclic stress of 400 MPa are shown in Figures 3.155 - 3.174.
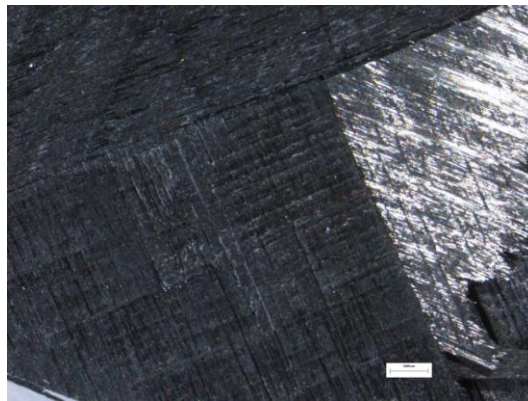
Figure 3.155: Fracture surface of control specimen at 6x magnification.
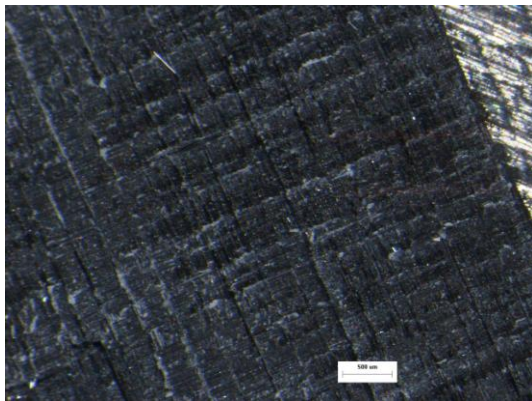
Figure 3.156: Close up of fracture surface of control specimen (shown in Figure 3.155) at 16x magnification. A slightly rough surface can be seen on the 45° ply.
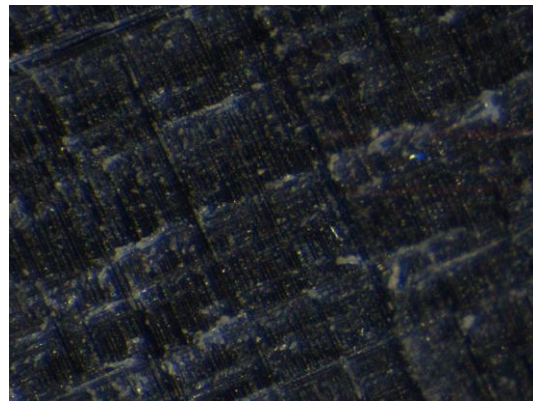
Figure 3.157: Close up of the slightly rough fracture surface of control specimen (shown in Figure 3.156) at 40x magnification.

From Figures 3.155 - 3.157, it appeared that the fracture surfaces of the control specimens (near the break point) were mostly flat, with some areas that were

slightly rough where one ply had separated from another during the fatigue test. The slightly rough area appeared to consist of epoxy.
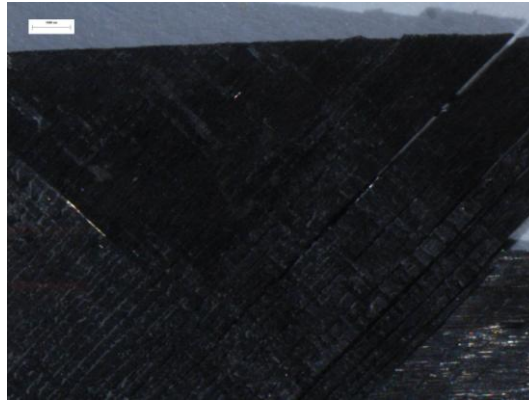
Figure 3.158: Fracture surface of the nanoNyplex interleaved specimen at 6x magnification.
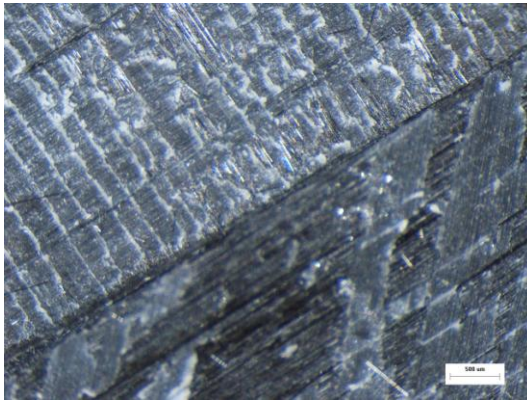
Figure 3.159: Close up of fracture surface of the nanoNyplex interleaved specimen (shown in Figure 3.158) at 16x magnification. A rough surface can be seen on both plies shown.
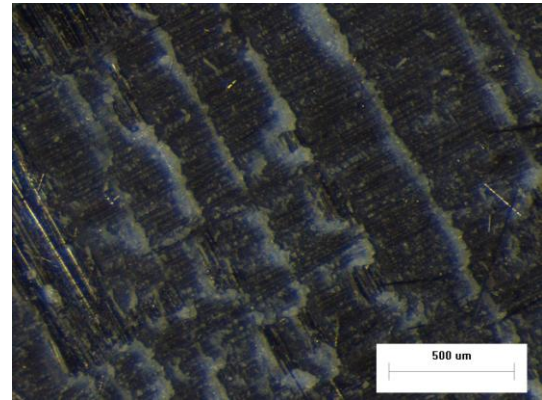
Figure 3.160: Close up of fracture surface of the nanoNyplex interleaved specimen (shown in Figure 3.158) at 40x magnification. The rough surface appears to be whiter in appearance than the rough areas of the control specimen (Figure 3.157).

From Figures 3.158 - 3.160, some of the fracture surfaces of the nanoNyplex interleaved specimen appeared rough. The rough surfaces also appeared white when viewed under the optical microscope. It is noted that the rough areas also seemed to be more abundant than the rough areas seen on the control specimen.
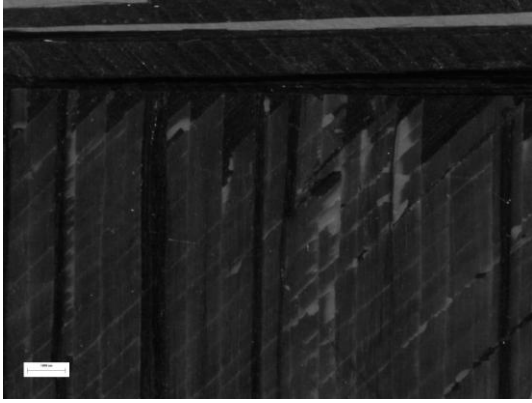
Figure 3.161: Whitened fracture surface of the nanoPMMA interleaved specimen (seen in Figure 3.142) at 6x magnification.
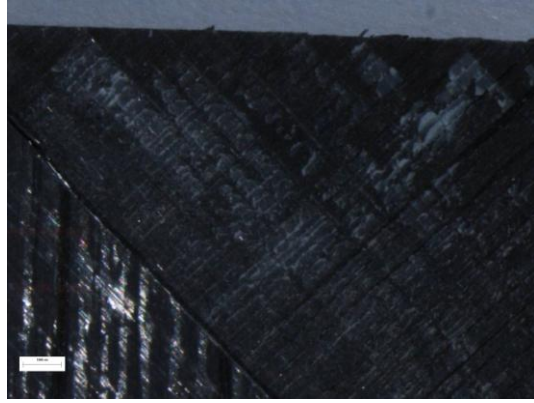
Figure 3.162: Fracture surface of the nanoPMMA interleaved specimen at 6x magnification.
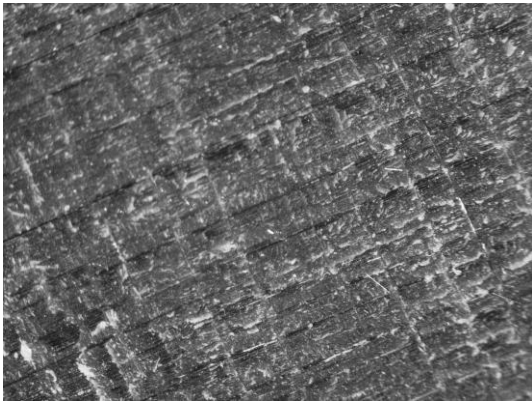
Figure 3.163: Fracture surface of the nanoPMMA interleaved specimen (shown in Figure 3.162) at 16x magnification.
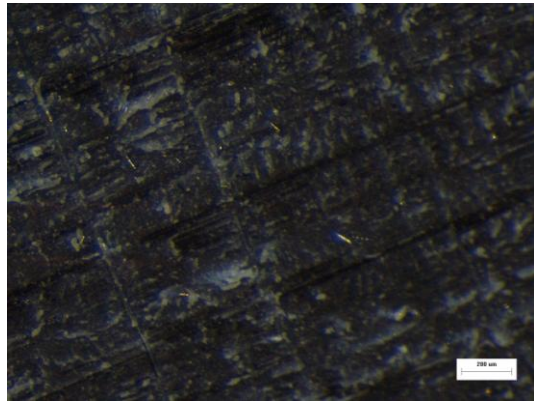
Figure 3.164: Fracture surface of the nanoPMMA interleaved specimen (shown in Figure 3.163) at 40x magnification.

The nanoPMMA interleaved specimens fracture surfaces (see Figures 3.162 - 3.164) were similar to the fracture surfaces of the nanoNyplex interleaved specimens (Figures 3.158 - 3.160). The rough areas on this specimen seemed to be more prevalent than on the control specimen.
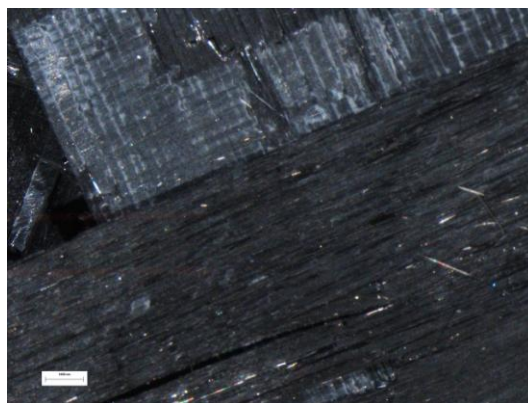
Figure 3.165: Fracture surface of the nanoPA6,6 interleaved specimen at 6x magnification.

176
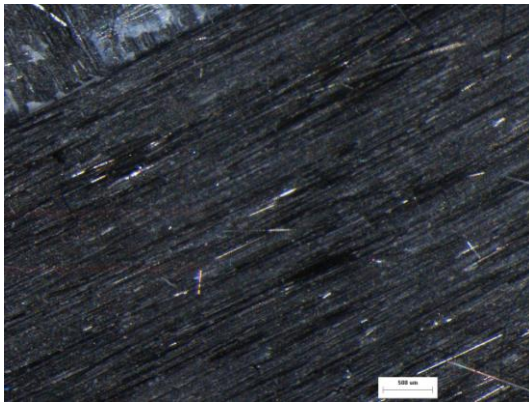
Figure 3.166: Close up of some of the fracture surface of the nanoPA6,6 interleaved specimen (shown in Figure 3.166) at 16x magnification.
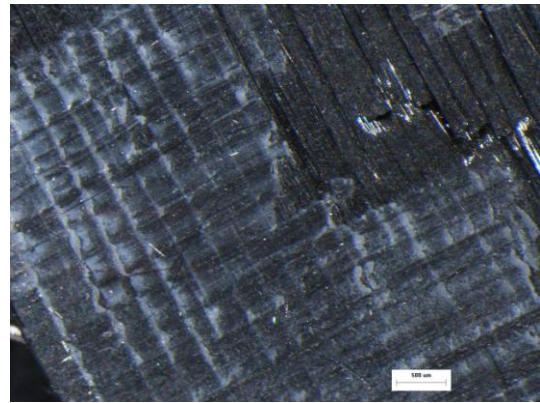
Figure 3.167: Close up of some of the fracture surface of the nanoPA6,6 interleaved specimen (shown in Figure 3.166) at 16x magnification.

Some of the fracture surfaces of the nanoPA6,6 interleaved specimens (see Figures 3.165 - 3.167) appeared to be rough while other plies seemed to be smooth. The rough areas were seen earlier in the visual inspection (see Figure 3.144) and seemed similar to that found on the nanoNyplex specimen.
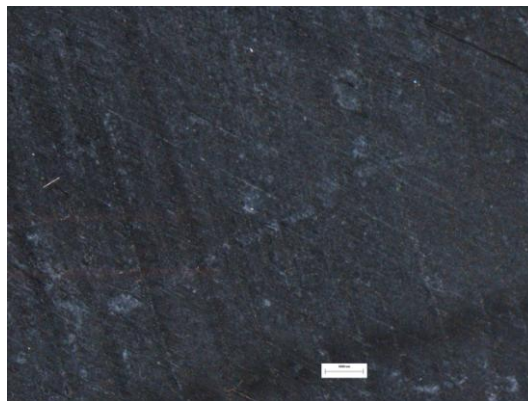
Figure 3.168: Fracture surface of the nanoPVB interleaved specimen at 6x magnification.
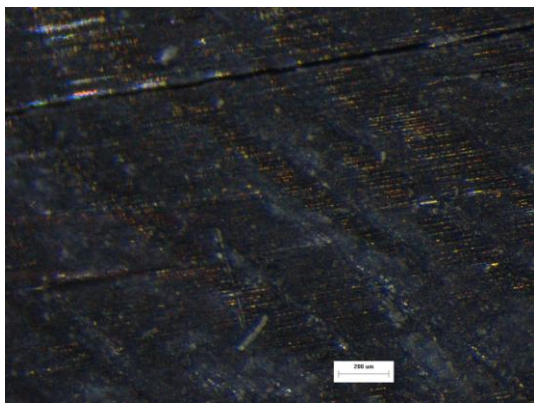
Figure 3.169: Close up of some of the fracture surface of the nanoPVB interleaved specimen (shown in Figure 3.166) at 16x magnification.
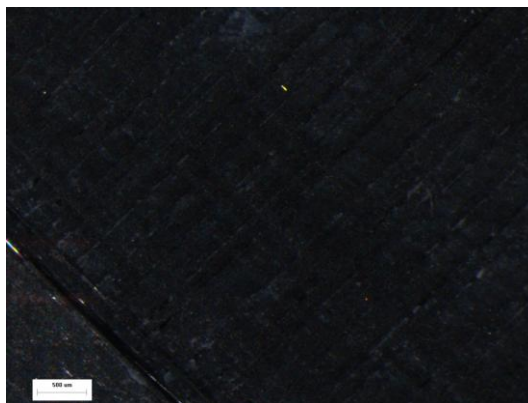
Figure 3.170: Close up of some of the fracture surface of the nanoPVB interleaved specimen (shown in Figure 3.168) at 16x magnification.

The fracture surfaces of the nanoPVB specimen (shown in Figures 3.168 - 3.170) seemed flat and dull in appearance. There was no evidence of rough areas that were observed on some of the other nanofibre interleaved specimens.

Similar to the nanoPA6,6 specimen, some areas of the fracture surfaces of the nanoPES interleaved specimens (see Figures 3.171 - 3.174) also appeared to be rough.
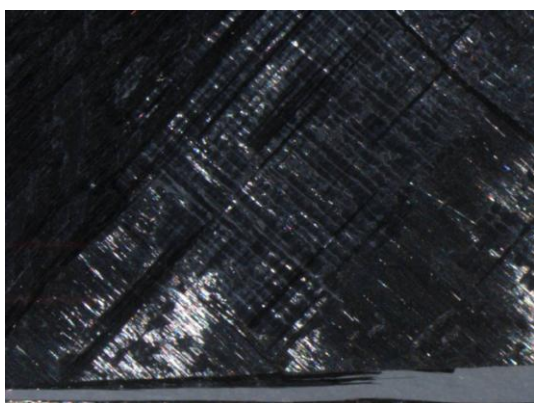
Figure 3.171: Fracture surface of the nanoPES interleaved specimen at 6x magnification.
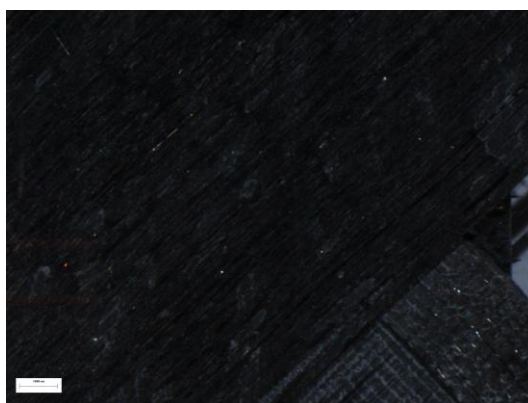
Figure 3.172: Fracture surface of the nanoPES interleaved specimen at 6x magnification.
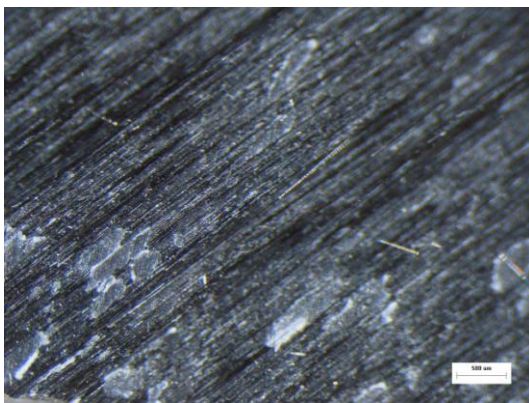
Figure 3.173: Close up of some of the fracture surface of the nanoPES interleaved specimen (shown in Figure 3.166) at 16x magnification.
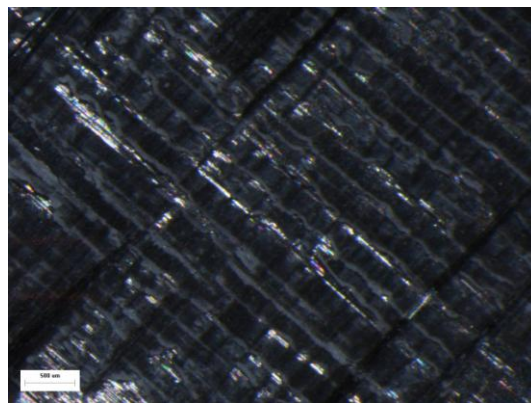
Figure 3.174: Close up of some of the fracture surface of the nanoPES interleaved specimen (shown in Figure 3.171) at 16x magnification.

Microfibre interleaved specimens

The images for the microfibre interleaved specimens are shown in Figures 3.175 - 3.192. The fracture surfaces of the microPPS specimen (Figures 3.175 - 3.178) and the microPEI specimen (Figures 3.179 and 3.180) appear to be rough and white in appearance. The PPS microfibre can be seen in Figures 3.177 and 3.178.
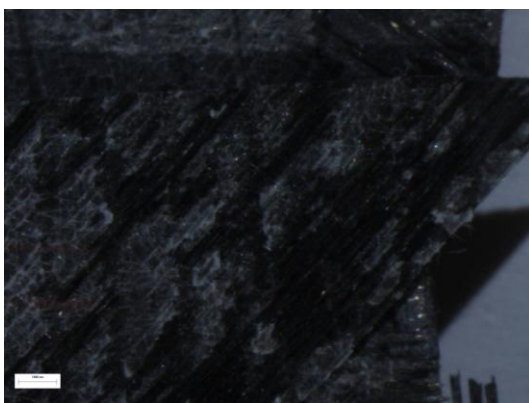
Figure 3.175: Fracture surface of the microPPS interleaved specimen at 6x magnification.
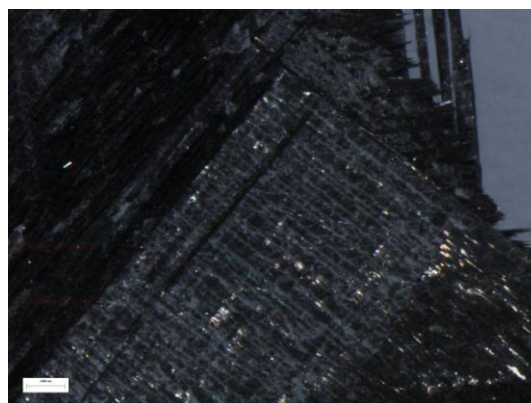
Figure 3.176: Fracture surface of the microPPS interleaved specimen at 6x magnification.
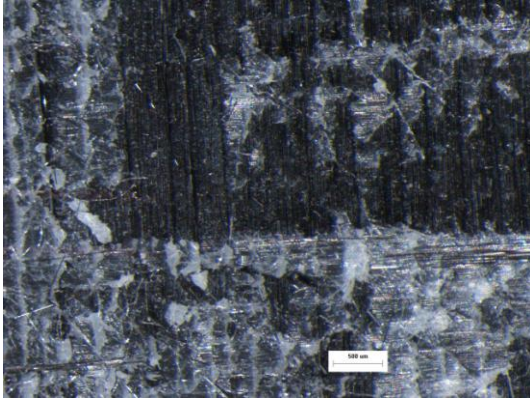
Figure 3.177: Close up of some of the fracture surface of the microPPS interleaved specimen (shown in Figure 3.175) at 16x magnification.
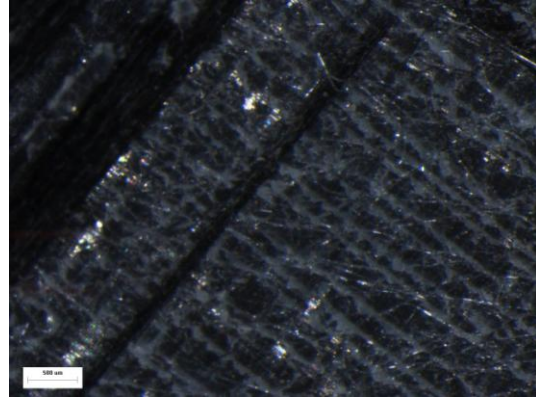
Figure 3.178: Close up of some of the fracture surface of the microPPS interleaved specimen (shown in Figure 3.176) at 16x magnification.
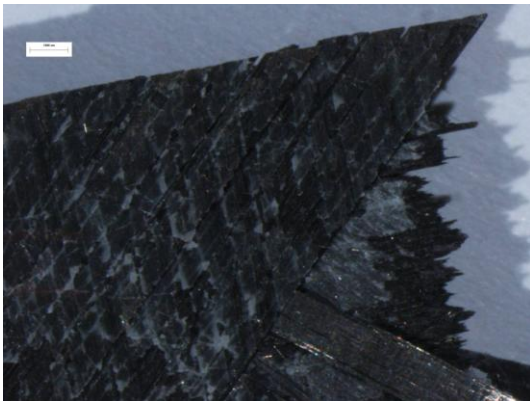
Figure 3.179: Fracture surface of the microPEI interleaved specimen at 6x magnification.
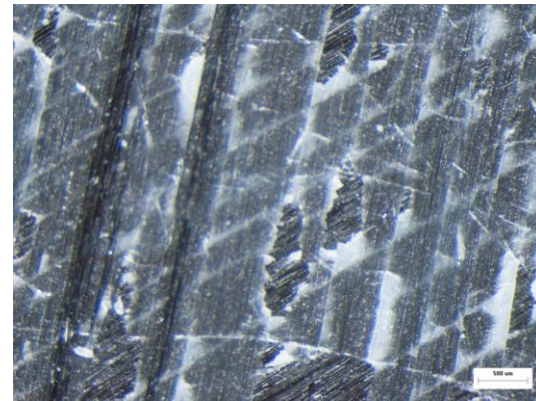
Figure 3.180: Close up of some of the fracture surface of the microPEI interleaved specimen (shown in Figure 3.179) at 16x magnification.

Some of the fracture surfaces of the microtricot interleaved specimen are shown in Figures 3.181 and 3.182. In Figure 3.181 the microfibre could clearly be seen. The plies appeared 'shiny' under the optical microscope. There did not appear to be any whitened areas.
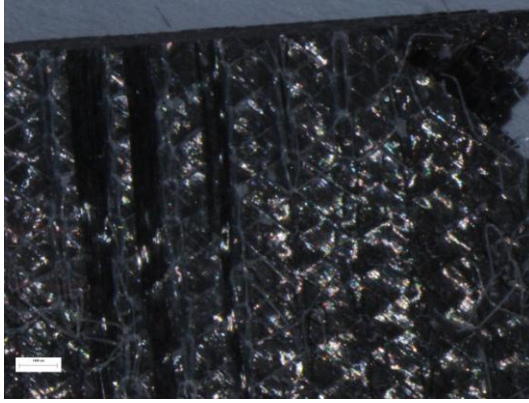
Figure 3.181: Fracture surface of the microtricot interleaved specimen at 6x magnification. The microfibre is clearly visible.
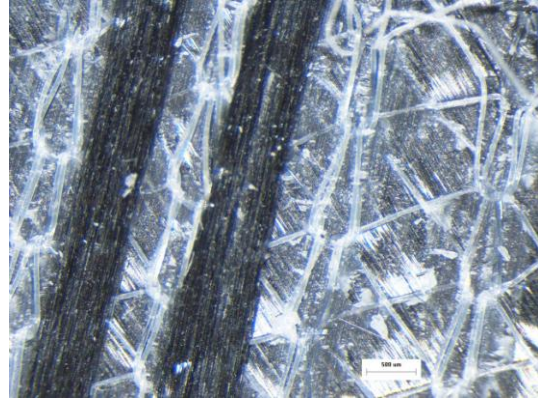
Figure 3.182: Close up of some of the fracture surface of the microtricot interleaved specimen (shown in Figure 3.181) at 16x magnification. The two parallel black blocks are 90° plies on the outside of the specimen that have not separated from the 45 ° plies underneath.

Microfibre-nanofibre combination interleaved specimens

Some fracture surfaces of the microPPSnanoPA6,6 specimen are shown in Figures 3.183- 3.185. From Figure 3.183, it can be seen that some of the fracture surfaces seem smooth, while some appear to be rough with whitened areas. In Figures 3.184 and 3.185, the PPS microfibre can be seen.

Figure 3.183: Some of the fracture surface of the microPPSnanoPA6,6 interleaved specimen at 6x magnification.
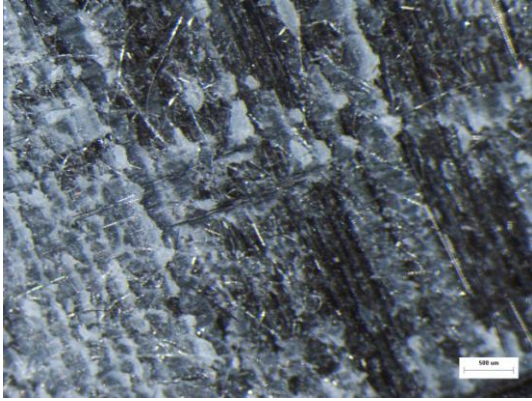
Figure 3.184: Close up of some of the fracture surface of the microPPSnanoPA6,6 interleaved specimen (shown in Figure 3.183) at 16x magnification.
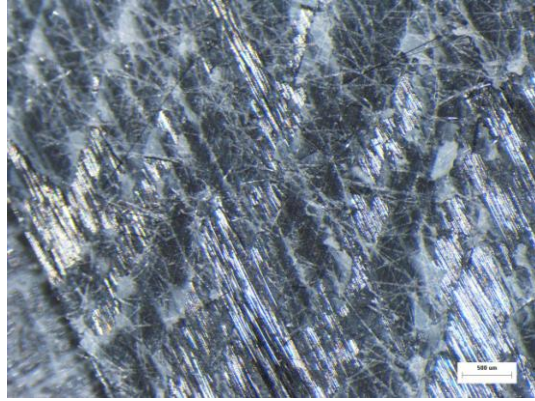
Figure 3.185: Close up of some of the fracture surface of the microPPSnanoPA6,6 interleaved specimen (shown in Figure 3.183) at 16x magnification.
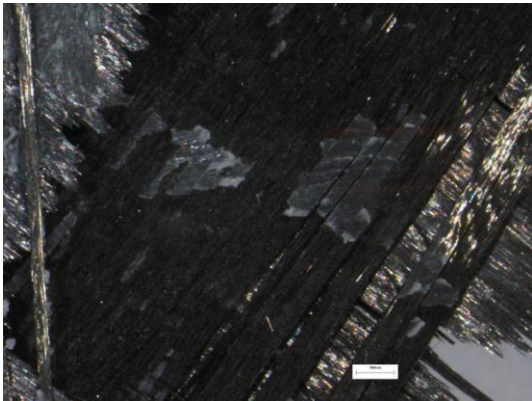
Figure 3.186: Fracture surface of the microPEInanoPA6,6 interleaved specimen at 6x magnification.
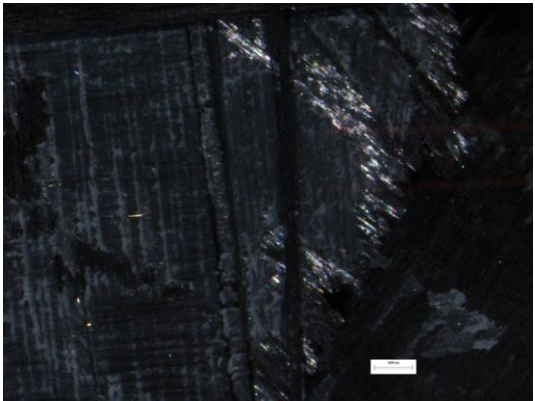
Figure 3.187: Fracture surface of the microPEInanoPA6,6 interleaved specimen at 6x magnification.
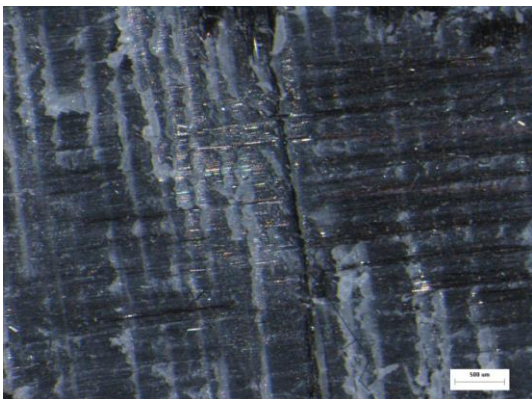
Figure 3.188: Close up of some of the fracture surface of the microPEInanoPA6,6 interleaved specimen (shown in Figure 3.183) at 16x magnification.
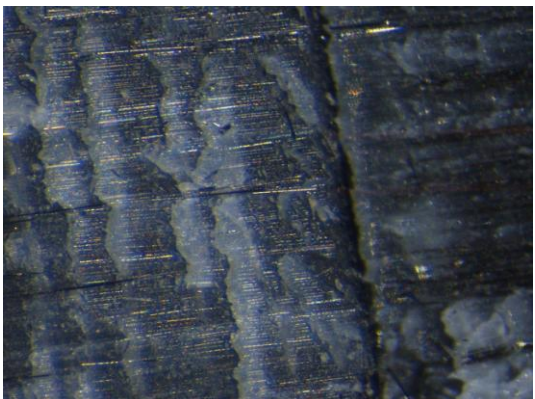
Figure 3.189: Close up of some of the fracture surface of the microPEInanoPA6,6 interleaved specimen (shown in Figure 3.183) at 40x magnification.

182

It also appeared that the fracture surfaces of the microPEInanoPA6,6 specimen (Figures 3.186 - 3.189) also had rough areas and areas that appeared white. The fracture surfaces of the microtricotnanoPA6,6 specimen also seemed to have the same features (see Figures 3.190 - 3.192).
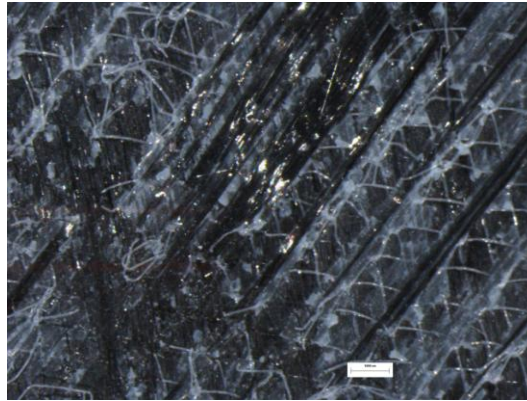
Figure 3.190: Fracture surface of the microtricotnanoPA6,6 interleaved specimen at 6x magnification.
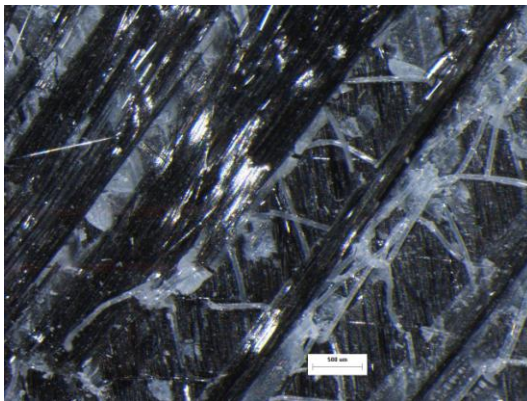
Figure 3.191: Close up of some of the fracture surface of the microtricotnanoPA6,6 interleaved specimen (shown in Figure 3.190) at 16x magnification.
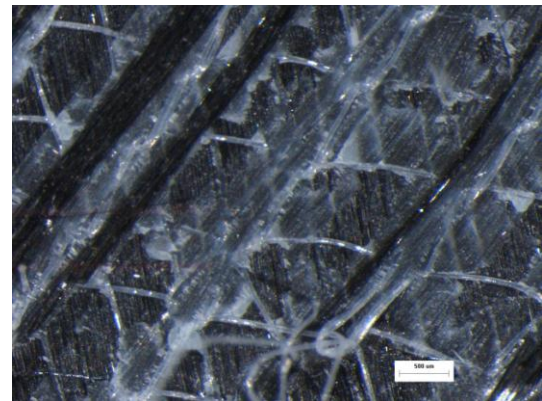
Figure 3.192: Close up of some of the fracture surface of the microtricotnanoPA6,6 interleaved specimen (shown in Figure 3.190) at 40x magnification.

3.5.4.3 SEM analysis

From optical inspection it seemed that parts of the fracture surfaces of the interleaved specimens appeared to be rougher than the control specimen fracture surfaces. SEM images were used to further investigate these areas of interest (see Section 2.7.1). As for the visual and optical inspection sections, only specimens tested at a maximum cyclic stress of 400 MPa were observed.
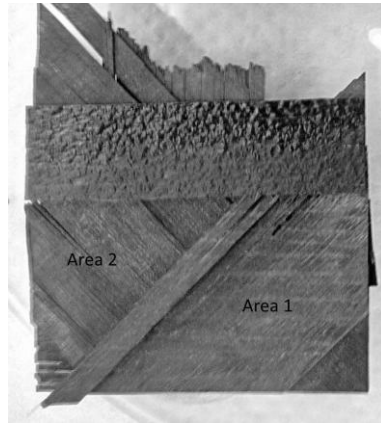
Figure 3.193: Broken end of the control specimen, showing two areas of interest where SEM images were taken.
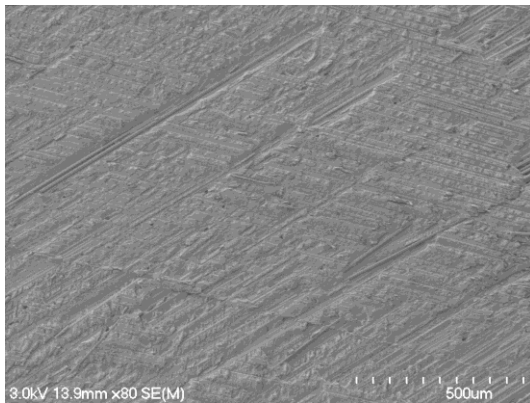
Figure 3.194: Area 1 of control specimen (see Figure 3.193), at 80x magnification.

Figure 3.195: Area 1 of control specimen (see Figure 3.193), at 200x magnification.
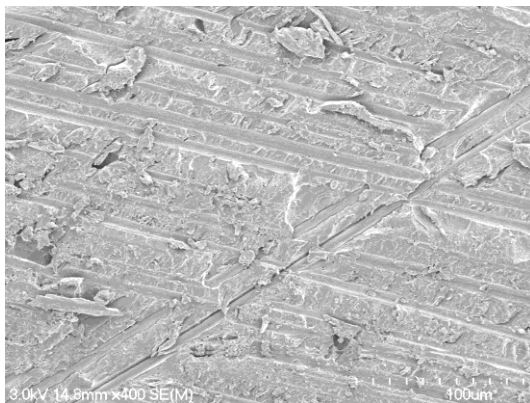
Figure 3.196: Area 1 of control specimen (see Figure 3.193), at 400x magnification.
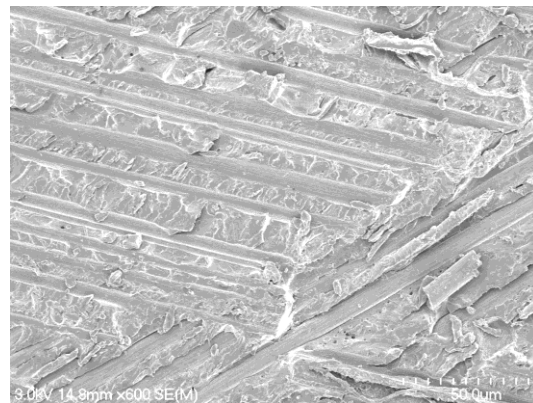
Figure 3.197: Area 1 of control specimen (see Figure 3.193), at 600x magnification.

SEM inspection of the surface of an exposed +45° ply (see Figures 3.194 - 3.197) showed troughs left from the carbon fibres (from the 90° ply above) that had debonded. Some carbon fibres were also visible.

Figure 3.198: Area 2 of control specimen (see Figure 3.193), at 80x magnification.

Figure 3.199: Area 2 of control specimen (see Figure 3.193), at 200x magnification.
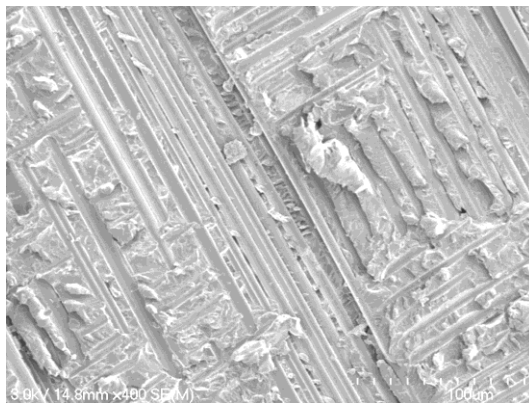
Figure 3.200: Area 2 of control specimen (see Figure 3.193), at 400x magnification.
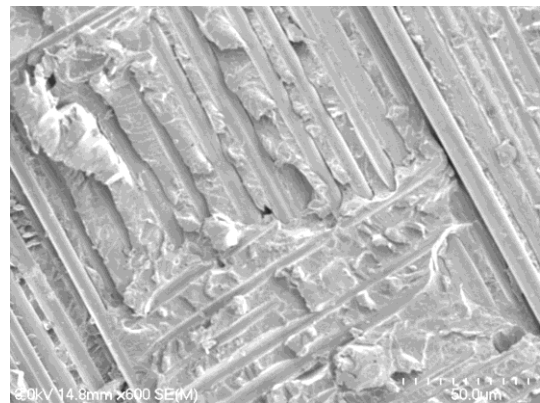
Figure 3.201: Area 2 of control specimen (see Figure 3.193), at 600x magnification.

SEM inspection of the -45 ° ply (shown in Figure 3.193) showed that the rough areas appeared to be epoxy that had peeled from the ply (see Figures 3.198 - 3.201). It is interesting to note the very small voids in some of the epoxy (see Figure 3.201).
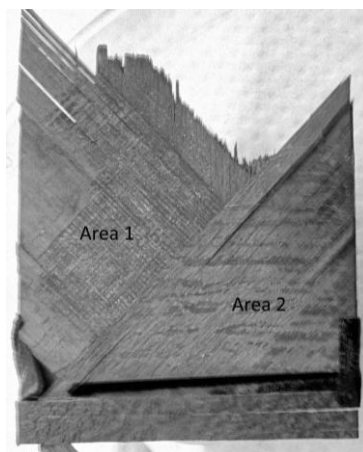
Figure 3.202: Broken end of the nanoNyplex interleaved specimen, showing two areas of interest where SEM images were taken.
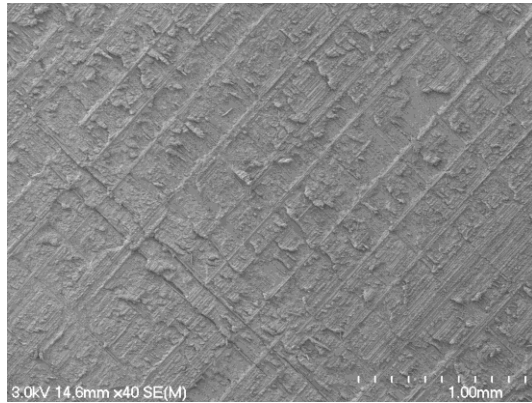
Figure 3.203: Area 1 of nanoNyplex interleaved specimen (see Figure 3.202), at 80x magnification.

Figure 3.204: Area 1 of nanoNyplex interleaved specimen (see Figure 3.202), at 200x magnification.
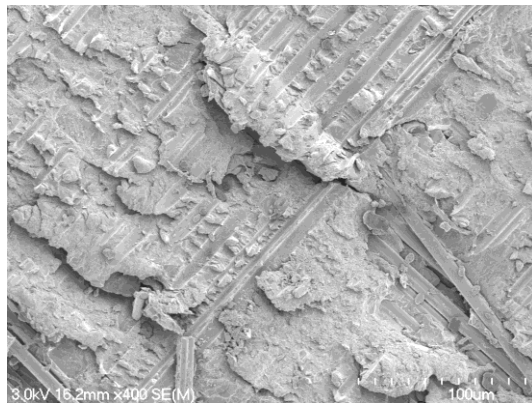
Figure 3.205: Area 1 of nanoNyplex interleaved specimen (see Figure 3.202), at 400x magnification.

Figure 3.206: Area 1 of nanoNyplex interleaved specimen (see Figure 3.202), at 600x magnification.

SEM inspection of the surface of an exposed -45° ply of the nanoNyplex specimen (inspected earlier using optical microscopy - see Figures 3.158 and 3.159) showed rough areas and troughs where the carbon fibres (of the ply above) had debonded (see Figures 3.203 - 3.206). The rough areas seem to be epoxy which has partially been 'peeled' away from the ply. This suggests that when cracks occurred between the -45° and +45° plies, the cracks were stopped, deflected and forced to propagate on a parallel plane, leaving a 'peeled' area.
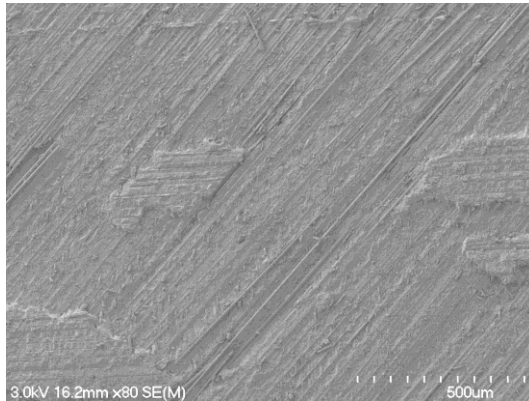
Figure 3.207: Area 2 of nanoNyplex interleaved specimen (see Figure 3.202), at 80x magnification.

Figure 3.208: Area 2 of nanoNyplex interleaved specimen (see Figure 3.202), at 200x magnification.
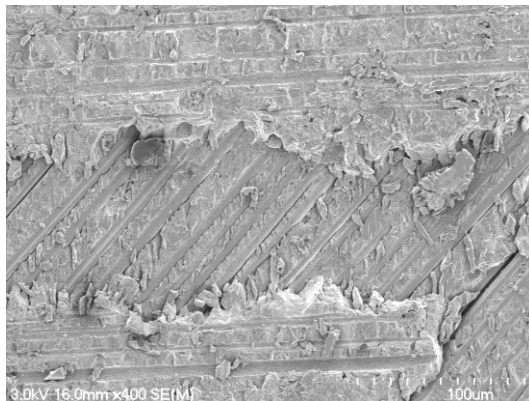
Figure 3.209: Area 2 of nanoNyplex interleaved specimen (see Figure 3.202), at 400x magnification.
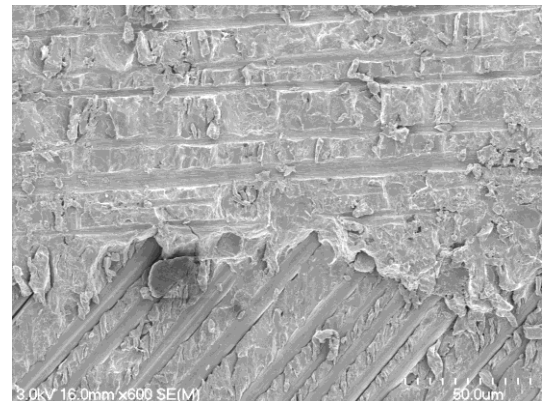
Figure 3.210: Area 2 of nanoNyplex interleaved specimen (see Figure 3.202), at 600x magnification.

SEM inspection of the surface of the exposed +45° ply of the nanoNyplex interleaved specimen showed exposed +45° carbon fibres, with some small 'islands' of matrix from between this ply and the 90° ply on top (it is noted that these were not seen on the +45° ply surface of the control specimen) (see Figures 3.207 - 3.210). The 'islands' suggest that when cracks propagated between the plies, the cracks encountered the interleaving and were deflected and forced to move onto a parallel plane.
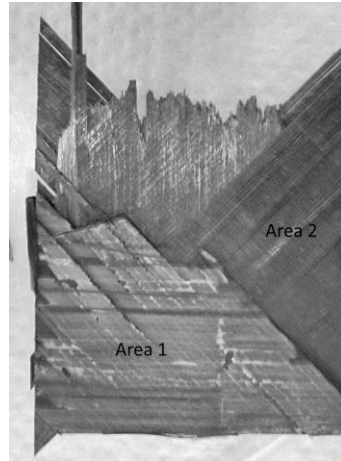
Figure 3.211: Broken end of the nanoPMMA interleaved specimen, showing two areas of interest where SEM images were taken.
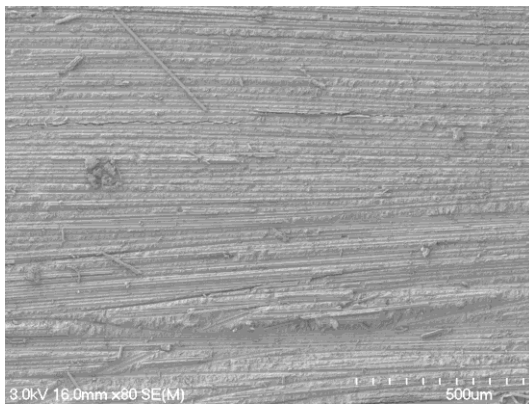
Figure 3.212: Area 1 of nanoPMMA interleaved specimen (see Figure 3.211), at 80x magnification.
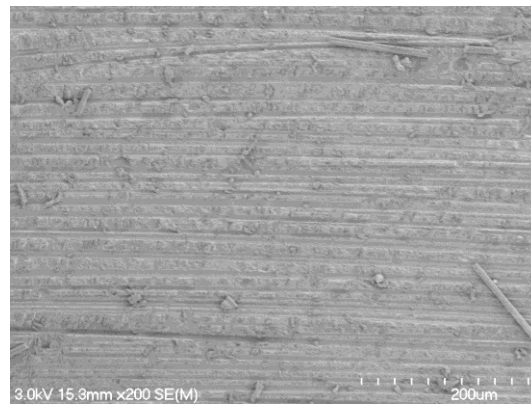
Figure 3.213: Area 1 of nanoPMMA interleaved specimen (see Figure 3.211), at 200x magnification.
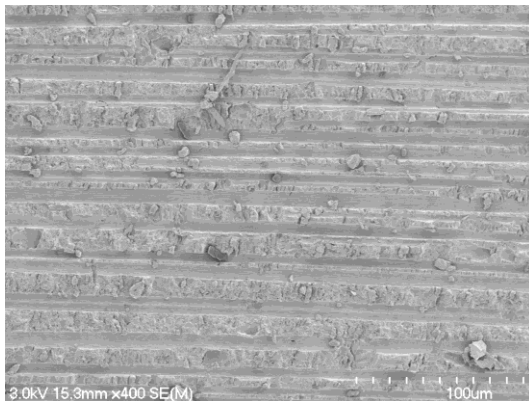
Figure 3.214: Area 1 of nanoPMMA interleaved specimen (see Figure 3.211), at 400x magnification.
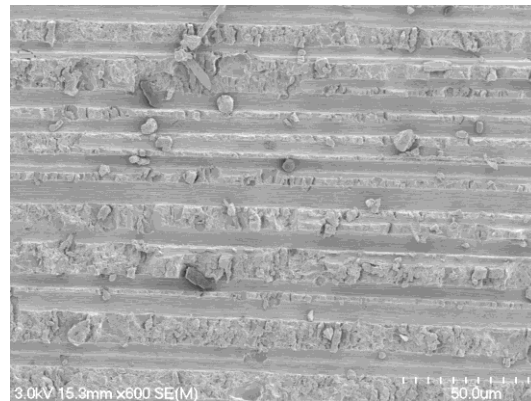
Figure 3.215: Area 1 of nanoPMMA interleaved specimen (see Figure 3.211), at 600x magnification.

SEM inspection of the surface of an exposed -45° ply of the nanoPMMA specimen showed a flat fracture surface with troughs where the carbon fibres from the 90° ply above had debonded (see Figures 3.211 - 3.215). Although the area appeared to be white (see Figure 3.211), on closer inspection little difference was

188

observed between this area and areas of the control specimen (see Figures 3.194 - 3.197).
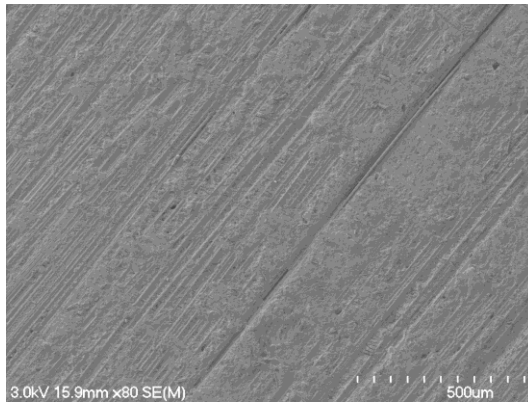
Figure 3.216: Area 2 of nanoPMMA interleaved specimen (see Figure 3.211), at 80x magnification.
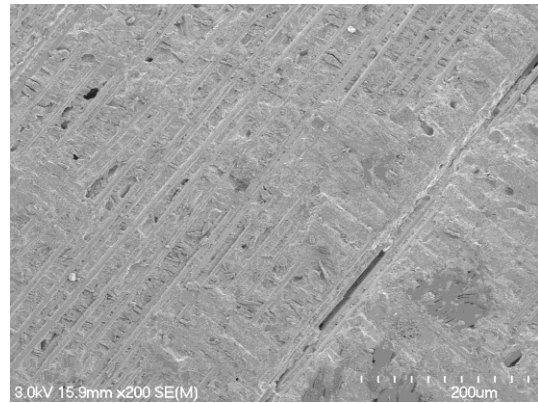
Figure 3.217: Area 2 of nanoPMMA interleaved specimen (see Figure 3.211), at 200x magnification.
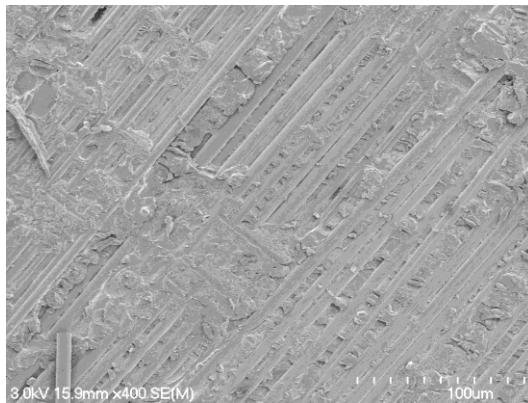
Figure 3.218: Area 2 of nanoPMMA interleaved specimen (see Figure 3.211), at 400x magnification.

Figure 3.219: Area 2 of nanoPMMA interleaved specimen (see Figure 3.211), at 600x magnification.

SEM inspection of the exposed $+45°$ ply (see Figures 3.216 - 3.219) showed some small 'islands' of matrix on top of the $+45°$ carbon fibres (as seen for the nanoNyplex interleaved specimen), suggesting that cracks were deflected by the nanoPMMA interleaving, as discussed earlier for the nanoNyplex specimen. It is interesting to note there was voids present in the specimen (see Figure 3.217).
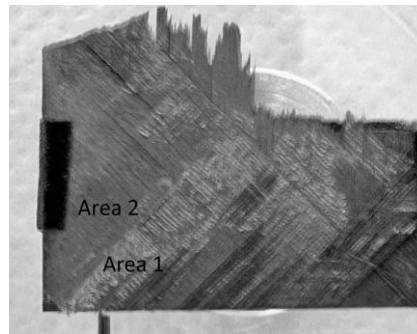
Figure 3.220: Broken end of the nanoPA6,6 interleaved specimen, showing two areas of interest where SEM images were taken.
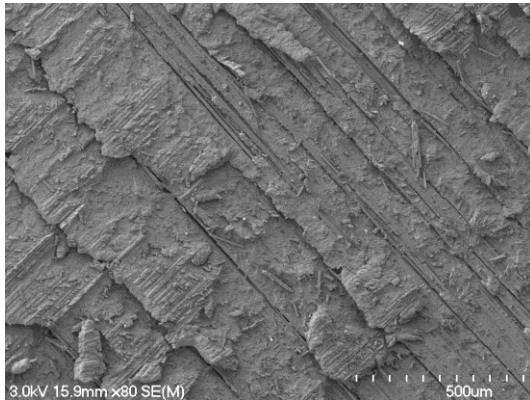
Figure 3.221: Area 1 of nanoPA6,6 interleaved specimen (see Figure 3.220), at 80x magnification.
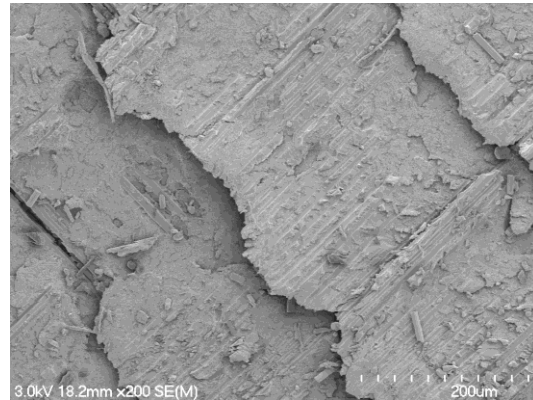
Figure 3.222: Area 1 of nanoPA6,6 interleaved specimen (see Figure 3.220), at 200x magnification.

Figure 3.223: Area 1 of nanoPA6,6 interleaved specimen (see Figure 3.220), at 400x magnification.

SEM inspection of the exposed -45° ply of the nanoPA6,6 specimen (see Figures 3.221 - 3.223), showed that the ply had split between the -45°carbon fibres. It also appears that there was some small 'islands' of matrix present on top of the ply (as seen on the nanoNyplex interleaved specimen surfaces).

190
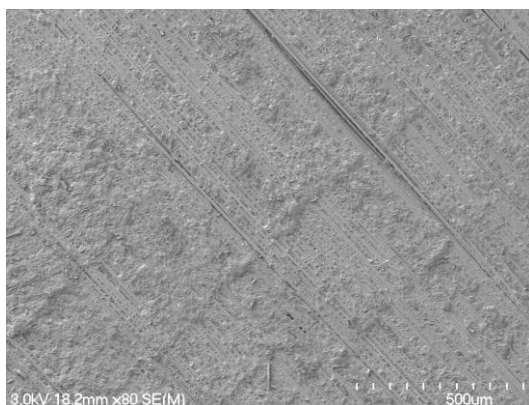
Figure 3.224: Area 2 of nanoPA6,6 interleaved specimen (see Figure 3.220), at 80x magnification.
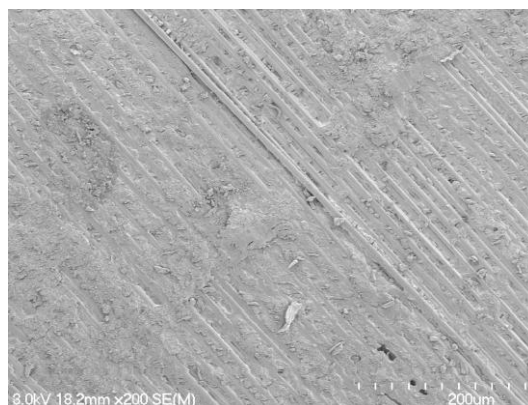
Figure 3.225: Area 2 of nanoPA6,6 interleaved specimen (see Figure 3.220), at 200x magnification.
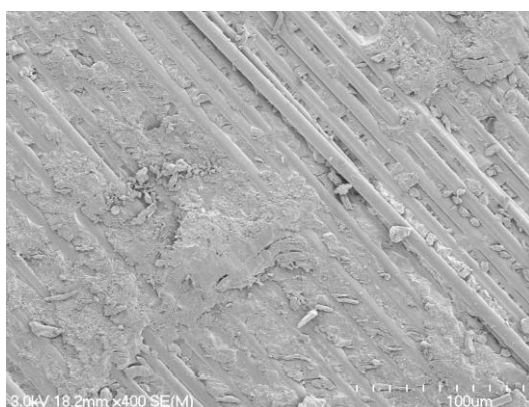
Figure 3.226: Area 2 of nanoPA6,6 interleaved specimen (see Figure 3.220), at 400x magnification.
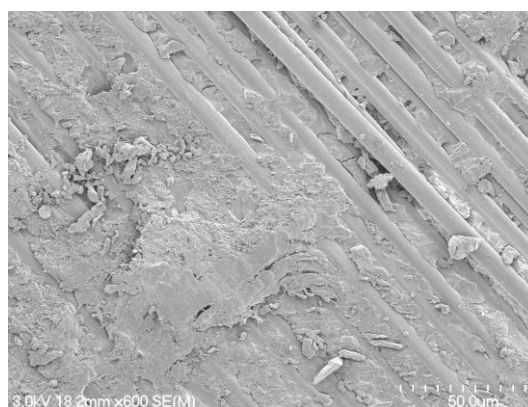
Figure 3.227: Area 2 of nanoPA6,6 interleaved specimen (see Figure 3.220), at 600x magnification.
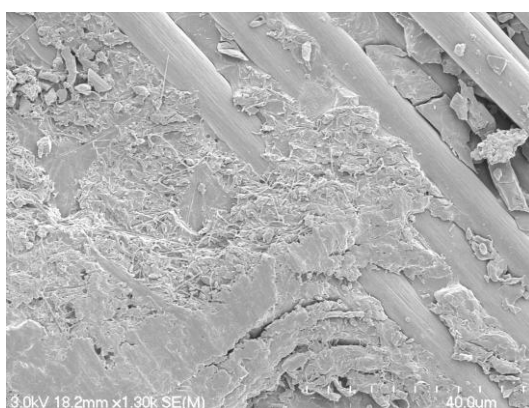
Figure 3.228: Area 2 of nanoPA6,6 interleaved specimen (see Figure 3.220), at 1300x magnification.
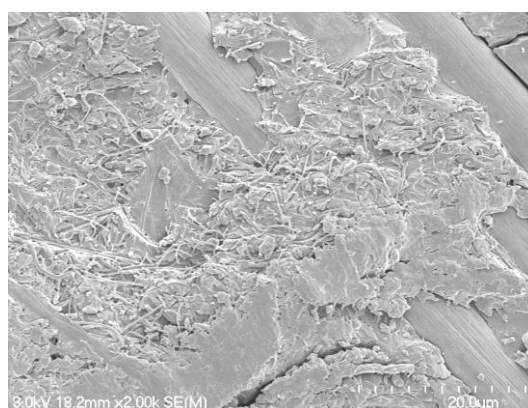
Figure 3.229: Area 2 of nanoPA6,6 interleaved specimen (see Figure 3.220), at 2000x magnification.

SEM inspection of the surface of the exposed -45° ply, (shown in Figure 3.220) showed that this surface was also rough due to the presence of some small 'islands' on top of the ply (see Figures 3.224 - 3.229). When magnified, the

191

'islands' appear to consist of epoxy and nanoPA6,6 fibre (see Figures 3.228 and 3.229). Thus, cracks seem to have been deflected by the presence of the interleaving. From these images it also appears that the nanofibre has debonded and pulled out of the epoxy matrix.
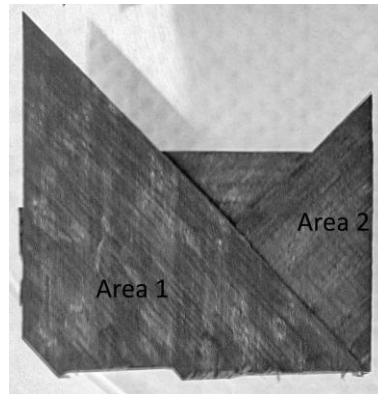
Figure 3.230: Broken end of the nanoPVB interleaved specimen, showing two areas of interest where SEM images were taken.
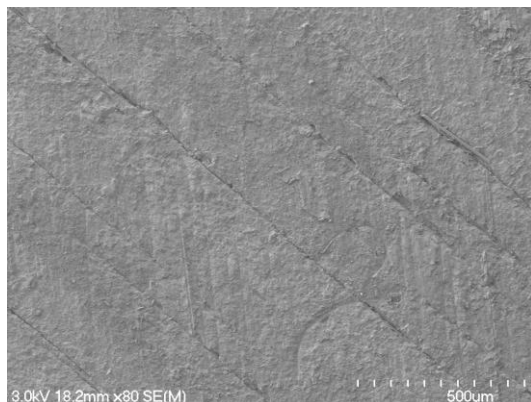
Figure 3.231: Area 1 of nanoPVB interleaved specimen (see Figure 3.230), at 80x magnification.
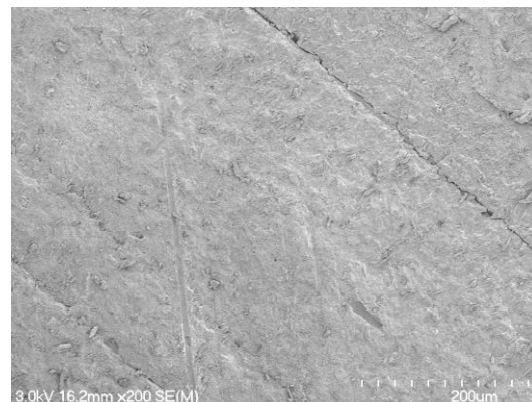
Figure 3.232: Area 1 of nanoPVB interleaved specimen (see Figure 3.230), at 200x magnification.

Figure 3.233: Area 1 of nanoPVB interleaved specimen (see Figure 3.230), at 400x magnification.
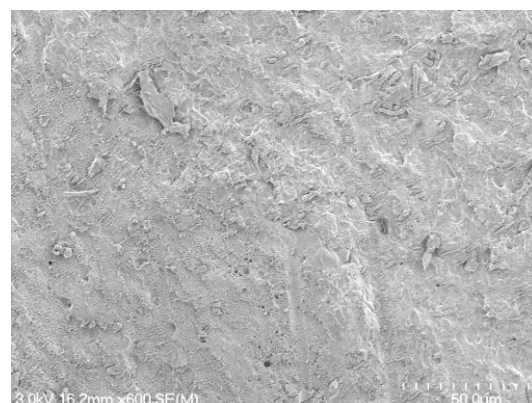
Figure 3.234: Area 1 of nanoPVB interleaved specimen (see Figure 3.230), at 600x magnification.
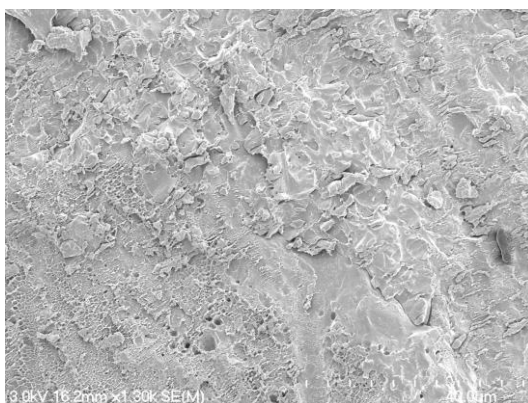
Figure 3.235: Area 1 of nanoPVB interleaved specimen (see Figure 3.230), at 1300x magnification.

SEM inspection of the surface of the exposed -45° ply of the nanoPVB specimen (see Figures 3.231 - 3.234) showed that there were very few troughs where the carbon fibre of the ply above had debonded (unlike ply surfaces of previous specimens). It appears that some of the ply was split between the -45° carbon fibres. No nanofibre was able to be seen from the images, although at high magnification the surface seemed rough (see Figures 3.234 and 3.235).

Figure 3.236: Area 2 of nanoPVB interleaved specimen (see Figure 3.230), at 200x magnification.
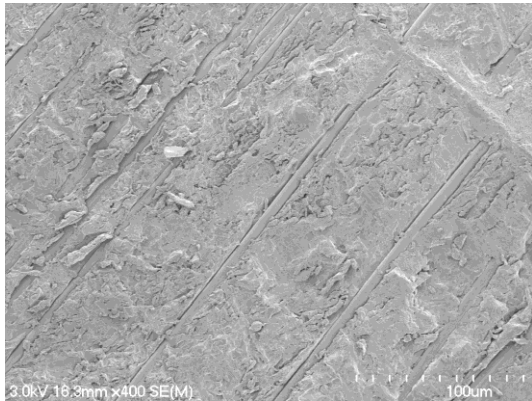
Figure 3.237: Area 2 of nanoPVB interleaved specimen (see Figure 3.230), at 400x magnification.
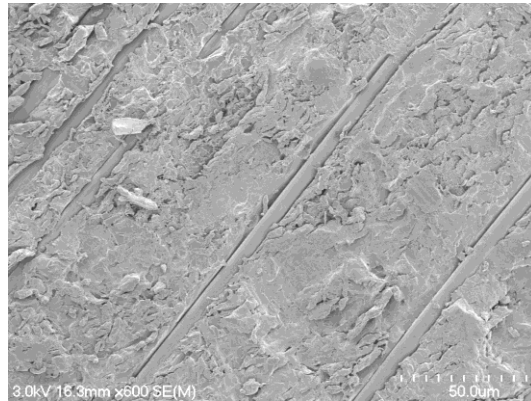
Figure 3.238: Area 2 of nanoPVB interleaved specimen (see Figure 3.230), at 600x magnification.

The SEM images of the second area (see Figures 3.236 - 3.238) show that the surface of this ply was similar in appearance to first area, although some carbon fibres were able to be seen.
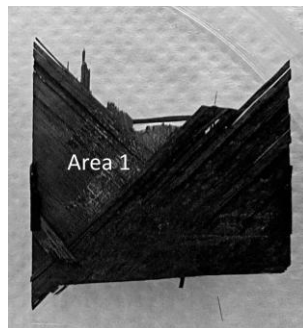
Figure 3.239: Broken end of the nanoPES interleaved specimen, showing one area of interest where SEM images were taken.
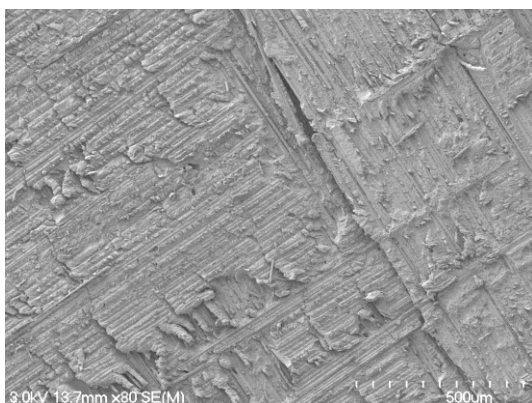
Figure 3.240: Area 1 of nanoPES interleaved specimen (see Figure 3.239), at 80x magnification.
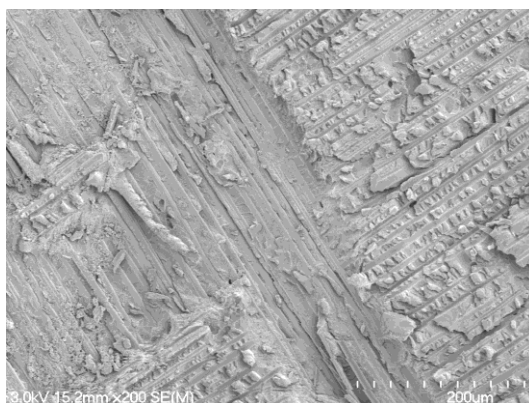
Figure 3.241: Area 1 of nanoPES interleaved specimen (see Figure 3.239), at 200x magnification.

Figure 3.242: Area 1 of nanoPES interleaved specimen (see Figure 3.239), at 400x magnification.

SEM inspection of the surface of the exposed -45° ply of the nanoPES specimen also showed some 'islands' of matrix, along with some troughs where the carbon fibres from the ply above had debonded (see Figures 3.240 - 3.242).
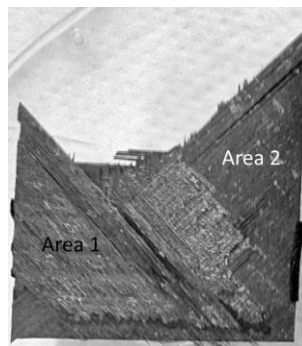
Figure 3.243: Broken end of the microPPS interleaved specimen, showing two areas of interest where SEM images were taken.
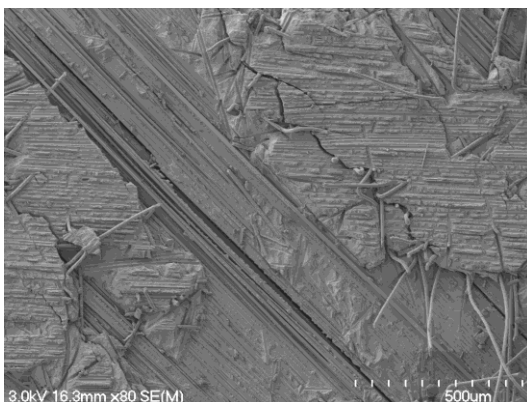
Figure 3.244: Area 1 of microPPS interleaved specimen (see Figure 3.243), at 80x magnification.
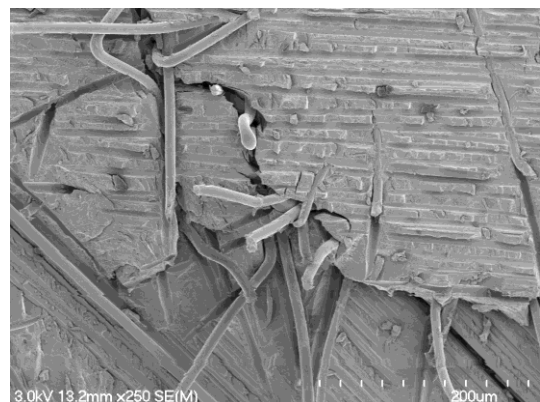
Figure 3.245: Area 1 of microPPS interleaved specimen (see Figure 3.243), at 250x magnification.
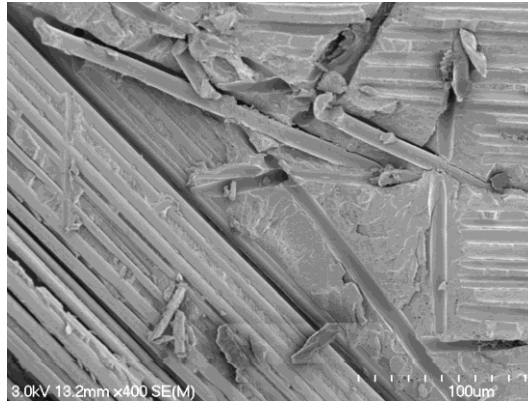
Figure 3.246: Area 1 of microPPS interleaved specimen (see Figure 3.243), at 400x magnification.

From SEM inspection of the exposed -45° ply of the microPPS specimen (see Figures 3.244 - 3.246), it seems that there were 'islands' of matrix that had not separated from the ply. The microfibre can be clearly seen in these 'islands'. The surface was very rough overall compared to the control specimen. Some of the microfibre appears to be embedded in the matrix. There is evidence that some microfibres had broken and pulled out of the matrix. It appears that the crack had been deflected and forced to move around these areas, onto a parallel plane.
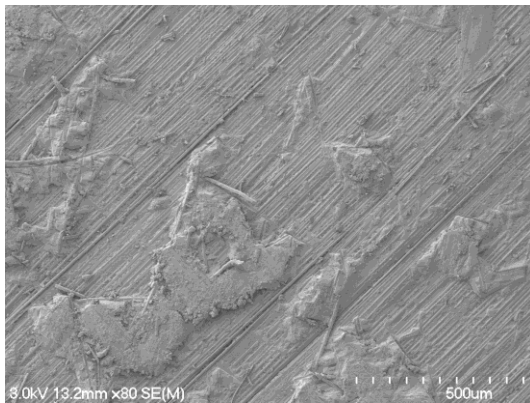
Figure 3.247: Area 2 of microPPS interleaved specimen (see Figure 3.243), at 80x magnification.
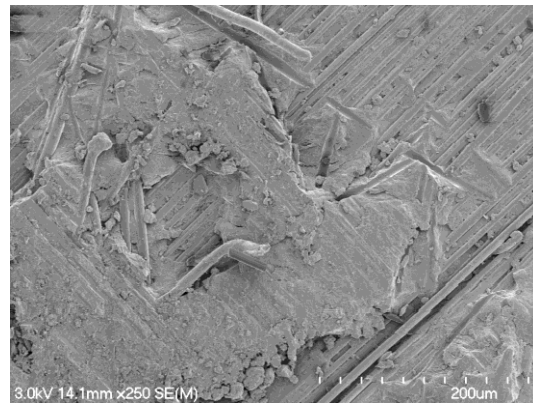
Figure 3.248: Area 2 of microPPS interleaved specimen (see Figure 3.243), at 250x magnification.

Figure 3.249: Area 2 of microPPS interleaved specimen (see Figure 3.243), at 400x magnification.

SEM inspection of the surface of an exposed +45° ply of the microPPS interleaved specimen (see Figures 3.247 - 3.249) showed similar attributes to the images taken of the previous area. SEM images (see Figures 3.251 - 3.254) of the two areas of the microPEI specimen investigated (see Figure 3.250) showed similar attributes to the microPEI specimen. Some troughs where the microfibre had pulled out of the epoxy were evident (although no PEI microfibre could be seen).
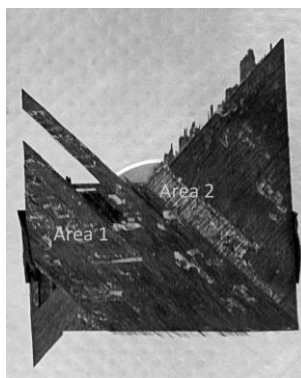
Figure 3.250: Broken end of the microPEI interleaved specimen, showing two areas of interest where SEM images were taken.
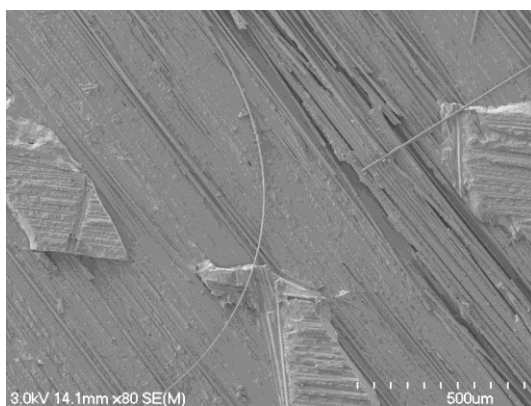
Figure 3.251: Area 1 of microPEI interleaved specimen (see Figure 3.250), at 80x magnification.

Figure 3.252: Area 1 of microPEI interleaved specimen (see Figure 3.250), at 250x magnification.

Figure 3.253: Area 1 of microPEI interleaved specimen (see Figure 3.250), at 400x magnification.
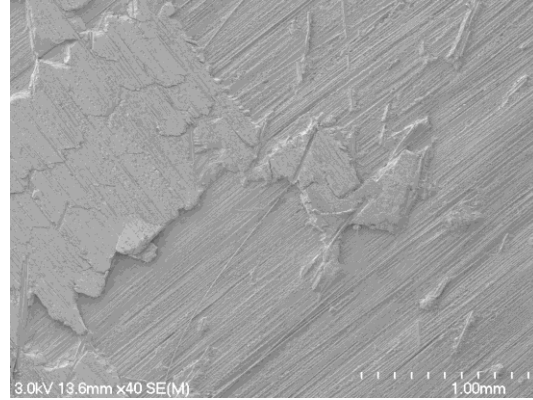
Figure 3.254: Area 2 of microPEI interleaved specimen (see Figure 3.250), at 40x magnification.
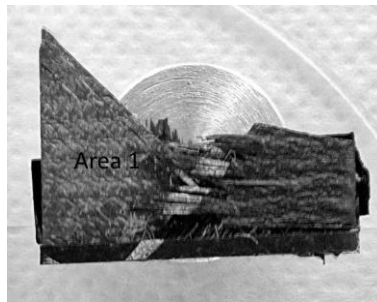
Figure 3.255: Broken end of the microtricot interleaved specimen, showing one area of interest where SEM images were taken.

Figure 3.256: Area 1 of microtricot interleaved specimen (see Figure 3.255), at 80x magnification.
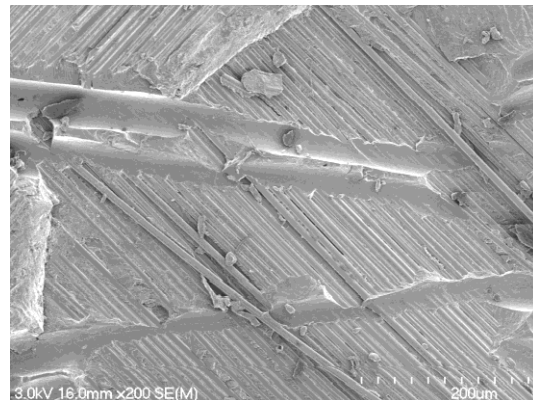
Figure 3.257: Area 1 of microtricot interleaved specimen (see Figure 3.255), at 200x magnification.

SEM inspection of the microtricot interleaved specimen (see Figures 3.255 - 3.257) also showed exposed carbon fibre plies with some 'islands' where the matrix between the plies still remained. There was also evidence of troughs where the microtricot fibres had pulled out from the ply.
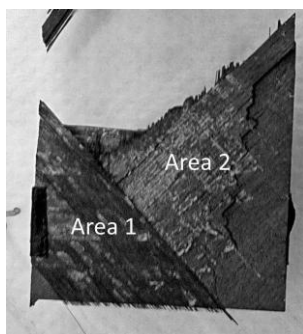
Figure 3.258: Broken end of the microPPSnanoPA6,6 interleaved specimen, showing two areas of interest where SEM images were taken.

Figure 3.259: Area 1 of microPPSnanoPA6,6 interleaved specimen (see Figure 3.258), at 80x magnification.

Figure 3.260: Area 1 of microPPSnanoPA6,6 interleaved specimen (see Figure 3.258), at 250x magnification.
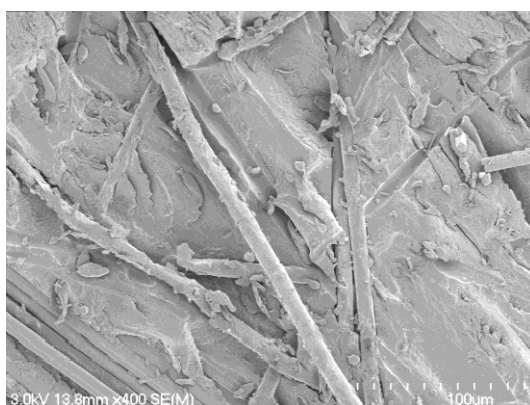
Figure 3.261: Area 1 of microPPSnanoPA6,6 interleaved specimen (see Figure 3.258), at 400x magnification.

SEM inspection of the exposed +45° ply of the microPPSnanoPA6,6 specimen showed that some of the matrix still remained on the surface of the ply and within these areas the PPS microfibre could be seen (see Figures 3.260 and 3.261). Some of the microfibre appears to be embedded in the matrix. Some microfibres have

broken and pulled out of the matrix (similar to microfibres seen on the microPPS interleaved specimen). The nanofibre was not visible from these images.
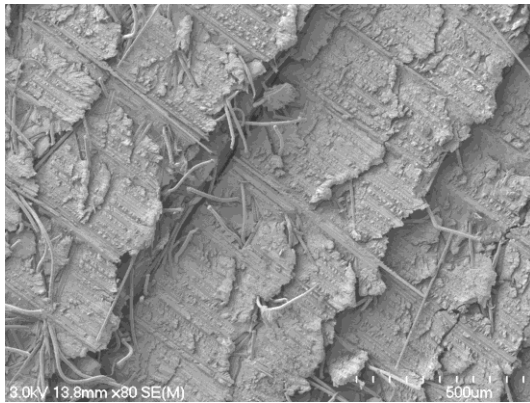
Figure 3.262: Area 2 of microPPSnanoPA6,6 interleaved specimen (see Figure 3.258), at 80x magnification.
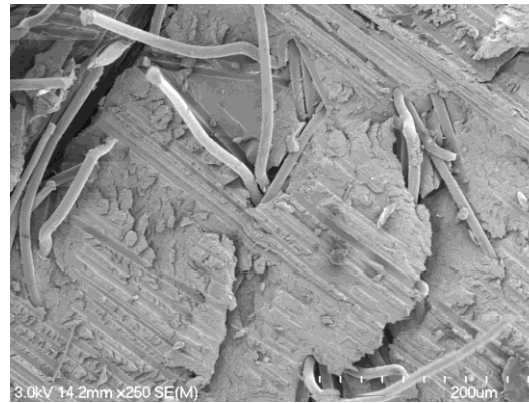
Figure 3.263: Area 2 of microPPSnanoPA6,6 interleaved specimen (see Figure 3.258), at 250x magnification.

SEM inspection of a different area of the microPPSnanoPA6,6 specimen show that this ply has broken along the +45° carbon fibres (see Figures 3.262 and 3.263). There also seems to be some (broken) carbon fibres from the ply above (-45°), that have remained on the surface of the +45° ply. The epoxy matrix seems to have torn in some areas; most likely giving the specimen the rough appearance seen in the optical microscopy section (see Figure 3.183). Similar to the previous area, the microfibre has appeared to have pulled out of the matrix and broken. The nanofibre does not appear visible from these images.

SEM inspection of the +45° ply of the microPEInanoPA6,6 specimen (see Figures 3.264 - 3.267) show that the specimen surface was similar to the microPPSnanoPA6,6 specimen.
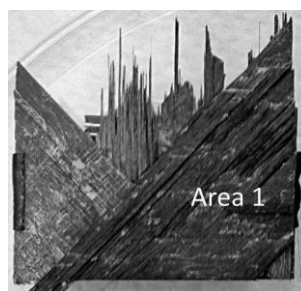
Figure 3.264: Broken end of the microPEInanoPA6,6 interleaved specimen, showing one area of interest where SEM images were taken.
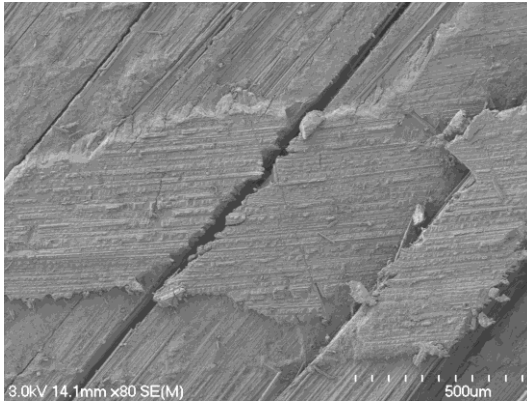
Figure 3.265: Area 1 of microPEInanoPA6,6 interleaved specimen (see Figure 3.264), at 80x magnification.

Figure 3.266: Area 1 of microPEInanoPA6,6 interleaved specimen (see Figure 3.264), at 250x magnification.
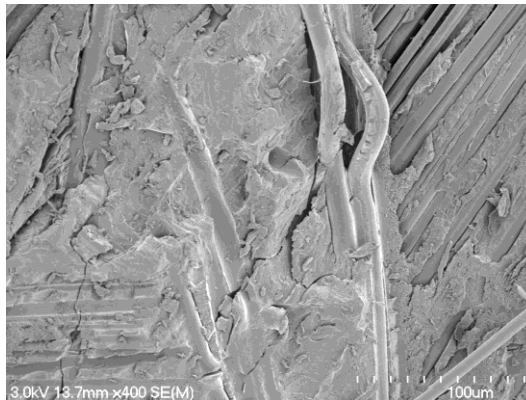
Figure 3.267: Area 1 of microPEInanoPA6,6 interleaved specimen (see Figure 3.264), at 400x magnification.

From SEM images of a -45° ply of the microtricotnanoPA6,6 specimen (see Figures 3.268 - 3.270) it appears that the microtricot fibres were not well bonded to the matrix. It also appears that there were no 'islands' previously seen with other interleaved specimens.
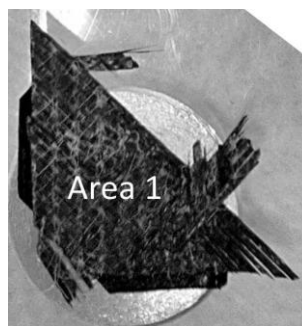
Figure 3.268: Broken end of the microtricotnanoPA6,6 interleaved specimen, showing one area of interest where SEM images were taken.

Figure 3.269: Area 1 of microtricotnanoPA6,6 interleaved specimen (see Figure 3.268), at 80x magnification.

Figure 3.270: Area 1 of microtricotnanoPA6,6 interleaved specimen (see Figure 3.268), at 250x magnification.

Overall, it appears the rough areas observed with optical microscopy was due to some remaining areas of matrix that were attached to the ply surface, forming what appeared to be 'islands' seen in SEM images. The 'islands' found on the nanoPA6,6 interleaved specimen were found to consist of epoxy and nanofibre. The 'islands' found on the microfibre interleaved specimens were found to consist of microfibre and epoxy. The 'islands' suggest that cracks were deflected by the interleavings and were forced to propagate onto a parallel plane. In addition to crack deflection, it appears that some of the interleaving fibres (nanoPA6,6, microPPS and microPEI fibres) had pulled out of the epoxy and broken. These mechanisms suggest that the amount of energy required for crack propagation was increased, as discussed in Section 3.5.3.

Chapter 4

Conclusions

During this research, a range of polymers were chosen to be assessed for production of veils via electrospinning for applications involving impact and cyclic loading. Of the polymers investigated, two nanofibre veils (nanoPMMA and nanoNyplex) were successfully produced. Various factors such as the solubility of the polymer in the solvents available and the solvent vapour pressures of the solvents meant that the remaining polymers were not able to be successfully electrospun to create interleaving veils.

The two veils produced, along with three other nanofibre veils (nanoPA6,6, nanoPVB and nanoPES), three microfibre veils (microPPS, microPEI and microtricot) and three microfibre/nanofibre combination veils (microPPSnanoPA6,6, microPEInanoPA6,6 and microtricotnanoPA6,6) were used as interleavings in carbon fibre reinforced laminate panels. Vibration damping, compression after impact and fatigue tests were undertaken using specimens cut from the panels.

The vibration damping study showed that the nanoNyplex interleaving improved the damping the most. This was thought to be due to movement (friction) of the nanoNyplex interleaving fibres within the matrix. Conversely, it was found that nanoPA6,6 interleaved specimens generally had the lowest tan delta, suggesting that fibre movement was restricted, possibly due to a higher degree of adhesion to the epoxy matrix.

Specimens interleaved with nanoPA6,6, microPPS, and microPPSnanoPA6,6 had the highest compression after impact (CAI) strengths. The high CAI strengths were thought to be due to the increased amount of energy required for crack propagation due to the veils providing toughening via crack deflection and other fibre reinforcement mechanisms. From further assessment, it appeared that in general, veils with high bulk polymer fracture toughness, large number of fibres

per unit area and high adhesion strength between the fibres and matrix seemed to increase the CAI strength the most, suggesting veils with these characteristics would be good to further investigate for use in applications such as aircraft panels.

It was found that most interleavings (apart from microtricot) provided significant improvement in the fatigue performance, suggesting that interleaving veils could be used to extend the lives of parts such helicopter rotor blades that are subjected to cyclic loads during service. It was thought that the improvement was also due to toughening via fibre reinforcement mechanisms mentioned previously. Through further assessment, it appeared (in general), that veils that had a large number of fibres per unit area and a higher degree of adhesion between the matrix and the fibres increased the number of cycles to failure the most.

Post fatigue SEM analysis showed some evidence of crack deflection, fibre pull out and fibre breakage (or a combination of some of these) on the fracture surfaces of nanoPA6,6, microPPS, microPEI, microPPSnanoPA6,6 and microPEInanoPA6,6 interleaved specimens, correlating with those that performed best mechanically.

Chapter 5

Recommendations for further work

Of the six polymers chosen to be investigated during the solution development phase of this research, suitable electrospinning solutions (or solutions that spun well) could not be found for ASA, ABS, CPVC, PC and PS. In most cases, the polymer either did not dissolve successfully in the chosen solvents, or appeared to dissolve but did not electrospin well. Solubility could have been affected by additives in the polymer granules, so in future research it would be recommended for trials that a more pure form of each polymer be used to avoid this.

Trials that did not electrospin well were often found to use solvents with unsuitable vapour pressures. In future, a wider range of solvents with suitable vapour pressures could be used or a blend of solvents could be investigated in order to tailor the vapour pressure.

During the vibration damping testing, it appears that resonance occurred, which produced peaks and negative values in the data collected. In future research it would be recommended that the tests undertaken also use a different test rig (such as the rig outlined in the ASTM E756) to assess whether it was related to the machine or the samples. It would also be recommended that tests be conducted at different temperatures as well as frequencies, as it would be likely that the damping performance would be highly temperature dependent. This would give a better idea of damping over temperature ranges that would likely to be used for a chosen application.

It would also be recommended that ultrasonic C scan analysis be used in the CAI study. This would be useful to check specimens for flaws before impacting. The damaged area could also be scanned after being impacted to give information on the degree of damage induced in the samples during the initial impact and separate impact damage from that produced by compression.

It would also be recommended in future work that more replicate specimens be tested for both the CAI and fatigue studies, as the lack of data made it difficult to assess the amount of variability and to therefore assess the degree of influence of the properties of the veils that influenced toughness. For both CAI and fatigue investigations, it would also be worthwhile investigating more interleaves with characteristics of the more successful veils, such as high bulk polymer fracture toughness, large amount of fibres per unit area and medium high adhesion strength with the matrix.

References

[1] Bhardwaj, N., & Kundu, S. C. (2010). Electrospinning: a fascinating fiber fabrication technique. *Biotechnol Adv, 28*(3), 325-47.

[2] Vasita, R., & Katti, D. S. (2006). Nanofibers and their applications in tissue engineering. *International Journal of Nanomedicine, 1*(1), 15-30.

[3] Wendorff, J. H., Agarwal, S., & Greiner, A. (2012). *Electrospinning: Materials, Processing, and Applications*: Wiley.

[4] Moon, S. C., & Farris, R. J. (2008). The morphology, mechanical properties, and flammability of aligned electrospun polycarbonate (PC) nanofibers. *Polymer Engineering & Science, 48*(9), 1848-1854.

[5] Ramakrishna, S., Fujihara, K., Teo, W.-E., Yong, T., Ma, Z., & Ramaseshan, R. (2006). Electrospun nanofibers: solving global issues. *Materials Today, 9*(3), 40-50.

[6] ACS Symposium Series, Vol 981, Polymeric Nanofibers, Darrell, H. Reneker, Hao, Fong, Copyright 2006, with permission from American Chemical Society Symposium Series.

[7] ElectrospinTech. (2014). *ElectrospinTech: An electrospinning ecosystem for the evolution of nanofibers and its application.* Retrieved 10 June, 2014, from http://electrospintech.com/index.html

[8] Kim, G. T., Lee, J. S., Shin, J. H., Ahn, Y. C., Jeong, K. H., Sung, C. M., & Lee, J. K. (2004). Effect of Humidity on the Microstructures of Electrospun Polystyrene Nanofibers. *Microscopy and Microanalysis, 10*(S02), 554-555.

[9] Golin, A. (2014). *Humidity effect on the structure of electrospun core-shell PCL-PEG fibers for tissue regeneration applications.* Masters thesis, The University of Western Ontario.

[10] Zargham, S., Bazgir, S., Tavakoli, A., Rashidi, A. S., & Damerchely, R. (2012). The Effect of Flow Rate on Morphology and Deposition Area of Electrospun Nylon 6 Nanofiber *Journal of Engineered Fibers and Fabrics 7*(4).

[11] Beachleya, V., & Wen, X. (2009). Effect of electrospinning parameters on the nanofiber diameter and length. *Materials Science and Engineering C: Materials for Biological Applications (Elsevier), 29*(3).

[12] Pattamaprom, C., Hongrojjanawiwat, W., Koombhongse, P., Supaphol, P., Jarusuwannapoo, T., & Rangkupan, R. (2006). The Influence of Solvent Properties and Functionality on the Electrospinnability of Polystyrene Nanofibers. *Macromolecular Materials and Engineering, 291*(7), 840-847.

[13] Luo, C. J., Nangrejo, M., & Edirisinghe, M. (2010). A novel method of selecting solvents for polymer electrospinning. *Polymer, 51*(7), 1654-1662.

[14] Garg, K., & Bowlin, G. L. (2011). Electrospinning jets and nanofibrous structures. *Biomicrofluidics (American Institute of Physics), 5*(1).

[15] Master Organic Chemistry. (2014). *Solvents*. Retrieved June, 2014, from http://www.masterorganicchemistry.com/2012/04/27/polar-protic-polar-aprotic-nonpolar-all-about-solvents/

[16] Luo, C. J., Stride, E., & Edirisinghe, M. (2012). Mapping the Influence of Solubility and Dielectric Constant on Electrospinning Polycaprolactone Solutions. *Macromolecules, 45*(11), 4669-4680.

[17] Wu, X. M., Branford-White, C. J., Zhu, L. M., Chatterton, N. P., & Yu, D. G. (2010). Ester prodrug-loaded electrospun cellulose acetate fiber mats as transdermal drug delivery systems. *J Mater Sci Mater Med, 21*(8), 2403-11.

[18] Wang, S., Bai, J., Li, C., Zhang, Y., & Zhang, J. (2012). Ag nanoparticle-embedded one-dimensional β-CD/PVP composite nanofibers prepared via electrospinning for use in antibacterial material. *Colloid and Polymer Science, 290*(7), 667-672.

[19] Lu, J. (2008). *High Dielectric Constant Polymer Nanocomposites for Embedded Capacitor Applications.* thesis, Georgia Institute of Technology, Atlanta, Georgia, United States.

[20] Matulevicius, J., Kliucininkas, L., Martuzevicius, D., Krugly, E., Tichonovas, M., & Baltrusaitis, J. (2014). Design and Characterization of Electrospun Polyamide Nanofiber Media for Air Filtration Applications. *Journal of Nanomaterials, 2014*, 1-13.

[21] Cai, S. (2013). *Electrospun Plant Protein Scaffolds with Fibers Oriented Randomly and Evenly in Three-Dimensions for Soft Tissue Engineering Applications.* Masters thesis, University of Nebraska.

[22] Choi, S. S., Lee, S. G., Im, S. S., Kim, S. H., & Joo, Y. L. (2003). Silica nanofibers from electrospinning/sol-gel process. *Journal of Materials Science Letters, 22*, 891-893.

[23] Burke, J. (1984). Solubility Parameters: Theory and Application. *The Book and Paper Group Annual, The American Institute for Conservation, 3*.

[24] Hansen, C. M. (2000). *Hansen Solubility Parameters, a User's handbook*. United States of America: CRC Press.

[25] Hansen, C. M. (2014). Hansen solubility parameters in practice [software].

[26] Woishnis, W. A., & Ebnesajjad, S. (2012). *Chemical Resistance of Thermoplastics*. Waltham, USA: Elsevier Inc.

[27] Santos, L. S. (2010). *Reactive Intermediates: MS Investigations in Solution*. Weinheim, Germany: Wiley-VCH.

[28] Boeing. (2014). *About the 787 Dreamliner family*. Retrieved June, 2014, from
http://www.boeing.com/boeing/commercial/787family/background.page

[29] Magniez, K., De Lavigne, C., & Fox, B. L. (2010). The effects of molecular weight and polymorphism on the fracture and thermo-mechanical properties of a carbon-fibre composite modified by electrospun poly (vinylidene fluoride) membranes. *Polymer, 51*(12), 2585-2596.

[30] Tsotsis, T. K. (2009). Interlayer toughening of composite materials. *Polymer Composites, 30*(1), 70-86.

[31] Zhang, J., Lin, T., & Wang, X. (2010). Electrospun nanofibre toughened carbon/epoxy composites: Effects of polyetherketone cardo (PEK-C) nanofibre diameter and interlayer thickness. *composites science and technology, 70*(11), 1660-1666.

[32] Akangah, P., Lingaiah, S., Shivakumar, K. (2010). Effect of Nylon-66 nano-fiber interleaving on impact damage resistance of epoxy/carbon fiber composite laminates. *Composite Structures, 92*(6), 1432-1439.

[33] Beckermann, G. W., & Pickering, K. L. (2015). Mode I and Mode II interlaminar fracture toughness of composite laminates interleaved with

electrospun nanofibre veils. *Composites Part A: Applied Science and Manufacturing, 72*(0), 11-21.

[34] Palazzetti, R., Zucchelli, A., Gualandi, C., Focarete, M. L., Donati, L., Minak, G., & Ramakrishna, S. (2012). Influence of electrospun Nylon 6,6 nanofibrous mats on the interlaminar properties of Gr–epoxy composite laminates. *Composite Structures, 94*(2), 571-579.

[35] Zhang, J., Yang, T., Lin, T., & Wang, C. H. (2012). Phase morphology of nanofibre interlayers: Critical factor for toughening carbon/epoxy composites. *Composites Science and Technology, 72*(2), 256-262.

[36] Matthews, F. L., & Rawlings, R. D. (1999). 2 - Reinforcements and the reinforcement–matrix interface. In F. L. Matthews & R. D. Rawlings (Eds.), *Composite materials: engineering and science* (pp. 29-77): Woodhead Publishing.

[37] DSM Engineering Plastics Ltd. (2014). *Gluing of Engineering Plastics.* [Pamphlet]. http://www.dsm.com/content/dam/dsm/automotive/en_US/documents/gluing-guide.pdf (accessed March 2015)

[38] Kaynak, C., Celikbilek, C., & Akovali, G. (2003). Use of silane coupling agents to improve epoxy–rubber interface. *European Polymer Journal, 39*(6), 1125-1132.

[39] Khan, S. U., Li, C. Y., Siddiqui, N. A., & Kim, J.-K. (2011). Vibration damping characteristics of carbon fiber-reinforced composites containing multi-walled carbon nanotubes. *Composites Science and Technology, 71*(12), 1486-1494.

[40] Verstappen, A. P., J. R. (2011). *Evaluation of Viscoelastic Vibration Damping Properties with a Dynamic Mechanical Analyser*. Paper presented at the 18th International Congress on Sound and Vibration.

[41] Grant, I. D., Lowe, A. T., & Thomas, S. (1997). 'Good vibrations', the science and application of intrinsically damped composite materials. *Composite Structures, 38*(1–4), 581-587.

[42] Miller, S. G. (2013). Evaluation of Nanomaterial Approaches to Damping in Epoxy Resin and Carbon Fiber/Epoxy Composite Structures by Dynamic Mechanical Analysis. *NASA*.

[43] PerkinElmer Inc. (2012). *DMA 8000 Dynamic Mechanical Analyser*.

[44] Menard, K. (2008). *Dynamic Mechanical Analysis, a Practical Introduction* (2nd Edition ed.). United States of America: CRC Press, Taylor and Francis Group Ltd.

[45] Raa Khimi. (2015). *Development of elastomeric composites from iron sand and natural rubber for vibration damping.* thesis, Univerisity of Waikato, Hamilton, New Zealand.

[46] Tehrani, M., Boroujeni, A. Y., Hartman, T. B., Haugh, T. P., Case, S. W., & Al-Haik, M. S. (2013). Mechanical characterization and impact damage assessment of a woven carbon fiber reinforced carbon nanotube–epoxy composite. *Composites Science and Technology, 75*(0), 42-48.

[47] Palazzetti, R., Zucchelli, A., & Trendafilova, I. (2013). The self-reinforcing effect of Nylon 6,6 nano-fibres on CFRP laminates subjected to low velocity impact. *Composite Structures, 106*(0), 661-671.

[48] Tehrani, M., Safdari, M., Boroujeni, A. Y., Razavi, Z., Case, S. W., Dahmen, K., Garmestani, H., & Al-Haik, M. S. (2013). Hybrid carbon fiber/carbon nanotube composites for structural damping applications. *Nanotechnology, 24*(15), 155704.

[49] Rajoria, H., & Jalili, N. (2005). Passive vibration damping enhancement using carbon nanotube-epoxy reinforced composites. *Composites Science and Technology, 65*(14), 2079-2093.

[50] Hodgkinson, J. M. (2000). *Mechanical Testing of Advanced Composites*. Cornwall, England: TJ International.

[51] Abrate, S. (1998). *Impact on Composite Structures*. Cambridge, United Kingdom: Cambridge University Press.

[52] Akangah, P., & Shivakumar, K. (2013). Assessment of Impact Damage Resistance and Tolerance of Polymer Nanofiber Interleaved Composite Laminates. *Journal of Chemical Science and Technology, 2*(2).

[53] Shivakumar, K., Lingaiah, S., Chen, H., Akangah, P., Swaminathan, G., Sharpe, M., Sadler, R. . (2009). *Polymer Nanofabric Interleaved Composite Laminates*. Paper presented at the 50th AIAA/ASME/ASCE/AHS/ASC Structures, Structural Dynamics, and Materials Conference

[54] Harris, B. (2003). *Fatigue in Composites*. Cambridge, England: Woodhead Publishing Ltd.

[55] Curtis, P. T. (1987). A review of fatigue of composite materials. (RAE, Farnbough).

[56] Matthews, F. L., & Rawlings, R. D. (1999). Fatigue and environmental effects. In *Composite materials: engineering and science*: Woodhead Publishing.

[57] Phong, N. T., Gabr, M. H., Okubo, K., Chuong, B., & Fujii, T. (2013). Improvement in the mechanical performances of carbon fiber/epoxy composite with addition of nano-(Polyvinyl alcohol) fibers. *Composite Structures, 99*(0), 380-387.

[58] Zhou, Y., Jeelani, S., & Lacy, T. (2013). Experimental study on the mechanical behavior of carbon/epoxy composites with a carbon nanofiber-modified matrix. *Journal of Composite Materials*.

[59] Hojo, M., Matsuda, S., Tanaka, M., Ochiai, S., & Murakami, A. (2006). Mode I delamination fatigue properties of interlayer-toughened CF/epoxy laminates. *Composites Science and Technology, 66*(5), 665-675.

[60] *Introduction to Polymers: A Property Database Online*. (2014). Retrieved March, 2014, from http://www.polymersdatabase.com/intro/index.jsp

[61] Henkel Loctite. (2011). *Loctite design guide for bonding plastics*.

[62] Placet, V., & Foltete, E. (2010). *Is Dynamic Mechanical Analysis (DMA) a non-resonance technique?* Paper presented at the ICEM 14 – 14th International Conference on Experimental Mechanics, retrieved from http://www.epj-conferences.org/articles/epjconf/abs/2010/05/epjconf_ICEM14_41004/epjconf_ICEM14_41004.html

[63] Hamerton, I. (1996). *Recent developments in epoxy resins.* Rapra Technology Ltd. (accessed

[64] Ghelli, D., & Minak, G. (2011). Low velocity impact and compression after impact tests on thin carbon/epoxy laminates. *Composites Part B: Engineering, 42*(7), 2067-2079.

[65] Xu, J., Li, Y., Ge, D., Liu, B., & Zhu, M. (2011). Experimental investigation on constitutive behavior of PVB under impact loading. *International Journal of Impact Engineering, 38*(2-3), 106-114.

[66] Kuraray America Inc. (2015). *Kuraray Mowital® and PIOLOFORM product information*. Retrieved March, 2015, from http://www.kuraray.us.com/products/resins/mowital-piolofor/

[67] Militky, J., & Ibrahim, S. (2009). 7 - Effect of textile processing on fatigue. In M. Miraftab (Ed.), *Fatigue Failure of Textile Fibres* (pp. 133-168): Woodhead Publishing.

Appendix

6.1 Solution development

6.1.1 Materials safety data

Table 6.1: Materals safety data for available solvents.

Name	CAS No.	Threshold Limit Value	NFPA 704 Health Rating	NFPA 704 Flammability Rating	LD50	EU Classification or GHS Classification	Comments
cyclohexane	110-82-7	300	1	3	Oral mouse 813 mg/kg	Danger flammable toxic	possibly mutagenic
toluene	108-88-3	50	2	3	Oral - rat - > 5,580 mg/kg Inhalation - rat - 4 h - 12,500 - 28,800 mg/m3 Dermal - rabbit - 12,196 mg/kg	Flammable, toxic to aquatic life	Suspected of damaging fertility, or unborn child
o-xylene	95-47-6	100	2	3	Intraperitoneal - mouse - 1,364 mg/kg	Flammable	
methyl ethyl ketone	78-93-3	200	1	3	Oral rat 2737 mg/kg inhalation mouse 32000 mg/m3	Danger highly flammable	
chloroform	67-66-3	10	2	0	-	Warning, toxic	Carcinogenic rats, mutagenic, suspected carcinogen for humans
n-propyl acetate	109-60-4	200	2	3	Oral - rat - 9,370 mg/kg Dermal - rabbit - > 17,740 mg/kg	Flammable, Irritant	
acetone	67-64-1	750	1	3	Oral rat 5800 mg/kg Inhalation rat 8h 50100 mg/m3	Danger highly flammable	
dichloromethane	75-09-2	50	2	1	Oral rat 2000 mg/kg Inhalation rat 52000 mg/kg	toxic	suspected carcinogen
ethyl acetate	141-78-6	400	1	3	Oral - rat 5620 mg/kg inhalation mouse 2h 45000 mg/m3	Danger	
n-methyl-2-pyrrolidone	872-50-4		2	1	Oral rat 3914 mg/kg LDLO inhalation rat 4h > 5100 ppm		Handle with gloves. Damage to fetus possible
tetrahydrofuran	109-99-9	200	2	3	Oral rat 2050 mg/kg	Flammable corrosive	possibly carcinogenic

Name	CAS No.	Threshold Limit Value	NFPA 704 Health Rating	NFPA 704 Flammability Rating	LD50	EU Classification or GHS Classification	Comments
n,n-dimethylacetamide	127-19-5	10	2	2	2.24 g/kg rabbit, 4.3g/kg rat (oral)	Toxic	
dimethyl sulfoxide	67-68-5		2	2	LC50 inhalation rat 4hr 40250 ppm oral rat 14.500 mg/kg		carcinogenic rats mice, reproductive toxicant rats, mice
n,n-dimethylformamide	68-12-2	10	1	2	Oral - rat - 2,800 mg/kg Inhalation - rat - 4 h - 9 - 15 mg/l	Flammable, Toxic,	Germ cell mutagen, presumed human reproductive toxicant.
acetic acid	64-19-7	10	3	2	Oral - rat - 3,310 mg/kg Inhalation - mouse - 1 h - 5620 ppm rat - 4 h - 11.4 mg/l Dermal - rabbit - 1,112 mg/kg	Flammable, Corrosive, toxic	
benzyl alcohol			1	1	Oral rat 1,230 mg/kg	Warning	Harmful if inhaled, swallowed. Can cause irritation to skin
formic acid			3	2	Oral - rat - 1,100 mg/kg Inhalation - rat - 4 h - 7.4 mg/l Inhalation - rat - 0.25 h - 15,000 mg/m3	Flammable, toxic, Corrosive, irritant, sensitizer	Reactivity 1. Toxic if inhaled
isopropyl alcohol	67-63-0	400	2	3	Oral - rat - 5,045 mg/kg Inhalation - rat - 8 h - 16000 ppm Dermal - rabbit - 12,800 mg/kg	Flammable	
ethanol	64-17-5	1000	0	3	Oral - rat - 7.060 mg/kg Inhalation - rat - 10 h - 20000 ppm	Flammable, Corrosive, toxic	Reproductive toxicity - Human - female - Oral
water							

*Sourced from available MSDS from various manufacturers

6.1.2 Grades and suppliers of polymers, solvents and additives

Table 6.2: Polymer grades and suppliers.

Polymer	Abbreviation	Source or grade
acrylonitrile butadiene styrene	ABS	LG Chem AF342 pellets, Supplier Axiam Engineering
acrylonitrile styrene acrylate	ASA	Starex WX-9130 pellets, Supplier Axiam Engineering
chlorinated PVC	CPVC	Ground high temperature piping
polyamide 6,6	PA6,6	BASF Ultramid A3K PA6'6
polycarbonate	PC	Bayer Makrolon 2407, pellets, Supplier Axiam Engineering
poly(methyl methacrylate)	PMMA	Evonik Plexiglas 8N, pellets, Supplier Axiam Engineering
polystyrene (expanded)	ExPS	packaging
polystyrene (high impact)	HIPS	LP8010F, Axiam Engineering
polystyrene (general purpose)	GPPS	Denka Styrol MW-1-321, Axiam Engineering

Table 6.3: Solvent grades and suppliers.

Solvent type	Solvent Grade and Supplier
acetic acid	Glacial, Manufacturer Ajax, Supplied by Thermofisher Scientific Ltd
acetone	Supplied by Marketing Chemicals Ltd
benzyl alcohol	98% reagent grade Manufacturer Ajax finechem, Supplier Thermofisher Scientific Ltd
dimethylformamide	AR grade manufacturer Scharlau, supplied by Global Science
ethanol	96% Manufacturer: Merck, Supplied by Global Science
ethyl acetate	Supplied by Bruce Scientific
formic acid	AR 99%, Manufacturer Ajax, Supplied by Thermofisher Scientific Ltd
methyl ether ketone	Manufacturer Analar Prolabo supplier Global Science
n-propyl acetate	Supplied by Bruce Scientific
n-methylpyrollidone	Supplied by Pure Science.
tetrahydrofuran	99.5% anyhdrous, stabilised with molecular sieves, manufacturer: Scharlau, supplied by Global Science.
xylene	98%, mix of isomers, manufacturer: Analar Normapur - VWR Int Ltd, supplied by Global Science

Table 6.4: Solution additives grades and suppliers

Additive	Grade and supplier
ammonium acetate	Reagent grade, ECP Ltd.
citric acid	Water residue cleaner, Anhydrous
lithium chloride	Molecular Biology grade, Manufacturer: Scharlau, Supplier Global Science
sodium dodecyl sulphate	Reagent grade, ECP Ltd.

Table 6.5: Fibre additives grades and suppliers

Additive	Grade and supplier
silver nitrate	Reagent Grade, Manufacturer Scharlau
poly(sodium 4-styrene sulfonate)	Ave Mw 70,000 Aldrich chemistry.
titanium dioxide	10 nm Anatase powder

6.2 SEM analysis of veils and composite panels

6.2.1 Fibre diameter calculations

Date:	17/06/2014 9:55			Legend	
Measurement Resolution (µm/pixel)	0.012				- Analysis Area
Contrast setting:	6				- Excluded Area
Number of Measurements:	1339				- Measured Diameter
Image Area Analyzed (%):	91%				- Out of Range Diameter
Selected Fiber Diameter Range (µm)	0.0 to 3.0				

Image #	Sample ID	Fiber Diameter (µm)			Average Orientation	Area Coverage (%)
		Average	Std Dev	Median		
1	Nyplex-e_q00.tif	0.141	0.070	0.138	79	28%

Figure 6.1: Fibre diameter measurements for nanoNyplex fibres.

217

		Fiber Diameter (µm)				
Date:		17/06/2014 9:55				
Measurement Resolution (µm/pixel)	0.011					
Contrast setting:	2					
Number of Measurements:	1057					
Image Area Analyzed (%):	89%					
Selected Fiber Diameter Range (µm)	0.06 to 0.65					

Legend
- Analysis Area
- Excluded Area
- Measured Diameter
- Out of Range Diameter

Image #	Sample ID	Fiber Diameter (µm)			Average Orientation	Area Coverage (%)
		Average	Std Dev	Median		
2	PA66-j_q00.tif	0.204	0.087	0.183	83	36%

Figure 6.2: Fibre diameter measurements for nanoPA6,6 fibres.

Date:		17/06/2014 9:55				
Measurement Resolution (µm/pixel)	0.022					
Contrast setting:	0					
Number of Measurements:	1455					
Image Area Analyzed (%):	94%					
Selected Fiber Diameter Range (µm)	0.06 to 0.65					

Legend
- Analysis Area
- Excluded Area
- Measured Diameter
- Out of Range Diameter

Image #	Sample ID	Fiber Diameter (µm)			Average Orientation	Area Coverage (%)
		Average	Std Dev	Median		
8	PMMA-f_q00.tif	0.274	0.108	0.265	92	32%

Figure 6.3: Fibre diameter measurements for nanoPMMA fibres.

		Fiber Diameter (µm)				
Date:		17/06/2014 9:55				
Measurement Resolution (µm/pixel		0.040				
Contrast setting:		0				
Number of Measurements:		1097				
Image Area Analyzed (%):		91%				
Selected Fiber Diameter Range (µm		0.0 to 3.0				

		Fiber Diameter (µm)				
Image #	Sample ID	Average	Std Dev	Median	Average Orientation	Area Coverage (%)
10	PVB-h_q00.tif	0.651	0.330	0.628	74	32%

Legend
- Analysis Area
- Excluded Area
- Measured Diameter
- Out of Range Diameter

Figure 6.4: Fibre diameter measurements for nanoPVB fibres.

Date:		17/06/2014 9:55				
Measurement Resolution (µm/pixel		0.011				
Contrast setting:		13				
Number of Measurements:		1135				
Image Area Analyzed (%):		90%				
Selected Fiber Diameter Range (µm		0.0 to 3.0				

		Fiber Diameter (µm)				
Image #	Sample ID	Average	Std Dev	Median	Average Orientation	Area Coverage (%)
7	PES-c_q00.tif	0.150	0.066	0.148	96	28%

Legend
- Analysis Area
- Excluded Area
- Measured Diameter
- Out of Range Diameter

Figure 6.5: Fibre diameter measurements for nanoPES fibres.

Date:	17/06/2014 9:55					Legend			
Measurement Resolution (µm/pixel)	0.396					☐ - Analysis Area			
Contrast setting:	0					☐ - Excluded Area			
Number of Measurements:	429					── - Measured Diameter			
Image Area Analyzed (%):	90%					── - Out of Range Diameter			
Selected Fiber Diameter Range (µm)	4.98 to 15.06								

Image #	Sample ID	Fiber Diameter (µm)			AverageOrientation	Area Coverage (%)
		Average	Std Dev	Median		
9	PPSVeil-d_q00.tif	9.465	1.640	9.641	71	19%

Figure 6.6: Fibre diameter measurements for microPPS fibres.

Date:	17/06/2014 9:55					Legend			
Measurement Resolution (µm/pixel)	0.396					☐ - Analysis Area			
Contrast setting:	-59					☐ - Excluded Area			
Number of Measurements:	79					── - Measured Diameter			
Image Area Analyzed (%):	-19%					── - Out of Range Diameter			
Selected Fiber Diameter Range (µm)	5.0 to 30.0								

Image #	Sample ID	Fiber Diameter (µm)			AverageOrientation	Area Coverage (%)
		Average	Std Dev	Median		
6	PEIVeil-a_q00.tif	15.405	3.372	16.404	79	16%

Figure 6.7: Fibre diameter measurements for microPEI fibres.

					Legend	
Date:	17/06/2014 9:55					- Analysis Area
Measurement Resolution (µm/pixel)	2.831					- Excluded Area
Contrast setting:	30					- Measured Diameter
Number of Measurements:	503					- Out of Range Diameter
Image Area Analyzed (%):	92%					
Selected Fiber Diameter Range (µm)	24.93 to 50.0					

Image #	Sample ID	Fiber Diameter (µm)			erageOrientation	Area Coverage (%)
		Average	Std Dev	Median		
11	Tricot-a_q00.tif	37.627	6.802	36.807	87	12%

Figure 6.8: Fibre diameter measurements for microtricot fibres.

					Legend	
Date:	17/06/2014 9:55					- Analysis Area
Measurement Resolution (µm/pixel)	0.011					- Excluded Area
Contrast setting:	4					- Measured Diameter
Number of Measurements:	1197					- Out of Range Diameter
Image Area Analyzed (%):	92%					
Selected Fiber Diameter Range (µm)	0.06 to 0.65					

Image #	Sample ID	Fiber Diameter (µm)			erageOrientation	Area Coverage (%)
		Average	Std Dev	Median		
4	PA66PPS-d_q00.	0.179	0.080	0.160	84	35%

Figure 6.9: Fibre diameter measurements for the PA6,6 nanofibre in the microPPSnanoPA6,6veil.

Date:		17/06/2014 9:55					Legend			
Measurement Resolution (µm/pixel)		0.011						- Analysis Area		
Contrast setting:		41						- Excluded Area		
Number of Measurements:		1092						- Measured Diameter		
Image Area Analyzed (%):		91%						- Out of Range Diameter		
Selected Fiber Diameter Range (µm)		0.06 to 0.65								

Image #	Sample ID	Fiber Diameter (µm)			Average Orientation	Area Coverage (%)
		Average	Std Dev	Median		
3	PA66PEI-d_q00.t	0.200	0.082	0.177	99	36%

Figure 6.10: Fibre diameter measurements for the PA6,6 nanofibre in the microPEInanoPA6,6 veil.

Date:		17/06/2014 9:55					Legend			
Measurement Resolution (µm/pixel)		0.011						- Analysis Area		
Contrast setting:		16						- Excluded Area		
Number of Measurements:		1312						- Measured Diameter		
Image Area Analyzed (%):		93%						- Out of Range Diameter		
Selected Fiber Diameter Range (µm)		0.06 to 0.65								

Image #	Sample ID	Fiber Diameter (µm)			Average Orientation	Area Coverage (%)
		Average	Std Dev	Median		
5	PA66tricot-d_q00	0.173	0.062	0.163	82	37%

Figure 6.11: Fibre diameter measurements for the PA6,6 nanofibre in the microtricotnanoPA6,6 veil.

6.3 Vibration damping analysis

6.3.1 Initial test results for each sample

Table 6.6: Results for control samples (no interleaving).

Sample:	1A - control			Sample:	1B- control			Sample:	1C- control				Average of control samples		
Frequency	Storage Modulus	Loss Modulus	Tan Delta	Frequency	Storage Modulus	Loss Modulus	Tan Delta	Frequency	Storage Modulus	Loss Modulus	Tan Delta	Frequency	Storage Modulus	Loss Modulus	Tan Delta
Hz	Pa	Pa		Hz	Pa	Pa		Hz	Pa	Pa		Hz	Pa	Pa	
0.100	5.22E+09	5.44E+07	1.04E-02	0.119	5.32E+09	6.75E+07	1.27E-02	0.188	7.26E+09	1.32E+08	1.81E-02				
0.158	5.23E+09	7.89E+07	1.51E-02	0.158	5.33E+09	1.04E+08	1.94E-02	0.158	7.28E+09	1.29E+08	1.77E-02	0.158	5.94E+09	1.04E+08	1.74E-02
0.251	5.24E+09	5.29E+07	1.01E-02	0.251	5.33E+09	6.32E+07	1.18E-02	0.251	7.29E+09	9.02E+07	1.24E-02	0.251	5.95E+09	6.88E+07	1.14E-02
0.398	5.24E+09	1.13E+08	2.15E-02	0.398	5.34E+09	1.45E+08	2.72E-02	0.398	7.31E+09	1.20E+07	1.64E-03	0.398	5.96E+09	9.01E+07	1.68E-02
0.631	5.25E+09	6.79E+07	1.29E-02	0.631	5.35E+09	7.50E+07	1.40E-02	0.631	7.32E+09	1.05E+08	1.44E-02	0.631	5.97E+09	8.28E+07	1.38E-02
1.000	5.26E+09	6.40E+07	1.22E-02	1.000	5.36E+09	7.60E+07	1.42E-02	1.000	7.33E+09	1.03E+08	1.41E-02	1.000	5.98E+09	8.11E+07	1.35E-02
1.585	5.26E+09	6.48E+07	1.23E-02	1.585	5.37E+09	7.93E+07	1.48E-02	1.585	7.35E+09	1.03E+08	1.41E-02	1.585	5.99E+09	8.25E+07	1.37E-02
2.512	5.27E+09	6.90E+07	1.31E-02	2.512	5.38E+09	7.08E+07	1.32E-02	2.512	7.36E+09	9.32E+07	1.27E-02	2.512	6.00E+09	7.77E+07	1.30E-02
3.981	5.28E+09	6.53E+07	1.24E-02	3.981	5.39E+09	7.56E+07	1.40E-02	3.981	7.37E+09	1.00E+08	1.36E-02	3.981	6.01E+09	8.04E+07	1.33E-02
6.310	5.29E+09	6.97E+07	1.32E-02	6.310	5.39E+09	7.80E+07	1.45E-02	6.310	7.40E+09	8.31E+07	1.12E-02	6.310	6.02E+09	7.69E+07	1.30E-02
10.000	5.30E+09	6.91E+07	1.30E-02	10.000	5.40E+09	7.56E+07	1.40E-02	10.000	7.40E+09	9.10E+07	1.23E-02	10.000	6.04E+09	7.86E+07	1.31E-02
15.849	5.31E+09	6.33E+07	1.19E-02	15.849	5.42E+09	7.67E+07	1.42E-02	15.849	7.42E+09	9.71E+07	1.31E-02	15.849	6.05E+09	7.90E+07	1.31E-02
25.119	5.32E+09	6.03E+07	1.13E-02	25.119	5.46E+09	6.83E+07	1.25E-02	25.119	7.44E+09	8.76E+07	1.18E-02	25.119	6.07E+09	7.21E+07	1.19E-02
39.811	5.33E+09	5.03E+07	9.44E-03	39.811	5.48E+09	4.62E+07	8.43E-03	39.811	7.49E+09	8.97E+07	1.20E-02	39.811	6.10E+09	6.21E+07	9.95E-03
63.096	5.41E+09	2.30E+08	4.25E-02	63.096	5.85E+09	4.70E+08	8.04E-02	63.096	7.61E+09	-1.44E+08	-1.89E-02	63.096	6.29E+09	1.85E+08	3.46E-02
100.000	5.33E+09	9.36E+07	1.76E-02	100.000	5.51E+09	7.87E+07	1.43E-02	100.000	7.59E+09	6.10E+07	8.04E-03	100.000	6.14E+09	7.78E+07	1.33E-02

Table 6.7: Results for nanoNyplex fibre interleaved samples.

Sample:	Nyplex nanofibre interleaved		2A	Sample:	Nyplex nanofibre interleaved		2B	Sample:	Nyplex nanofibre interleaved		2C	Sample:	Nyplex nanofibre interleaved		2D	average of Nyplex nanofibre interleaved samples			
Frequency	Storage Modulus	Loss Modulus	Tan Delta	Frequency	Storage Modulus	Loss Modulus	Tan Delta	Frequency	Storage Modulus	Loss Modulus	Tan Delta	Frequency	Storage Modulus	Loss Modulus	Tan Delta	Frequency	Storage Modulus	Loss Modulus	Tan Delta
Hz	Pa	Pa		Hz	Pa	Pa		Hz	Pa	Pa		Hz	Pa	Pa		Hz	Pa	Pa	
0.100	5.58E+09	9.99E+07	1.79E-02	0.193	5.64E+09	6.02E+07	1.07E-02	0.175	7.58E+09	1.33E+08	1.75E-02								
0.158	5.59E+09	1.31E+08	2.34E-02	0.158	5.65E+09	8.72E+07	1.54E-02	0.158	7.59E+09	1.41E+08	1.85E-02	0.158	6.28E+09	1.20E+08	1.91E-02	0.16	6.28E+09	1.20E+08	1.91E-02
0.251	5.61E+09	9.74E+07	1.74E-02	0.251	5.67E+09	5.52E+07	9.74E-03	0.251	7.61E+09	9.12E+07	1.20E-02	0.251	6.29E+09	8.13E+07	1.30E-02	0.25	6.29E+09	8.13E+07	1.30E-02
0.398	5.61E+09	1.20E+08	2.15E-02	0.398	5.65E+09	-4.16E+07	-7.37E-03	0.398	7.63E+09	7.20E+07	9.44E-03	0.398	6.30E+09	5.03E+07	7.84E-03	0.40	6.30E+09	5.03E+07	7.84E-03
0.631	5.63E+09	1.13E+08	2.01E-02	0.631	5.69E+09	7.79E+07	1.37E-02	0.631	7.64E+09	1.26E+08	1.65E-02	0.631	6.32E+09	1.06E+08	1.68E-02	0.63	6.32E+09	1.06E+08	1.68E-02
1.000	5.63E+09	1.00E+08	1.77E-02	1.000	5.69E+09	6.55E+07	1.15E-02	1.000	7.65E+09	1.15E+08	1.51E-02	1.000	6.33E+09	9.36E+07	1.48E-02	1.00	6.33E+09	9.36E+07	1.48E-02
1.585	5.64E+09	9.60E+07	1.70E-02	1.585	5.70E+09	6.39E+07	1.12E-02	1.585	7.67E+09	1.15E+08	1.50E-02	1.585	6.34E+09	9.16E+07	1.44E-02	1.58	6.34E+09	9.16E+07	1.44E-02
2.512	5.65E+09	9.41E+07	1.67E-02	2.512	5.70E+09	6.17E+07	1.08E-02	2.512	7.69E+09	1.13E+08	1.47E-02	2.512	6.35E+09	8.95E+07	1.40E-02	2.51	6.35E+09	8.95E+07	1.40E-02
3.981	5.66E+09	9.41E+07	1.66E-02	3.981	5.72E+09	6.53E+07	1.14E-02	3.981	7.70E+09	1.10E+08	1.42E-02	3.981	6.36E+09	8.97E+07	1.41E-02	3.98	6.36E+09	8.97E+07	1.41E-02
6.310	5.68E+09	8.07E+07	1.42E-02	6.310	5.73E+09	5.44E+07	9.49E-03	6.310	7.71E+09	1.03E+08	1.33E-02	6.310	6.37E+09	7.92E+07	1.23E-02	6.31	6.37E+09	7.92E+07	1.23E-02
10.000	5.69E+09	8.85E+07	1.56E-02	10.000	5.74E+09	6.24E+07	1.09E-02	10.000	7.74E+09	1.12E+08	1.45E-02	10.000	6.39E+09	8.76E+07	1.36E-02	10.00	6.39E+09	8.76E+07	1.36E-02
15.849	5.69E+09	8.75E+07	1.54E-02	15.849	5.75E+09	5.78E+07	1.01E-02	15.849	7.76E+09	1.10E+08	1.42E-02	15.849	6.40E+09	8.52E+07	1.32E-02	15.85	6.40E+09	8.52E+07	1.32E-02
25.119	5.72E+09	8.14E+07	1.42E-02	25.119	5.76E+09	5.51E+07	9.57E-03	25.119	7.78E+09	1.10E+08	1.41E-02	25.119	6.42E+09	8.21E+07	1.26E-02	25.12	6.42E+09	8.21E+07	1.26E-02
39.811	5.72E+09	8.06E+07	1.41E-02	39.811	5.79E+09	4.05E+07	6.99E-03	39.811	7.83E+09	1.05E+08	1.35E-02	39.811	6.44E+09	7.55E+07	1.15E-02	39.81	6.44E+09	7.55E+07	1.15E-02
63.096	5.94E+09	-3.14E+08	-5.28E-02	63.096	5.64E+09	2.95E+08	5.22E-02	63.096	8.06E+09	1.17E+08	1.45E-02	63.096	6.55E+09	3.27E+07	4.64E-03	63.10	6.55E+09	3.27E+07	4.64E-03
100.000	5.78E+09	2.72E+07	4.71E-03	100.000	5.87E+09	3.87E+07	6.60E-03	100.000	7.94E+09	1.04E+08	1.31E-02	100.000	6.53E+09	5.67E+07	8.14E-03	100.00	6.53E+09	5.67E+07	8.14E-03

Table 6.8: Results for nanoPMMA fibre interleaved samples.

Sample:	PMMA nanofibre interleaved		3A	Sample:	PMMA nanofibre interleaved		3B	Sample:	PMMA nanofibre interleaved		3C	Average of PMMA nanofibre interleaved samples			
Frequency	Storage Modulus	Loss Modulus	Tan Delta	Frequency	Storage Modulus	Loss Modulus	Tan Delta	Frequency	Storage Modulus	Loss Modulus	Tan Delta	Frequency	Storage Modulus	Loss Modulus	Tan Delta
Hz	Pa	Pa		Hz	Pa	Pa		Hz	Pa	Pa		Hz	Pa	Pa	
0.100	7.37E+09	1.16E+08	1.57E-02	0.100	5.46E+09	1.23E+08	2.26E-02	0.100	7.15E+09	1.20E+08	1.68E-02	0.100	6.66E+09	1.20E+08	1.84E-02
0.158	7.39E+09	1.31E+08	1.77E-02	0.158	5.47E+09	1.10E+08	2.01E-02	0.158	7.17E+09	1.24E+08	1.74E-02	0.158	6.68E+09	1.22E+08	1.84E-02
0.251	7.41E+09	7.97E+07	1.08E-02	0.251	5.47E+09	8.31E+07	1.52E-02	0.251	7.19E+09	7.47E+07	1.04E-02	0.251	6.69E+09	7.92E+07	1.21E-02
0.398	7.42E+09	4.39E+07	5.92E-03	0.398	5.46E+09	2.41E+07	4.40E-03	0.398	7.20E+09	4.09E+07	5.68E-03	0.398	6.70E+09	3.63E+07	5.33E-03
0.631	7.44E+09	1.08E+08	1.45E-02	0.631	5.49E+09	1.03E+08	1.87E-02	0.631	7.22E+09	9.99E+07	1.38E-02	0.631	6.72E+09	1.04E+08	1.57E-02
1.000	7.44E+09	9.12E+07	1.23E-02	1.000	5.50E+09	1.04E+08	1.89E-02	1.000	7.22E+09	9.33E+07	1.29E-02	1.000	6.72E+09	9.62E+07	1.47E-02
1.585	7.45E+09	8.44E+07	1.13E-02	1.585	5.51E+09	9.91E+07	1.80E-02	1.585	7.23E+09	9.54E+07	1.32E-02	1.585	6.73E+09	9.30E+07	1.42E-02
2.512	7.47E+09	8.42E+07	1.13E-02	2.512	5.51E+09	9.85E+07	1.79E-02	2.512	7.25E+09	9.41E+07	1.30E-02	2.512	6.74E+09	9.23E+07	1.40E-02
3.981	7.48E+09	8.24E+07	1.10E-02	3.981	5.52E+09	9.78E+07	1.77E-02	3.981	7.27E+09	9.56E+07	1.32E-02	3.981	6.76E+09	9.19E+07	1.40E-02
6.310	7.51E+09	1.03E+08	1.37E-02	6.310	5.55E+09	9.92E+07	1.79E-02	6.310	7.29E+09	9.72E+07	1.33E-02	6.310	6.78E+09	9.98E+07	1.50E-02
10.000	7.52E+09	6.74E+07	8.97E-03	10.000	5.55E+09	1.07E+08	1.93E-02	10.000	7.29E+09	9.03E+07	1.24E-02	10.000	6.79E+09	8.82E+07	1.35E-02
15.849	7.54E+09	7.84E+07	1.04E-02	15.849	5.56E+09	9.65E+07	1.74E-02	15.849	7.31E+09	8.48E+07	1.16E-02	15.849	6.80E+09	8.66E+07	1.31E-02
25.119	7.56E+09	7.21E+07	9.54E-03	25.119	5.57E+09	8.79E+07	1.58E-02	25.119	7.34E+09	8.54E+07	1.16E-02	25.119	6.82E+09	8.18E+07	1.23E-02
39.811	7.61E+09	8.79E+07	1.15E-02	39.811	5.60E+09	8.22E+07	1.47E-02	39.811	7.35E+09	6.79E+07	9.25E-03	39.811	6.85E+09	7.93E+07	1.18E-02
63.096	8.09E+09	-6.98E+08	-8.64E-02	63.096	5.39E+09	-5.65E+08	-1.05E-01	63.096	7.09E+09	-1.74E+08	-2.46E-02	63.096	6.86E+09	-4.79E+08	-7.19E-02
100.000	7.74E+09	1.35E+07	1.75E-03	100.000	5.72E+09	1.36E+08	2.38E-02	100.000	7.48E+09	3.51E+07	4.69E-03	100.000	6.98E+09	6.16E+07	1.01E-02

Table 6.9: Results for nanoPA6,6 fibre interleaved samples.

Sample:	PA6,6 nanofibre interleaved		4a	Sample:	PA6,6 nanofibre interleaved		4b	Sample:	PA6,6 nanofibre interleaved		4c		average of PA6,6 interleaved samples		
Frequency	Storage Modulus	Loss Modulus	Tan Delta	Frequency	Storage Modulus	Loss Modulus	Tan Delta	Frequency	Storage Modulus	Loss Modulus	Tan Delta	Frequency	Storage Modulus	Loss Modulus	Tan Delta
Hz	Pa	Pa		Hz	Pa	Pa		Hz	Pa	Pa		Hz	Pa	Pa	
0.100	6.37E+09	1.23E+08	1.92E-02	0.100	7.17E+09	1.32E+08	1.85E-02	0.100	7.09E+09	1.30E+08	1.84E-02	0.100	6.87E+09	1.28E+08	1.87E-02
0.158	6.35E+09	1.14E+08	1.80E-02	0.158	7.18E+09	1.18E+08	1.64E-02	0.158	7.12E+09	1.36E+08	1.91E-02	0.158	6.88E+09	1.23E+08	1.78E-02
0.251	6.36E+09	7.57E+07	1.19E-02	0.251	7.19E+09	6.75E+07	9.39E-03	0.251	7.14E+09	8.55E+07	1.20E-02	0.251	6.89E+09	7.62E+07	1.11E-02
0.398	6.36E+09	5.59E+07	8.79E-03	0.398	7.20E+09	4.62E+07	6.42E-03	0.398	7.16E+09	5.08E+07	7.10E-03	0.398	6.91E+09	5.10E+07	7.43E-03
0.631	6.37E+09	1.01E+08	1.58E-02	0.631	7.22E+09	9.28E+07	1.28E-02	0.631	7.17E+09	1.11E+08	1.54E-02	0.631	6.92E+09	1.01E+08	1.47E-02
1.000	6.40E+09	1.03E+08	1.61E-02	1.000	7.24E+09	9.28E+07	1.28E-02	1.000	7.18E+09	9.36E+07	1.30E-02	1.000	6.94E+09	9.64E+07	1.40E-02
1.585	6.40E+09	1.03E+08	1.61E-02	1.585	7.25E+09	8.93E+07	1.23E-02	1.585	7.19E+09	9.98E+07	1.39E-02	1.585	6.95E+09	9.75E+07	1.41E-02
2.512	6.42E+09	1.01E+08	1.58E-02	2.512	7.26E+09	9.00E+07	1.24E-02	2.512	7.21E+09	8.62E+07	1.20E-02	2.512	6.96E+09	9.24E+07	1.34E-02
3.981	6.43E+09	1.13E+08	1.75E-02	3.981	7.28E+09	9.26E+07	1.27E-02	3.981	7.23E+09	7.92E+07	1.10E-02	3.981	6.98E+09	9.48E+07	1.37E-02
6.310	6.43E+09	1.06E+08	1.66E-02	6.310	7.29E+09	1.16E+08	1.59E-02	6.310	7.25E+09	9.37E+07	1.29E-02	6.310	6.99E+09	1.05E+08	1.51E-02
10.000	6.46E+09	9.05E+07	1.40E-02	10.000	7.32E+09	1.02E+08	1.40E-02	10.000	7.26E+09	7.73E+07	1.06E-02	10.000	7.01E+09	9.00E+07	1.29E-02
15.849	6.46E+09	9.85E+07	1.53E-02	15.849	7.34E+09	8.89E+07	1.21E-02	15.849	7.28E+09	6.40E+07	8.79E-03	15.849	7.02E+09	8.38E+07	1.21E-02
25.119	6.48E+09	8.56E+07	1.32E-02	25.119	7.36E+09	8.21E+07	1.12E-02	25.119	7.29E+09	7.46E+07	1.02E-02	25.119	7.04E+09	8.08E+07	1.15E-02
39.811	6.49E+09	7.56E+07	1.16E-02	39.811	7.37E+09	7.27E+07	9.86E-03	39.811	7.33E+09	4.65E+07	6.34E-03	39.811	7.06E+09	6.49E+07	9.28E-03
63.096	5.91E+09	6.71E+08	1.14E-01	63.096	7.53E+09	1.40E+09	1.85E-01	63.096	7.08E+09	1.36E+08	1.92E-02	63.096	6.84E+09	7.34E+08	1.06E-01
100.000	6.57E+09	1.46E+08	2.22E-02	100.000	7.42E+09	1.11E+08	1.50E-02	100.000	7.58E+09	1.16E+08	1.53E-02	100.000	7.19E+09	1.24E+08	1.75E-02

Table 6.10: Results for nanoPVB fibre interleaved samples.

Sample:	PVB nanofibre interleaved		5a	Sample:	PVB nanofibre interleaved			Sample:	PVB nanofibre interleaved				average PVB nanofibre interleaved samples		
Frequency	Storage Modulus	Loss Modulus	Tan Delta	Frequency	Storage Modulus	Loss Modulus	Tan Delta	Frequency	Storage Modulus	Loss Modulus	Tan Delta	Frequency	Storage Modulus	Loss Modulus	Tan Delta
Hz	Pa	Pa		Hz	Pa	Pa		Hz	Pa	Pa		Hz	Pa	Pa	
0.100	6.11E+09	1.03E+08	1.68E-02	0.137	6.83E+09	1.23E+08	1.80E-02	0.100	7.14E+09	1.32E+08	1.85E-02				
0.158	6.11E+09	9.19E+07	1.50E-02	0.158	6.83E+09	1.38E+08	2.02E-02	0.158	7.15E+09	1.17E+08	1.63E-02	0.158	6.70E+09	1.16E+08	1.72E-02
0.251	6.13E+09	5.87E+07	9.57E-03	0.251	6.85E+09	9.86E+07	1.44E-02	0.251	7.17E+09	7.73E+07	1.08E-02	0.251	6.72E+09	7.82E+07	1.16E-02
0.398	6.14E+09	4.74E+07	7.73E-03	0.398	6.86E+09	4.12E+07	6.00E-03	0.398	7.19E+09	1.37E+07	1.91E-03	0.398	6.73E+09	3.41E+07	5.21E-03
0.631	6.17E+09	8.81E+07	1.43E-02	0.631	6.88E+09	1.20E+08	1.75E-02	0.631	7.21E+09	1.01E+08	1.40E-02	0.631	6.75E+09	1.03E+08	1.53E-02
1.000	6.17E+09	7.82E+07	1.27E-02	1.000	6.88E+09	1.05E+08	1.53E-02	1.000	7.23E+09	9.24E+07	1.28E-02	1.000	6.76E+09	9.19E+07	1.36E-02
1.585	6.19E+09	7.35E+07	1.19E-02	1.585	6.90E+09	1.06E+08	1.53E-02	1.585	7.24E+09	8.91E+07	1.23E-02	1.585	6.78E+09	8.95E+07	1.32E-02
2.512	6.20E+09	6.66E+07	1.08E-02	2.512	6.90E+09	1.02E+08	1.48E-02	2.512	7.26E+09	8.99E+07	1.24E-02	2.512	6.79E+09	8.61E+07	1.26E-02
3.981	6.21E+09	6.84E+07	1.10E-02	3.981	6.93E+09	1.02E+08	1.47E-02	3.981	7.27E+09	8.10E+07	1.11E-02	3.981	6.81E+09	8.38E+07	1.23E-02
6.310	6.21E+09	8.70E+07	1.40E-02	6.310	6.91E+09	7.51E+07	1.09E-02	6.310	7.29E+09	8.69E+07	1.19E-02	6.310	6.80E+09	8.30E+07	1.23E-02
10.000	6.24E+09	6.62E+07	1.06E-02	10.000	6.95E+09	1.02E+08	1.47E-02	10.000	7.30E+09	7.59E+07	1.04E-02	10.000	6.83E+09	8.15E+07	1.19E-02
15.849	6.26E+09	6.43E+07	1.03E-02	15.849	6.96E+09	9.01E+07	1.29E-02	15.849	7.32E+09	6.84E+07	9.34E-03	15.849	6.85E+09	7.43E+07	1.09E-02
25.119	6.27E+09	6.06E+07	9.66E-03	25.119	6.99E+09	9.20E+07	1.32E-02	25.119	7.34E+09	6.49E+07	8.84E-03	25.119	6.87E+09	7.25E+07	1.06E-02
39.811	6.30E+09	3.46E+07	5.49E-03	39.811	7.01E+09	5.43E+07	7.75E-03	39.811	7.39E+09	4.05E+07	5.48E-03	39.811	6.90E+09	4.31E+07	6.24E-03
63.096	6.49E+09	-1.67E+08	-2.57E-02	63.096	7.04E+09	3.43E+06	4.88E-04	63.096	7.49E+09	4.33E+07	5.78E-03	63.096	7.01E+09	-4.01E+07	-6.48E-03
100.000	6.39E+09	5.14E+06	8.04E-04	100.000	7.10E+09	7.52E+07	1.06E-02	100.000	7.50E+09	4.53E+07	6.04E-03	100.000	7.00E+09	4.19E+07	5.81E-03

Table 6.11: Results for nanoPES fibre interleaved samples.

sample:	nanofibre PES interleaved		12a	sample:	nanofibre PES interleaved		12b	sample:	nanofibre PES interleaved		12c	average for nanofibre PES interleaved samples			
Frequency	Storage Modulus	Loss Modulus	Tan Delta	Frequency	Storage Modulus	Loss Modulus	Tan Delta	Frequency	Storage Modulus	Loss Modulus	Tan Delta	Frequency	Storage Modulus	Loss Modulus	Tan Delta
Hz	Pa	Pa		Hz	Pa	Pa		Hz	Pa	Pa		Hz	Pa	Pa	
0.100	5.84E+09	9.68E+07	1.66E-02	0.188	7.05E+09	1.31E+08	1.86E-02	0.233	6.76E+09	1.24E+08	1.83E-02				
0.158	5.84E+09	1.06E+08	1.82E-02	0.158	7.06E+09	1.35E+08	1.91E-02	0.158	6.77E+09	1.30E+08	1.92E-02	0.158	6.56E+09	1.24E+08	1.88E-02
0.251	5.85E+09	7.21E+07	1.23E-02	0.251	7.07E+09	8.53E+07	1.21E-02	0.251	6.78E+09	8.75E+07	1.29E-02	0.251	6.57E+09	8.17E+07	1.24E-02
0.398	5.87E+09	1.11E+08	1.89E-02	0.398	7.09E+09	3.11E+07	4.39E-03	0.398	6.80E+09	1.84E+07	2.71E-03	0.398	6.59E+09	5.34E+07	8.65E-03
0.631	5.89E+09	8.24E+07	1.40E-02	0.631	7.10E+09	1.07E+08	1.50E-02	0.631	6.81E+09	1.12E+08	1.65E-02	0.631	6.60E+09	1.00E+08	1.52E-02
1.000	5.90E+09	7.80E+07	1.32E-02	1.000	7.12E+09	8.84E+07	1.24E-02	1.000	6.82E+09	8.94E+07	1.31E-02	1.000	6.61E+09	8.53E+07	1.29E-02
1.585	5.91E+09	7.73E+07	1.31E-02	1.585	7.13E+09	8.91E+07	1.25E-02	1.585	6.83E+09	8.82E+07	1.29E-02	1.585	6.62E+09	8.48E+07	1.28E-02
2.512	5.92E+09	6.95E+07	1.17E-02	2.512	7.15E+09	8.55E+07	1.20E-02	2.512	6.84E+09	8.75E+07	1.28E-02	2.512	6.64E+09	8.08E+07	1.22E-02
3.981	5.93E+09	6.71E+07	1.13E-02	3.981	7.17E+09	8.44E+07	1.18E-02	3.981	6.85E+09	8.47E+07	1.24E-02	3.981	6.65E+09	7.88E+07	1.18E-02
6.310	5.94E+09	7.21E+07	1.21E-02	6.310	7.19E+09	7.40E+07	1.03E-02	6.310	6.85E+09	8.36E+07	1.22E-02	6.310	6.66E+09	7.66E+07	1.15E-02
10.000	5.95E+09	6.75E+07	1.13E-02	10.000	7.19E+09	7.31E+07	1.02E-02	10.000	6.87E+09	7.69E+07	1.12E-02	10.000	6.67E+09	7.25E+07	1.09E-02
15.849	5.96E+09	6.57E+07	1.10E-02	15.849	7.21E+09	7.54E+07	1.04E-02	15.849	6.89E+09	8.00E+07	1.16E-02	15.849	6.69E+09	7.37E+07	1.10E-02
25.119	5.98E+09	5.79E+07	9.67E-03	25.119	7.24E+09	6.32E+07	8.73E-03	25.119	6.90E+09	7.46E+07	1.08E-02	25.119	6.71E+09	6.52E+07	9.74E-03
39.811	5.99E+09	4.61E+07	7.69E-03	39.811	7.28E+09	4.64E+07	6.37E-03	39.811	6.94E+09	6.90E+07	9.94E-03	39.811	6.74E+09	5.38E+07	8.00E-03
63.096	5.73E+09	3.66E+07	6.40E-03	63.096	7.18E+09	2.98E+08	4.14E-02	63.096	7.06E+09	6.42E+08	9.09E-02	63.096	6.66E+09	3.25E+08	4.62E-02
100.000	6.09E+09	2.28E+07	3.75E-03	100.000	7.40E+09	2.92E+07	3.94E-03	100.000	6.93E+09	7.61E+07	1.10E-02	100.000	6.81E+09	4.27E+07	6.22E-03

Table 6.12: Results for microPPS interleaved samples.

Sample:	microfibre PPS interleaved		6a	Sample:	microfibre PPS interleaved		6b	Sample:	microfibre PPS interleaved		6c	average of microfibre PPS interleaved samples			
Frequency	Storage Modulus	Loss Modulus	Tan Delta	Frequency	Storage Modulus	Loss Modulus	Tan Delta	Frequency	Storage Modulus	Loss Modulus	Tan Delta	Frequency	Storage Modulus	Loss Modulus	Tan Delta
Hz	Pa	Pa		Hz	Pa	Pa		Hz	Pa	Pa		Hz	Pa	Pa	
0.324	7.13E+09	6.10E+07	8.56E-03	0.100	7.13E+09	1.25E+08	1.75E-02	0.100	6.70E+09	1.38E+08	2.07E-02				
0.158	7.10E+09	1.08E+08	1.51E-02	0.158	7.14E+09	1.33E+08	1.86E-02	0.158	6.72E+09	1.14E+08	1.69E-02	0.158	6.99E+09	1.18E+08	1.69E-02
0.251	7.14E+09	6.68E+07	9.35E-03	0.251	7.16E+09	8.24E+07	1.15E-02	0.251	6.73E+09	6.93E+07	1.03E-02	0.251	7.01E+09	7.28E+07	1.04E-02
0.398	7.15E+09	1.15E+07	1.61E-03	0.398	7.18E+09	4.31E+07	6.01E-03	0.398	6.75E+09	-2.37E+07	-3.51E-03	0.398	7.02E+09	1.03E+07	1.37E-03
0.631	7.17E+09	8.96E+07	1.25E-02	0.631	7.19E+09	1.05E+08	1.46E-02	0.631	6.76E+09	8.49E+07	1.26E-02	0.631	7.04E+09	9.32E+07	1.32E-02
1.000	7.19E+09	8.42E+07	1.17E-02	1.000	7.20E+09	8.10E+07	1.12E-02	1.000	6.77E+09	8.52E+07	1.26E-02	1.000	7.05E+09	8.35E+07	1.18E-02
1.585	7.21E+09	8.09E+07	1.12E-02	1.585	7.21E+09	8.51E+07	1.18E-02	1.585	6.79E+09	8.27E+07	1.22E-02	1.585	7.07E+09	8.29E+07	1.17E-02
2.512	7.20E+09	8.22E+07	1.14E-02	2.512	7.22E+09	8.06E+07	1.12E-02	2.512	6.80E+09	7.72E+07	1.13E-02	2.512	7.08E+09	8.00E+07	1.13E-02
3.981	7.23E+09	7.47E+07	1.03E-02	3.981	7.22E+09	8.02E+07	1.11E-02	3.981	6.81E+09	8.09E+07	1.19E-02	3.981	7.09E+09	7.86E+07	1.11E-02
6.310	7.24E+09	9.01E+07	1.24E-02	6.310	7.23E+09	7.06E+07	9.76E-03	6.310	6.82E+09	7.81E+07	1.15E-02	6.310	7.10E+09	7.96E+07	1.12E-02
10.000	7.24E+09	6.34E+07	8.75E-03	10.000	7.26E+09	8.38E+07	1.15E-02	10.000	6.84E+09	7.70E+07	1.13E-02	10.000	7.12E+09	7.47E+07	1.05E-02
15.849	7.28E+09	7.01E+07	9.63E-03	15.849	7.27E+09	8.25E+07	1.13E-02	15.849	6.86E+09	7.74E+07	1.13E-02	15.849	7.14E+09	7.67E+07	1.08E-02
25.119	7.30E+09	6.05E+07	8.28E-03	25.119	7.30E+09	7.81E+07	1.07E-02	25.119	6.88E+09	6.58E+07	9.57E-03	25.119	7.16E+09	6.82E+07	9.52E-03
39.811	7.33E+09	3.39E+07	4.62E-03	39.811	7.32E+09	8.46E+07	1.16E-02	39.811	6.91E+09	4.77E+07	6.91E-03	39.811	7.18E+09	5.54E+07	7.70E-03
63.096	8.03E+09	-6.01E+08	-7.48E-02	63.096	6.82E+09	6.47E+08	9.48E-02	63.096	6.31E+09	1.64E+08	2.61E-02	63.096	7.05E+09	7.01E+07	1.54E-02
100.000	7.41E+09	9.27E+07	1.25E-02	100.000	7.47E+09	2.53E+07	3.38E-03	100.000	7.05E+09	6.29E+07	8.93E-03	100.000	7.31E+09	6.03E+07	8.27E-03

Table 6.13: Results for microPEI interleaved samples.

Sample: microfibre PEI interleaved			7a	Sample: microfibre PEI interleaved			7b	Sample: microfibre PEI interleaved			7c	average of microfibre PEI interleaved samples			
Frequency	Storage Modulus	Loss Modulus	Tan Delta	Frequency	Storage Modulus	Loss Modulus	Tan Delta	Frequency	Storage Modulus	Loss Modulus	Tan Delta	Frequency	Storage Modulus	Loss Modulus	Tan Delta
Hz	Pa	Pa		Hz	Pa	Pa		Hz	Pa	Pa		Hz	Pa	Pa	
0.193	6.87E+09	1.00E+08	1.46E-02	0.100	6.09E+09	1.28E+08	2.10E-02	0.100	7.19E+09	1.34E+08	1.87E-02				
0.158	6.87E+09	1.27E+08	1.85E-02	0.158	6.10E+09	1.20E+08	1.97E-02	0.158	7.21E+09	1.31E+08	1.81E-02	0.158	6.73E+09	1.26E+08	1.88E-02
0.251	6.89E+09	8.45E+07	1.23E-02	0.251	6.12E+09	8.54E+07	1.39E-02	0.251	7.23E+09	8.10E+07	1.12E-02	0.251	6.75E+09	8.36E+07	1.25E-02
0.398	6.90E+09	4.71E+07	6.82E-03	0.398	6.13E+09	3.03E+07	4.94E-03	0.398	7.24E+09	4.27E+07	5.89E-03	0.398	6.76E+09	4.00E+07	5.88E-03
0.631	6.92E+09	1.18E+08	1.70E-02	0.631	6.14E+09	1.00E+08	1.63E-02	0.631	7.25E+09	1.13E+08	1.56E-02	0.631	6.77E+09	1.10E+08	1.63E-02
1.000	6.92E+09	9.41E+07	1.36E-02	1.000	6.16E+09	9.76E+07	1.58E-02	1.000	7.27E+09	9.48E+07	1.30E-02	1.000	6.78E+09	9.55E+07	1.42E-02
1.585	6.93E+09	9.56E+07	1.38E-02	1.585	6.16E+09	9.40E+07	1.53E-02	1.585	7.27E+09	1.01E+08	1.39E-02	1.585	6.79E+09	9.68E+07	1.43E-02
2.512	6.96E+09	8.25E+07	1.18E-02	2.512	6.18E+09	9.14E+07	1.48E-02	2.512	7.29E+09	9.66E+07	1.33E-02	2.512	6.81E+09	9.01E+07	1.33E-02
3.981	6.97E+09	8.09E+07	1.16E-02	3.981	6.19E+09	8.80E+07	1.42E-02	3.981	7.30E+09	9.46E+07	1.30E-02	3.981	6.82E+09	8.78E+07	1.29E-02
6.310	6.97E+09	7.36E+07	1.06E-02	6.310	6.21E+09	9.78E+07	1.58E-02	6.310	7.30E+09	9.37E+07	1.28E-02	6.310	6.83E+09	8.84E+07	1.31E-02
10.000	6.99E+09	9.32E+07	1.33E-02	10.000	6.21E+09	9.14E+07	1.47E-02	10.000	7.33E+09	9.12E+07	1.24E-02	10.000	6.84E+09	9.19E+07	1.35E-02
15.849	7.01E+09	9.38E+07	1.34E-02	15.849	6.22E+09	8.35E+07	1.34E-02	15.849	7.33E+09	9.78E+07	1.33E-02	15.849	6.86E+09	9.17E+07	1.34E-02
25.119	7.03E+09	6.55E+07	9.33E-03	25.119	6.24E+09	8.14E+07	1.30E-02	25.119	7.35E+09	9.00E+07	1.22E-02	25.119	6.87E+09	7.90E+07	1.15E-02
39.811	7.08E+09	4.13E+07	5.84E-03	39.811	6.28E+09	8.31E+07	1.32E-02	39.811	7.39E+09	7.94E+07	1.07E-02	39.811	6.92E+09	6.79E+07	9.94E-03
63.096	6.54E+09	7.14E+08	1.09E-01	63.096	6.18E+09	-4.21E+06	-6.81E-04	63.096	7.54E+09	-1.00E+08	-1.33E-02	63.096	6.75E+09	2.03E+08	3.18E-02
100.000	7.14E+09	1.02E+08	1.43E-02	100.000	6.36E+09	9.81E+07	1.54E-02	100.000	7.49E+09	8.51E+07	1.14E-02	100.000	7.00E+09	9.51E+07	1.37E-02

Table 6.14: Results for microtricot interleaved samples.

Sample:	Tricot microfibre interleaved		8a	Sample:	Tricot microfibre interleaved		8b	Sample:	Tricot microfibre interleaved		8c	average of tricot interleaved samples			
Frequency	Storage Modulus	Loss Modulus	Tan Delta	Frequency	Storage Modulus	Loss Modulus	Tan Delta	Frequency	Storage Modulus	Loss Modulus	Tan Delta	Frequenc	Storage Modulus	Loss Modulus	Tan Delta
Hz	Pa	Pa		Hz	Pa	Pa		Hz	Pa	Pa		Hz	Pa	Pa	
0.324	6.87E+09	1.12E+08	1.63E-02	0.100	6.47E+09	9.86E+07	1.52E-02	0.187	8.05E+09	1.51E+08	1.87E-02				
0.158	6.86E+09	1.55E+08	2.26E-02	0.158	6.47E+09	8.92E+07	1.38E-02	0.158	8.05E+09	1.22E+08	1.52E-02	0.158	7.13E+09	1.22E+08	1.72E-02
0.251	6.89E+09	1.02E+08	1.48E-02	0.251	6.49E+09	4.42E+07	6.81E-03	0.251	8.08E+09	9.23E+07	1.14E-02	0.251	7.15E+09	7.94E+07	1.10E-02
0.398	6.91E+09	8.33E+07	1.20E-02	0.398	6.51E+09	7.96E+06	1.22E-03	0.398	8.11E+09	9.25E+07	1.14E-02	0.398	7.18E+09	6.12E+07	8.23E-03
0.631	6.93E+09	1.22E+08	1.76E-02	0.631	6.52E+09	7.80E+07	1.20E-02	0.631	8.11E+09	1.31E+08	1.62E-02	0.631	7.19E+09	1.10E+08	1.52E-02
1.000	6.96E+09	1.24E+08	1.78E-02	1.000	6.53E+09	7.05E+07	1.08E-02	1.000	8.14E+09	1.18E+08	1.45E-02	1.000	7.21E+09	1.04E+08	1.44E-02
1.585	6.97E+09	1.23E+08	1.77E-02	1.585	6.55E+09	6.67E+07	1.02E-02	1.585	8.16E+09	1.26E+08	1.55E-02	1.585	7.22E+09	1.05E+08	1.44E-02
2.512	6.98E+09	1.19E+08	1.70E-02	2.512	6.55E+09	6.47E+07	9.88E-03	2.512	8.17E+09	1.22E+08	1.49E-02	2.512	7.23E+09	1.02E+08	1.39E-02
3.981	6.99E+09	1.09E+08	1.55E-02	3.981	6.57E+09	6.80E+07	1.04E-02	3.981	8.19E+09	1.14E+08	1.40E-02	3.981	7.25E+09	9.70E+07	1.33E-02
6.310	7.00E+09	1.27E+08	1.81E-02	6.310	6.58E+09	7.21E+07	1.10E-02	6.310	8.21E+09	9.60E+07	1.17E-02	6.310	7.26E+09	9.84E+07	1.36E-02
10.000	7.03E+09	1.23E+08	1.74E-02	10.000	6.59E+09	5.52E+07	8.38E-03	10.000	8.22E+09	1.22E+08	1.48E-02	10.000	7.28E+09	9.99E+07	1.35E-02
15.849	7.06E+09	1.07E+08	1.52E-02	15.849	6.61E+09	5.66E+07	8.56E-03	15.849	8.25E+09	1.05E+08	1.28E-02	15.849	7.31E+09	8.98E+07	1.22E-02
25.119	7.06E+09	1.15E+08	1.63E-02	25.119	6.62E+09	5.07E+07	7.65E-03	25.119	8.28E+09	1.20E+08	1.45E-02	25.119	7.32E+09	9.54E+07	1.28E-02
39.811	7.10E+09	9.16E+07	1.29E-02	39.811	6.65E+09	2.71E+07	4.08E-03	39.811	8.31E+09	9.27E+07	1.12E-02	39.811	7.35E+09	7.05E+07	9.38E-03
63.096	7.66E+09	7.69E+08	1.00E-01	63.096	6.75E+09	-1.40E+08	-2.08E-02	63.096	8.00E+09	3.32E+08	4.15E-02	63.096	7.47E+09	3.20E+08	4.04E-02
100.000	7.23E+09	1.09E+08	1.51E-02	100.000	6.73E+09	-6.60E+07	-9.82E-03	100.000	8.41E+09	9.19E+07	1.09E-02	100.000	7.46E+09	4.50E+07	5.41E-03

Table 6.15: Results for microPPSnanoPA6,6 interleaved samples.

Sample:	microPPSnanoPA6,6 interleaved		9a	Sample:	microPPSnanoPA6,6 interleaved		9b	Sample:	microPPSnanoPA6,6 interleaved		9c	average of microPPSnanoPA6,6 interleaved samples		
Frequency	Storage Modulus	Loss Modulus	Tan Delta	Frequency	Storage Modulus	Loss Modulus	Tan Delta	Frequency	Storage Modulus	Loss Modulus	Tan Delta	Frequency	Storage Modulus	Loss Modulus	Tan Delta
Hz	Pa	Pa		Hz	Pa	Pa		Hz	Pa	Pa		Hz	Pa	Pa	
0.100	6.57E+09	1.33E+08	2.02E-02	0.100	6.77E+09	2.04E+08	3.01E-02	0.211	7.31E+09	1.56E+08	2.14E-02				
0.158	6.59E+09	1.29E+08	1.96E-02	0.158	6.75E+09	2.15E+08	3.18E-02	0.158	7.33E+09	1.53E+08	2.09E-02	0.158	6.89E+09	1.66E+08	2.41E-02
0.251	6.61E+09	8.37E+07	1.27E-02	0.251	6.76E+09	1.51E+08	2.23E-02	0.251	7.35E+09	1.07E+08	1.46E-02	0.251	6.90E+09	1.14E+08	1.65E-02
0.398	6.61E+09	3.24E+07	4.90E-03	0.398	6.77E+09	1.40E+08	2.06E-02	0.398	7.36E+09	1.01E+08	1.37E-02	0.398	6.91E+09	9.09E+07	1.31E-02
0.631	6.62E+09	1.08E+08	1.63E-02	0.631	6.79E+09	1.86E+08	2.74E-02	0.631	7.37E+09	1.38E+08	1.87E-02	0.631	6.93E+09	1.44E+08	2.08E-02
1.000	6.64E+09	1.02E+08	1.54E-02	1.000	6.81E+09	1.89E+08	2.77E-02	1.000	7.39E+09	1.21E+08	1.64E-02	1.000	6.94E+09	1.37E+08	1.98E-02
1.585	6.65E+09	9.95E+07	1.50E-02	1.585	6.83E+09	1.85E+08	2.70E-02	1.585	7.39E+09	1.13E+08	1.53E-02	1.585	6.96E+09	1.32E+08	1.91E-02
2.512	6.65E+09	1.03E+08	1.56E-02	2.512	6.85E+09	1.80E+08	2.63E-02	2.512	7.41E+09	1.17E+08	1.58E-02	2.512	6.97E+09	1.34E+08	1.92E-02
3.981	6.67E+09	1.04E+08	1.57E-02	3.981	6.86E+09	1.93E+08	2.82E-02	3.981	7.43E+09	1.12E+08	1.51E-02	3.981	6.99E+09	1.37E+08	1.96E-02
6.310	6.68E+09	9.94E+07	1.49E-02	6.310	6.87E+09	1.80E+08	2.62E-02	6.310	7.44E+09	9.54E+07	1.28E-02	6.310	7.00E+09	1.25E+08	1.80E-02
10.000	6.68E+09	9.91E+07	1.48E-02	10.000	6.91E+09	1.73E+08	2.51E-02	10.000	7.46E+09	1.19E+08	1.60E-02	10.000	7.02E+09	1.30E+08	1.86E-02
15.849	6.70E+09	9.76E+07	1.46E-02	15.849	6.93E+09	1.69E+08	2.44E-02	15.849	7.48E+09	1.06E+08	1.42E-02	15.849	7.04E+09	1.24E+08	1.77E-02
25.119	6.71E+09	1.01E+08	1.51E-02	25.119	6.96E+09	1.54E+08	2.21E-02	25.119	7.50E+09	9.92E+07	1.32E-02	25.119	7.06E+09	1.18E+08	1.68E-02
39.811	6.73E+09	6.59E+07	9.80E-03	39.811	6.99E+09	1.31E+08	1.87E-02	39.811	7.53E+09	6.73E+07	8.95E-03	39.811	7.08E+09	8.80E+07	1.25E-02
63.096	7.30E+09	2.02E+08	2.76E-02	63.096	7.01E+09	-3.08E+07	-4.40E-03	63.096	7.49E+09	-7.00E+07	-9.34E-03	63.096	7.27E+09	3.36E+07	4.63E-03
100.000	6.86E+09	1.11E+08	1.62E-02	100.000	7.21E+09	1.09E+08	1.52E-02	100.000	7.63E+09	1.45E+08	1.90E-02	100.000	7.23E+09	1.22E+08	1.68E-02

Table 6.16: Results for microPEInanoPA6,6 interleaved samples.

Sample:	microPEInanoPA6,6 interleaved		10a	Sample:	microPEInanoPA6,6 interleaved		1b	Sample:	microPEInanoPA6,6 interleaved		10c	average of microPEInanoPA6,6 interleaved samples			
Frequency	Storage Modulus	Loss Modulus	Tan Delta	Frequency	Storage Modulus	Loss Modulus	Tan Delta	Frequency	Storage Modulus	Loss Modulus	Tan Delta	Frequency	Storage Modulus	Loss Modulus	Tan Delta
Hz	Pa	Pa		Hz	Pa	Pa		Hz	Pa	Pa		Hz	Pa	Pa	
0.100	6.55E+09	1.11E+08	1.70E-02	0.122	7.85E+09	1.58E+08	2.01E-02	0.100	6.81E+09	1.58E+08	2.31E-02				
0.158	6.56E+09	1.22E+08	1.86E-02	0.158	7.87E+09	1.01E+08	1.29E-02	0.158	6.82E+09	1.50E+08	2.20E-02	0.158	7.09E+09	1.24E+08	1.78E-02
0.251	6.58E+09	6.94E+07	1.06E-02	0.251	7.90E+09	7.14E+07	9.04E-03	0.251	6.84E+09	1.01E+08	1.47E-02	0.251	7.11E+09	8.05E+07	1.14E-02
0.398	6.59E+09	4.75E+07	7.21E-03	0.398	7.91E+09	8.78E+07	1.11E-02	0.398	6.86E+09	8.63E+07	1.26E-02	0.398	7.12E+09	7.39E+07	1.03E-02
0.631	6.61E+09	9.09E+07	1.37E-02	0.631	7.91E+09	1.27E+08	1.60E-02	0.631	6.87E+09	1.31E+08	1.91E-02	0.631	7.13E+09	1.16E+08	1.63E-02
1.000	6.63E+09	8.17E+07	1.23E-02	1.000	7.93E+09	1.26E+08	1.58E-02	1.000	6.88E+09	1.20E+08	1.74E-02	1.000	7.15E+09	1.09E+08	1.52E-02
1.585	6.64E+09	7.75E+07	1.17E-02	1.585	7.94E+09	1.14E+08	1.43E-02	1.585	6.89E+09	1.14E+08	1.65E-02	1.585	7.16E+09	1.02E+08	1.42E-02
2.512	6.65E+09	7.50E+07	1.13E-02	2.512	7.95E+09	1.14E+08	1.43E-02	2.512	6.90E+09	1.18E+08	1.71E-02	2.512	7.17E+09	1.02E+08	1.42E-02
3.981	6.67E+09	6.92E+07	1.04E-02	3.981	7.96E+09	1.10E+08	1.39E-02	3.981	6.92E+09	1.16E+08	1.67E-02	3.981	7.18E+09	9.84E+07	1.36E-02
6.310	6.67E+09	6.91E+07	1.03E-02	6.310	7.97E+09	1.16E+08	1.45E-02	6.310	6.93E+09	1.11E+08	1.60E-02	6.310	7.19E+09	9.85E+07	1.36E-02
10.000	6.70E+09	7.07E+07	1.06E-02	10.000	8.00E+09	1.20E+08	1.50E-02	10.000	6.94E+09	1.11E+08	1.59E-02	10.000	7.21E+09	1.01E+08	1.38E-02
15.849	6.72E+09	5.95E+07	8.86E-03	15.849	8.03E+09	1.20E+08	1.50E-02	15.849	6.97E+09	1.10E+08	1.58E-02	15.849	7.24E+09	9.67E+07	1.32E-02
25.119	6.74E+09	6.63E+07	9.84E-03	25.119	8.03E+09	1.14E+08	1.41E-02	25.119	6.99E+09	9.95E+07	1.42E-02	25.119	7.25E+09	9.31E+07	1.27E-02
39.811	6.75E+09	5.03E+07	7.46E-03	39.811	8.06E+09	9.93E+07	1.23E-02	39.811	7.00E+09	7.34E+07	1.05E-02	39.811	7.27E+09	7.43E+07	1.01E-02
63.096	6.50E+09	-1.03E+08	-1.59E-02	63.096	8.15E+09	2.17E+08	2.67E-02	63.096	6.75E+09	2.44E+08	3.62E-02	63.096	7.13E+09	1.20E+08	1.57E-02
100.000	6.88E+09	4.04E+07	5.86E-03	100.000	8.20E+09	8.26E+07	1.01E-02	100.000	7.10E+09	1.28E+08	1.81E-02	100.000	7.39E+09	8.37E+07	1.13E-02

Table 6.17: Results for microtricotnanoPA6,6 interleaved samples.

Sample:	tricot nano PA6,6 interleaved		11a	Sample:	tricot nano PA6,6 interleaved		11b	Sample:	tricot nano PA6,6 interleaved		11c	average of tricot nanoPA6,6 interleaved samples			
Frequency	Storage Modulus	Loss Modulus	Tan Delta	Frequency	Storage Modulus	Loss Modulus	Tan Delta	Frequency	Storage Modulus	Loss Modulus	Tan Delta	Frequenc	Storage Modulus	Loss Modulus	Tan Delta
Hz	Pa	Pa		Hz	Pa	Pa		Hz	Pa	Pa		Hz	Pa	Pa	
0.233	7.42E+09	1.07E+08	1.45E-02	0.100	7.72E+09	1.12E+08	1.45E-02	0.133	6.42E+09	1.48E+08	2.30E-02				
0.158	7.44E+09	9.53E+07	1.28E-02	0.158	7.74E+09	8.54E+07	1.10E-02	0.158	6.44E+09	1.47E+08	2.28E-02	0.158	7.21E+09	1.09E+08	1.55E-02
0.251	7.45E+09	8.56E+07	1.15E-02	0.251	7.77E+09	1.11E+08	1.42E-02	0.251	6.46E+09	9.93E+07	1.54E-02	0.251	7.23E+09	9.85E+07	1.37E-02
0.398	7.45E+09	5.78E+07	7.76E-03	0.398	7.77E+09	7.59E+07	9.77E-03	0.398	6.47E+09	1.02E+08	1.58E-02	0.398	7.23E+09	7.87E+07	1.11E-02
0.631	7.46E+09	9.52E+07	1.28E-02	0.631	7.79E+09	1.11E+08	1.42E-02	0.631	6.48E+09	1.34E+08	2.07E-02	0.631	7.24E+09	1.13E+08	1.59E-02
1.000	7.49E+09	9.36E+07	1.25E-02	1.000	7.81E+09	9.48E+07	1.21E-02	1.000	6.49E+09	1.16E+08	1.79E-02	1.000	7.26E+09	1.02E+08	1.42E-02
1.585	7.50E+09	8.48E+07	1.13E-02	1.585	7.83E+09	9.12E+07	1.17E-02	1.585	6.50E+09	1.17E+08	1.79E-02	1.585	7.28E+09	9.76E+07	1.36E-02
2.512	7.52E+09	9.27E+07	1.23E-02	2.512	7.85E+09	9.55E+07	1.22E-02	2.512	6.51E+09	1.10E+08	1.69E-02	2.512	7.29E+09	9.93E+07	1.38E-02
3.981	7.53E+09	8.15E+07	1.08E-02	3.981	7.85E+09	8.94E+07	1.14E-02	3.981	6.52E+09	1.04E+08	1.60E-02	3.981	7.30E+09	9.17E+07	1.27E-02
6.310	7.56E+09	6.92E+07	9.15E-03	6.310	7.87E+09	6.84E+07	8.70E-03	6.310	6.53E+09	1.25E+08	1.91E-02	6.310	7.32E+09	8.76E+07	1.23E-02
10.000	7.56E+09	8.74E+07	1.16E-02	10.000	7.89E+09	9.43E+07	1.20E-02	10.000	6.55E+09	1.13E+08	1.72E-02	10.000	7.34E+09	9.82E+07	1.36E-02
15.849	7.58E+09	7.26E+07	9.58E-03	15.849	7.91E+09	8.95E+07	1.13E-02	15.849	6.57E+09	1.21E+08	1.84E-02	15.849	7.35E+09	9.43E+07	1.31E-02
25.119	7.62E+09	6.35E+07	8.33E-03	25.119	7.94E+09	7.35E+07	9.26E-03	25.119	6.58E+09	1.18E+08	1.79E-02	25.119	7.38E+09	8.49E+07	1.18E-02
39.811	7.66E+09	4.54E+07	5.92E-03	39.811	7.96E+09	5.19E+07	6.52E-03	39.811	6.59E+09	8.26E+07	1.25E-02	39.811	7.41E+09	6.00E+07	8.32E-03
63.096	7.11E+09	-3.35E+07	-4.72E-03	63.096	8.25E+09	1.15E+08	1.39E-02	63.096	6.08E+09	3.20E+08	5.26E-02	63.096	7.14E+09	1.34E+08	2.06E-02
100.000	7.93E+09	8.28E+07	1.05E-02	100.000	8.21E+09	1.36E+08	1.66E-02	100.000	6.71E+09	1.98E+07	2.95E-03	100.000	7.62E+09	7.96E+07	9.99E-03

6.3.2 Complete retesting results

Table 6.18: Retest results for control samples

Table 6.19: Retest results for control specimens.

Sample:	1A - control			Sample:	1B- control			Sample:	1C-Control			Sample:	1D- Control				Average of control samples		
Frequency	Storage Modulus	Loss Modulus	Tan Delta	Frequency	Storage Modulus	Loss Modulus	Tan Delta	Frequency	Storage Modulus	Loss Modulus	Tan Delta	Frequency	Storage Modulus	Loss Modulus	Tan Delta	Frequency	Storage Modulus	Loss Modulus	Tan Delta
Hz	Pa	Pa		Hz	Pa	Pa		Hz	Pa	Pa		Hz	Pa	Pa		Hz	Pa	Pa	
0.100	6.82E+09	1.15E+08	1.69E-02	0.125	7.30E+09	1.37E+08	1.88E-02	0.122	6.16E+09	9.30E+07	1.51E-02	0.100	7.10E+09	1.56E+08	2.20E-02				
0.158	6.83E+09	1.09E+08	1.60E-02	0.158	7.32E+09	1.40E+08	1.91E-02	0.158	6.18E+09	1.03E+08	1.66E-02	0.158	7.13E+09	1.42E+08	1.99E-02	0.158	6.86E+09	1.23E+08	1.79E-02
0.251	6.85E+09	6.88E+07	1.00E-02	0.251	7.33E+09	9.65E+07	1.32E-02	0.251	6.19E+09	6.13E+07	9.92E-03	0.251	7.14E+09	8.98E+07	1.26E-02	0.251	6.88E+09	7.91E+07	1.14E-02
0.398	6.86E+09	1.97E+07	2.88E-03	0.398	7.34E+09	5.20E+07	7.08E-03	0.398	6.20E+09	2.13E+07	3.43E-03	0.398	7.17E+09	3.26E+06	4.55E-04	0.398	6.89E+09	2.41E+07	3.46E-03
0.631	6.87E+09	9.61E+07	1.40E-02	0.631	7.34E+09	1.17E+08	1.60E-02	0.631	6.22E+09	8.18E+07	1.32E-02	0.631	7.18E+09	1.19E+08	1.66E-02	0.631	6.90E+09	1.04E+08	1.49E-02
1.000	6.87E+09	8.42E+07	1.23E-02	1.000	7.36E+09	1.19E+08	1.62E-02	1.000	6.22E+09	7.22E+07	1.16E-02	1.000	7.19E+09	1.14E+08	1.58E-02	1.000	6.91E+09	9.74E+07	1.40E-02
1.585	6.89E+09	8.92E+07	1.30E-02	1.585	7.35E+09	1.16E+08	1.58E-02	1.585	6.23E+09	6.95E+07	1.12E-02	1.585	7.20E+09	1.06E+08	1.48E-02	1.585	6.92E+09	9.54E+07	1.37E-02
2.512	6.90E+09	8.29E+07	1.20E-02	2.512	7.38E+09	1.20E+08	1.62E-02	2.512	6.24E+09	6.84E+07	1.10E-02	2.512	7.21E+09	1.05E+08	1.46E-02	2.512	6.93E+09	9.41E+07	1.34E-02
3.981	6.91E+09	8.86E+07	1.28E-02	3.981	7.39E+09	1.20E+08	1.63E-02	3.981	6.26E+09	6.12E+07	9.79E-03	3.981	7.22E+09	1.09E+08	1.51E-02	3.981	6.94E+09	9.48E+07	1.35E-02
6.310	6.94E+09	8.15E+07	1.18E-02	6.310	7.39E+09	1.23E+08	1.66E-02	6.310	6.27E+09	6.35E+07	1.01E-02	6.310	7.23E+09	1.04E+08	1.44E-02	6.310	6.95E+09	9.31E+07	1.32E-02
10.000	6.95E+09	8.38E+07	1.21E-02	10.000	7.41E+09	1.03E+08	1.39E-02	10.000	6.28E+09	5.73E+07	9.12E-03	10.000	7.26E+09	9.54E+07	1.31E-02	10.000	6.97E+09	8.49E+07	1.21E-02
15.849	6.96E+09	8.82E+07	1.27E-02	15.849	7.42E+09	1.11E+08	1.50E-02	15.849	6.29E+09	6.76E+07	1.07E-02	15.849	7.27E+09	9.49E+07	1.31E-02	15.849	6.98E+09	9.04E+07	1.29E-02
25.119	6.96E+09	8.09E+07	1.16E-02	25.119	7.45E+09	1.21E+08	1.63E-02	25.119	6.31E+09	5.29E+07	8.38E-03	25.119	7.28E+09	9.14E+07	1.25E-02	25.119	7.00E+09	8.67E+07	1.22E-02
39.811	7.02E+09	8.60E+07	1.23E-02	39.811	7.48E+09	1.06E+08	1.41E-02	39.811	6.27E+09	1.21E+08	1.93E-02	39.811	7.32E+09	7.57E+07	1.04E-02	39.811	7.02E+09	9.70E+07	1.40E-02
63.096	7.32E+09	-1.07E+08	-1.46E-02	63.096	7.37E+09	-7.19E+07	-9.76E-03	63.096	6.47E+09	3.38E+08	5.23E-02	63.096	7.47E+09	3.94E+08	5.28E-02	63.096	7.15E+09	1.38E+08	2.02E-02
100.000	7.05E+09	9.19E+07	1.30E-02	100.000	7.60E+09	5.91E+07	7.78E-03	100.000	6.35E+09	7.53E+07	1.19E-02	100.000	7.39E+09	1.19E+08	1.62E-02	100.000	7.10E+09	8.64E+07	1.22E-02

Table 6.20: Retest results for nanoNyplex fibre interleaved samples.

Sample:	Nyplex nanofibre interleaved		2A	Sample:	Nyplex nanofibre interleaved		2B	Sample:	Nyplex nanofibre interleaved		2C	Sample:	Nyplex nanofibre interleaved		2D	average of Nyplex nanofibre interleaved samples			
Frequency	Storage Modulus	Loss Modulus	Tan Delta	Frequency	Storage Modulus	Loss Modulus	Tan Delta	Frequency	Storage Modulus	Loss Modulus	Tan Delta	Frequency	Storage Modulus	Loss Modulus	Tan Delta	Frequency	Storage Modulus	Loss Modulus	Tan Delta
Hz	Pa	Pa		Hz	Pa	Pa		Hz	Pa	Pa		Hz	Pa	Pa		Hz	Pa	Pa	
0.100	7.02E+09	1.30E+08	1.86E-02	0.125	7.09E+09	1.45E+08	2.04E-02	0.187	6.89E+09	1.16E+08	1.69E-02	0.100	7.41E+09	1.49E+08	2.01E-02				
0.158	7.03E+09	1.31E+08	1.87E-02	0.158	7.11E+09	1.61E+08	2.26E-02	0.158	6.90E+09	1.51E+08	2.19E-02	0.158	7.42E+09	1.66E+08	2.23E-02	0.158	7.12E+09	1.52E+08	2.14E-02
0.251	7.05E+09	7.79E+07	1.10E-02	0.251	7.13E+09	1.01E+08	1.42E-02	0.251	6.91E+09	8.50E+07	1.23E-02	0.251	7.44E+09	9.19E+07	1.24E-02	0.251	7.13E+09	8.90E+07	1.25E-02
0.398	7.07E+09	3.84E+07	5.43E-03	0.398	7.15E+09	5.56E+07	7.78E-03	0.398	6.93E+09	5.11E+07	7.39E-03	0.398	7.46E+09	6.54E+07	8.76E-03	0.398	7.15E+09	5.26E+07	7.34E-03
0.631	7.08E+09	1.05E+08	1.48E-02	0.631	7.16E+09	1.25E+08	1.74E-02	0.631	6.94E+09	1.06E+08	1.52E-02	0.631	7.48E+09	1.18E+08	1.58E-02	0.631	7.16E+09	1.13E+08	1.58E-02
1.000	7.10E+09	9.55E+07	1.34E-02	1.000	7.17E+09	1.10E+08	1.54E-02	1.000	6.96E+09	1.05E+08	1.50E-02	1.000	7.50E+09	1.07E+08	1.43E-02	1.000	7.18E+09	1.04E+08	1.45E-02
1.585	7.11E+09	9.75E+07	1.37E-02	1.585	7.19E+09	1.06E+08	1.48E-02	1.585	6.97E+09	9.81E+07	1.41E-02	1.585	7.51E+09	1.08E+08	1.44E-02	1.585	7.20E+09	1.02E+08	1.42E-02
2.512	7.13E+09	8.78E+07	1.23E-02	2.512	7.20E+09	1.12E+08	1.56E-02	2.512	6.99E+09	9.74E+07	1.39E-02	2.512	7.53E+09	1.07E+08	1.42E-02	2.512	7.21E+09	1.01E+08	1.40E-02
3.981	7.14E+09	9.54E+07	1.34E-02	3.981	7.21E+09	1.09E+08	1.52E-02	3.981	7.01E+09	9.70E+07	1.38E-02	3.981	7.54E+09	1.09E+08	1.44E-02	3.981	7.23E+09	1.03E+08	1.42E-02
6.310	7.17E+09	9.12E+07	1.27E-02	6.310	7.22E+09	1.12E+08	1.55E-02	6.310	7.03E+09	9.85E+07	1.40E-02	6.310	7.55E+09	1.02E+08	1.35E-02	6.310	7.24E+09	1.01E+08	1.39E-02
10.000	7.17E+09	8.76E+07	1.22E-02	10.000	7.25E+09	9.86E+07	1.36E-02	10.000	7.04E+09	9.61E+07	1.37E-02	10.000	7.59E+09	9.65E+07	1.27E-02	10.000	7.26E+09	9.47E+07	1.30E-02
15.849	7.20E+09	8.60E+07	1.19E-02	15.849	7.26E+09	1.05E+08	1.45E-02	15.849	7.05E+09	9.48E+07	1.34E-02	15.849	7.60E+09	9.84E+07	1.29E-02	15.849	7.28E+09	9.61E+07	1.32E-02
25.119	7.22E+09	7.27E+07	1.01E-02	25.119	7.29E+09	9.04E+07	1.24E-02	25.119	7.07E+09	9.06E+07	1.28E-02	25.119	7.62E+09	8.89E+07	1.17E-02	25.119	7.30E+09	8.56E+07	1.17E-02
39.811	7.25E+09	6.95E+07	9.59E-03	39.811	7.31E+09	7.10E+07	9.70E-03	39.811	7.12E+09	8.04E+07	1.13E-02	39.811	7.63E+09	8.57E+07	1.12E-02	39.811	7.33E+09	7.66E+07	1.05E-02
63.096	7.76E+09	1.67E+08	2.15E-02	63.096	7.14E+09	-2.90E+08	-4.07E-02	63.096	6.98E+09	-1.23E+08	-1.76E-02	63.096	8.18E+09	6.01E+07	7.35E-03	63.096	7.52E+09	-4.65E+07	-7.34E-03
100.000	7.38E+09	1.38E+07	1.88E-03	100.000	7.42E+09	1.48E+08	2.00E-02	100.000	7.24E+09	7.48E+07	1.03E-02	100.000	7.62E+09	1.23E+08	1.61E-02	100.000	7.42E+09	9.00E+07	1.21E-02

Table 6.21: Retest results for nanoPMMA fibre interleaved samples.

Sample:	PMMA nanofibre interleaved		3A	Sample:	PMMA nanofibre interleaved		3B	Sample:	PMMA nanofibre interleaved		3C	Sample:	PMMA nanofibre interleaved		3D	Average of PMMA nanofibre interleaved samples			
Frequency	Storage Modulus	Loss Modulus	Tan Delta	Frequency	Storage Modulus	Loss Modulus	Tan Delta	Frequency	Storage Modulus	Loss Modulus	Tan Delta	Frequency	Storage Modulus	Loss Modulus	Tan Delta	Frequency	Storage Modulus	Loss Modulus	Tan Delta
Hz	Pa	Pa		Hz	Pa	Pa		Hz	Pa	Pa		Hz	Pa	Pa		Hz	Pa	Pa	
0.211	6.14E+09	1.08E+08	1.76E-02	0.100	6.96E+09	1.47E+08	2.11E-02	0.150	6.69E+09	1.07E+08	1.61E-02	0.100	7.14E+09	1.20E+08	1.68E-02				
0.158	6.14E+09	1.02E+08	1.66E-02	0.158	6.98E+09	1.45E+08	2.07E-02	0.158	6.70E+09	1.25E+08	1.87E-02	0.158	7.17E+09	1.22E+08	1.71E-02	0.158	6.75E+09	1.24E+08	1.83E-02
0.251	6.15E+09	6.68E+07	1.09E-02	0.251	6.99E+09	9.61E+07	1.37E-02	0.251	6.72E+09	7.98E+07	1.19E-02	0.251	7.19E+09	7.93E+07	1.10E-02	0.251	6.76E+09	8.05E+07	1.19E-02
0.398	6.16E+09	4.30E+06	6.98E-04	0.398	7.01E+09	7.26E+07	1.04E-02	0.398	6.73E+09	3.67E+07	5.45E-03	0.398	7.21E+09	4.47E+07	6.20E-03	0.398	6.78E+09	3.96E+07	5.68E-03
0.631	6.17E+09	9.13E+07	1.48E-02	0.631	7.02E+09	1.25E+08	1.78E-02	0.631	6.74E+09	1.08E+08	1.60E-02	0.631	7.23E+09	9.57E+07	1.32E-02	0.631	6.79E+09	1.05E+08	1.55E-02
1.000	6.18E+09	8.87E+07	1.44E-02	1.000	7.04E+09	1.19E+08	1.68E-02	1.000	6.75E+09	8.78E+07	1.30E-02	1.000	7.24E+09	9.33E+07	1.29E-02	1.000	6.80E+09	9.71E+07	1.43E-02
1.585	6.19E+09	9.23E+07	1.49E-02	1.585	7.06E+09	1.18E+08	1.68E-02	1.585	6.76E+09	8.64E+07	1.28E-02	1.585	7.24E+09	7.91E+07	1.09E-02	1.585	6.81E+09	9.40E+07	1.38E-02
2.512	6.20E+09	8.81E+07	1.42E-02	2.512	7.07E+09	1.11E+08	1.57E-02	2.512	6.78E+09	8.67E+07	1.28E-02	2.512	7.26E+09	7.71E+07	1.06E-02	2.512	6.83E+09	9.08E+07	1.33E-02
3.981	6.20E+09	8.92E+07	1.44E-02	3.981	7.08E+09	1.20E+08	1.69E-02	3.981	6.79E+09	8.56E+07	1.26E-02	3.981	7.27E+09	7.97E+07	1.10E-02	3.981	6.83E+09	9.35E+07	1.37E-02
6.310	6.21E+09	8.01E+07	1.29E-02	6.310	7.08E+09	1.18E+08	1.67E-02	6.310	6.80E+09	7.61E+07	1.12E-02	6.310	7.28E+09	6.63E+07	9.12E-03	6.310	6.84E+09	8.52E+07	1.25E-02
10.000	6.23E+09	9.50E+07	1.52E-02	10.000	7.09E+09	1.27E+08	1.79E-02	10.000	6.81E+09	8.56E+07	1.26E-02	10.000	7.30E+09	7.83E+07	1.07E-02	10.000	6.86E+09	9.64E+07	1.41E-02
15.849	6.24E+09	8.72E+07	1.40E-02	15.849	7.12E+09	1.18E+08	1.65E-02	15.849	6.83E+09	7.40E+07	1.08E-02	15.849	7.32E+09	7.76E+07	1.06E-02	15.849	6.88E+09	8.91E+07	1.30E-02
25.119	6.26E+09	7.96E+07	1.27E-02	25.119	7.14E+09	1.04E+08	1.46E-02	25.119	6.85E+09	7.15E+07	1.04E-02	25.119	7.35E+09	6.71E+07	9.13E-03	25.119	6.90E+09	8.06E+07	1.17E-02
39.811	6.27E+09	8.16E+07	1.30E-02	39.811	7.15E+09	1.13E+08	1.57E-02	39.811	6.87E+09	5.88E+07	8.56E-03	39.811	7.37E+09	5.06E+07	6.86E-03	39.811	6.92E+09	7.59E+07	1.10E-02
63.096	6.83E+09	-7.21E+07	-1.06E-02	63.096	7.68E+09	4.17E+07	5.42E-03	63.096	7.27E+09	6.42E+08	8.83E-02	63.096	7.18E+09	-3.02E+08	-4.21E-02	63.096	7.24E+09	7.75E+07	1.03E-02
100.000	6.32E+09	9.16E+07	1.45E-02	100.000	7.25E+09	1.57E+08	2.16E-02	100.000	6.98E+09	6.84E+07	9.80E-03	100.000	7.49E+09	6.09E+07	8.13E-03	100.000	7.01E+09	9.44E+07	1.35E-02
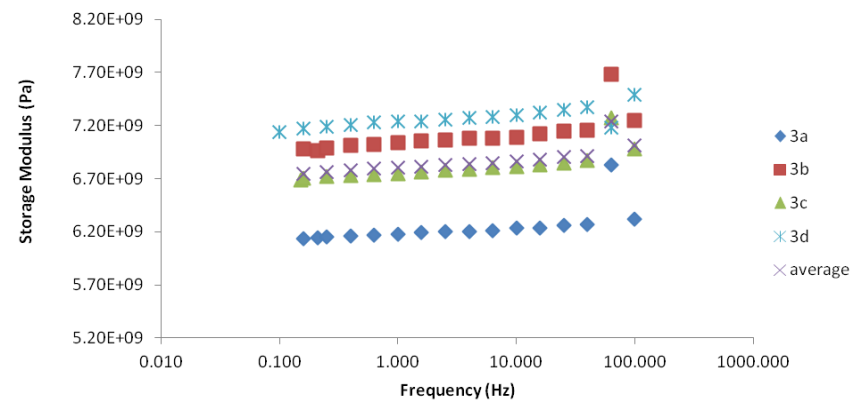
Figure 6.12: Storage modulus vs. frequency for nanoPMMA fibre interleaved samples.

Figure 6.13: Loss modulus vs. frequency for nanoPMMA interleaved samples.

Figure 6.14: Tan delta vs. frequency for nanoPMMA interleaved samples.

Figure 6.15: Loss modulus vs. frequency for nanoPMMA interleaved samples excluding 63 and 100 Hz.

Figure 6.16: Tan delta vs. frequency for nanoPMMA samples, excluding 63 and 100 Hz.

Table 6.22: Retest results for nanoPA6,6 fibre interleaved samples.

Sample:	PA6,6 nanofibre interleaved		4a	Sample:	PA6,6 nanofibre interleaved		4b	Sample:	PA6,6 nanofibre interleaved		4c	Sample:	PA6,6 nanofibre interleaved		4d		average of PA6,6 interleaved samples		
Frequency	Storage Modulus	Loss Modulus	Tan Delta	Frequency	Storage Modulus	Loss Modulus	Tan Delta	Frequency	Storage Modulus	Loss Modulus	Tan Delta	Frequency	Storage Modulus	Loss Modulus	Tan Delta	Frequency	Storage Modulus	Loss Modulus	Tan Delta
Hz	Pa	Pa		Hz	Pa	Pa		Hz	Pa	Pa		Hz	Pa	Pa		Hz	Pa	Pa	
0.100	6.73E+09	1.26E+08	1.87E-02	0.187	7.90E+09	1.03E+08	1.30E-02	0.100	7.14E+09	1.11E+08	1.55E-02	0.162	7.53E+09	1.10E+08	1.46E-02				
0.158	6.76E+09	1.14E+08	1.69E-02	0.158	7.90E+09	1.53E+08	1.94E-02	0.158	7.16E+09	1.28E+08	1.79E-02	0.158	7.53E+09	1.43E+08	1.90E-02	0.158	7.34E+09	1.35E+08	1.83E-02
0.251	6.78E+09	6.95E+07	1.02E-02	0.251	7.91E+09	6.39E+07	8.07E-03	0.251	7.17E+09	7.11E+07	9.91E-03	0.251	7.55E+09	8.82E+07	1.17E-02	0.251	7.35E+09	7.31E+07	9.98E-03
0.398	6.79E+09	8.01E+06	1.18E-03	0.398	7.93E+09	4.74E+07	5.98E-03	0.398	7.18E+09	5.73E+07	7.97E-03	0.398	7.57E+09	5.24E+07	6.92E-03	0.398	7.37E+09	4.13E+07	5.51E-03
0.631	6.80E+09	9.73E+07	1.43E-02	0.631	7.96E+09	9.88E+07	1.24E-02	0.631	7.20E+09	1.03E+08	1.43E-02	0.631	7.60E+09	1.13E+08	1.49E-02	0.631	7.39E+09	1.03E+08	1.40E-02
1.000	6.81E+09	7.45E+07	1.09E-02	1.000	7.98E+09	9.17E+07	1.15E-02	1.000	7.21E+09	9.01E+07	1.25E-02	1.000	7.59E+09	8.75E+07	1.15E-02	1.000	7.40E+09	8.59E+07	1.16E-02
1.585	6.82E+09	7.63E+07	1.12E-02	1.585	7.99E+09	8.58E+07	1.07E-02	1.585	7.23E+09	8.72E+07	1.21E-02	1.585	7.58E+09	9.92E+07	1.31E-02	1.585	7.40E+09	8.71E+07	1.18E-02
2.512	6.83E+09	7.55E+07	1.11E-02	2.512	8.00E+09	9.05E+07	1.13E-02	2.512	7.23E+09	8.40E+07	1.16E-02	2.512	7.61E+09	8.59E+07	1.13E-02	2.512	7.42E+09	8.40E+07	1.13E-02
3.981	6.84E+09	7.01E+07	1.02E-02	3.981	8.02E+09	1.06E+08	1.33E-02	3.981	7.25E+09	7.90E+07	1.09E-02	3.981	7.60E+09	8.48E+07	1.11E-02	3.981	7.43E+09	8.51E+07	1.14E-02
6.310	6.85E+09	6.11E+07	8.92E-03	6.310	8.04E+09	9.75E+07	1.21E-02	6.310	7.25E+09	7.40E+07	1.02E-02	6.310	7.61E+09	8.59E+07	1.13E-02	6.310	7.44E+09	7.96E+07	1.06E-02
10.000	6.89E+09	7.06E+07	1.02E-02	10.000	8.05E+09	6.98E+07	8.67E-03	10.000	7.27E+09	7.74E+07	1.06E-02	10.000	7.63E+09	8.43E+07	1.10E-02	10.000	7.46E+09	7.55E+07	1.01E-02
15.849	6.88E+09	6.55E+07	9.52E-03	15.849	8.07E+09	9.41E+07	1.17E-02	15.849	7.30E+09	8.54E+07	1.17E-02	15.849	7.61E+09	8.51E+07	1.12E-02	15.849	7.47E+09	8.25E+07	1.10E-02
25.119	6.91E+09	5.70E+07	8.25E-03	25.119	8.10E+09	7.72E+07	9.53E-03	25.119	7.31E+09	8.80E+07	1.20E-02	25.119	7.64E+09	8.31E+07	1.09E-02	25.119	7.49E+09	7.63E+07	1.02E-02
39.811	6.96E+09	5.84E+07	8.39E-03	39.811	8.14E+09	6.64E+07	8.15E-03	39.811	7.34E+09	7.50E+07	1.02E-02	39.811	7.64E+09	3.77E+07	4.93E-03	39.811	7.52E+09	5.93E+07	7.92E-03
63.096	7.38E+09	2.52E+08	3.42E-02	63.096	8.15E+09	2.33E+08	2.86E-02	63.096	6.94E+09	6.99E+08	1.01E-01	63.096	7.78E+09	-2.85E+08	-3.67E-02	63.096	7.56E+09	2.25E+08	3.18E-02
100.000	7.07E+09	3.68E+07	5.20E-03	100.000	8.20E+09	1.39E+08	1.69E-03	100.000	7.39E+09	5.41E+07	7.32E-03	100.000	7.79E+09	2.31E+07	2.96E-03	100.000	7.61E+09	3.20E+07	4.29E-03

Figure 6.17: Storage modulus vs. frequency for nanoPA6,6 interleaved samples.

Figure 6.18: Loss modulus vs. frequency for nanoPA6,6 interleaved samples.

Figure 6.19: Tan delta vs. frequency for nanoPA6,6 interleaved samples.

Figure 6.20: Loss modulus vs. frequency for nanoPA6,6 interleaved samples excluding 63 and 100 Hz.

Figure 6.21: Tan delta vs. frequency for nanoPA6,6 interleaved samples excluding 63 and 100 Hz.

Table 6.23: Retest results for nanoPVB interleaved samples.

Sample: PVB nanofibre interleaved 5a Frequency Hz	Storage Modulus Pa	Loss Modulus Pa	Tan Delta	Sample: PVB nanofibre interleaved 5b Frequency Hz	Storage Modulus Pa	Loss Modulus Pa	Tan Delta	Sample: PVB nanofibre interleaved 5c Frequency Hz	Storage Modulus Pa	Loss Modulus Pa	Tan Delta	Sample: PVB nanofibre interleaved 5d Frequency Hz	Storage Modulus Pa	Loss Modulus Pa	Tan Delta	average PVB nanofibre interleaved samples Frequency Hz	Storage Modulus Pa	Loss Modulus Pa	Tan Delta
0.100	7.41E+09	1.33E+08	1.80E-02	0.233	6.90E+09	1.20E+08	1.74E-02	0.277	6.70E+09	1.13E+08	1.69E-02	0.144	6.78E+09	1.24E+08	1.83E-02				
0.158	7.42E+09	1.18E+08	1.59E-02	0.158	6.91E+09	1.32E+08	1.91E-02	0.158	6.69E+09	1.15E+08	1.72E-02	0.158	6.80E+09	1.27E+08	1.87E-02	0.158	6.96E+09	1.23E+08	1.77E-02
0.251	7.43E+09	6.82E+07	9.18E-03	0.251	6.93E+09	8.57E+07	1.24E-02	0.251	6.71E+09	7.33E+07	1.09E-02	0.251	6.81E+09	1.01E+08	1.48E-02	0.251	6.97E+09	8.20E+07	1.18E-02
0.398	7.46E+09	5.51E+06	7.39E-04	0.398	6.95E+09	3.59E+07	5.17E-03	0.398	6.73E+09	4.02E+07	5.98E-03	0.398	6.81E+09	3.64E+07	5.35E-03	0.398	6.98E+09	2.95E+07	4.31E-03
0.631	7.47E+09	9.32E+07	1.25E-02	0.631	6.95E+09	1.03E+08	1.49E-02	0.631	6.74E+09	9.38E+07	1.39E-02	0.631	6.82E+09	1.12E+08	1.65E-02	0.631	7.00E+09	1.01E+08	1.44E-02
1.000	7.49E+09	9.15E+07	1.22E-02	1.000	6.97E+09	9.37E+07	1.34E-02	1.000	6.76E+09	8.79E+07	1.30E-02	1.000	6.82E+09	1.01E+08	1.48E-02	1.000	7.01E+09	9.35E+07	1.34E-02
1.585	7.50E+09	9.32E+07	1.24E-02	1.585	6.99E+09	1.16E+08	1.66E-02	1.585	6.77E+09	8.88E+07	1.31E-02	1.585	6.83E+09	8.92E+07	1.31E-02	1.585	7.02E+09	9.68E+07	1.38E-02
2.512	7.52E+09	8.35E+07	1.11E-02	2.512	7.00E+09	8.91E+07	1.27E-02	2.512	6.78E+09	8.64E+07	1.27E-02	2.512	6.85E+09	9.93E+07	1.45E-02	2.512	7.04E+09	8.96E+07	1.28E-02
3.981	7.52E+09	9.11E+07	1.21E-02	3.981	7.01E+09	8.31E+07	1.19E-02	3.981	6.80E+09	7.97E+07	1.17E-02	3.981	6.86E+09	9.31E+07	1.36E-02	3.981	7.05E+09	8.68E+07	1.23E-02
6.310	7.54E+09	8.69E+07	1.15E-02	6.310	7.04E+09	8.93E+07	1.27E-02	6.310	6.81E+09	7.10E+07	1.04E-02	6.310	6.87E+09	9.02E+07	1.31E-02	6.310	7.06E+09	8.44E+07	1.19E-02
10.000	7.56E+09	8.52E+07	1.13E-02	10.000	7.04E+09	9.51E+07	1.35E-02	10.000	6.82E+09	8.74E+07	1.28E-02	10.000	6.89E+09	8.27E+07	1.20E-02	10.000	7.08E+09	8.76E+07	1.24E-02
15.849	7.58E+09	8.54E+07	1.13E-02	15.849	7.06E+09	8.43E+07	1.19E-02	15.849	6.84E+09	7.70E+07	1.12E-02	15.849	6.90E+09	9.34E+07	1.35E-02	15.849	7.10E+09	8.50E+07	1.20E-02
25.119	7.59E+09	7.90E+07	1.04E-02	25.119	7.08E+09	7.77E+07	1.10E-02	25.119	6.86E+09	7.65E+07	1.12E-02	25.119	6.92E+09	8.71E+07	1.26E-02	25.119	7.12E+09	8.01E+07	1.13E-02
39.811	7.61E+09	4.70E+07	6.18E-03	39.811	7.09E+09	7.60E+07	1.07E-02	39.811	6.89E+09	6.88E+07	9.98E-03	39.811	6.94E+09	9.76E+07	1.41E-02	39.811	7.13E+09	7.23E+07	1.02E-02
63.096	7.94E+09	1.83E+08	2.30E-02	63.096	7.24E+09	-2.04E+08	-2.81E-02	63.096	7.32E+09	4.68E+08	6.39E-02	63.096	6.69E+09	-1.57E+08	-2.35E-02	63.096	7.30E+09	7.23E+07	8.81E-03
100.000	7.76E+09	1.13E+08	1.46E-02	100.000	7.24E+09	1.18E+08	1.63E-02	100.000	6.97E+09	1.17E+08	1.68E-02	100.000	7.05E+09	1.30E+08	1.85E-02	100.000	7.25E+09	1.19E+08	1.65E-02
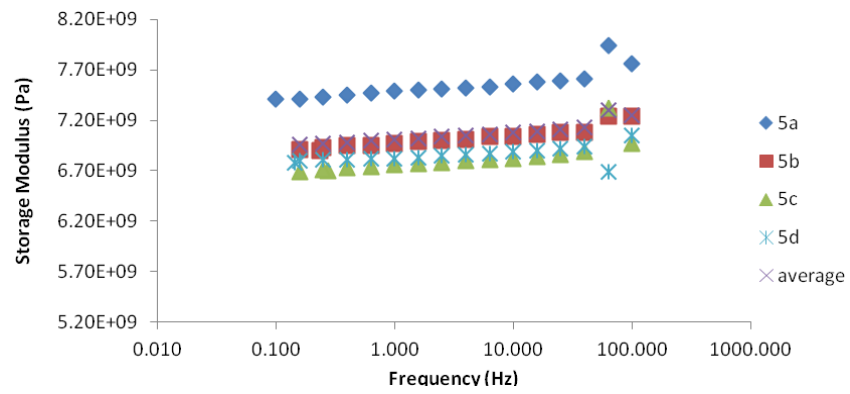
Figure 6.22: Storage modulus vs. frequency for nanoPVB interleaved specimens.
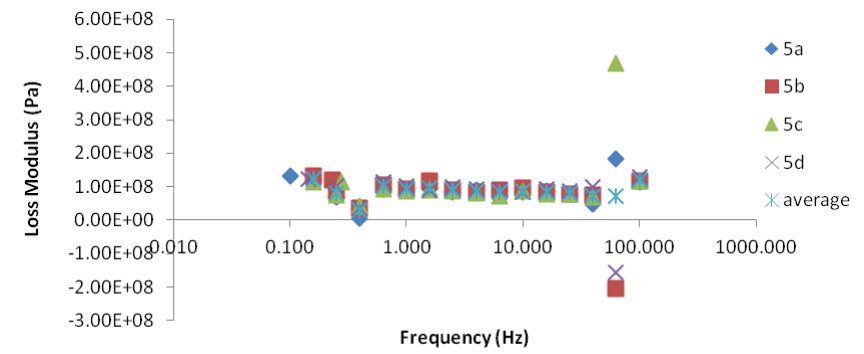
Figure 6.23: Loss modulus vs. frequency for nanoPVB interleaved specimens.
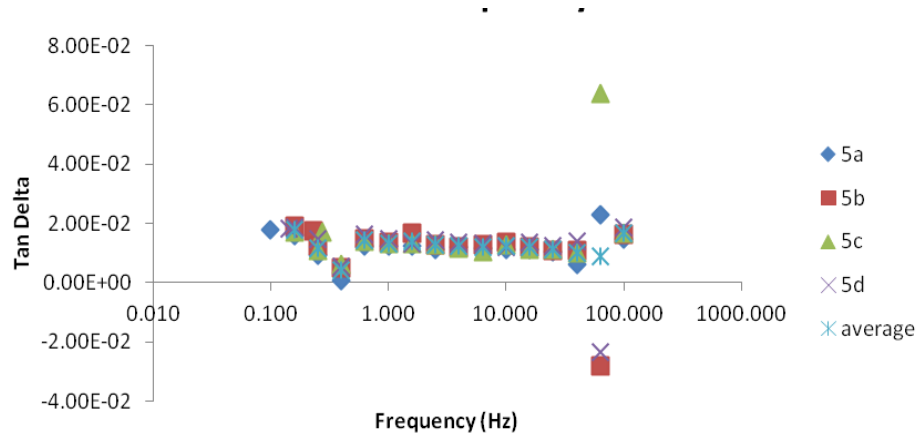
Figure 6.24 Tan delta vs. frequency for nanoPVB interleaved specimens.

Figure 6.25: Loss modulus vs. frequency for nanoPVB interleaved specimens excluding 63 and 100 Hz.
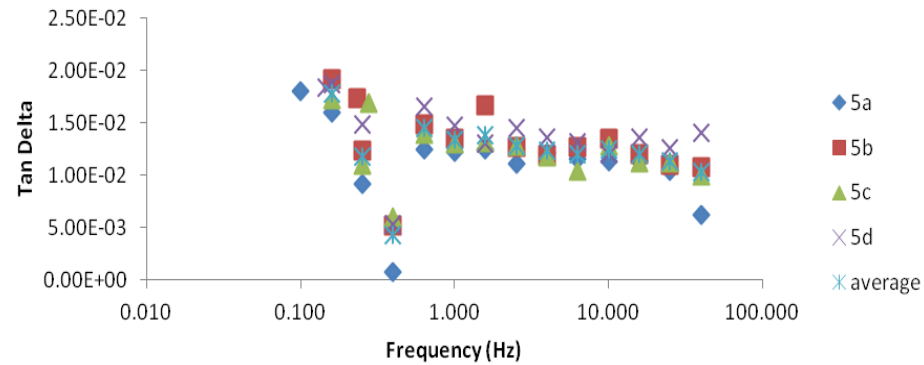
Figure 6.26 Tan delta vs. frequency for nanoPVB specimens excluding 63, 100 Hz.

Table 6.24: Results for nanoPES interleaved samples.

| sample:	nanofibre PES interleaved		12a	sample:	nanofibre PES interleaved		12b	sample:	nanofibre PES interleaved		12c	sample:	nanofibre PES interleaved		12d	average for nanofibre PES interleaved samples			
Frequency	Storage Modulus	Loss Modulus	Tan Delta	Frequency	Storage Modulus	Loss Modulus	Tan Delta	Frequency	Storage Modulus	Loss Modulus	Tan Delta	Frequency	Storage Modulus	Loss Modulus	Tan Delta	Frequency	Storage Modulus	Loss Modulus	Tan Delta
Hz	Pa	Pa		Hz	Pa	Pa		Hz	Pa	Pa		Hz	Pa	Pa		Hz	Pa	Pa	
0.233	6.85E+09	1.09E+08	1.59E-02	0.125	6.98E+09	1.30E+08	1.87E-02	0.187	7.14E+09	1.09E+08	1.52E-02	0.144	6.96E+09	1.40E+08	2.01E-02				
0.158	6.85E+09	1.08E+08	1.57E-02	0.158	6.99E+09	1.50E+08	2.14E-02	0.158	7.15E+09	1.31E+08	1.83E-02	0.158	6.98E+09	1.47E+08	2.11E-02	0.158	6.99E+09	1.30E+08	1.85E-02
0.251	6.86E+09	6.65E+07	9.70E-03	0.251	7.01E+09	9.17E+07	1.31E-02	0.251	7.17E+09	8.44E+07	1.18E-02	0.251	7.00E+09	1.05E+08	1.49E-02	0.251	7.01E+09	8.09E+07	1.15E-02
0.398	6.87E+09	-1.17E+07	-1.70E-03	0.398	7.03E+09	5.90E+07	8.40E-03	0.398	7.19E+09	4.67E+07	6.49E-03	0.398	7.02E+09	6.42E+07	9.14E-03	0.398	7.03E+09	3.13E+07	4.40E-03
0.631	6.88E+09	8.44E+07	1.23E-02	0.631	7.04E+09	1.09E+08	1.54E-02	0.631	7.20E+09	1.10E+08	1.53E-02	0.631	7.04E+09	1.20E+08	1.71E-02	0.631	7.04E+09	1.01E+08	1.43E-02
1.000	6.90E+09	8.59E+07	1.24E-02	1.000	7.06E+09	1.08E+08	1.53E-02	1.000	7.21E+09	9.94E+07	1.38E-02	1.000	7.05E+09	1.06E+08	1.50E-02	1.000	7.06E+09	9.78E+07	1.38E-02
1.585	6.91E+09	8.46E+07	1.22E-02	1.585	7.07E+09	9.73E+07	1.38E-02	1.585	7.23E+09	9.53E+07	1.32E-02	1.585	7.07E+09	9.96E+07	1.41E-02	1.585	7.07E+09	9.24E+07	1.31E-02
2.512	6.93E+09	8.75E+07	1.26E-02	2.512	7.09E+09	1.00E+08	1.42E-02	2.512	7.24E+09	9.30E+07	1.28E-02	2.512	7.08E+09	1.03E+08	1.46E-02	2.512	7.09E+09	9.36E+07	1.32E-02
3.981	6.94E+09	7.99E+07	1.15E-02	3.981	7.11E+09	8.92E+07	1.25E-02	3.981	7.25E+09	9.22E+07	1.27E-02	3.981	7.10E+09	9.78E+07	1.38E-02	3.981	7.10E+09	8.71E+07	1.23E-02
6.310	6.96E+09	8.01E+07	1.15E-02	6.310	7.13E+09	8.43E+07	1.18E-02	6.310	7.25E+09	1.07E+08	1.47E-02	6.310	7.12E+09	8.06E+07	1.13E-02	6.310	7.11E+09	9.04E+07	1.27E-02
10.000	6.97E+09	9.26E+07	1.33E-02	10.000	7.15E+09	9.09E+07	1.27E-02	10.000	7.29E+09	8.04E+07	1.10E-02	10.000	7.14E+09	8.66E+07	1.21E-02	10.000	7.14E+09	8.79E+07	1.23E-02
15.849	6.98E+09	7.90E+07	1.13E-02	15.849	7.15E+09	8.85E+07	1.24E-02	15.849	7.29E+09	7.85E+07	1.08E-02	15.849	7.15E+09	9.23E+07	1.29E-02	15.849	7.14E+09	8.20E+07	1.15E-02
25.119	7.00E+09	6.74E+07	9.63E-03	25.119	7.18E+09	7.24E+07	1.01E-02	25.119	7.32E+09	6.86E+07	9.38E-03	25.119	7.17E+09	8.60E+07	1.20E-02	25.119	7.16E+09	6.95E+07	9.70E-03
39.811	7.03E+09	6.62E+07	9.42E-03	39.811	7.21E+09	7.69E+07	1.07E-02	39.811	7.36E+09	6.03E+07	8.20E-03	39.811	7.20E+09	7.27E+07	1.01E-02	39.811	7.20E+09	6.78E+07	9.43E-03
63.096	7.05E+09	-2.31E+08	-3.28E-02	63.096	6.62E+09	8.82E+07	1.33E-02	63.096	7.37E+09	-7.08E+08	-9.61E-02	63.096	7.46E+09	2.25E+08	3.01E-02	63.096	7.01E+09	-2.84E+08	-3.85E-02
100.000	7.12E+09	4.09E+07	5.75E-03	100.000	7.29E+09	4.76E+07	6.53E-03	100.000	7.49E+09	-3.56E+06	-4.76E-04	100.000	7.23E+09	-1.46E+07	-2.02E-03	100.000	7.30E+09	2.83E+07	3.93E-03
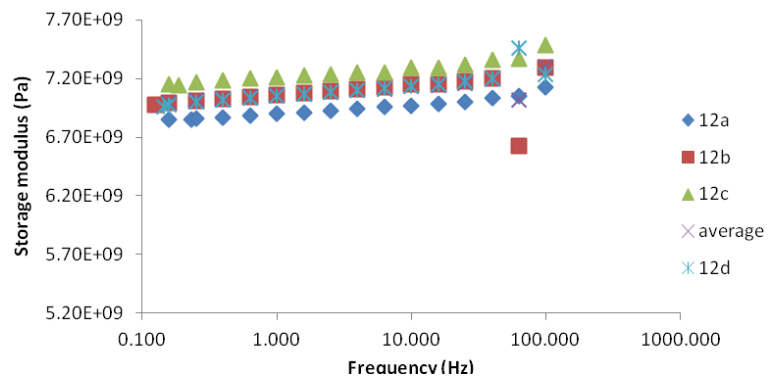
Figure 6.27: Storage modulus vs. frequency for nanoPES interleaved samples.
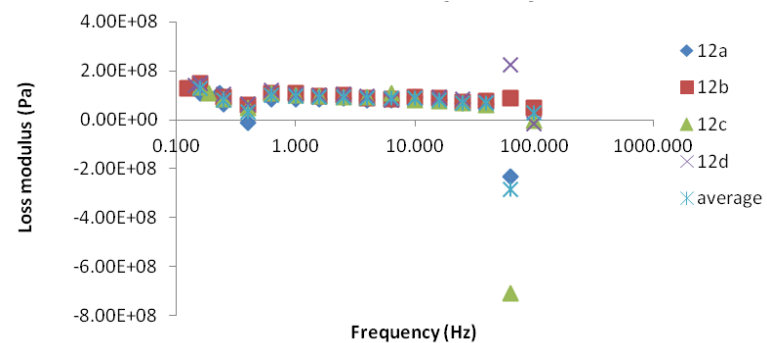
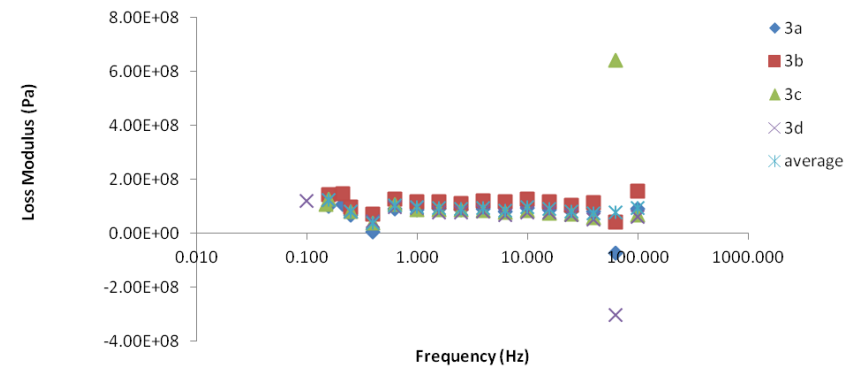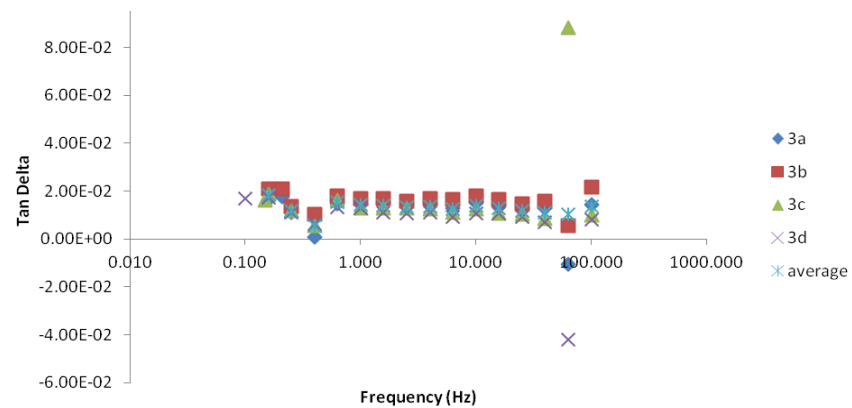Figure 6.28: Loss modulus vs. frequency for nanoPES interleaved samples.
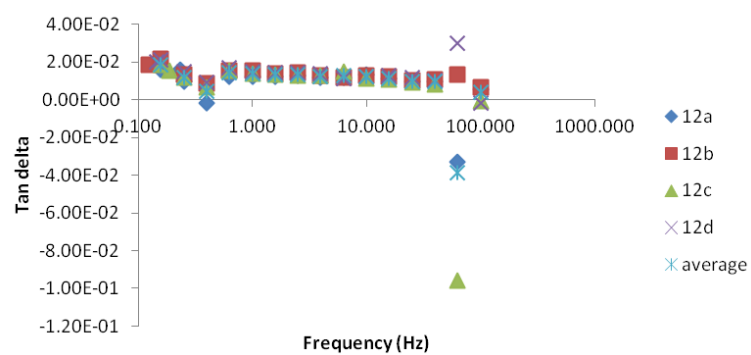
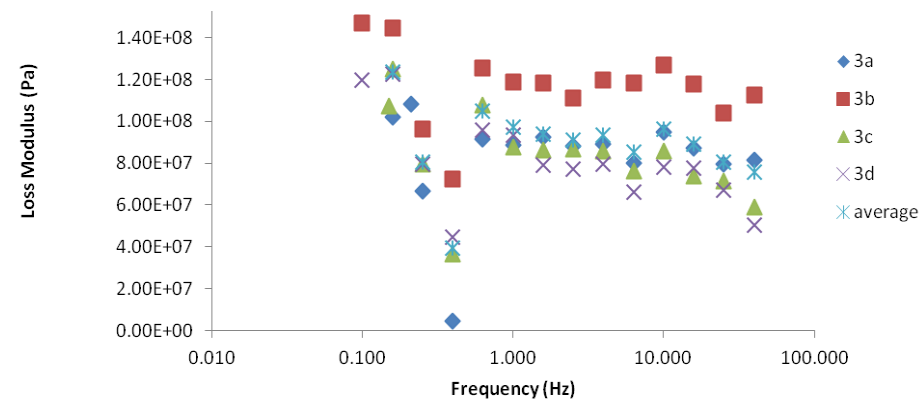Figure 6.29: Tan delta vs. frequency for nanoPES interleaved samples.

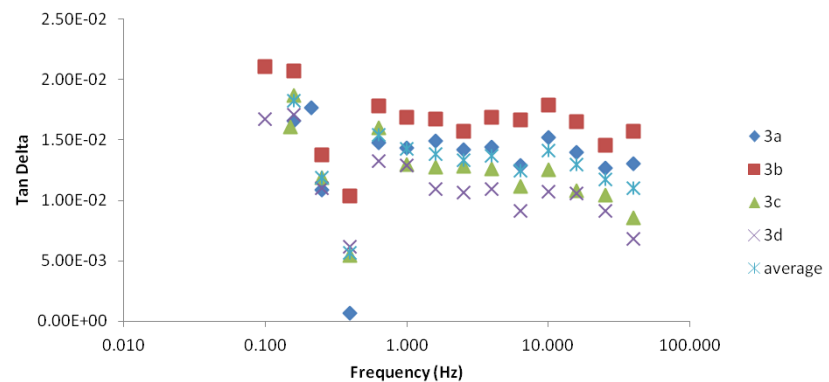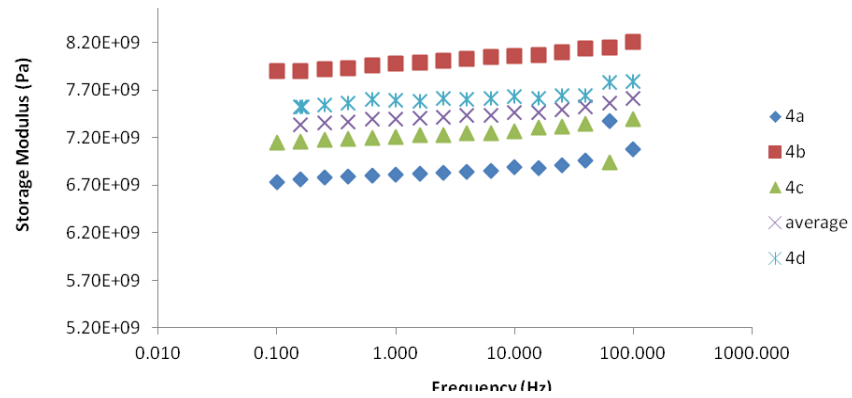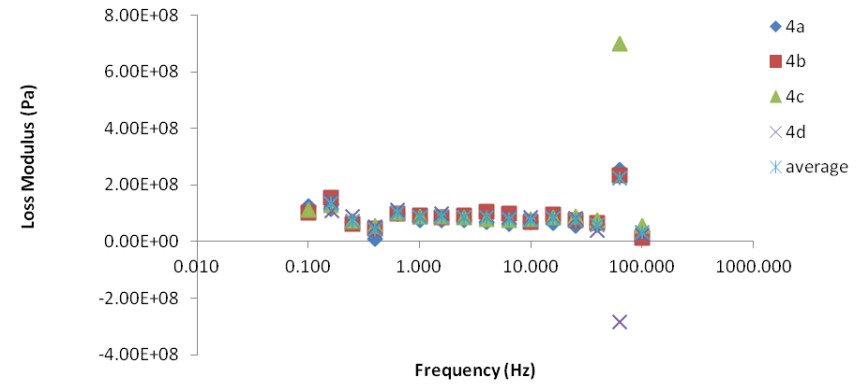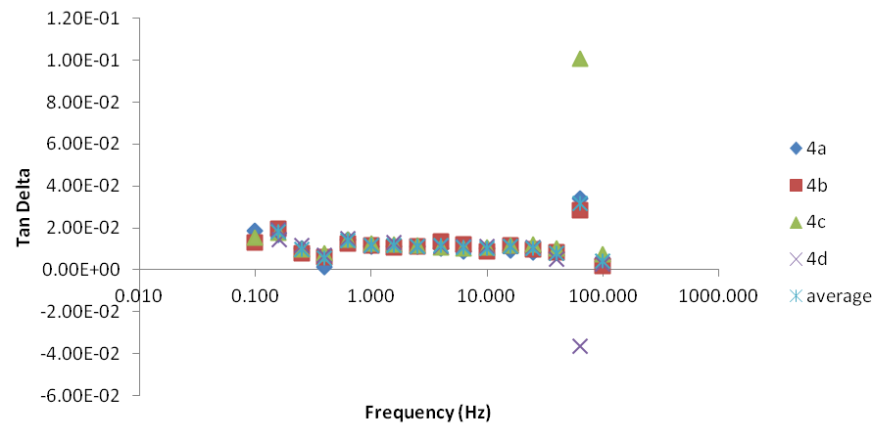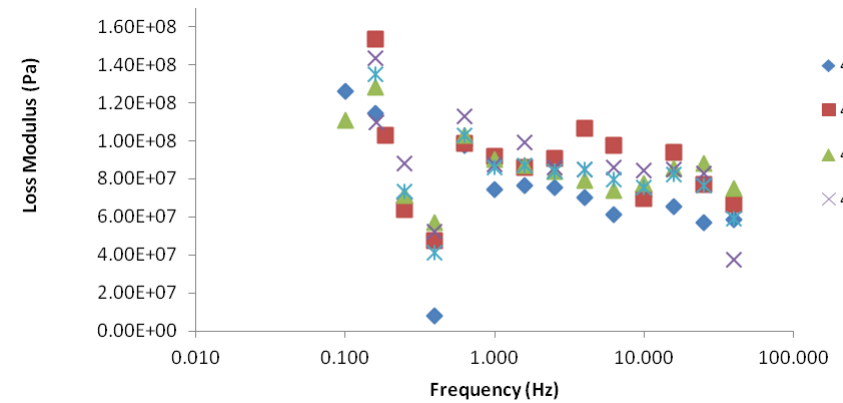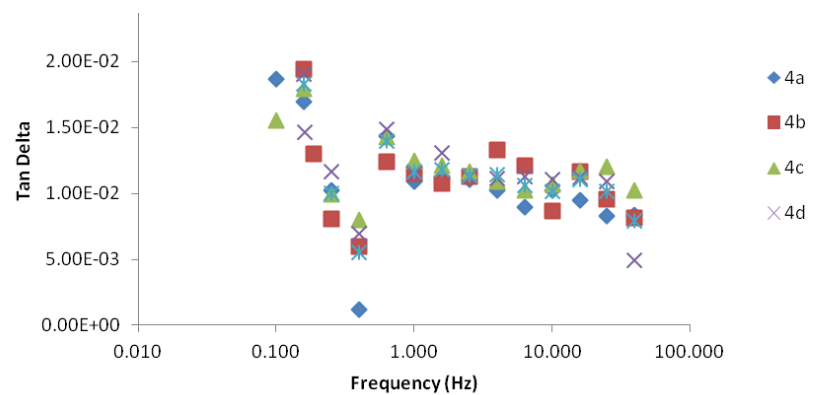Figure 6.30: Loss modulus vs. frequency for nanoPES interleaved samples excluding 63 and 100 Hz.

Figure 6.31: Tan delta vs. frequency for nanoPES interleaved samples excluding 63 and 100 Hz.

Table 6.25: Results for microPPS interleaved samples.

Sample:	microfibre PPS interleaved		6a	Sample:	microfibre PPS interleaved		6b	Sample:	microfibre PPS interleaved		6c	Sample:	microfibre PPS interleaved		6d	average of microfibre PPS interleaved samples		
Frequency	Storage Modulus	Loss Modulus	Tan Delta	Frequency	Storage Modulus	Loss Modulus	Tan Delta	Frequency	Storage Modulus	Loss Modulus	Tan Delta	Frequency	Storage Modulus	Loss Modulus	Tan Delta	Frequency	Storage Modulus	Loss Modulus	Tan Delta
Hz	Pa	Pa		Hz	Pa	Pa		Hz	Pa	Pa		Hz	Pa	Pa		Hz	Pa	Pa	
0.150	7.51E+09	1.32E+08	1.76E-02	0.100	7.13E+09	1.47E+08	2.06E-02	0.188	6.97E+09	1.10E+08	1.58E-02	0.175	6.42E+09	1.16E+08	1.80E-02				
0.158	7.53E+09	1.61E+08	2.14E-02	0.158	7.17E+09	1.56E+08	2.17E-02	0.158	6.98E+09	1.06E+08	1.52E-02	0.158	6.41E+09	1.31E+08	2.05E-02	0.158	7.03E+09	1.39E+08	1.97E-02
0.251	7.55E+09	1.02E+08	1.34E-02	0.251	7.17E+09	1.07E+08	1.50E-02	0.251	7.00E+09	6.36E+07	9.08E-03	0.251	6.43E+09	1.00E+08	1.55E-02	0.251	7.04E+09	9.31E+07	1.33E-02
0.398	7.57E+09	4.34E+07	5.74E-03	0.398	7.19E+09	7.46E+07	1.04E-02	0.398	7.01E+09	-4.54E+05	-6.47E-05	0.398	6.45E+09	6.60E+07	1.02E-02	0.398	7.06E+09	4.59E+07	6.57E-03
0.631	7.59E+09	1.22E+08	1.61E-02	0.631	7.20E+09	1.34E+08	1.87E-02	0.631	7.02E+09	8.60E+07	1.23E-02	0.631	6.46E+09	1.17E+08	1.81E-02	0.631	7.07E+09	1.15E+08	1.63E-02
1.000	7.59E+09	1.07E+08	1.40E-02	1.000	7.22E+09	1.20E+08	1.66E-02	1.000	7.04E+09	7.43E+07	1.06E-02	1.000	6.47E+09	1.06E+08	1.64E-02	1.000	7.08E+09	1.02E+08	1.44E-02
1.585	7.60E+09	1.03E+08	1.35E-02	1.585	7.24E+09	1.13E+08	1.57E-02	1.585	7.05E+09	7.16E+07	1.02E-02	1.585	6.49E+09	9.96E+07	1.54E-02	1.585	7.10E+09	9.69E+07	1.37E-02
2.512	7.62E+09	1.01E+08	1.33E-02	2.512	7.24E+09	1.11E+08	1.54E-02	2.512	7.06E+09	7.31E+07	1.04E-02	2.512	6.50E+09	1.03E+08	1.58E-02	2.512	7.10E+09	9.71E+07	1.37E-02
3.981	7.63E+09	1.00E+08	1.32E-02	3.981	7.26E+09	1.16E+08	1.60E-02	3.981	7.07E+09	7.33E+07	1.04E-02	3.981	6.51E+09	9.67E+07	1.49E-02	3.981	7.12E+09	9.67E+07	1.36E-02
6.310	7.64E+09	9.33E+07	1.22E-02	6.310	7.28E+09	1.01E+08	1.38E-02	6.310	7.08E+09	7.07E+07	9.98E-03	6.310	6.52E+09	1.01E+08	1.55E-02	6.310	7.13E+09	9.14E+07	1.29E-02
10.000	7.67E+09	8.62E+07	1.12E-02	10.000	7.29E+09	1.25E+08	1.71E-02	10.000	7.10E+09	7.41E+07	1.04E-02	10.000	6.53E+09	8.62E+07	1.32E-02	10.000	7.15E+09	9.27E+07	1.30E-02
15.849	7.68E+09	8.89E+07	1.16E-02	15.849	7.30E+09	1.11E+08	1.51E-02	15.849	7.11E+09	6.76E+07	9.50E-03	15.849	6.55E+09	1.05E+08	1.61E-02	15.849	7.16E+09	9.31E+07	1.31E-02
25.119	7.70E+09	9.96E+07	1.29E-02	25.119	7.33E+09	1.09E+08	1.48E-02	25.119	7.13E+09	5.65E+07	7.92E-03	25.119	6.56E+09	9.09E+07	1.39E-02	25.119	7.18E+09	8.90E+07	1.24E-02
39.811	7.70E+09	1.06E+08	1.38E-02	39.811	7.35E+09	9.07E+07	1.23E-02	39.811	7.14E+09	5.63E+07	7.89E-03	39.811	6.59E+09	8.64E+07	1.31E-02	39.811	7.19E+09	8.49E+07	1.18E-02
63.096	8.15E+09	-1.72E+08	-2.11E-02	63.096	7.11E+09	4.82E+08	6.79E-02	63.096	6.94E+09	-3.09E+07	-4.45E-03	63.096	6.48E+09	2.43E+08	3.75E-02	63.096	7.17E+09	1.31E+08	2.00E-02
100.000	7.81E+09	9.81E+07	1.26E-02	100.000	7.43E+09	8.84E+07	1.19E-02	100.000	7.23E+09	2.61E+06	3.61E-04	100.000	6.66E+09	1.41E+08	2.12E-02	100.000	7.28E+09	8.26E+07	1.15E-02
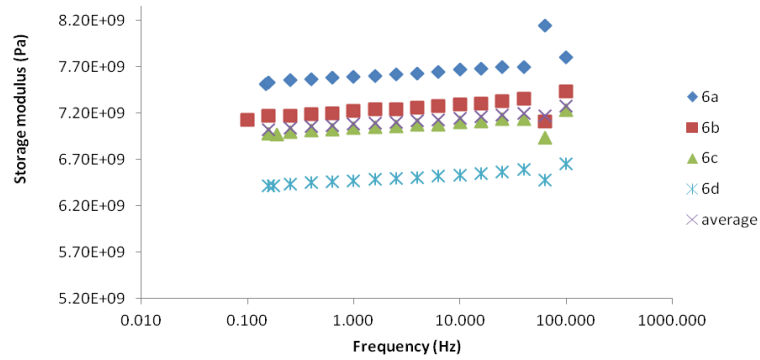
Figure 6.32: Storage modulus vs. frequency for microPPS interleaved samples.

Figure 6.33: Loss modulus vs. frequency for microPPS interleaved samples.

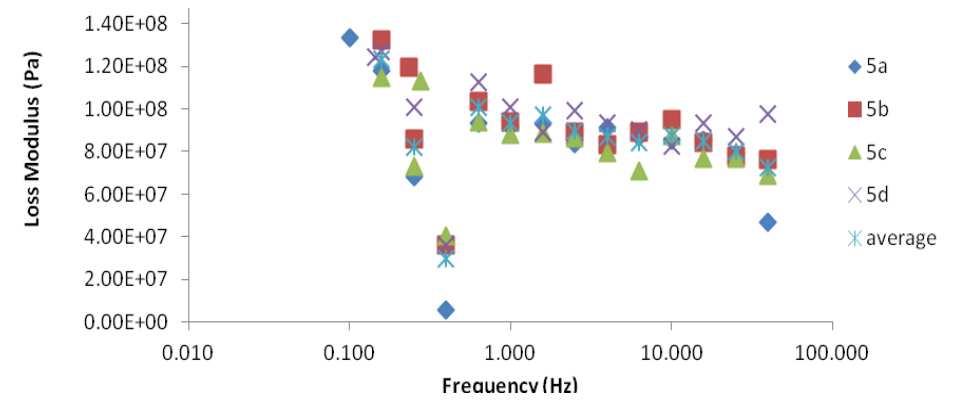**Figure 6.34: Tan delta vs. frequency for microPPS interleaved samples.**

Figure 6.35: Loss modulus vs. frequency for microPPS interleaved samples excluding 63 and 100 Hz.

Figure 6.36: Tan delta vs. frequency for microPPS interleaved samples excluding 63, 100 Hz.

Table 6.26: Results for microPEI interleaved samples.

Sample:	microfibre PEI interleaved		7a	Sample:	microfibre PEI interleaved		7b	Sample:	microfibre PEI interleaved		7c	Sample:	microfibre PEI interleaved		7d	average of microfibre PEI interleaved samples			
Frequency	Storage Modulus	Loss Modulus	Tan Delta	Frequency	Storage Modulus	Loss Modulus	Tan Delta	Frequency	Storage Modulus	Loss Modulus	Tan Delta	Frequenc	Storage Modulus	Loss Modulus	Tan Delta	Frequenc	Storage Modulus	Loss Modulus	Tan Delta
Hz	Pa	Pa		Hz	Pa	Pa		Hz	Pa	Pa		Hz	Pa	Pa		Hz	Pa	Pa	
0.193	7.19E+09	1.25E+08	1.74E-02	0.100	7.80E+09	1.44E+08	1.85E-02	0.100	7.49E+09	1.39E+08	1.85E-02	0.137	6.52E+09	1.13E+08	1.73E-02				
0.158	7.20E+09	1.32E+08	1.83E-02	0.158	7.81E+09	1.72E+08	2.21E-02	0.158	7.50E+09	1.46E+08	1.95E-02	0.158	6.53E+09	1.18E+08	1.80E-02	0.158	7.26E+09	1.42E+08	1.95E-02
0.251	7.21E+09	8.83E+07	1.22E-02	0.251	7.83E+09	9.99E+07	1.28E-02	0.251	7.52E+09	8.44E+07	1.12E-02	0.251	6.55E+09	8.07E+07	1.23E-02	0.251	7.28E+09	8.83E+07	1.21E-02
0.398	7.23E+09	3.83E+07	5.30E-03	0.398	7.84E+09	7.98E+07	1.02E-02	0.398	7.53E+09	8.11E+07	1.08E-02	0.398	6.56E+09	5.84E+07	8.89E-03	0.398	7.29E+09	6.44E+07	8.78E-03
0.631	7.24E+09	1.09E+08	1.51E-02	0.631	7.86E+09	1.31E+08	1.67E-02	0.631	7.57E+09	1.29E+08	1.70E-02	0.631	6.58E+09	1.03E+08	1.57E-02	0.631	7.31E+09	1.18E+08	1.61E-02
1.000	7.25E+09	9.85E+07	1.36E-02	1.000	7.88E+09	1.11E+08	1.42E-02	1.000	7.59E+09	9.75E+07	1.29E-02	1.000	6.59E+09	9.46E+07	1.44E-02	1.000	7.33E+09	1.01E+08	1.37E-02
1.585	7.26E+09	9.12E+07	1.26E-02	1.585	7.89E+09	1.14E+08	1.45E-02	1.585	7.60E+09	8.35E+07	1.10E-02	1.585	6.60E+09	9.01E+07	1.37E-02	1.585	7.34E+09	9.48E+07	1.29E-02
2.512	7.28E+09	9.29E+07	1.28E-02	2.512	7.91E+09	1.04E+08	1.31E-02	2.512	7.60E+09	1.02E+08	1.35E-02	2.512	6.60E+09	9.02E+07	1.37E-02	2.512	7.35E+09	9.73E+07	1.32E-02
3.981	7.29E+09	1.02E+08	1.39E-02	3.981	7.92E+09	1.10E+08	1.39E-02	3.981	7.62E+09	9.70E+07	1.27E-02	3.981	6.64E+09	9.44E+07	1.42E-02	3.981	7.37E+09	1.01E+08	1.37E-02
6.310	7.31E+09	8.76E+07	1.20E-02	6.310	7.94E+09	9.64E+07	1.21E-02	6.310	7.62E+09	8.53E+07	1.12E-02	6.310	6.63E+09	8.53E+07	1.29E-02	6.310	7.38E+09	8.86E+07	1.20E-02
10.000	7.33E+09	8.95E+07	1.22E-02	10.000	7.95E+09	1.04E+08	1.31E-02	10.000	7.61E+09	1.10E+08	1.44E-02	10.000	6.65E+09	9.30E+07	1.40E-02	10.000	7.39E+09	9.92E+07	1.34E-02
15.849	7.34E+09	8.66E+07	1.18E-02	15.849	7.97E+09	1.07E+08	1.35E-02	15.849	7.63E+09	9.93E+07	1.30E-02	15.849	6.67E+09	9.89E+07	1.48E-02	15.849	7.40E+09	9.81E+07	1.33E-02
25.119	7.37E+09	7.64E+07	1.04E-02	25.119	8.00E+09	9.73E+07	1.22E-02	25.119	7.65E+09	8.83E+07	1.15E-02	25.119	6.69E+09	9.42E+07	1.41E-02	25.119	7.43E+09	8.90E+07	1.20E-02
39.811	7.39E+09	8.23E+07	1.11E-02	39.811	8.02E+09	1.05E+08	1.31E-02	39.811	7.70E+09	1.06E+08	1.38E-02	39.811	6.72E+09	6.51E+07	9.69E-03	39.811	7.45E+09	8.96E+07	1.19E-02
63.096	7.16E+09	3.94E+08	5.50E-02	63.096	7.86E+09	1.78E+08	2.26E-02	63.096	7.31E+09	1.83E+08	2.51E-02	63.096	6.72E+09	1.10E+08	1.63E-02	63.096	7.26E+09	2.16E+08	2.98E-02
100.000	7.46E+09	3.33E+07	4.46E-03	100.000	8.14E+09	4.47E+07	5.50E-03	100.000	7.82E+09	1.56E+08	1.99E-02	100.000	6.78E+09	8.55E+07	1.26E-02	100.000	7.55E+09	7.98E+07	1.06E-02

Figure 6.37: Storage modulus vs. frequency for microfibre PEI interleaved samples.

Figure 6.38: Loss modulus vs. frequency for microfibre PEI interleaved samples.
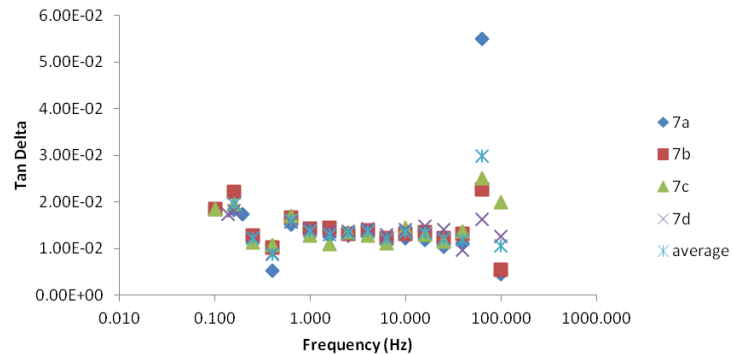
Figure 6.39: Tan delta vs. frequency for microfibre PEI interleaved samples.
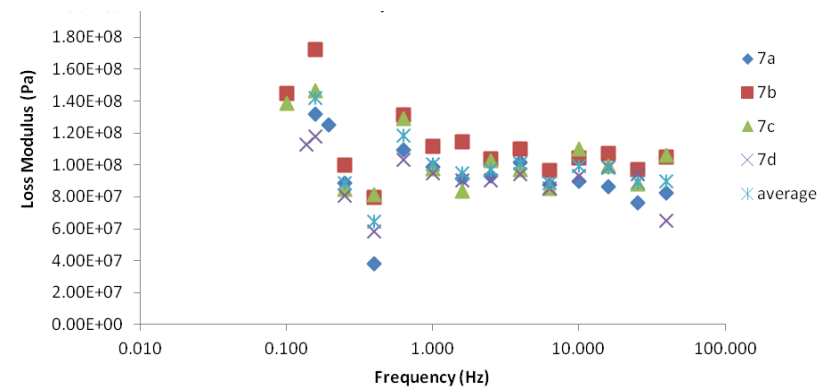
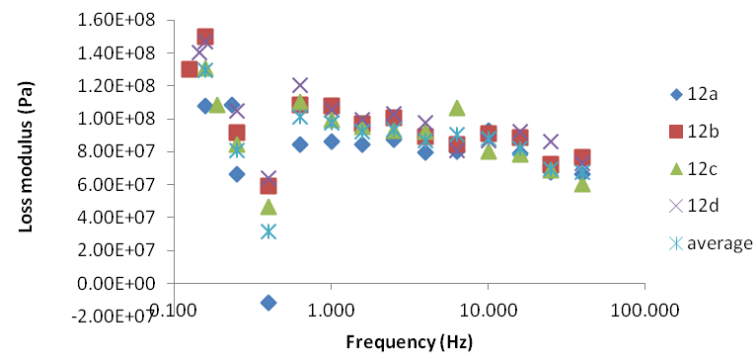**Figure 6.40: Loss modulus vs. frequency for microfibre PEI samples excluding 63 and 100 Hz.**
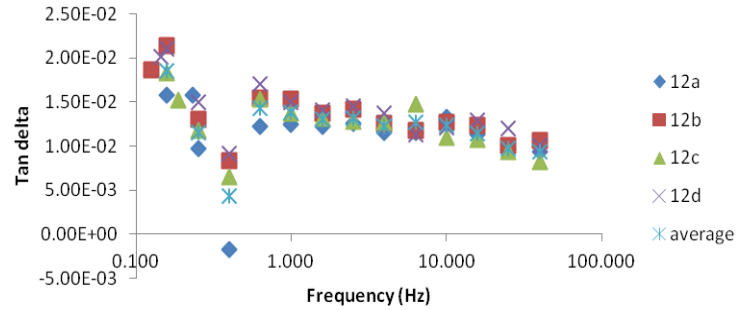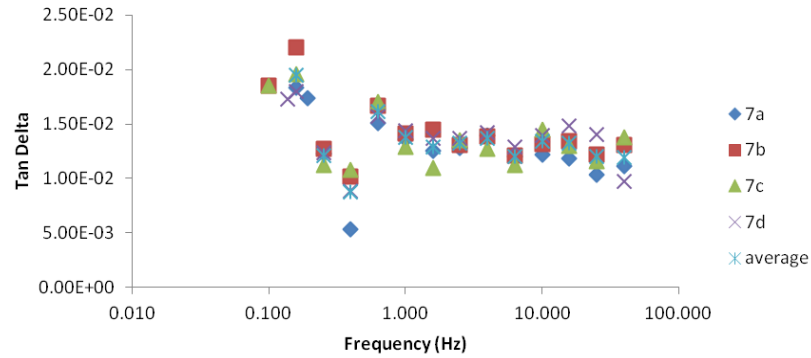
Figure 6.41: Tan delta vs. frequency for microfibre PEI interleaved samples excluding 63 and 100 Hz.

Table 6.27: Results for microtricot interleaved samples.

| Sample:	Tricot microfibre interleaved		8a	Sample:	Tricot microfibre interleaved		8b	Sample:	Tricot microfibre interleaved		8c	Sample:	Tricot microfibre interleaved		8d	average of tricot interleaved samples			
Frequency	Storage Modulus	Loss Modulus	Tan Delta	Frequency	Storage Modulus	Loss Modulus	Tan Delta	Frequency	Storage Modulus	Loss Modulus	Tan Delta	Frequenc	Storage Modulus	Loss Modulus	Tan Delta	Frequenc	Storage Modulus	Loss Modulus	Tan Delta
Hz	Pa	Pa		Hz	Pa	Pa		Hz	Pa	Pa		Hz	Pa	Pa		Hz	Pa	Pa	
0.162	7.05E+09	1.19E+08	1.69E-02	0.100	6.95E+09	1.14E+08	1.65E-02	0.211	7.17E+09	1.31E+08	1.83E-02	0.162	7.60E+09	1.23E+08	1.61E-02				
0.158	7.06E+09	1.48E+08	2.10E-02	0.158	6.96E+09	9.70E+07	1.39E-02	0.158	7.17E+09	1.21E+08	1.68E-02	0.158	7.62E+09	1.20E+08	1.57E-02	0.158	7.20E+09	1.21E+08	1.69E-02
0.251	7.06E+09	7.66E+07	1.09E-02	0.251	6.98E+09	5.57E+07	7.98E-03	0.251	7.18E+09	7.45E+07	1.04E-02	0.251	7.63E+09	7.45E+07	9.76E-03	0.251	7.21E+09	7.03E+07	9.74E-03
0.398	7.07E+09	4.47E+07	6.32E-03	0.398	6.99E+09	3.88E+07	5.56E-03	0.398	7.19E+09	6.24E+07	8.68E-03	0.398	7.65E+09	7.85E+07	1.03E-02	0.398	7.23E+09	5.61E+07	7.71E-03
0.631	7.08E+09	9.60E+07	1.36E-02	0.631	7.00E+09	9.08E+07	1.30E-02	0.631	7.20E+09	1.14E+08	1.58E-02	0.631	7.66E+09	1.19E+08	1.55E-02	0.631	7.24E+09	1.05E+08	1.45E-02
1.000	7.11E+09	1.02E+08	1.43E-02	1.000	7.01E+09	7.74E+07	1.10E-02	1.000	7.23E+09	1.13E+08	1.56E-02	1.000	7.68E+09	9.56E+07	1.24E-02	1.000	7.26E+09	9.69E+07	1.34E-02
1.585	7.12E+09	9.73E+07	1.37E-02	1.585	7.03E+09	7.76E+07	1.10E-02	1.585	7.24E+09	1.08E+08	1.49E-02	1.585	7.69E+09	9.85E+07	1.28E-02	1.585	7.27E+09	9.53E+07	1.31E-02
2.512	7.14E+09	1.07E+08	1.49E-02	2.512	7.04E+09	6.86E+07	9.74E-03	2.512	7.25E+09	1.00E+08	1.38E-02	2.512	7.71E+09	9.60E+07	1.25E-02	2.512	7.28E+09	9.29E+07	1.27E-02
3.981	7.15E+09	9.84E+07	1.38E-02	3.981	7.05E+09	7.09E+07	1.01E-02	3.981	7.26E+09	1.03E+08	1.41E-02	3.981	7.72E+09	8.90E+07	1.15E-02	3.981	7.29E+09	9.03E+07	1.24E-02
6.310	7.15E+09	8.29E+07	1.16E-02	6.310	7.06E+09	6.98E+07	9.88E-03	6.310	7.29E+09	1.27E+08	1.74E-02	6.310	7.74E+09	7.81E+07	1.01E-02	6.310	7.31E+09	8.94E+07	1.22E-02
10.000	7.19E+09	9.57E+07	1.33E-02	10.000	7.06E+09	5.49E+07	7.77E-03	10.000	7.30E+09	1.08E+08	1.48E-02	10.000	7.74E+09	7.87E+07	1.02E-02	10.000	7.32E+09	8.43E+07	1.15E-02
15.849	7.19E+09	9.74E+07	1.36E-02	15.849	7.09E+09	6.88E+07	9.70E-03	15.849	7.31E+09	1.01E+08	1.37E-02	15.849	7.78E+09	8.92E+07	1.15E-02	15.849	7.34E+09	8.90E+07	1.21E-02
25.119	7.22E+09	9.10E+07	1.26E-02	25.119	7.11E+09	6.05E+07	8.50E-03	25.119	7.34E+09	9.26E+07	1.26E-02	25.119	7.80E+09	7.74E+07	9.93E-03	25.119	7.37E+09	8.04E+07	1.09E-02
39.811	7.24E+09	8.50E+07	1.17E-02	39.811	7.13E+09	6.16E+07	8.65E-03	39.811	7.37E+09	9.67E+07	1.31E-02	39.811	7.83E+09	6.66E+07	8.51E-03	39.811	7.39E+09	7.75E+07	1.05E-02
63.096	6.68E+09	6.59E+08	9.87E-02	63.096	8.08E+09	1.59E+08	1.97E-02	63.096	7.37E+09	-2.50E+06	-3.39E-04	63.096	8.06E+09	3.46E+08	4.30E-02	63.096	7.55E+09	2.90E+08	4.02E-02
100.000	7.31E+09	7.86E+07	1.08E-02	100.000	7.18E+09	5.67E+07	7.90E-03	100.000	7.47E+09	9.43E+07	1.26E-02	100.000	7.99E+09	5.85E+07	7.32E-03	100.000	7.49E+09	7.20E+07	9.65E-03
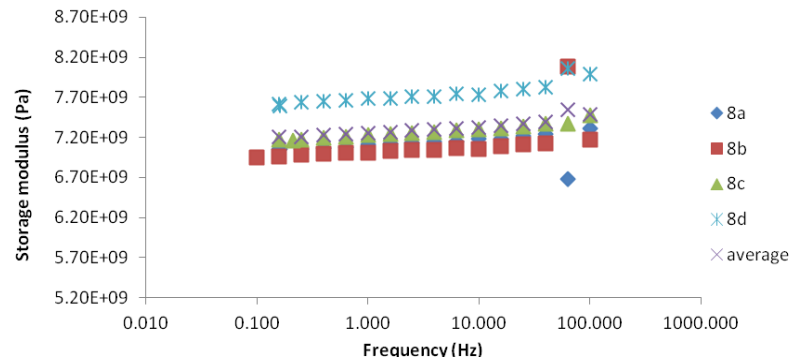
Figure 6.42: Storage modulus vs. frequency for microtricot interleaved samples.
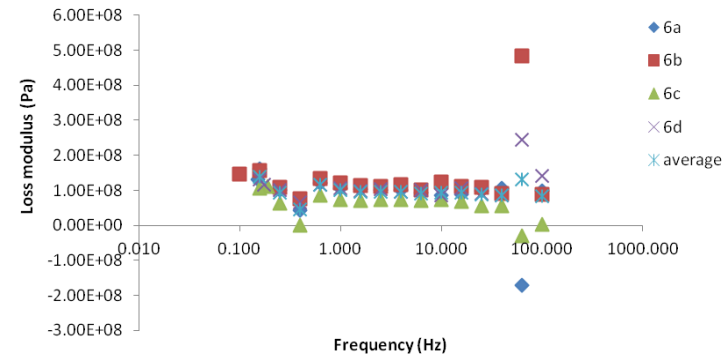

Figure 6.43: Loss modulus vs. frequency for microtricot interleaved samples.
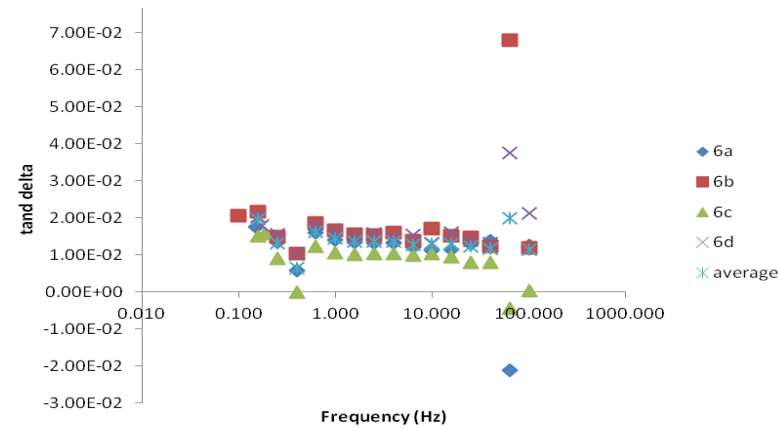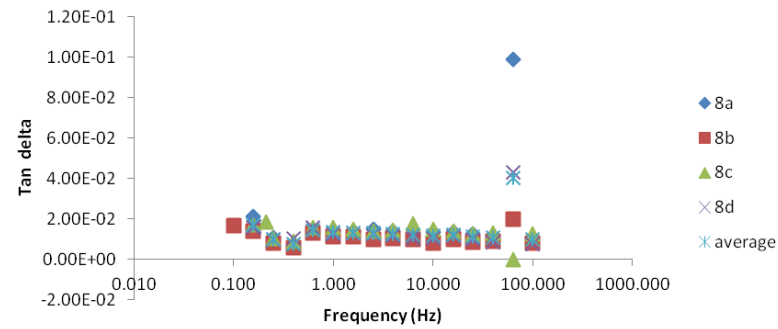

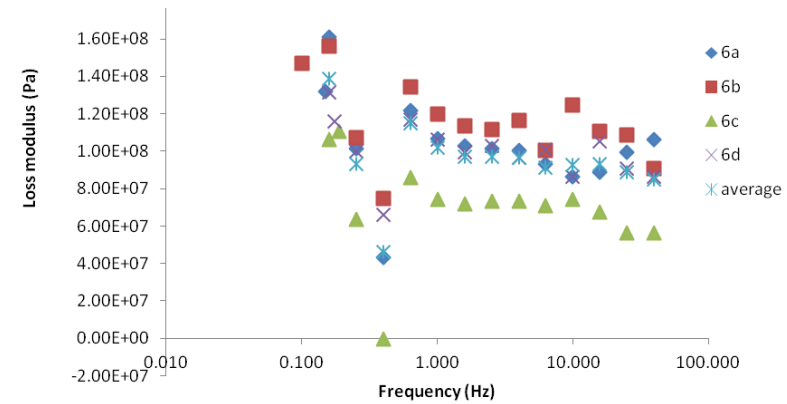**Figure 6.44: Tan delta vs. frequency for microtricot interleaved samples.**

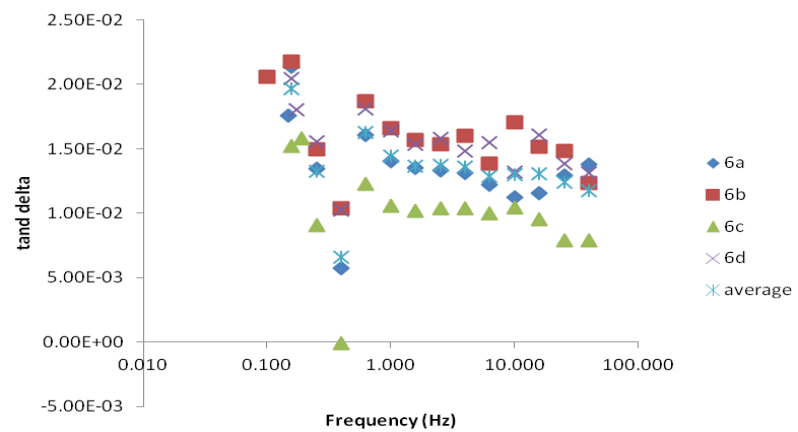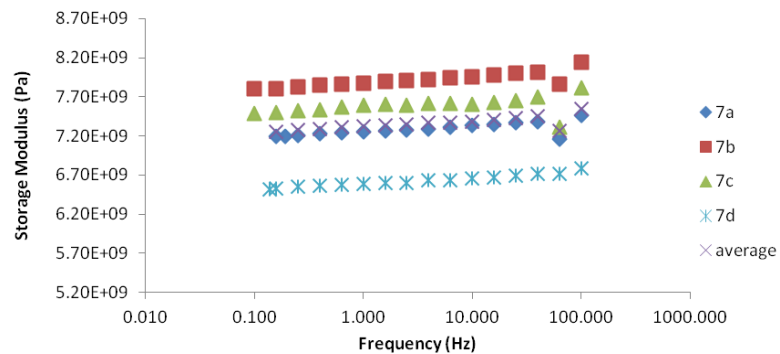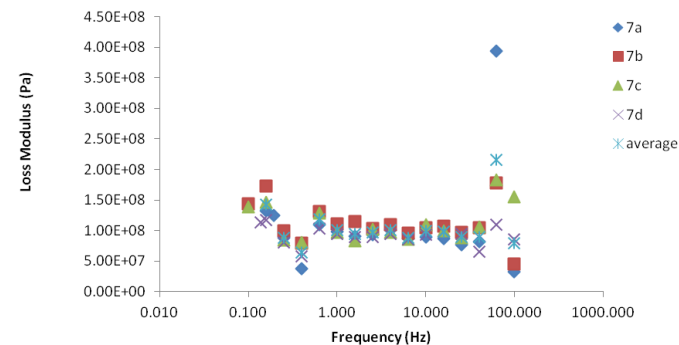**Figure 6.45: Loss modulus vs. frequency for microtricot interleaved samples excluding 63 and 100 Hz.**
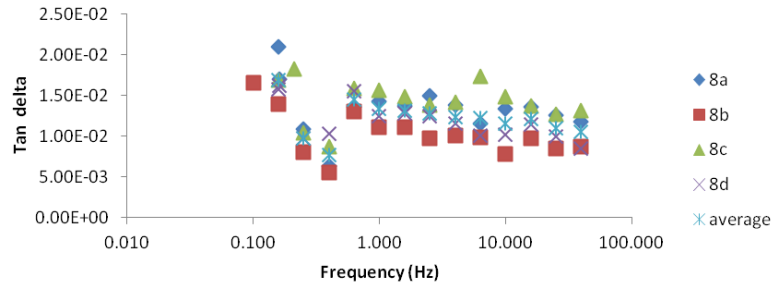
Figure 6.46: Tan delta vs. frequency for microtricot interleaved samples excluding 63 and 100 Hz.

Table 6.28: Results for microPPSnanoPA6,6 interleaved samples.

Sample:	microPPSnanoPA6,6 interleaved 9a			Sample:	microPPSnanoPA6,6 interleaved 9b			Sample:	microPPSnanoPA6,6 interleaved 9c			Sample:	microPPSnanoPA6,6 interleaved 9d			average of microPPSnanoPA6,6 interleaved samples			
Frequency	Storage Modulus	Loss Modulus	Tan Delta	Frequency	Storage Modulus	Loss Modulus	Tan Delta	Frequency	Storage Modulus	Loss Modulus	Tan Delta	Frequenc	Storage Modulus	Loss Modulus	Tan Delta	Frequenc	Storage Modulus	Loss Modulus	Tan Delta
Hz	Pa	Pa		Hz	Pa	Pa		Hz	Pa	Pa		Hz	Pa	Pa		Hz	Pa	Pa	
0.100	7.90E+09	1.35E+08	1.71E-02	0.100	6.99E+09	1.70E+08	2.44E-02	0.162	6.24E+09	1.03E+08	1.66E-02	0.122	7.29E+09	1.19E+08	1.63E-02				
0.158	7.94E+09	1.35E+08	1.70E-02	0.158	7.01E+09	1.53E+08	2.19E-02	0.158	6.26E+09	1.17E+08	1.87E-02	0.158	7.32E+09	1.46E+08	1.99E-02	0.158	7.13E+09	1.38E+08	1.94E-02
0.251	7.96E+09	7.71E+07	9.68E-03	0.251	7.03E+09	1.03E+08	1.47E-02	0.251	6.27E+09	8.66E+07	1.38E-02	0.251	7.34E+09	8.13E+07	1.11E-02	0.251	7.15E+09	8.71E+07	1.23E-02
0.398	7.97E+09	7.98E+07	1.00E-02	0.398	7.07E+09	9.77E+07	1.38E-02	0.398	6.28E+09	1.52E+07	2.43E-03	0.398	7.36E+09	7.22E+07	9.81E-03	0.398	7.17E+09	6.62E+07	9.02E-03
0.631	7.99E+09	1.18E+08	1.48E-02	0.631	7.08E+09	1.34E+08	1.89E-02	0.631	6.28E+09	9.12E+07	1.45E-02	0.631	7.37E+09	1.11E+08	1.50E-02	0.631	7.18E+09	1.13E+08	1.58E-02
1.000	7.99E+09	9.79E+07	1.23E-02	1.000	7.09E+09	1.28E+08	1.81E-02	1.000	6.29E+09	9.07E+07	1.44E-02	1.000	7.38E+09	8.69E+07	1.18E-02	1.000	7.19E+09	1.01E+08	1.41E-02
1.585	8.02E+09	8.93E+07	1.11E-02	1.585	7.11E+09	1.17E+08	1.65E-02	1.585	6.31E+09	8.46E+07	1.34E-02	1.585	7.40E+09	8.58E+07	1.16E-02	1.585	7.21E+09	9.43E+07	1.32E-02
2.512	8.03E+09	9.01E+07	1.12E-02	2.512	7.09E+09	1.03E+08	1.45E-02	2.512	6.31E+09	7.37E+07	1.17E-02	2.512	7.41E+09	7.73E+07	1.04E-02	2.512	7.21E+09	8.60E+07	1.20E-02
3.981	8.04E+09	8.62E+07	1.07E-02	3.981	7.11E+09	9.99E+07	1.41E-02	3.981	6.31E+09	8.36E+07	1.33E-02	3.981	7.43E+09	7.47E+07	1.01E-02	3.981	7.22E+09	8.61E+07	1.20E-02
6.310	8.05E+09	9.07E+07	1.13E-02	6.310	7.11E+09	1.01E+08	1.43E-02	6.310	6.32E+09	7.80E+07	1.23E-02	6.310	7.44E+09	7.28E+07	9.80E-03	6.310	7.23E+09	8.57E+07	1.19E-02
10.000	8.07E+09	9.52E+07	1.18E-02	10.000	7.14E+09	1.22E+08	1.71E-02	10.000	6.29E+09	6.89E+07	1.09E-02	10.000	7.47E+09	7.83E+07	1.05E-02	10.000	7.24E+09	9.11E+07	1.26E-02
15.849	8.10E+09	7.66E+07	9.45E-03	15.849	7.17E+09	1.01E+08	1.42E-02	15.849	6.31E+09	7.88E+07	1.25E-02	15.849	7.48E+09	7.42E+07	9.91E-03	15.849	7.27E+09	8.28E+07	1.15E-02
25.119	8.12E+09	7.36E+07	9.07E-03	25.119	7.19E+09	1.03E+08	1.43E-02	25.119	6.36E+09	6.23E+07	9.80E-03	25.119	7.51E+09	7.62E+07	1.01E-02	25.119	7.30E+09	7.88E+07	1.08E-02
39.811	8.15E+09	5.35E+07	6.56E-03	39.811	7.22E+09	7.89E+07	1.09E-02	39.811	6.37E+09	5.74E+07	9.01E-03	39.811	7.53E+09	4.06E+07	5.40E-03	39.811	7.32E+09	5.76E+07	7.97E-03
63.096	8.28E+09	-2.77E+08	-3.35E-02	63.096	6.93E+09	-3.94E+08	-5.68E-02	63.096	6.58E+09	-3.24E+08	-4.93E-02	63.096	7.69E+09	-7.99E+08	-1.04E-01	63.096	7.37E+09	-4.49E+08	-6.09E-02
100.000	8.28E+09	2.80E+07	3.38E-03	100.000	7.27E+09	9.11E+07	1.25E-02	100.000	6.42E+09	7.12E+07	1.11E-02	100.000	7.70E+09	7.52E+07	9.76E-03	100.000	7.42E+09	6.64E+07	9.19E-03
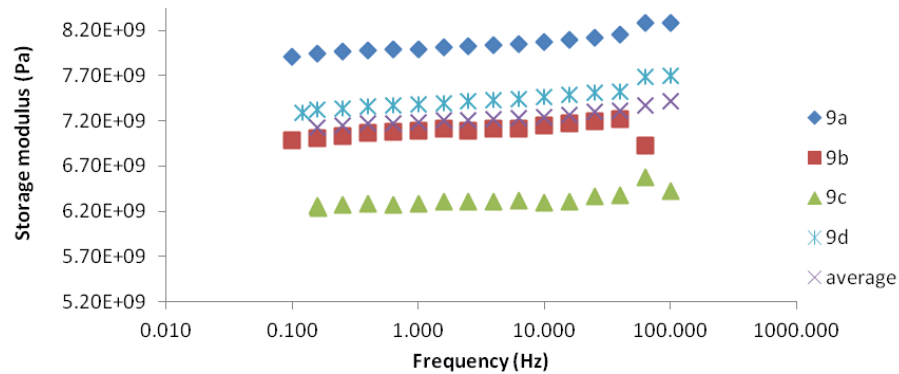
Figure 6.47: Storage modulus vs. frequency for microPPSnanoPA6,6 interleaved samples.

Figure 6.48: Loss modulus vs. frequency for microPPSnanoPA6,6 interleaved samples.

Figure 6.49: Tan delta vs. frequency for microPPSnanoPA6,6 interleaved samples.

Figure 6.50: Loss modulus vs. frequency for microPPSnanoPA6,6 interleaved samples excluding 63 and 100 Hz.
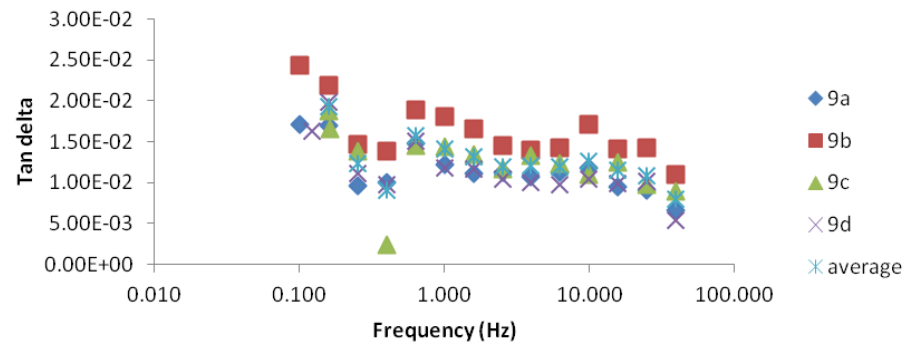
Figure 6.51: Tan delta vs, frequency for microPPSnanoPA6,6 interleaved samples.

Table 6.29: Results for microPEInanoPA6,6 interleaved samples.

Sample:	microPEInanoPA6,6 interleaved	10a		Sample:	microPEInanoPA6,6 interleaved	10b		Sample:	microPEInanoPA6,6 interleaved	10c		Sample:	microPEInanoPA6,6 interleaved	10d	average of microPEInanoPA6,6 interleaved samples		
Frequency	Storage Modulus	Loss Modulus	Tan Delta	Frequency	Storage Modulus	Loss Modulus	Tan Delta	Frequency	Storage Modulus	Loss Modulus	Tan Delta	Frequenc	Storage Modulus	Loss Modulus	Tan Delta	Frequenc	Storage Modulus	Loss Modulus	Tan Delta
Hz	Pa	Pa		Hz	Pa	Pa		Hz	Pa	Pa		Hz	Pa	Pa		Hz	Pa	Pa	
0.100	6.43E+09	1.26E+08	1.96E-02	0.122	7.49E+09	1.46E+08	1.95E-02	0.100	6.80E+09	1.25E+08	1.84E-02	0.100	7.30E+09	1.37E+08	1.87E-02				
0.158	6.43E+09	1.30E+08	2.02E-02	0.158	7.48E+09	1.31E+08	1.75E-02	0.158	6.81E+09	1.46E+08	2.15E-02	0.158	7.32E+09	1.07E+08	1.46E-02	0.158	7.01E+09	1.28E+08	1.84E-02
0.251	6.45E+09	7.29E+07	1.13E-02	0.251	7.50E+09	7.77E+07	1.04E-02	0.251	6.83E+09	8.44E+07	1.24E-02	0.251	7.35E+09	7.03E+07	9.57E-03	0.251	7.03E+09	7.63E+07	1.09E-02
0.398	6.46E+09	6.13E+07	9.48E-03	0.398	7.52E+09	7.21E+07	9.58E-03	0.398	6.85E+09	5.44E+07	7.94E-03	0.398	7.37E+09	7.41E+07	1.00E-02	0.398	7.05E+09	6.55E+07	9.26E-03
0.631	6.48E+09	1.02E+08	1.57E-02	0.631	7.53E+09	1.15E+08	1.52E-02	0.631	6.85E+09	1.11E+08	1.61E-02	0.631	7.39E+09	1.18E+08	1.60E-02	0.631	7.06E+09	1.11E+08	1.58E-02
1.000	6.49E+09	9.56E+07	1.47E-02	1.000	7.57E+09	1.22E+08	1.61E-02	1.000	6.88E+09	9.42E+07	1.37E-02	1.000	7.39E+09	1.01E+08	1.37E-02	1.000	7.08E+09	1.03E+08	1.46E-02
1.585	6.49E+09	8.63E+07	1.33E-02	1.585	7.58E+09	1.22E+08	1.61E-02	1.585	6.90E+09	8.93E+07	1.29E-02	1.585	7.41E+09	9.28E+07	1.25E-02	1.585	7.10E+09	9.77E+07	1.37E-02
2.512	6.51E+09	8.28E+07	1.27E-02	2.512	7.58E+09	1.09E+08	1.44E-02	2.512	6.90E+09	8.12E+07	1.18E-02	2.512	7.43E+09	9.12E+07	1.23E-02	2.512	7.11E+09	9.11E+07	1.28E-02
3.981	6.52E+09	7.67E+07	1.18E-02	3.981	7.60E+09	1.16E+08	1.53E-02	3.981	6.91E+09	8.16E+07	1.18E-02	3.981	7.45E+09	9.21E+07	1.24E-02	3.981	7.12E+09	9.17E+07	1.28E-02
6.310	6.54E+09	7.54E+07	1.15E-02	6.310	7.60E+09	1.10E+08	1.45E-02	6.310	6.92E+09	8.98E+07	1.30E-02	6.310	7.46E+09	7.90E+07	1.06E-02	6.310	7.13E+09	8.85E+07	1.24E-02
10.000	6.55E+09	8.09E+07	1.24E-02	10.000	7.63E+09	1.13E+08	1.49E-02	10.000	6.95E+09	8.19E+07	1.18E-02	10.000	7.47E+09	1.04E+08	1.39E-02	10.000	7.15E+09	9.51E+07	1.32E-02
15.849	6.57E+09	7.71E+07	1.17E-02	15.849	7.65E+09	1.06E+08	1.38E-02	15.849	6.97E+09	7.87E+07	1.13E-02	15.849	7.50E+09	9.27E+07	1.24E-02	15.849	7.17E+09	8.86E+07	1.23E-02
25.119	6.58E+09	6.33E+07	9.62E-03	25.119	7.68E+09	1.03E+08	1.34E-02	25.119	6.95E+09	6.33E+07	9.12E-03	25.119	7.53E+09	8.68E+07	1.15E-02	25.119	7.18E+09	7.91E+07	1.09E-02
39.811	6.62E+09	5.52E+07	8.33E-03	39.811	7.71E+09	8.57E+07	1.11E-02	39.811	7.03E+09	5.00E+07	7.11E-03	39.811	7.58E+09	1.05E+08	1.38E-02	39.811	7.23E+09	7.39E+07	1.01E-02
63.096	7.36E+09	-1.84E+08	-2.50E-02	63.096	7.94E+09	2.55E+08	3.22E-02	63.096	6.47E+09	3.70E+06	5.71E-04	63.096	7.20E+09	6.00E+08	8.33E-03	63.096	7.24E+09	1.69E+08	2.28E-02
100.000	6.55E+09	7.33E+07	1.12E-02	100.000	7.92E+09	5.85E+07	7.39E-03	100.000	7.13E+09	8.19E+06	1.15E-03	100.000	7.63E+09	1.10E+08	1.45E-02	100.000	7.31E+09	6.26E+07	8.54E-03

Figure 6.52: Storage modulus vs. frequency for microPEInanoPA6,6 interleaved samples.

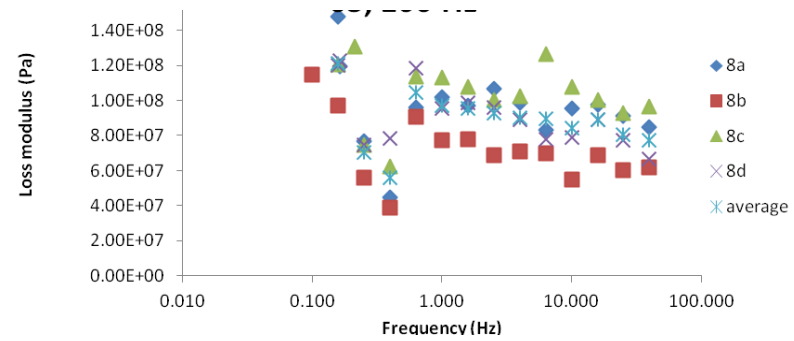**Figure 6.53: Loss modulus vs. frequency for microPEInanoPA6,6 interleaved samples.**

Figure 6.54: Tan delta vs. frequency for microPEInanoPA6,6 interleaved samples.

Figure 6.55: Loss modulus vs. frequency for microPEInanoPA6,6 interleaved samples.
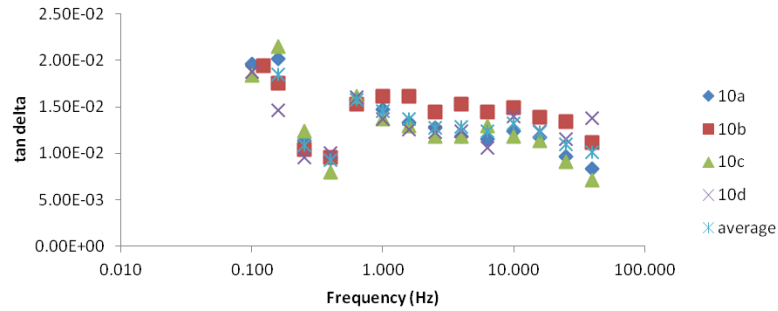
Figure 6.56: Tan delta vs. frequency for microPEInanoPA6,6 6 interleaved samples.

Table 6.30: Results for microtricotnanoPA6,6 interleaved samples.

| Sample:	tricot nano PA6,6 interleaved		11a	Sample:	tricot nano PA6,6 interleaved		11b	Sample:	tricot nano PA6,6 interleaved		11c	Sample:	tricot nano PA6,6 interleaved		11d	average of tricot nanoPA6,6 interleaved samples			
Frequency	Storage Modulus	Loss Modulus	Tan Delta	Frequency	Storage Modulus	Loss Modulus	Tan Delta	Frequency	Storage Modulus	Loss Modulus	Tan Delta	Frequenc	Storage Modulus	Loss Modulus	Tan Delta	Frequenc	Storage Modulus	Loss Modulus	Tan Delta
Hz	Pa	Pa		Hz	Pa	Pa		Hz	Pa	Pa		Hz	Pa	Pa		Hz	Pa	Pa	
0.100	7.71E+09	1.26E+08	1.63E-02	0.211	6.77E+09	1.19E+08	1.76E-02	0.211	6.90E+09	1.16E+08	1.68E-02	0.100	7.20E+09	1.36E+08	1.90E-02				
0.158	7.74E+09	1.03E+08	1.33E-02	0.158	6.78E+09	8.95E+07	1.32E-02	0.158	6.89E+09	9.91E+07	1.44E-02	0.158	7.21E+09	9.10E+07	1.26E-02	0.158	7.16E+09	9.57E+07	1.34E-02
0.251	7.77E+09	1.22E+08	1.58E-02	0.251	6.79E+09	5.46E+07	8.03E-03	0.251	6.90E+09	5.32E+07	7.71E-03	0.251	7.24E+09	7.19E+07	9.92E-03	0.251	7.18E+09	7.55E+07	1.04E-02
0.398	7.78E+09	8.36E+07	1.07E-02	0.398	6.81E+09	5.57E+07	8.17E-03	0.398	6.93E+09	5.90E+07	8.52E-03	0.398	7.26E+09	7.40E+07	1.02E-02	0.398	7.19E+09	6.81E+07	9.41E-03
0.631	7.79E+09	1.33E+08	1.71E-02	0.631	6.82E+09	9.73E+07	1.43E-02	0.631	6.94E+09	9.13E+07	1.32E-02	0.631	7.27E+09	9.95E+07	1.37E-02	0.631	7.20E+09	1.05E+08	1.46E-02
1.000	7.82E+09	1.06E+08	1.35E-02	1.000	6.84E+09	9.00E+07	1.32E-02	1.000	6.97E+09	9.15E+07	1.31E-02	1.000	7.28E+09	1.01E+08	1.39E-02	1.000	7.23E+09	9.72E+07	1.34E-02
1.585	7.83E+09	1.03E+08	1.32E-02	1.585	6.86E+09	8.64E+07	1.26E-02	1.585	6.98E+09	8.57E+07	1.23E-02	1.585	7.30E+09	9.71E+07	1.33E-02	1.585	7.24E+09	9.31E+07	1.28E-02
2.512	7.85E+09	1.11E+08	1.42E-02	2.512	6.87E+09	8.19E+07	1.19E-02	2.512	7.00E+09	8.57E+07	1.22E-02	2.512	7.32E+09	9.32E+07	1.27E-02	2.512	7.26E+09	9.30E+07	1.28E-02
3.981	7.86E+09	9.64E+07	1.23E-02	3.981	6.89E+09	7.62E+07	1.11E-02	3.981	7.03E+09	8.13E+07	1.16E-02	3.981	7.34E+09	8.96E+07	1.22E-02	3.981	7.28E+09	8.59E+07	1.18E-02
6.310	7.88E+09	1.08E+08	1.38E-02	6.310	6.91E+09	7.22E+07	1.05E-02	6.310	7.04E+09	8.36E+07	1.19E-02	6.310	7.36E+09	8.11E+07	1.10E-02	6.310	7.30E+09	8.63E+07	1.18E-02
10.000	7.90E+09	1.04E+08	1.32E-02	10.000	6.92E+09	7.83E+07	1.13E-02	10.000	7.04E+09	7.21E+07	1.02E-02	10.000	7.38E+09	8.24E+07	1.12E-02	10.000	7.31E+09	8.43E+07	1.15E-02
15.849	7.92E+09	9.57E+07	1.21E-02	15.849	6.94E+09	7.09E+07	1.02E-02	15.849	7.07E+09	7.48E+07	1.06E-02	15.849	7.40E+09	8.15E+07	1.10E-02	15.849	7.33E+09	8.07E+07	1.10E-02
25.119	7.94E+09	7.66E+07	9.64E-03	25.119	6.97E+09	7.16E+07	1.03E-02	25.119	7.10E+09	7.26E+07	1.02E-02	25.119	7.41E+09	7.46E+07	1.01E-02	25.119	7.36E+09	7.39E+07	1.01E-02
39.811	8.00E+09	4.96E+07	6.19E-03	39.811	6.98E+09	4.79E+07	6.86E-03	39.811	7.11E+09	5.49E+07	7.72E-03	39.811	7.45E+09	5.05E+07	6.78E-03	39.811	7.39E+09	5.07E+07	6.89E-03
63.096	8.08E+09	-2.07E+08	-2.56E-02	63.096	7.66E+09	4.13E+08	5.39E-02	63.096	7.09E+09	3.89E+08	5.49E-02	63.096	7.21E+09	-3.20E+08	-4.44E-02	63.096	7.51E+09	6.88E+07	9.72E-03
100.000	8.11E+09	4.61E+07	5.69E-03	100.000	7.10E+09	8.65E+07	1.22E-02	100.000	7.22E+09	4.89E+07	6.77E-03	100.000	7.60E+09	-4.45E+07	-5.86E-03	100.000	7.51E+09	3.43E+07	4.70E-03
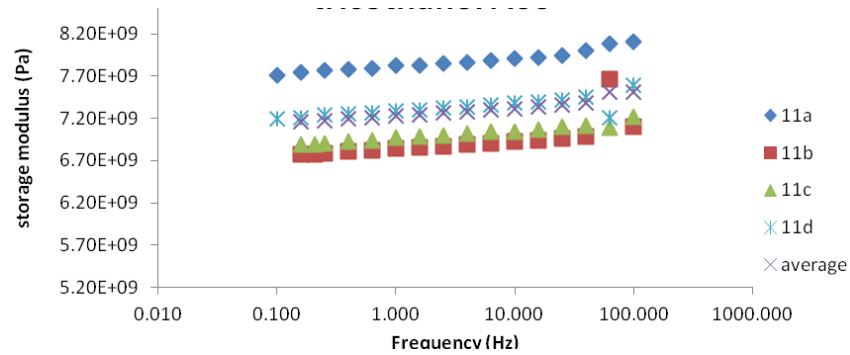
Figure 6.57: Storage modulus vs. frequency for microtricotnanoPA6,6 interleaved samples.
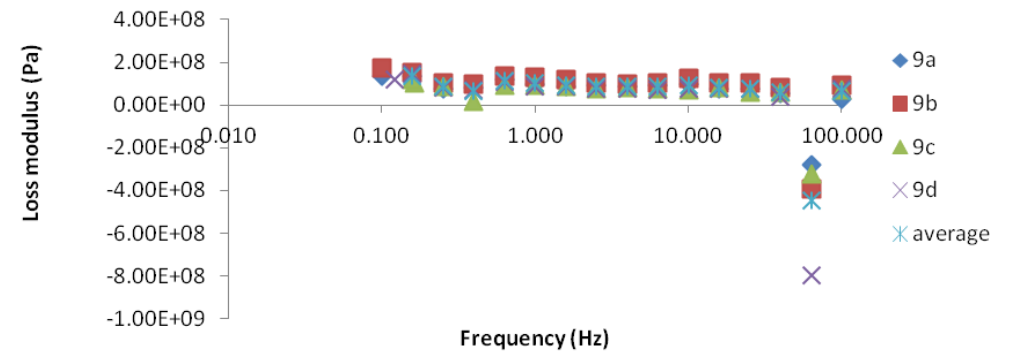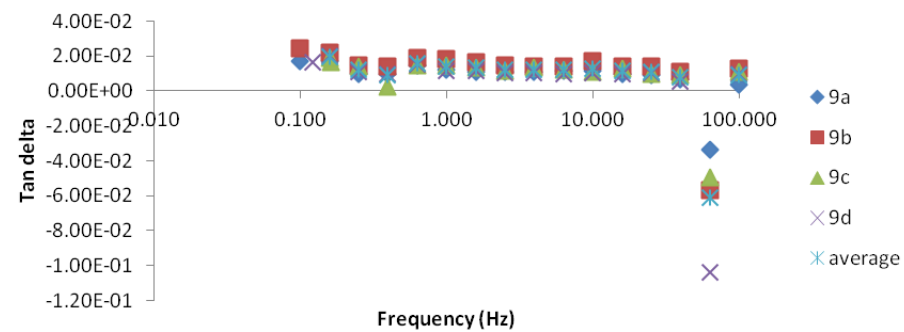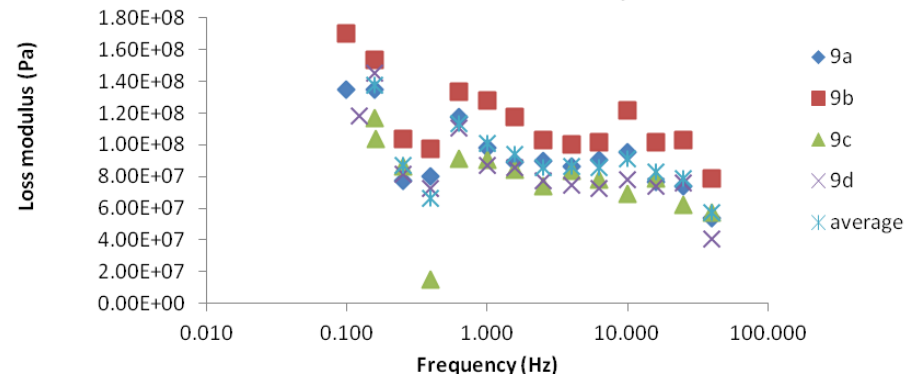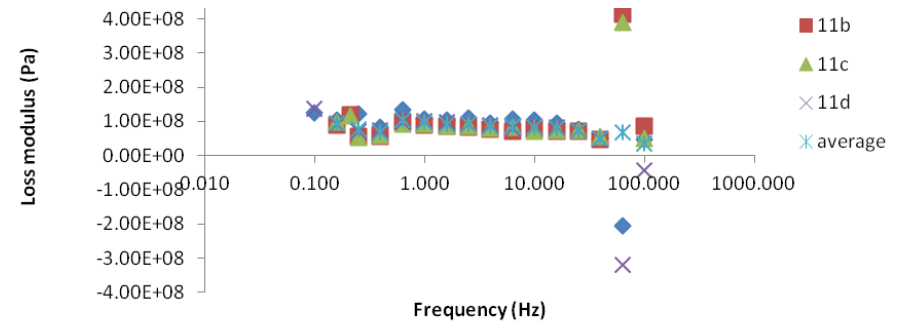

Figure 6.58: Loss modulus vs. frequency for microtricotnanoPA6,6 interleaved samples.
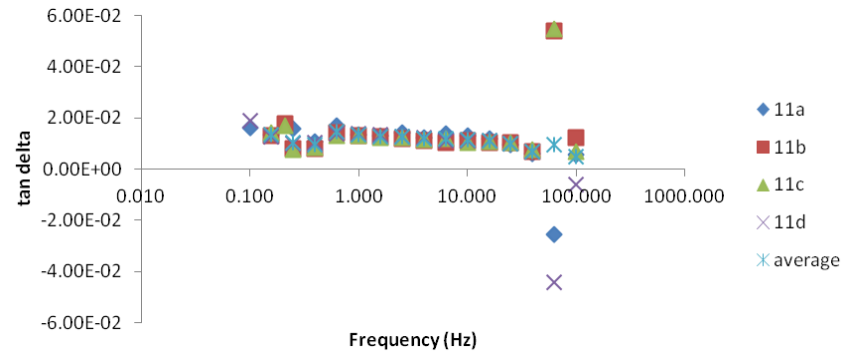
Figure 6.59: Tan delta vs. frequency for microtricotnanoPA6,6 interleaved samples.

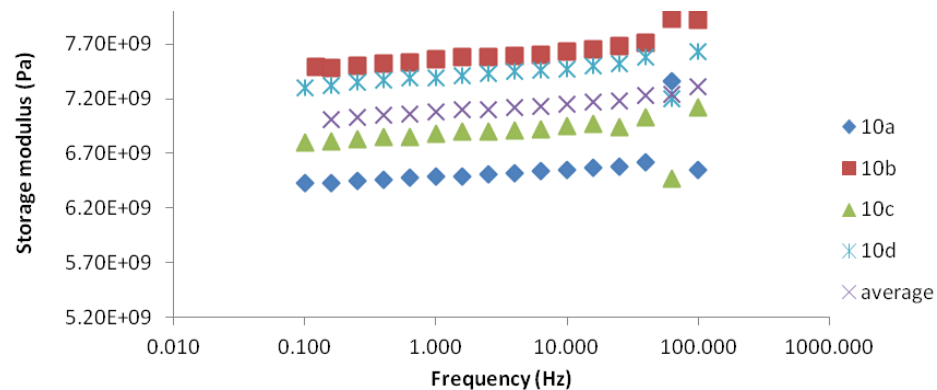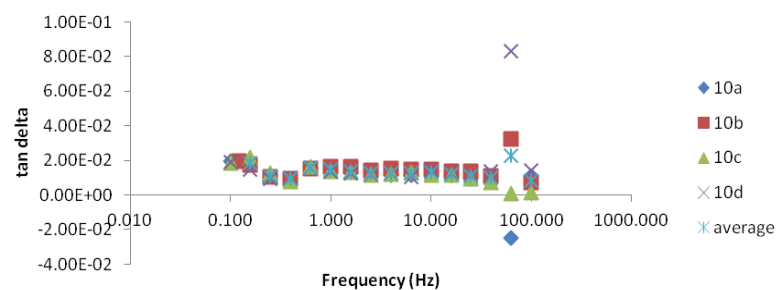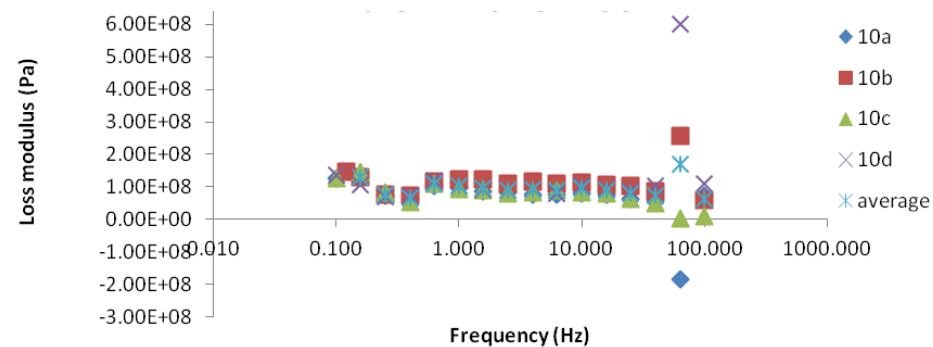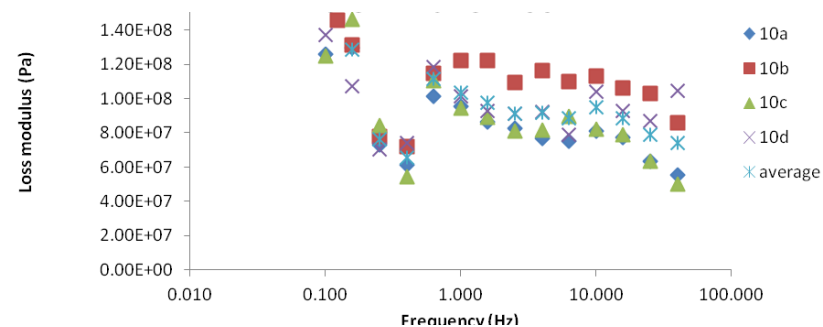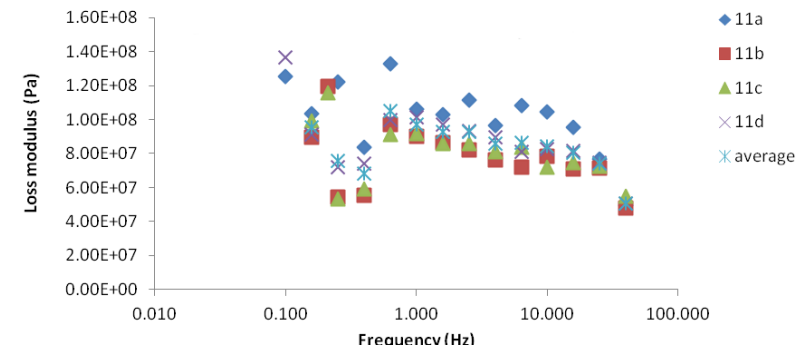**Figure 6.60: Loss modulus vs. frequency for microtricotnanoPA6,6 interleaved samples excluding 63 and 100 Hz.**
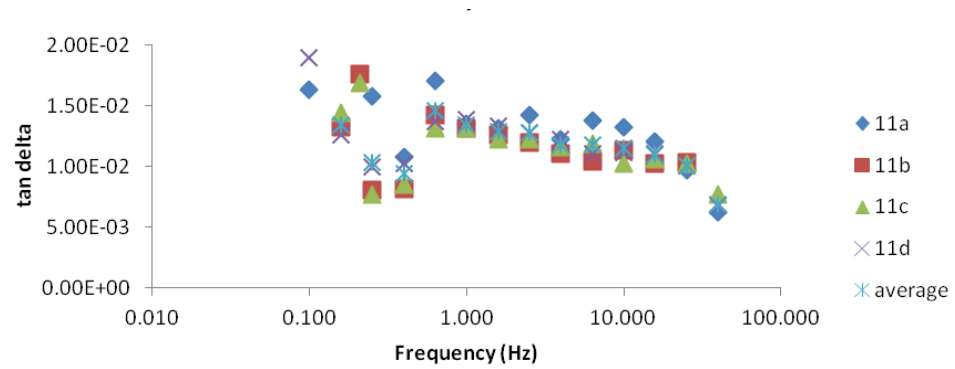
Figure 6.61: Tan delta vs. frequency for microtricotnanoPA6,6 interleaved samples excluding 63 and 100 Hz.

6.4   Compression after impact

Table 6.31: Specimen measurements, data and results for control specimens.

Laminate:		1								
Laminate Description:		Control								
Specimen #	Drop Weight (kg)	Drop Height (mm)	Impact Velocity (m/s)	Spec. Length (mm)	Spec. Width (mm)	Spec. Thickness (mm)	Failure Load (kN)	Target Impact Energy (J)	Actual Impact Energy (J)	CAI Strength (MPa)
1a	5.4	197	1.97	148	99.96	3.56	72.245	10	10.435878	203.0165999
1b	5.4	269	2.30	148.02	100.05	3.54	74.277	15	14.250006	209.7171753
1c	5.4	384	2.74	147.87	100.06	3.54	70.79	20	20.342016	199.8518403
1e	5.4	479	3.07	147.74	100.02	3.53	61.826	25	25.374546	175.109454
1f	5.4	573	3.35	147.76	99.95	3.5	58.46	30	30.354102	167.1121275
1d	5.4	666	3.61	147.88	100.06	3.52	51.599	35	35.280684	146.5001681

Table 6.32: Specimen measurements, data and results for nanoNyplex interleaved specimens.

Laminate:		2								
Laminate Description:		Nyplex interleaved								
Specimen #	Drop Weight (kg)	Drop Height (mm)	Impact Velocity (m/s)	Spec. Length (mm)	Spec. Width (mm)	Spec. Thickness (mm)	Failure Load (kN)	Target Impact Energy (J)	Actual Impact Energy (J)	CAI Strength (MPa)
2a	5.4	197	1.97	147.93	100.09	3.66	80.294	10	10.435878	219.1852469
2b	5.4	269	2.30	147.87	100.04	3.62	85.032	15	14.250006	234.8011072
2c	5.4	384	2.74	147.8	100.02	3.6	74.214	20	20.342016	206.1087782
2d	5.4	479	3.07	147.82	100.06	3.66	62.085	25	25.374546	169.5294299
2e	5.4	573	3.35	147.8	100.05	3.655	56.486	30	30.354102	154.467226
2f	5.4	666	3.61	147.83	99.93	3.62	62.533	35	35.280684	172.8640988

Table 6.33: Specimen measurements, data and results for nanoPMMA interleaved specimens.

Laminate:	3									
Laminate Description:	PMMA interleaved									
Specimen #	Drop Weight (kg)	Drop Height (mm)	Impact Velocity (m/s)	Spec. Length (mm)	Spec. Width (mm)	Spec. Thickness (mm)	Failure Load (kN)	Target Impact Energy (J)	Actual Impact Energy (J)	CAI Strength (MPa)
3b	5.4	197	1.97	147.77	100.01	3.555	77.534	10	10.435878	218.0766452
3c	5.4	269	2.30	147.94	99.98	3.61	81.093	15	14.250006	224.6792849
3d	5.4	384	2.74	147.76	99.99	3.59		20	20.342016	
3e	5.4	479	3.07	147.75	100.09	3.58	43.127	25	25.374546	120.3581581
3f	5.4	573	3.35	147.78	99.93	3.54	49.857	30	30.354102	140.9376394
3a	5.4	666	3.61	147.78	100.03	3.55	45.461	35	35.280684	128.0207487

Table 6.34: Specimen measurements, data and results for nanoPA6,6 interleaved specimens.

Laminate:	4									
Laminate Description:	PA66 interleaved									
Specimen #	Drop Weight (kg)	Drop Height (mm)	Impact Velocity (m/s)	Spec. Length (mm)	Spec. Width (mm)	Spec. Thickness (mm)	Failure Load (kN)	Target Impact Energy (J)	Actual Impact Energy (J)	CAI Strength (MPa)
4a	5.4	197	1.97	147.94	100.03	3.65		10	10.435878	
4e	5.4	269	2.30	147.97	100.05	3.67		15	14.250006	
4b	5.4	384	2.74	147.88	100.07	3.64	79.79	20	20.342016	219.0499617
4c	5.4	479	3.07	147.81	100.01	3.59	64.61	25	25.374546	179.9541494
4d	5.4	573	3.35	147.71	100	3.62	69.932	30	30.354102	193.1823204
4f	5.4	666	3.61	147.8	99.89	3.59	63.72	35	35.280684	177.6884936

Table 6.35: Specimen measurements, data and results for nanoPVB interleaved specimens.

Laminate:	5									
Laminate Description:	PVB interleaved									
Specimen #	Drop Weight (kg)	Drop Height (mm)	Impact Velocity (m/s)	Spec. Length (mm)	Spec. Width (mm)	Spec. Thickness (mm)	Failure Load (kN)	Target Impact Energy (J)	Actual Impact Energy (J)	CAI Strength (MPa)
5a	5.4	197	1.97	150.02	100.01	3.57		10	10.435878	
5b	5.4	269	2.30	150.02	100.03	3.58	68.428	15	14.250006	191.0823401
5c	5.4	384	2.74	147.74	100.01	3.54	69.734	20	20.342016	196.9690037
5e	5.4	479	3.07	147.68	100.04	3.55	60.317	25	25.374546	169.8391066
5f	5.4	573	3.35	147.69	99.98	3.52	57.271	30	30.354102	162.7342514
5d	5.4	666	3.61	146.3	100.09	3.57	57.057	35	35.280684	159.6798176

Table 6.36: Specimen measurements, data and results for microPPS interleaved specimens.

Laminate:	6									
Laminate Description:	Micro PPS interleaved									
Specimen #	Drop Weight (kg)	Drop Height (mm)	Impact Velocity (m/s)	Spec. Length (mm)	Spec. Width (mm)	Spec. Thickness (mm)	Failure Load (kN)	Target Impact Energy (J)	Actual Impact Energy (J)	CAI Strength (MPa)
6a	5.4	197	1.97	147.89	100	3.6		10	10.435878	
6b	5.4	269	2.30	147.92	100	3.59	85.314	15	14.250006	237.643454
6c	5.4	384	2.74	147.87	99.99	3.58	69.457	20	20.342016	194.0333698
6d	5.4	479	3.07	147.76	100.02	3.55	67.572	25	25.374546	190.3056009
6e	5.4	573	3.35	147.76	100	3.56	67.323	30	30.354102	189.1095506
6f	5.4	666	3.61	147.73	99.9	3.57	68.186	35	35.280684	191.1883873

Table 6.37: Specimen measurements, data and results for microPEI interleaved specimens.

Laminate:	7									
Laminate Description:	Micro PEI interleaved									
Specimen #	Drop Weight (kg)	Drop Height (mm)	Impact Velocity (m/s)	Spec. Length (mm)	Spec. Width (mm)	Spec. Thickness (mm)	Failure Load (kN)	Target Impact Energy (J)	Actual Impact Energy (J)	CAI Strength (MPa)
7a	5.4	197	1.97	147.85	100.11	3.54	77.912	10	10.435878	219.8485621
7b	5.4	269	2.30	147.87	100.01	3.59	78.172	15	14.250006	217.7275309
7c	5.4	384	2.74	147.78	99.95	3.57	73.279	20	20.342016	205.3659883
7d	5.4	479	3.07	147.83	100.01	3.59	58.073	25	25.374546	161.7470565
7e	5.4	573	3.35	147.78	100.03	3.58	56.625	30	30.354102	158.1229542
7f	5.4	666	3.61	147.68	100.03	3.55	61.363	35	35.280684	172.8016806

Table 6.38: Specimen measurements, data and results for microtricot interleaved specimens.

Laminate:	8									
Laminate Description:	Tricot interleaved									
Specimen #	Drop Weight (kg)	Drop Height (mm)	Impact Velocity (m/s)	Spec. Length (mm)	Spec. Width (mm)	Spec. Thickness (mm)	Failure Load (kN)	Target Impact Energy (J)	Actual Impact Energy (J)	CAI Strength (MPa)
8a	5.4	197	1.97	147.31	100.03	3.69		10	10.435878	
8b	5.4	269	2.30	150.01	100.02	3.74		15	14.250006	
8c	5.4	384	2.74	149.95	100.01	3.7		20	20.342016	
8e	5.4	479	3.07	150	100	3.75		25	25.374546	
8f	5.4	573	3.35	150.02	99.89	3.69	65.5	30	30.354102	177.7022475
8d	5.4	666	3.61	150.12	99.96	3.71		35	35.280684	

Table 6.39: Specimen measurements, data and results for microPPSnanoPA6,6 interleaved specimens.

Laminate:	9									
Laminate Description:	Micro PPS and nano PA66 interleaved									
Specimen #	**Drop Weight (kg)**	**Drop Height (mm)**	**Impact Velocity (m/s)**	**Spec. Length (mm)**	**Spec. Width (mm)**	**Spec. Thickness (mm)**	**Failure Load (kN)**	**Target Impact Energy (J)**	**Actual Impact Energy (J)**	**CAI Strength (MPa)**
9b	5.4	197	1.97	147.66	99.98	3.69		10	10.435878	
9c	5.4	269	2.30	149.98	99.92	3.68		15	14.250006	
9d	5.4	384	2.74	149.99	99.94	3.68	80.824	20	20.342016	219.7622922
9e	5.4	479	3.07	147.78	100	3.67	76.349	25	25.374546	208.0354223
9f	5.4	573	3.35	147.76	99.85	3.66	68.699	30	30.354102	187.984162
9a	5.4	666	3.61	147.83	99.95	3.66	69.557	35	35.280684	190.1415188

Table 6.40: Specimen measurements, data and results for microPEInanoPA6,6 interleaved specimens.

Laminate:	10									
Laminate Description:	Micro PEI and nano PA66 interleaved									
Specimen #	**Drop Weight (kg)**	**Drop Height (mm)**	**Impact Velocity (m/s)**	**Spec. Length (mm)**	**Spec. Width (mm)**	**Spec. Thickness (mm)**	**Failure Load (kN)**	**Target Impact Energy (J)**	**Actual Impact Energy (J)**	**CAI Strength (MPa)**
10a	5.4	197	1.97	147.87	100.01	3.7		10	10.435878	
10b	5.4	269	2.30	147.83	100.1	3.68		15	14.250006	
10c	5.4	384	2.74	147.74	100.04	3.68		20	20.342016	
10e	5.4	479	3.07	147.74	100.11	3.755	67.001	25	25.374546	178.2353659
10f	5.4	573	3.35	147.75	99.95	3.77	64.068	30	30.354102	170.0266579
10d	5.4	666	3.61	147.78	100.12	3.66	66.164	35	35.280684	180.5592851

Table 6.41: Specimen measurements, data and results for microtricotnanoPA6,6 interleaved specimens.

Laminate:	11								
Laminate Description:	Tricot and nano PA66 interleaved								

Specimen #	Drop Weight (kg)	Drop Height (mm)	Impact Velocity (m/s)	Spec. Length (mm)	Spec. Width (mm)	Spec. Thickness (mm)	Failure Load (kN)	Target Impact Energy (J)	Actual Impact Energy (J)	CAI Strength (MPa)
11b	5.4	197	1.97	147.14	100.11	3.84		10	10.435878	
11c	5.4	269	2.30	150.07	100.03	3.82		15	14.250006	
11d	5.4	384	2.74	149.18	100	3.84	71.85	20	20.342016	187.109375
11e	5.4	479	3.07	150.06	99.98	3.87		25	25.374546	
11f	5.4	573	3.35	150.05	99.95	3.83	67.329	30	30.354102	175.8816745
11a	5.4	666	3.61	150.08	100.13	3.855		35	35.280684	

Table 6.42: Specimen measurements, data and results for nanoPES interleaved specimens.

Laminate:	12								
Laminate Description:	PES interleaved								

Specimen #	Drop Weight (kg)	Drop Height (mm)	Impact Velocity (m/s)	Spec. Length (mm)	Spec. Width (mm)	Spec. Thickness (mm)	Failure Load (kN)	Target Impact Energy (J)	Actual Impact Energy (J)	CAI Strength (MPa)
12a	5.4	197	1.97	146.96	100.04	3.6		10	10.435878	
12b	5.4	269	2.30	146.98	100.06	3.54	79.938	15	14.250006	225.6781524
12c	5.4	384	2.74	148.25	100.06	3.52	69.72	20	20.342016	197.9494122
12e	5.4	479	3.07	150.07	100.1	3.51		25	25.374546	
12f	5.4	573	3.35	150.13	99.99	3.54	60.388	30	30.354102	170.6046311
12d	5.4	666	3.61	150.09	100.07	3.58	65.561	35	35.280684	183.0031827

6.5 Fatigue

Table 6.43: Results for control specimens.

Specimen #	Spec. Width (mm)	Spec. Thickness (mm)	Max. cyclic stress (MPa)	Cycles to failure	Comments
1i	25.15	3.57	400	349586	55 mm tabs
1j	25.16	3.56	500	1753	55 mm tabs
1k	25.21	3.53	450	16974	55 mm tabs

Table 6.44: Results for nanoNyplex interleaved specimens.

Specimen #	Spec. Width (mm)	Spec. Thickness (mm)	Max. cyclic stress (MPa)	Cycles to failure	Comments
2h	25.15	3.65	500	5768	no tabs
2i	25.17	3.66	400	818617	55 mm tabs, interupted test due to cooling water turned off
2k	25.2	3.67	450	28152	55mm tabs

Table 6.45: Results for nanoPMMA interleaved specimens.

Specimen #	Spec. Width (mm)	Spec. Thickness (mm)	Max. cyclic stress (MPa)	Cycles to failure	Comments
3h	25.11	3.57	450	34164	55 mm tabs
3i	25.16	3.62	400	141710	55 mm tabs
3j	25.15	3.62	500	3186	interupted test, no tabs

Table 6.46: Results for nanoPA6,6 interleaved specimens.

Specimen #	Spec. Width (mm)	Spec. Thickness (mm)	Max. cyclic stress (MPa)	Cycles to failure	Comments
4h	25.14	3.65	400	1123801	55 mm tabs
4i	25.17	3.66	400	201931	55 mm tabs
4j	25.14	3.63	450	66892	55 mm tabs
4k	25.14	3.68	500	4827	55 mm tabs

Table 6.47: Results for nanoPVB interleaved specimens.

Specimen #	Spec. Width (mm)	Spec. Thickness (mm)	Max. cyclic stress (MPa)	Cycles to failure	Comments
5g	25.15	3.57	500	3100	no tabs
5h			450	65895	no tabs
5j	25.17	3.59	400	837232	tabs 60 mm

Table 6.48: Results for nanoPES interleaved specimens.

Specimen #	Spec. Width (mm)	Spec. Thickness (mm)	Max. cyclic stress (MPa)	Cycles to failure	Comments
12g			500	8648	no tabs
12h	25.19	3.59	400	660060	55mm tabs
12k			450	100038	interupted test, no tabs

Table 6.49: Results for microPPS interleaved specimens.

Specimen #	Spec. Width (mm)	Spec. Thickness (mm)	Max. cyclic stress (MPa)	Cycles to failure	Comments
6g	25.12	3.6	400	512264	
6h	25.15	3.61	500	-	tab failure
6i	25.14	3.62	500	7130	55 mm tabs, surface of specimen uneven from vacuum bagging
6j	25.11	3.58	450	63340	
6k	25.22	3.62	450	-	tab faiure

Table 6.50: Results for microPEI interleaved specimens.

Specimen #	Spec. Width (mm)	Spec. Thickness (mm)	Max. cyclic stress (MPa)	Cycles to failure	Comments
7g	25.15	3.62	400	1155098	55 mm tabs. Interupted test due to overheating
7h	25.16	3.62	500	-	tab failure
7i	25.17	3.6	450	28298	55 mm tabs
7j	25.15	3.57	500	5637	55 mm tabs

Table 6.51: Results for microtricot interleaved specimens.

Specimen #	Spec. Width (mm)	Spec. Thickness (mm)	Max. cyclic stress (MPa)	Cycles to failure	Comments
8h	25.19	3.75	500	1912	tabs 60 mm
8i	25.18	3.75	500	1369	interupted test, no tabs
8j			450	19138	interupted test, no tabs
8k	25.21	3.65	400	39746	55 mm tabs

Table 6.52: Results for microPPSnanoPA6,6 interleaved specimens.

Specimen #	Spec. Width (mm)	Spec. Thickness (mm)	Max. cyclic stress (MPa)	Cycles to failure	Comments
9g	25.17	3.74	400	141510	55 mm tabs
9h	25.15	3.73	500	15058	55 mm tabs
9j	25.15	3.72	450	56202	55 mm tabs

Table 6.53: Results for microPEInanoPA6,6 interleaved specimens.

Specimen #	Spec. Width (mm)	Spec. Thickness (mm)	Max. cyclic stress (MPa)	Cycles to failure	Comments
10g	25.14	3.76	400	672202	55 mm tabs
10h	25.14	3.75	500	5314	55 mm tabs
10i	25.17	3.75	450	16730	55 mm tabs

Table 6.54: Results for microtricotnanoPA6,6 interleaved specimens.

Specimen #	Spec. Width (mm)	Spec. Thickness (mm)	Max. cyclic stress (MPa)	Cycles to failure	Comments
11g	25.14	3.85	500	-	interupted test, no tabs
11h	25.12	3.85	450	29597	60 mm tabs
11i	25.17	3.85	400	139352	55 mm tabs
11j	25.18	3.86	500	5123	55 mm tabs